Targeting fungal growth with novel antifungal drugs

A thesis submitted to The University of Manchester for the degree of Doctor of Philosophy in the Faculty of Biology, Medicine and Health

2017

Saskia du Pré

School of Biological Sciences

Division of Infection, Immunity and Respiratory Medicine

List of contents

Supplementary CD containing movies (included in CD pocket inside the back cover)

Final word count: 44,240

List of figures

List of tables

List of appendix figures

List of supplementary movies (CD)

Abbreviations

ABC	ATP-binding cassette
ABPA	Allergic bronchopulmonary aspergillosis
AIDS	Acquired immune deficiency syndrome
AMA	Autonomously maintained in *Aspergillus*
ATG	Autophagy-related protein
ATP	Adenosine triphosphate
cDNA	Complementary DNA
CDP	Cytidine diphosphate
CDP-DAG	CDP-diacylglycerol
CDR	*Candida* drug resistance
CFW	Calcofluor white
CLSI	Clinical & laboratory standards institute
CMAC	7-amino-4-chloromethylcoumarin
CMP	Cytidine monophosphate
ConA	Concanavalin A
COPD	Chronic obstructive pulmonary disease
CoQ	Coenzyme Q, Ubiquinone
CPA	Chronic pulmonary aspergillosis
CTP	Cytidine triphosphate
CYP51	Lanosterol-14 alpha-demethylase
DCIP	2,6-dichloroinophenol
dCDP	Deoxy cytidine diphosphate
dCMP	Deoxy cytidine monophosphate
DHO	Dihydroorotate
DHODH	Dihydroorotate dehydrogenase
DHR-123	Dihydrorhodamine-123
DiBAC	Bis-(1,3-dibutylbarbituric acid)trimethine oxonol
DIC	Differential Interference Contrast
dNTPS	Deoxy nucleotides
DMSO	Dimethylsulfoxide
DNA	Desoxyribonucleic Acid
dTMP	Deoxy thymidine monophosphate

dUMP	Deoxy uridine monophosphate
ER	Endoplasmatic reticulum
ERG	Ergosterol biosynthesis genes
ETC	Electon transport chain
FITC	Fluoroisothiocyanate
FKS	1,3-ß-glucan synthase genes
FMN	Flavin mononucleotide
$FMNH_2$	Reduced FMN
GAG	Galactosaminoglycan
GECI	Genetically encoded calcium indicator
Gly-Ala	Glycyl-alanine
GFP	Green Fluorescent Protein
GPI	Glycosylphosphatidylinositol
HIV	Human immunodeficiency virus
HOG	High osmolarity glycerol
Hsp90	Heat shock protein 90
IC_{50}	Half maximal inhibitory concentration
IPTG	Isopropyl-beta-D-thiogalactopyranoside
IV	Intravenously
LB	Lysogeny broth
MFC	Minimum Fungicidal Concentration
MIC	Minimal Inhibitory Concentration
MMP	Mitochondrial membrane potential
MTS	Mitochondrial Targeting Signal
NA	Numerical Aperture
NAD^+	Nicotinamide adenine dinucleotide
NBD	Nitrobenzofurazan
OD	Optical Density
OMP	Orotidine monophosphate
PCP	*Pneumocystis* pneumonia
PCR	Polymerase chain reaction
PBS	Phosphate Buffered Saline
PBST	Phosphate Buffered Saline with Tween
PCD	Programmed Cell Death

PEG	Polyethylene glycol
PI	Propidium Iodide
RNA	Ribonucleic Acid
ROS	Reactive oxygen species
RPMI-1640	Roswell Park Memorial Institute 1640 medium
SAB	Sabouraud
SABUU	SAB medium containing uracil and uridine
SAFS	Severe asthma with fungal sensitization
SALA	Salicylate 1-monooxygenase
SAR	Structure-activity relationship
SD	Standard Deviation
TEM	Transmission Electron Microscopy
TPEN	N,N,N',N'-Tetrakis(2-pyridylmethyl)ethylenediamine
UDP	Uridine diphosphate
UMP	Uridine monophosphate
UTP	Uridine triphosphate
UU	Uridine uracil
UV	Ultraviolet
VMM	Vogel's Minimal Medium
VMMUU	VMM containing uridine and uracil
WGA	Wheat Germ Agglutinin
WGA-orange	WGA-tetramethylrhodamine
X-GAL	5-bromo-4-chloro-3-indolyl-beta-D-galacto-pyranoside
Z-VAD-FMK	carbobenzoxy-valyl-alanyl-aspartyl –[O-methyl]-fluoromethylketone

Abstract

Targeting fungal growth with novel antifungal drugs

A PhD thesis submitted to The University of Manchester by Saskia du Pré MSc, School of Biological Sciences, December 2017

Every year approximately 1.5 million people die due to systemic fungal infections. Issues with diagnosis, limited treatment options and resistance to antifungal drugs have led to a high mortality rate. Currently, only five classes of antifungal drugs are available: the azoles, the polyenes (amphotericin B), pyrimidine analogues (flucytosine), the echinocandins and the allylamines/thiocarbamates. The azoles are frequently the first line of treatment, but the emergence of resistance against drugs in this class is a growing problem. Although new drugs are approved for clinical use occasionally, they usually belong to an existing class. The development of new antifungal drugs, acting on new targets is difficult, due to the phylogenetic relatedness between human and fungi: potential antifungal drugs often have unacceptably high levels of toxicity, making them unsuitable for treatment. Recently, F901318, a first-in-class orotomide antifungal developed by F2G Ltd., has gone into clinical development for invasive aspergillosis. During this PhD project, the effects of F901318 on the human pathogenic fungus *Aspergillus fumigatus* were investigated.

F901318 inhibits dihydroorotate dehydrogenase (DHODH), thereby blocking the *de novo* pyrimidine biosynthesis pathway. Pyrimidines play key roles in several important cellular processes, such as DNA/RNA synthesis, cell cycle regulation, protein synthesis and cell wall synthesis. Live-cell, time lapse confocal fluorescence microscopy was utilized to analyze the effect of DHODH inhibition by F901318 in *A. fumigatus*. Growth and viability was analyzed, as well as the morphology of intracellular structures affected by pyrimidine biosynthesis inhibition. Furthermore, a fluorescent analogue of F901318 was demonstrated to be a valuable tool in analyzing drug uptake and distribution. Together, the results have led to the conclusion that F901318 is a time-dependent fungicidal drug, by causing growth arrest and hyphal swelling that over time leads to cell lysis. Morphological rearrangements of multiple cellular structures, such as the cell wall, the vacuoles and the nuclei, show that inhibition of the pyrimidine biosynthesis pathway affects many key cellular processes.

Declaration

No portion of the work referred to in the thesis has been submitted in support of an application for another degree or qualification of this or any other university or other institute of learning

Copyright statement

i. The author of this thesis (including any appendices and/or schedules to this thesis) owns certain copyright or related rights in it (the "Copyright") and s/he has given The University of Manchester certain rights to use such Copyright, including for administrative purposes.

ii. Copies of this thesis, either in full or in extracts and whether in hard or electronic copy, may be made **only** in accordance with the Copyright, Designs and Patents Act 1988 (as amended) and regulation issued under it or, where appropriate, in accordance with licensing agreements which the University has from time to time. This page must form part of any such copies made.

iii. The ownership of certain Copyrights, patents, designs, trademarks and other intellectual property (the "Intellectual Property") and any reproductions of copyright works in the thesis, for example graphs and table ("Reproductions"), which may be described in this thesis, may not be owned by the author and may be owned by third parties. Such Intellectual Property and Reproductions cannot and must not be made available for use without the prior written permission of the owner(s) of the relevant Intellectual Property and/or Reproductions.

iv. Further information on the conditions under which disclosure publication and commercialization of this thesis, the Copyright and any intellectual Property and/or Reproductions described in it may take place is available in the university IP policy (see http://documents.manchester.ac.uk/DocuInfo.aspx?DocID=24420), in any relevant Thesis restriction declarations deposited in the University Library, The University Library's regulations (see http://www.library.manchester.ac.uk/about/regulations/) and in The University's policy on Presentation of Theses.

Acknowledgements

I would like to thank everyone at F2G, especially my supervisor Dr. Jason Oliver, as well as Dr. Mike Birch and Dr. Nicola Beckmann for their support and advice during this PhD project. I would also like to thank my University supervisor Prof. Nick Read for his support and advice and a big thanks to everyone in the Manchester Fungal Infection Group, especially to the members of the Read group.

Also, a big thanks to everyone involved in the FungiBrain ITN and Marie Curie, it was an amazing experience and great to share this with each of you. It has been a great opportunity to visit all the labs and learn various techniques. I will certainly never forget this experience.

Finally, I want to thank my family and friends for their support during this PhD project. Especially a huge thanks to my mum, dad and sister, for their support, help, caring, guidance and so much more. I could have never done this without the three of you, dank jullie wel! Big hug and kisses!

CHAPTER 1

Introduction

1.1 Overview of the thesis

This thesis was written in the alternative journal thesis style. Chapter 1 covers the introduction, chapter 2 the materials and methods, chapters 3-6 are the results chapters written as papers and chapter 7 is the general discussion and future work. An appendix is included which covers some additional experiments that were performed, but were not included in the results chapters. It also includes a copy of a paper by my supervisor Dr. Jason D. Oliver, on which I was one of the co-authors. Additionally, a supplementary CD is included which contains movies of the time lapse sequences that were performed during this work. References to the appropriate movie on the CD are made in the text.

For the purposes of this thesis, the manuscript style of the papers was rearranged according to a thesis style format, with figures and tables inserted in the text after being referenced to in the text. The following is an overview of the four results chapters, along with the role of each author.

Chapter 3: The effect of the novel antifungal drug F901318 on the growth and viability of *Aspergillus fumigatus*

Saskia du Pré, Nicola Beckmann, Mariana Cruz Almeida, Graham E. M. Sibley, Derek Law, Alexandra C. Brand, Mike Birch, Nick D. Read and Jason D. Oliver.

This paper investigates how F901318 affects growth and viability of *A. fumigatus*, utilizing live-cell, time lapse imaging, viability staining and biomass and liquid growth assays. Due to be submitted to Antimicrobial Agents and Chemotherapy (AAC) in December 2017.

Authors' contributions:

Saskia du Pré:	author, microscopy experiments
Nicola Beckmann:	growth recovery assays
Mariana Cruz Almeida:	assisted with TEM
Graham E. M. Sibley:	designed F901318
Derek Law:	support and advice
Alexandra C. Brand:	support with TEM
Mike Birch:	support and advice

Nick D. Read:	University supervisor
Jason D. Oliver:	project supervisor

Chapter 4: The dynamic influence of F901318 on the morphology of *Aspergillus fumigatus*

Saskia du Pré, Mike Birch, Nick D. Read and Jason D. Oliver

This paper investigates the effects of F901318 on intracellular structures of *A. fumigatus*, utilizing GFP-labelling and fluorescent staining and live-cell, time lapse imaging.

Authors' contributions:

Saskia du Pré:	author, all experiments
Mike Birch:	support and advice
Nick D. Read:	University supervisor
Jason D. Oliver:	project supervisor

Chapter 5: Analysis of uptake and intracellular distribution of the orotomide antifungal agent F901318 using a fluorescent analogue

Saskia du Pré, Graham E. M. Sibley, Nicola Beckmann, Nick D. Read, Mike Birch and Jason D. Oliver

This paper investigated the use of a fluorescent analogue as a tool to study distribution and uptake of the F901318.

Authors' contributions:

Saskia du Pré:	author, protein isolation, IC_{50}, fluorescent scans, growth assays, microscopy
Graham E. M. Sibley:	designed F901318 and the fluorescent analogues
Nicola Beckmann:	MICs
Nick D. Read:	University supervisor
Mike Birch:	support and advice
Jason D. Oliver:	protein isolation, IC_{50}, project supervisor

Chapter 6: F901318-induced killing of *A. fumigatus*: an investigation into the mechanism of cell death

Saskia du Pré, Nick D. Read, Mike Birch and Jason D. Oliver

This paper is the start of an investigation into how F901318 kills *A. fumigatus*. Markers for apoptosis and autophagy are investigated, as well as the mitochondrial membrane potential and the intracellular calcium concentration.

Authors' contributions:

Saskia du Pré:	author, all experiments
Nick D. Read:	University supervisor
Mike Birch:	support and advice
Jason D. Oliver:	project supervisor

1.2 Review of the literature

1.2.1 Fungi in our daily lives

Fungi are eukaryotic microorganisms that are classified as a kingdom separate from plants and animals. For a long time, fungi were part of the kingdom of plants due to their apparent similarities in both morphology and lifestyle. However, since the introduction of various modern molecular research techniques, such as DNA sequencing and PCR, it was found that fungi weren't as similar to plants as initially thought. Fungi were found to be more closely related to animals, but distinct enough to be given their own kingdom. The kingdom of Fungi harbours more than 100,000 known species, but recently it was estimated that there could be as many as 5.1 million fungal species inhabiting our planet (1). One of the most important differences between fungi and plants, is the presence of chitin in their cell wall. Also, they do not have chloroplasts and they do not photosynthesise. Fungi are heterotrophic organisms and require the uptake of organic compounds from their environment.

Fungi are divided into budding yeasts and filamentous fungi. Yeasts reproduce by budding or binary fission, but most fungal cells are elongated cells that grow at their tips forming hyphae that contain multiple nuclei, these are the filamentous fungi. Some fungi can switch between a yeast and a hyphal form, these are the so called dimorphic fungi. Fungi are microorganisms that can form a fruiting body (mushroom) or a colony

of which the size of can be enormous. For example, in the Malheur National Forest in Oregon a single *Armillaria ostoyae* colony has been allowed to grow an underground hyphal network for about the last 2,400 years and it now covers more than 8 km^2. Though the hyphal network itself is invisible above ground, in autumn it forms honey mushrooms that pop up above ground, showing the enormous size of this colony.

Though not always obvious, fungi play a very important role in our daily lives. Fungi might be best known as the mushrooms we eat or for the yeasts used in brewing, making wine and baking bread (*Saccharomyces*). They are also used in the production of cheeses (Roquefort, Stilton, Gorgonzola etc.; *Penicillium*) and meat substitutes (Quorn; *Fusarium*). Fungi, especially filamentous fungi, also naturally produce several compounds that can be used for various applications. Medically important applications include the production of the β-lactam group of antibiotics, such as penicillin (*Penicillium*) and cephalosporin (*Acremonium*, previously *Cephalosporium*) (2). Other clinically important compounds produced by filamentous fungi are cyclosporine (*Tolypocladium inflatum*), an immunosuppressive agent; lovastatin (*Pleurotus*), a cholesterol-lowering agent and griseofulvin (*Penicillium*), an antifungal agent (2). Filamentous fungi are used in the field of biotechnology to produce a wealth of other compounds that are used for several processes in various industries. They produce acids, enzymes, exopolysaccharides, secondary metabolites and other compounds that are used in the food and beverage industry, textile industry, detergent industry, cosmetics industry, pharmaceutical industry, in oil production and in starch processing (2). So, fungi make a very important contribution to various aspects in our everyday lives, unfortunately, they are also well known for the unwanted moulds in our houses, for causing food to rot and for causing diseases to crops and animals.

1.2.2 Fungal diseases

Fungal infections can range from simple superficial skin infections to severe invasive infections (3). The superficial infections are best known, as fungi most commonly cause various types of superficial infections to the skin and nails. These kinds of infections are usually caused by dermatophytes (*Trichophyton*, *Microsporum* and *Epidermophyton*), yeasts (*Candida* and *Malassezia furfur*) or non-dermatophytic moulds (*Neoscytalidium, Scopulariopsis* and *Aspergillus*). Examples include: athlete's foot, ringworm of the groin and scalp and nail infections (4, 5). The incidence of these infections is high with more than 20 – 25% of the human population suffering from

skin and nail infections (5). Athlete's foot occurs in 20% of the adult population, ringworm of the scalp is thought to affect more than 200 million people and about 10% of the world population suffers from nail infections. Superficial mucosal infections of oral and genital tracts are mostly caused by *Candida* species, causing oral candidiasis and vaginal and vulvovaginal candidiasis. These kinds of infections are also very common with for example 50 – 75% of young women likely to suffer at least once from vulvovaginitis (4). Even though many people suffer from superficial infections, they are usually easily treatable, which is not the case for systemic fungal infections.

Although cases of systemic fungal diseases have been known for some time, such as the first described cases of aspergillosis in animals and humans in the 19th century, there has been an increase in occurrence since the 1980s (6–8). Several factors have contributed to this, such as the increase in organ transplantations, the development of aggressive therapies and drugs to fight cancer and autoimmune diseases, the insertion of medical devices, the rise of immunocompromised individuals because of immunosuppressive infections like HIV/AIDS, the increase in people's life expectation, etc (4, 7–10). Many people are affected by mycoses and the mortality rate is high, with an estimated 1.5 million people dying each year due to a fungal infection (4).

Systemic fungal infections can occur in both healthy (endemic infections) and in immunocompromised individuals (opportunistic infections). Examples of fungi causing endemic mycoses are *Histoplasma capsulatum*, *Coccidioides immitis* and *Blastomyces dermatitidis* (3). Opportunistic mycoses can be caused by several species and recently more and more fungal species are emerging as pathogens, such as *Fusarium* spp., *Scedosporium* spp. and *Rhizopus* spp (11, 12). However, more than 90% of deaths due to fungal infections are caused by a species belonging to either the *Pneumocystis*, *Cryptococcus*, *Candida* or *Aspergillus* genus (4, 8).

1.2.2.1 *Pneumocystis*

Individuals with impaired immunity, especially HIV/AIDS patients, are very susceptible to pneumonia caused by *Pneumocystis jirovecii* (PCP) (4). PCP is an AIDS defining disease, although there are other groups at risk as well, such as individuals with hematologic diseases, transplant patients and individuals on prolonged immunosuppressive therapy (4). As PCP is difficult to diagnose, it is not known exactly how many cases arise every year. An estimation based on the number of HIV-

infected individuals worldwide suggests that there are at least 400,000 cases each year, with a mortality rate between 20 and 80%. In addition to the number of HIV-infected individuals with PCP, *Pneumocystis* spp. are also likely to contribute to the deaths attributed to chronic obstructive pulmonary disease (COPD) (4).

1.2.2.2 *Cryptococcus*

Nearly all cases of cryptococcosis are caused by *Cryptococcus neoformans* and *C. gattii* (4). Cryptococcosis is caused by *C. neoformans* in immunocompromised individuals, *C. gattii* causes cryptococcosis in individuals that are seemingly healthy, not having any or hardly any deficiencies of the immune system (4, 13). When *Cryptococcus* cells are inhaled, and colonise the lungs, they can cause lung infection and pneumonia and without a proper immune reaction the *Cryptococcus* cells can spread to the brain and cause meningoencephalitis (4, 13). *C. neoformans* especially causes cryptococcosis in people suffering from AIDS. In fact, since the start of the HIV/AIDS epidemic, numbers of cases of cryptococcosis caused by *C. neoformans* have risen (13, 14). Estimates indicate that there are nearly 1 million cases of meningoencephalitis in AIDS patients annually, leading to about 624,700 deaths (14).

1.2.2.3 *Candida*

Species of the *Candida* genus cause both superficial and invasive infections in humans. Some *Candida* species are present on epithelial surfaces of most people as commensals, not causing any infections (4, 5, 15). Only when the host is weakened or immunocompromised can some *Candida* spp. become pathogenic and cause various kinds of infections. These infections range from superficial infections that affect skin or the mucous membrane, to life-threatening invasive infections when this yeast invades the bloodstream and spreads to internal organs (15). Individuals who are susceptible to contracting a form of candidiasis are individuals who are immunocompromised, have had surgery, have burns, were hospitalised for a long time and people that have used broad-spectrum antibiotics and immunosuppressants (4, 15). Other factors that have contributed to fungal invasion and colonisation of *Candida* are medical advances in for example chemotherapy, organ transplantation, hemodialysis and central venous catheters (15). 90% of *Candida* related invasive infections are caused by *Candida albicans*, *C. glabrata*, *C. tropicalis*, *C. parapsilosis* and *C. krusei*

(15). Because these infections are often misdiagnosed and treatment options are limited, mortality rates of candidiasis are high, possibly as high as 45% (15).

1.2.2.4 *Aspergillus*

Some species of the *Aspergillus* genus can cause life-threatening diseases in humans, which are collectively called aspergillosis (16). Pathogenic aspergilli include *A. flavus, A. terreus, A. niger, A. nidulans,* but the most common pathogen in the *Aspergillus* genus is *Aspergillus fumigatus*, causing about 90% of the aspergillosis cases (6, 10).
Aspergillus species belong to the phylum of Ascomycota and are a widespread and diverse group of filamentous fungi, comprising over a hundred species. They grow as saprotrophs, living on dead and decaying matter, degrading organic compounds by producing and secreting proteins (17). This characteristic is exploited by biotechnology, where *Aspergillus* and other filamentous fungi are used to produce proteins, from either fungal origin or non-fungal origin (2). Several *Aspergillus* species, including *A. niger, A. terreus, A. oryzae* and *A. phoenicis*, are used in biotechnology, not only producing proteins, but also secondary metabolites that are of commercial importance and are used for various industrial processes (2). In the field of fungal genetics, *Aspergillus* species such as *A. nidulans* and *A. niger*, are utilised to study several genetic and cellular processes, such as regulation of metabolic pathways, growth, division and genetic recombination.
For a long time, it was thought that *A. fumigatus* only reproduced asexually, however, in a recent study they discovered that this fungus does also has a sexual life cycle (18). The asexual life cycle is far more common and is very simple (Figure 1.1). It all starts with conidiophores producing spores called conidia. The conidia are very small, only 2 -3 μm in diameter, and disperse easily through the air (10). In favourable conditions the conidia will germinate; the conidia will first undergo isotropic growth and when the right size is reached, a germ tube will emerge, in this stage they are called germlings. The germ tube in the germlings will continue to extend and become a hypha. Along hyphae branches will appear and together the hyphae will form a dense hyphal network in which new conidiophores will be made, allowing for the asexual life cycle to start over again.

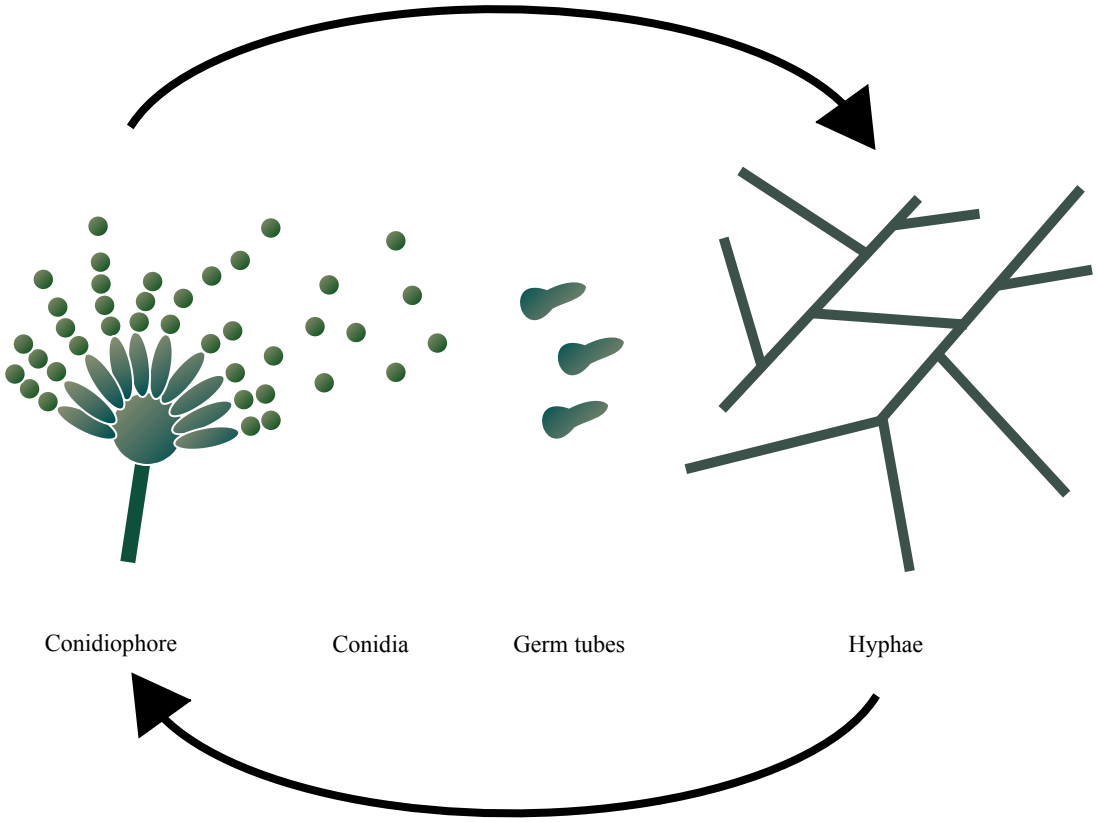

Figure 1.1 The asexual life cycle of *Aspergillus fumigatus*. Spores called conidia are produced by conidiophores. In favourable conditions, a germ tube will emerge from the conidia to form germlings, and they will extend further to form hyphae. A hyphal network will form in which new conidiophores are made, producing new conidia.

When the conidia are dispersed from the conidiophores into the air, they can invade our lungs when they are inhaled, which is why *A. fumigatus* related diseases usually start in the lungs, but they can disseminate throughout the body (10). Usually, inhaling conidia causes no harm to humans, because our immune system effectively removes these conidia. However, in atopic individuals, individuals with an underlying disease and immunocompromised individuals, *A. fumigatus* can cause allergies and severe infections (10, 19). Atopic individuals with asthma are susceptible to contracting allergic bronchopulmonary aspergillosis (ABPA) or severe asthma with fungal sensitisation (SAFS) (19). Between 3.5 and 15 million adults with asthma are thought to be affected by SAFS worldwide and 4.8 million people with asthma and cystic fibrosis are estimated to suffer from ABPA (20). In individuals with an underlying pulmonary condition or disease, such as tuberculosis, ABPA, COPD or SAFS, *A. fumigatus* can cause chronic pulmonary aspergillosis (CPA), with mortality rates of 20 - 33% in the short term and up to 50% in the long term (16, 19, 21). About 1.2 million individuals worldwide are affected by CPA after having suffered from pulmonary

tuberculosis and even more people suffer from CPA in general (21). In immunocompromised individuals, especially individuals with decreased neutrophils, solid organ transplant recipients, patients on immunosuppressants and patients with chronic obstructive pulmonary disease (COPD), *A. fumigatus* can cause severe invasive aspergillosis (4). It is estimated that each year there are more than 200,000 new cases of aspergillosis and if undiagnosed or untreated, the mortality rate is nearly 100% and even if treated, the mortality rate is still about 50% (4, 22).

1.2.3 Antifungal drugs

Currently, there are five major classes of antifungal drugs that are used for treatment of fungal infections: the polyenes, the azoles, the pyrimidine analogues, the echinocandins and the allylamines/thiocarbamates (8, 22). The first four classes are used for the treatment of invasive fungal infections, whereas the latter class is mostly used for treating infections caused by dermatophytes (23). In addition to the five mentioned classes, there is another class called the morpholines (agriculture) and the antifungal compound griseofulvin (dermatophytes).

The limited availability of antifungal drugs is a problem in treating fungal infections, but another increasing problem is the emergence of resistance to these available drugs (9, 23–25). Fungal species can be either naturally resistant (intrinsic) to an antifungal compound or resistance can be acquired by constant exposure during therapy. Additionally, agricultural use of these antifungal drug classes also contributes to the increasing emergence of resistance (26). For example, azoles are commonly used in agriculture; over 25% of fungicide sales are azoles and most are triazoles (20). Fungicides difenoconazole, propiconazole, epoxiconazole, bromuconazole and tebuconazole have a structure similar to the three medical triazoles itraconazole, voriconazole and posaconazole and they bind CYP51A in a similar manner (20, 27). A double mutation resistance mechanism called TR_{34}/L98H, is found in many resistant isolates from patients worldwide, and is also found in isolates from the environment (20, 27). It is very unlikely that clinically used azoles are responsible for environmental azole resistance, because the annual use of fungicides is much higher than the annual use of clinically used azoles (20). Furthermore, before the introduction of the mentioned azole fungicides, no TR_{34}/L98H resistance isolates were found (20). All this evidence strongly suggests that agricultural used azoles are at least partly responsible for azole resistance found in clinical isolates. Besides azoles, it has also

been suggested that agricultural use of polyenes has also led to medical polyene resistance (28).

The following sections describe the mode of action of the available antifungal drug classes and the resistance mechanisms that fungi have developed against them.

1.2.3.1 Polyenes

Drugs of this class interact with ergosterol in the fungal cell membrane, leading to the formation of pores through which the cells leak their cellular constituents (Figure 1.2) (8, 15, 29–31). The first polyenes were discovered in the fifties and they are produced by *Streptomyces* bacteria (8, 15, 22, 29). The most commonly used polyenes are nystatin, produced by *Streptomyces noursei* and amphotericin B, produced by *S. nodosum* (8, 22). Systemic toxicity, especially nephrotoxicity, caused by polyenes when administered in humans, used to limit their use, but novel drug delivery systems have been developed (8, 22, 29). Amphotericin B, for example, is now administered as a lipid formulation, which is less toxic, but the drug does not lose its efficacy (29). Amphotericin B is used for treating candidiasis, aspergillosis and cryptococcosis (22). Amphotericin B was the main antifungal drug for a long time, but several fungal pathogens are now showing microbiological resistance. Resistance in *Candida* spp. remains rare (15), but in filamentous fungi resistance is more frequent. Mutations in the *ERG3* and possibly in the *ERG6* gene, which prevents the conversion of 14α-methylfecosterol to 14α-methyl-3,6-diol, replacing ergosterol with other sterols, which results in a functional membrane with a lower ergosterol content, leading to less interaction of polyenes with the membrane so no pores are formed (9, 15, 30–33). Another mechanism might be increasing the catalase activity, which decreases susceptibility to oxidative damage caused by polyenes (30, 31).

1.2.3.2 Azoles

Most commonly prescribed antifungal drug class that act by causing a decrease in sterol content, which leads to loss of viability. Azoles target lanosterol 14α-demethylase (*CYP51*), a cytochrome p450 dependent enzyme in the ergosterol biosynthesis pathway, inhibiting ergosterol synthesis (Figure 1.2) (8, 15, 29–31, 34). The first developed azoles were the imidazoles, for example clotrimazole, miconazole and ketoconazole (8). Later on, modifications were made to the imidazole ring in the structure, which led to the introduction of the triazoles (8, 22). The most commonly

clinically used triazoles include fluconazole, itraconazole, voriconazole, posaconazole and isavuconazole, the newest triazole. Azoles are useful in preventing and treating both superficial and systemic fungal infections caused by *Candida* spp. and *Aspergillus* spp., but are also used for cryptococcal infections and infections caused by dermatophytes (22).

Drugs in this antifungal drug class are the most widely prescribed drugs and this has led to resistance (26). In *Candida* spp. resistance is usually due to one or a combination of the following four mechanisms: (1) decreased intracellular drug concentrations, achieved by activating efflux pumps and by altering permeability of the fungal cell, (2) target site alteration, by mutations in *CYP51*, (3) overexpression of target enzyme, achieved by gene amplification, increased transcription or decreased degradation of *CYP51* and/or (4) development of bypass pathways by mutations in ERG3, leading to a fungal cell membrane with other sterols than ergosterol, so that the effect of azoles on ergosterol is no longer a problem (9, 15, 30–32). The structural similarity of clinically used azoles has led to cross-resistance among *Candida* species, which is thus yet another way to acquire resistance (15, 31–33). In *Aspergillus* spp., resistance to azoles is achieved by expression of efflux pumps, modification of 14α-sterol demethylase enzyme by mutations in *CYP51* and overexpression of this enzyme (30, 33).

1.2.3.3 Pyrimidine analogues

Flucytosine is the only antifungal compound in this class of antifungal drugs (30, 31). In fungi, flucytosine is converted to 5-fluorouracil by cytosine deaminase (15, 22, 29). Phosphorylation of this compound produces toxic fluorinated nucleotides that interfere with DNA/RNA synthesis (Figure 1.2) (15, 22). The enzymes needed for this conversion, are not present in the human genome, so this antifungal agent is not toxic to humans (29). Flucytosine is mostly used to treat cryptococcal meningitis (29).

Resistance to flucytosine has also been reported. Microbiological resistance to flucytosine is associated with mutations in three enzymes: Purine-cytosine permease, responsible for taking up the drugs into the fungal cell, cytosine deaminase, conversion to 5-fluorouracil and uracil phosphoribosyl transferase, conversion of 5-fluorouracil to 5-fluorouridine monophosphate (15, 30, 31). Because of the development of resistance to flucytosine, this drug is now usually administered in combination with another antifungal drug (31–33).

1.2.3.4 Echinocandins

The echinocandins were the last new class of antifungal drugs to be approved for clinical use, which was in 2000. They are semi-synthetic lipopeptides derived from secondary metabolites produced by fungi (8, 22, 29). They are the only clinically approved antifungal drug class that target the fungal cell wall, by inhibiting the β-1,3-D-glucan synthase complex (Figure 1.2) (8, 15, 22, 29–31). Currently, three echinocandins are in clinical use: caspofungin, derived from pneumocandin B (*Glarea lozoyensis*), micafungin, a semi-synthetic lipopeptide synthesized by chemically modifying a fermentation product of *Coleophoma empetri* and anidulafungin, derived from echinocandin B (*Aspergillus nidulans*) (8). Echinocandins are used for fighting *Candida* spp. and *Aspergillus* spp. infections (15, 22, 29).

Resistance to echinocandins has been reported and has been rising in recent years. Mutations in the genes encoding the elements of the 1,3-β-D-glucan synthase complex are likely the main mechanism through which echinocandin resistance is established, especially point mutations in the *FKS1* and *FKS2* genes (15, 24, 30, 31, 33).

1.2.3.5 Allylamines/thiocarbamates

Allylamines/thiocarbamates are antifungal drugs that blocks ergosterol synthesis by inhibiting squalene epoxidase, an enzyme that catalyses the conversion of squalene to squalene 2,3-epoxide in the ergosterol biosynthesis pathway (Figure 1.2) (8, 15, 22, 34). The first discovered allylamine was naftifine, later on terbinafine was derived from this compound (22, 29). Terbinafine is used to fight infections caused by dermatophytes (8, 29). Tolnaftate is an example of a thiocarbamate and is used to prevent fungal nail infection (8).

For thiocarbamates, no resistance has been reported. For allylamines, resistance has not been reported either, but strains of *Candida* and *Aspergillus*, resistant to terbinafine, have been genetically generated in laboratories. A *C. glabrata* strain, resistant to fluconazole, became cross resistant to terbinafine (32). ATP-binding cassette (ABC) transporter genes called *Candida* Drug Resistance (CDR) genes appear to be reactive to terbinafine, which could be a potential mechanism of resistance to allylamines (32). An *A. fumigatus* strain, transformed with multiple copies of a plasmid harbouring *ERG1*, was resistant to terbinafine (35). UV mutated *A. nidulans* strains that showed resistance to terbinafine, had multiple copies of SALA, a salicylate 1-monooxygenase (36). An. *A. fumigatus* strain with an altered squalene epoxidase gene,

was also resistant to terbinafine (37). So even though no resistance to allylamine has been reported, the mechanisms to acquire resistance appear to be present in the genomes of *Candida* and *Aspergillus*.

1.2.3.6 Other antifungals

Griseofulvin was one of the first compounds found to selectively inhibit fungal growth (29). It is produced by the fungus *Penicillium griseofulvum* and the only antifungal known to block microtubule assembly in susceptible fungi and it does not block assembly of microtubules in humans (Figure 1.2) (15, 29). Griseofulvin is used to fight dermatophytes (29, 32).

Resistance to griseofulvin has been reported, but the precise mechanism is not known. Griseofulvin is transported into dermatophytes via an energy dependent transport process. Fungi that are not sensitive to griseofulvin, lack this kind of energy dependent transport system (32). This could be one of the mechanisms through which griseofulvin resistance is conferred.

Another antifungal drug class is called the morpholines. Although most morpholines are used in agriculture, there is one that is approved for clinical usage, it is called amorolfine and is used topically (29). Morpholines target sterol C_8-C_7 isomerase (*ERG2*) and sterol reductase (*ERG24*) (Figure 1.2) (34).

There are no reports for clinical resistance to amorolfine. But the *C. glabrata* strain that became cross resistant to terbinafine after exposure to fluconazole, also became cross resistant to amorolfine (32). Again, CDR genes also seem to be reactive to amorolfine (32).

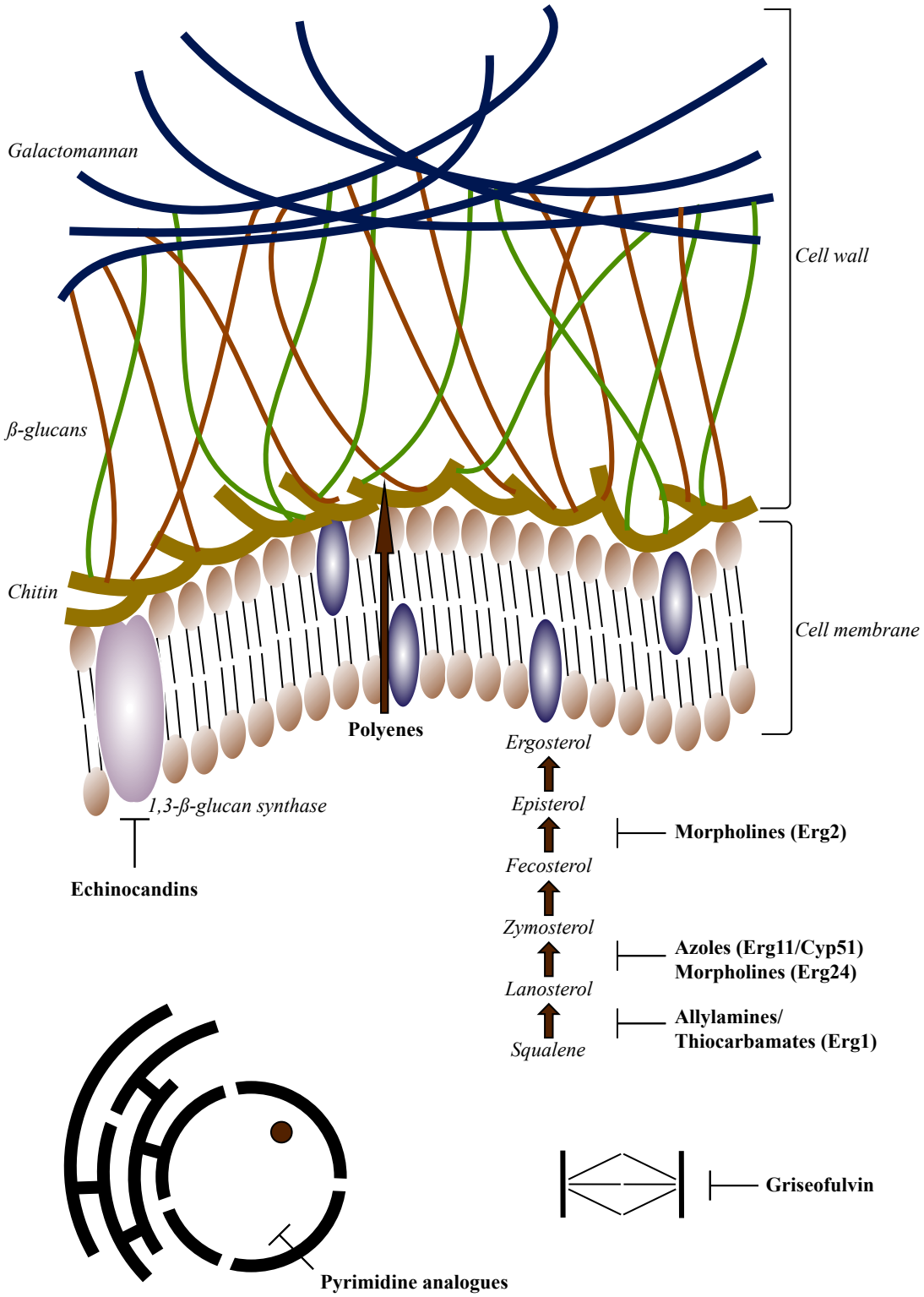

Figure 1.2 Overview of the modes of action of the antifungal drug classes. Polyenes interact with ergosterol, creating channels through which cell contents leak out. Morpholines, azoles and allylamines/thiocarbamates inhibit steps in the ergosterol synthesis pathway. The echinocandins inhibit 1,3-ß-glucan synthase. Pyrimidine analogues insert toxic pyrimidines into DNA during replication. Griseofulvin inhibits the formation of microtubule assembly.

1.2.4 Treatment of invasive fungal infections

The high mortality rate of invasive fungal infections can be attributed to several factors, such as limited treatment options (amphotericin B, azoles, echinocandins and flucytosine), toxicity and resistance. Another contributing factor is the difficulty in diagnosis of these kinds of infections (38). Early diagnosis and determination of the fungal pathogen is important for correct treatment as the activity of antifungal drugs is dependent on the fungal species. A common way to determine the susceptibility of antifungal compounds against fungal pathogens, is by determining the minimal inhibitory concentration (MIC). However, this test is merely a determination of the concentration at which growth is completely inhibited, it does not distinguish between fungistatic or fungicidal compounds. Therefore, the minimal fungicidal concentration (MFC) is commonly determined (39). The conidia from clear wells of an MIC test are transferred to plates, where they are left to form colonies. The lowest concentration where ≥99.9% of colony formation is inhibited, is the MFC of the compound. However, an antifungal compound is usually not specifically either fungistatic or fungicidal, it rather depends on a variety of factors, such as fungal species, concentration of the drug and the exposure time. In general, amphotericin is regarded as a fungicidal drug and the echinocandins are regarded as fungicidal against *Candida* species, but fungistatic against *Aspergillus* species. The azoles are more complicated, as some azoles are fungistatic, where others are fungicidal against the same species, which is also dependent on the exposure time. For example, voriconazole is fungicidal against *Aspergillus*, but only when exposed for a sufficient amount of time (40, 41). Additionally, for filamentous fungi the determination of MICs and MFCs are carried out with conidia, but an antifungal compound may have a different effect against the germinated forms of the fungus (42). Therefore, it is important to take all these factors into consideration when determining the course of treatment for invasive infections.

Azoles are commonly prescribed as antifungal treatment, however, for various reasons such as drug-drug interactions, resistance and acute and chronic side effects, other treatment options could be required (43). Alternatives are amphotericin B and the echinocandins, but they can only be administered intravenously (IV), requiring the patient to be hospitalised. Another downside to these antifungals is that amphotericin is very toxic and the echinocandins have a relatively narrow spectrum, being mostly active against *Candida* spp. Very often combinations of antifungal drugs are used, for example, for cryptococcal meningitis the combination of amphotericin and flucytosine

works quite well (11, 25, 44). For invasive aspergillosis that combination is also used on occasion, but combinations of azoles and amphotericin; echinocandins and amphotericin; and echinocandins and azoles are also used (11, 44, 45).

To try and prevent the development of invasive fungal infections in patients that are at risk, antifungal drugs are sometimes administered as prophylactic agents. Amphotericin B is usually not considered for prophylaxis due to its toxicity. Several studies have examined the use of echinocandins and azoles (posaconazole, fluconazole, itraconazole, and voriconazole) for prophylaxis (46, 47). Although especially posaconazole has been recommended as a prophylactic agent, the ideal prophylactic drug differs from patient to patient (46, 47). It depends on the underlying disease the patient is suffering from, but also on several individual toxicity factors, therefore some patients may be better off with an echinocandin instead of an azole for prophylaxis (46). Several studies have shown that antifungal prophylaxis is beneficial and can prevent the development of invasive fungal infections. There is, however, a concern that prophylaxis may contribute to the increasing emergence of resistant fungal pathogens (11, 46, 47).

1.2.5 Development of new antifungals

Over the years, advances have been made in antifungal drug development and improvements have been made in diagnostics, however, the mortality rate remains high and the increasing emergence of resistance to the available antifungals means there is a high need for new antifungals acting on novel targets.

Developing new fungal specific drugs is quite challenging, because humans and fungi are evolutionarily closely related, both being eukaryotes. The echinocandins represent the only class of antifungal drugs that act on a fungus-specific target, namely 1,3-β-glucan synthase. Other problems with antifungal development include issues with their spectrum of activity, pharmacokinetic profile, bioavailability, adverse effects, in vivo activity, drug-drug interactions etc. Potentially an antifungal compound could cause unacceptable levels of toxicity in the patients or the compound may not be effective as a treatment at all. These issues are all reasons why the development of novel antifungal drugs often fails. Many newly developed antifungals therefore don't even make it to clinical trials or if they do make it, the trial is stopped early on due to either one or a combination of these issues.

The last novel antifungal drug class with a novel mode of action, are the echinocandins and this class was licenced for clinical use in 2001 (44). New antifungal drugs still enter the market occasionally, but they usually belong to one of the existing classes. Especially new azoles are being developed regularly. The most recent clinically approved azole is isavuconazole and has the advantage that it is less toxic than other azoles and it has a higher efficacy (48, 49). Besides developing structurally similar antifungals, existing antifungals can also be reformulated. Amphotericin B is a highly toxic antifungal, causing nephrotoxicity in humans, but it is very effective against invasive fungal infections (11). It has been reformulated to make it less toxic and work to improve the formulation is still ongoing (50).

The disadvantage of developing antifungal drugs that belong to the existing classes is that fungal pathogens that are already resistant to a structurally similar compound, can develop resistance to these new compounds relatively fast. It is thus also very important that new antifungal drugs with novel targets are being developed. New antifungal compounds are often discovered by screening compound libraries or natural products, but this often leads to rediscovery of known compounds or compounds with high toxicity (51). Recently, big pharmaceutical companies are not very active in developing new antifungals because it is more lucrative to develop treatments against chronic diseases such as diabetes (44). Antifungal drug discovery is mostly done by small biotech companies and individual research labs, but if they find a potential antifungal, they will have difficulty in finding enough funds to get the compound through to clinical development, which is very expensive (44). Even when a compound has entered clinical development, there are still many things that can go wrong. It is a lengthy process that needs to be thoroughly regulated in order to be granted the final approval for clinical use.

Some small companies have been successful and have a compound in early clinical development (52–55). One example is T-2307, an arylamidine compound that causes a loss of mitochondrial membrane potential and has broad-spectrum activity against pathogenic fungal species such as *Candida* and *Aspergillus* species and *Cryptococcus neoformans* (56). Another example is APX001 (formerly E1210), inhibiting the 4th enzyme (Gwt1p) in the glycosylphosphatidylinositol (GPI) anchoring pathway and has broad-spectrum activity against *Candida* and *Aspergillus* species, but also against *Fusarium* and *Scedosporium* species (57). Haemofungin is another example that has good activity against various pathogenic fungi. Targeting haem synthesis, this

compound causes severe cell wall damage, possibly due to porphyrin poisoning (58). Another recently described new class of antifungals target the fungal sphingolipid glucosylceramide, the two compounds in this class showed promising MICs against *Cryptococcus* species (59). Other compounds in clinical development include CD101 (Cidara Therapeutics), a new echinocandin for treatment of invasive *Candida* infections (60) and SCY-078 (Scynexis), a glucan synthase inhibitor active against several *Candida* and *Aspergillosis* species (61). A company called Viamet currently have three CYP51 inhibitors in development; VT-1161, VT-1129 and VT-1598 which are being developed for the treatment of several invasive fungal infections (62). Another compound worth mentioning is Nikkomycin Z, a chitin synthase inhibitor discovered in the 1990s, but now in clinical development by Valley Fever Solutions for treatment of coccidioidomycosis (valley fever) caused by *Coccidioides* species (63).

Another way to improve antifungal drugs is to find combinations with other (antifungal) drugs that work in synergy (25). A screen of compounds in combination with sublethal doses of known antifungals led to the discovery of non-antifungal drugs that can be used for antifungal therapy. Especially inhibitors of heat shock protein 90 (hsp90) and calcineurin are found to increase the effectivity of caspofungin (64). Hsp90 activates calcineurin phosphatase, which plays a key role in stress responses and cell wall repair mechanisms.

Natural compounds can also exhibit antifungal activities, an example of this is griseofulvin. In nature when organisms are competing against each other, some organisms produce compounds that exert antifungal activities. Compounds like that could be developed into a clinically used antifungal drug. Another approach is antifungal immunotherapy, though still in development, in the future this might be a promising way to treat fungal infections (65, 66).

1.2.6 The orotomides; a new antifungal drug class

This PhD project has focused on the new antifungal drug F901318, which was discovered and developed by F2G Ltd, a small biotech company that started in 2000 as a spin-out company from the University of Manchester. This new antifungal compound is currently in clinical development for treatment of invasive aspergillosis. F901318 is the lead compound of the so called F3 series, which was initially discovered via screening a library of small compounds for antifungal activity. The

initial compound showed good activity against some *Aspergillus* species and was further developed to improve spectrum and activity. F901318 was chosen as the lead compound as it showed excellent *in vitro* activity against all pathogenic *Aspergilli*, including azole resistant strains, with a minimal inhibitory concentration (MIC) of <0.1 µg/ml (67, 68). Furthermore, F901318 has also showed potent activity against *Scedosporium* species including *Lomentospora prolificans* (69)

The mode of action was identified by performing a genetic screen, using *A. nidulans* strains that had been transformed with Autonomously Maintained in Aspergillus (pAMA1) plasmids that carried the *A. nidulans* genomic library (67). As pAMA1 plasmids are autonomously maintained in the transformed strain, multiple copies of the genes present on the plasmid are expressed, creating a higher level of expression of these genes than in the wild type. Target overexpression should lead to resistance to the drug, so by exposing the pAMA1 transformed strains to F901318, genes could be identified that provide resistance to F901318. Resistant clones were obtained and the gene that was found to provide resistance to F901318 was *pyrE*, encoding for dihydroorotate dehydrogenase (DHODH) (67). DHODH catalyses the fourth step in the pyrimidine biosynthesis pathway and is a novel antifungal drug target (Figure 1.3). The class of antifungals to which this drug belongs has been named the orotomides.

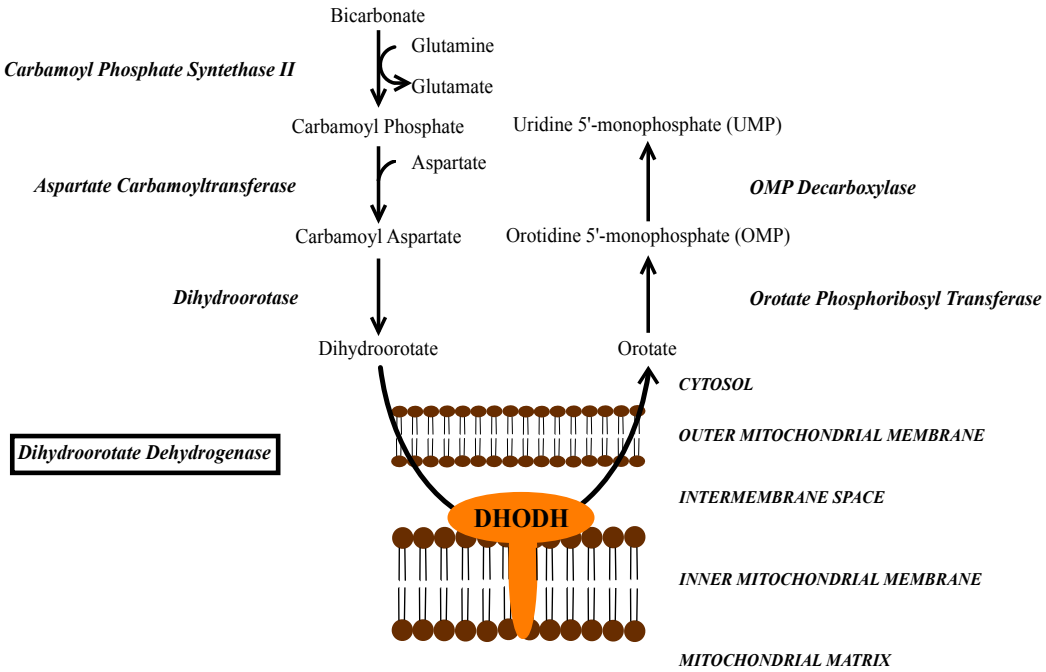

Figure 1.3 The *de novo* pyrimidine biosynthesis pathway. F901318 inhibits the enzyme that catalyses the fourth step: dihydroorotate dehydrogenase.

1.2.6.1 DHODH

The *de novo* pyrimidine biosynthesis pathway is a highly conserved pathway among prokaryotes and eukaryotes (70). DHODH is a flavoenzyme that catalyses the fourth of six steps in the pyrimidine biosynthesis pathway (Figure 1.4). It is a redox reaction where dihydroorotate (DHO) is oxidised to orotate, while FMN is reduced to $FMNH_2$ (71). $FMNH_2$ is recycled via re-oxidation by a cofactor, which is ubiquinone in the case of *A. fumigatus*.

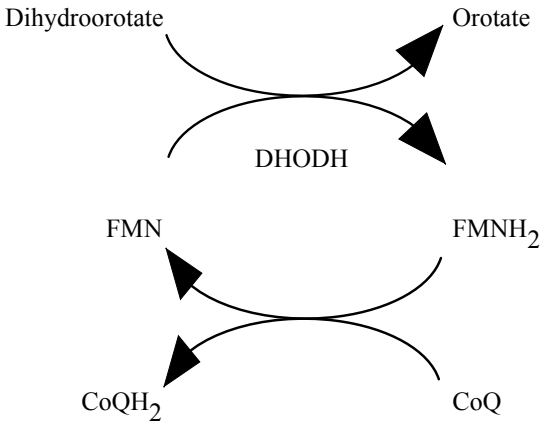

Figure 1.4 Redox reaction catalyzed by DHODH. Dihydroorotate is oxidised to orotate, while FMN is reduced. FMN is recycled by Coenzyme Q10 (CoQ, ubiquinone) in *A. fumigatus*.

Based on sequence similarity, subcellular location and cofactor used, DHODHs are divided into two classes, *i.e.*, Class 1 and Class 2. Class 1 DHODHs are cytosolic, homodimeric proteins (Class 1A) or heterotetrameric proteins, dimers of two heterodimers (Class 1B). Class 1A and Class 1B DHODHs are found for example in gram positive bacteria and yeast, some possess both classes of DHODH. Class 2 DHODHs are membrane bound monomeric proteins. In eukaryotes DHODH is inserted in the inner mitochondria membrane, facing the intermembrane space. In some prokaryotes, such as *Escherichia coli*, DHODH is bound to the cytosolic membrane. Class 1A DHODH use fumarate as a cofactor to re-oxidise $FMNH_2$ and class 1B uses NAD^+ while class 2 DHODH use ubiquinone, linking pyrimidine synthesis to the electron transport chain. Although not previously studied, as *Aspergillus fumigatus* is a eukaryote, it is likely that it has a class 2 DHODH (*pyrE*), bound to the mitochondria. From its sequence, it appears a mitochondrial targeting sequence could be present.

There is no crystal structure for *A. fumigatus* DHODH, but to gain some insight, a homology model was created using structures of other class 2 DHODH enzymes (67). As DHODH catalyses two redox reactions, two redox sites are present in the structure, one for the oxidation of DHO to orotate and one for the oxidation of $FMNH_2$ to FMN. DHODH contains an N-terminal sequence that targets the enzyme to the inner mitochondrial membrane. The long N-terminal extension forms a hydrophobic tunnel that leads into the $FMNH_2$-ubiquinone redox site (71). It is here that human DHODH inhibitor teriflunomide binds and it also believed to be the location where F901318 binds (67, 71). It is suggested that F901318 is a competitive inhibitor for ubiquinone binding, preventing re-oxidation of $FMNH_2$. This channel is also a location where most variation exists between DHODH of different species, explaining why F901318 only targets DHODH of amongst others *Aspergillus* and *Scedosporium* species, but not human DHODH or *Candida* DHODH for example.

1.2.6.2 Pyrimidine biosynthesis as a drug target

Studies in various pathogenic fungi have shown that mutants in the pyrimidine biosynthesis pathway leads to a decrease in virulence. In *C. albicans* a *URA3* mutant showed attenuated levels of virulence (72). In *Histoplasma capsulatum* a *URA5* mutant was avirulent in murine and human cells (73). In *C. neoformans* a *URA4* mutant was affected in various virulence factors (74).

Besides *de novo* synthesis, pyrimidines can also be acquired via salvage pathways. Studies with human lymphocytes have shown that in a resting state, the *de novo* pyrimidine biosynthesis is virtually inactive, the metabolic requirements are met by the salvage pathways (75). In proliferating cells, however, the salvage pathways do not provide the cells with sufficient pyrimidines and so the pyrimidine *de novo* biosynthesis pathway becomes fully active.

The pyrimidine salvage pathway in *A. fumigatus* does not appear to be sufficient during treatment with F901318. MICs for F901318 carried out in presence of increasing concentrations of uridine and uracil show that at least 5 mM of each is required to reverse the antifungal effect of F901318 (67). This was confirmed by *in vivo* infection studies, in which F901318 increased the survival rates, indicating that sufficient pyrimidines cannot be taken from the host. Furthermore, in a murine model of invasive aspergillosis with an *A. fumigatus pyrG* mutant strain, it was shown that this strain was non-pathogenic and unable to germinate (76). Their results suggest that

the concentration of uridine and uracil required to restore wild type growth is higher than the concentration present in the human body. Thus, *A. fumigatus* pyrimidine biosynthesis mutants cannot be supplied with sufficient uridine and uracil for the pyrimidine salvage pathways. All these results show that the enzymes in the pyrimidine biosynthesis pathway, including DHODH, could be promising antifungal drug targets.

Inhibitors of DHODH are already used to treat rheumatoid arthritis, multiple sclerosis, psoriasis and cancer, but also infections caused by viruses, bacteria and *Plasmodium falciparum* (77, 78). Even though the function of DHODH is conserved among eukaryotes, *Aspergillus* DHODH and mammalian DHODH share only about 30% homology (67). Leflunomide is a prodrug that is metabolised into teriflunomide that is active against human DHODH, but not against *Aspergillus* DHODH. F901318 was confirmed to be inactive against human DHODH by determining its half maximal inhibitory concentration (IC_{50}) against human and *A. fumigatus* DHODH. Redox indicator 2,6-dichloroinophenol (DCIP) was used as an artificial electron acceptor when DHO is oxidised to orotate. F901318 was found to inhibit *A. fumigatus* DHODH >2,200-fold more potently than human DHODH (67). Teriflunomide was active against human DHODH, but not against *A. fumigatus* DHODH.

1.2.6.3 Pyrimidines are important for several processes

Pyrimidine biosynthesis is required for synthesising three out of the five nucleobases of DNA and RNA, but the products formed in the pyrimidine biosynthesis pathway are essential for other processes in the cell as well (79)(Figure 1.5).

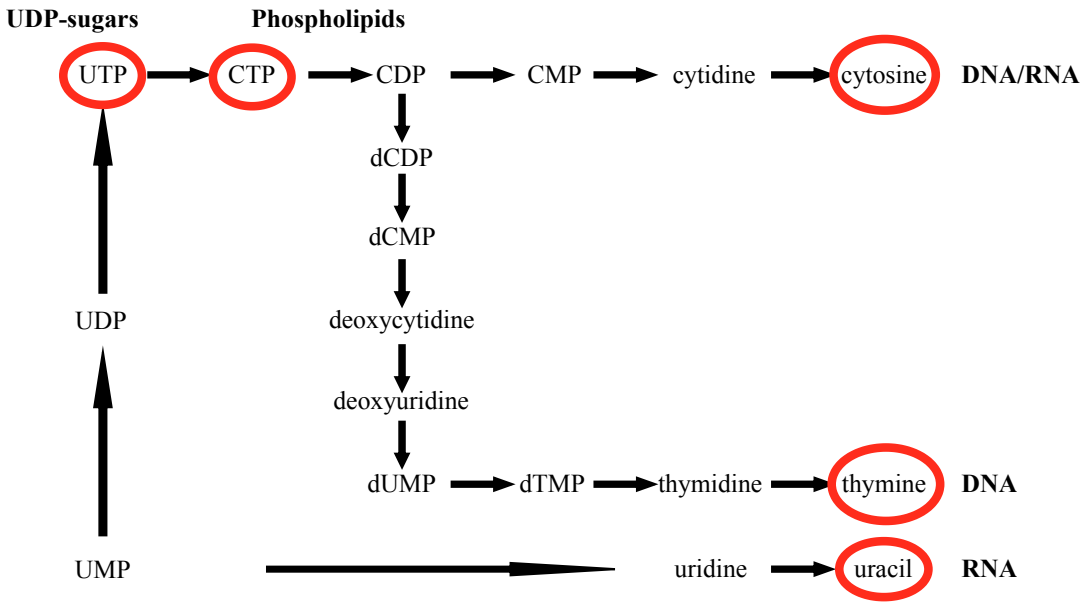

Figure 1.5 Products of pyrimidine synthesis are required for several processes. UTP is required for the synthesis of UDP-sugars which are required for synthesis of cell wall components. CTP is required for phospholipid synthesis. Cytosine, thymine and uracil are nucleobases for DNA and/or RNA.

UTP is important for the synthesis of UDP-sugars that in turn are important for the synthesis of cell wall components in *A. fumigatus* (79). The cell wall forms a protective layer around the fungal conidia and hyphae. As can be seen in figure 1.2, the cell wall mainly consists of chitin, ß-glucans and galactomannan (80). Conidia additionally also have a rodlet and a melanin layer (80). Melanin is what gives the *A. fumigatus* conidia their distinctive black green colour. The two main components 1,3-ß-glucan and chitin both require UTP for their production (Figure 1.6).

The direct precursor of chitin is UDP-*N*-acetyl-glucosamine (81). Not only is this compound required for the synthesis of chitin, it is also involved in glycosylation of proteins, glycolipid synthesis and GPI-anchored protein synthesis. Due to the importance of this compound, UDP-*N*-acetylglucosamine pyrophosphorylase has been suggested as a potential drug target, inhibiting the formation of UDP-*N*-acetyl-glucosamine (82).

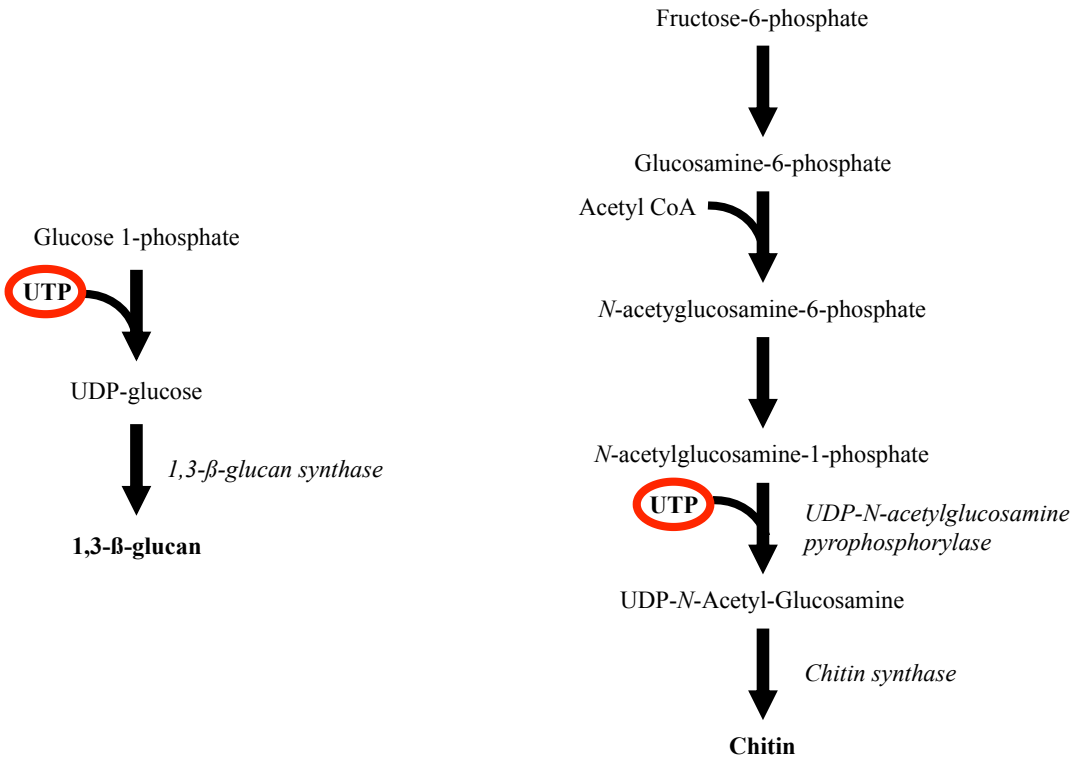

Figure 1.6 Biosynthesis pathway of the two main components of the cell wall chitin and 1,3-ß-glucan, which require UTP for their synthesis.

The CTP pathway is important for the synthesis of membrane phospholipids. They are the major components of the cellular and organelle membranes, but they are also involved in regulatory processes. Though mostly studied in other fungi, a transcriptome analysis recently showed that *A. fumigatus* has similar phospholipid pathways to the other fungi (83). CTP is the direct precursor of the phospholipid pathways for CDP-diacylglycerol (CDP-DAG), CDP-choline and CDP-ethanolamine (the latter two are known as the Kennedy pathway) (84). CDP-DAG is the precursor for the biosynthesis of other phospholipids, such as glycophosphatidylinositol (GPI) and the sphingolipids (84). The latter are involved in a number of processes, which include transport, calcium signalling, cell cycle control and nutrient uptake (85). For this reason, they have been considered as a potential promising target for antifungal drugs. In general, due to the importance of the cell membrane, it has been suggested that it could be a promising antifungal drug target (86).

Pyrimidine biosynthesis leads to the formation of the three pyrimidine nucleobases cytosine (DNA and RNA), thymine (DNA) and uracil (RNA). A study showed that a significant increase in available pyrimidines was correlated with the transition of the G1 to the S phase (75), meaning that proper pyrimidine synthesis is required before a

cell can go into S-phase. In filamentous fungi, the cell cycle is often called duplication cycle, as the cells do not separate after mitosis. When in favourable conditions, *A. fumigatus* uninucleate conidia will start to grow isotropically until they reach a certain size and then the first mitosis takes place, which is after 4h 15 min (87). A germ tube will then emerge from the conidia and this is the start of polarised growth. Subsequent mitosis rounds take place approximately every 45 minutes and occurs synchronously, meaning that all nuclei in a germling/hypha undergo mitosis at the same time (87). Mitosis is also important for septation, indeed septum inhibitors diepoxyoctane and hydroxyurea are also known to inhibit mitosis (88). In 21% of the *A. fumigatus* germlings, the first septum was formed after having undergone four rounds of mitosis (87). After each subsequent round of mitosis, septa are formed at regular distances, dividing the hypha into compartments that each contain roughly 8 nuclei (87).

Cells do not seem to undergo mitosis until they are of a certain size, so it seems that cell size is an important trigger in the cell cycle. Vacuoles are very important contributors to the size of a cell. Indeed, in *C. albicans* they found that the hyphal cell cycle was affected by genes that control the volume of the vacuoles (89). Also, cell cycle mutants were found to have changes in vacuole volume (90). The timing of the cell cycle thus seems to be strongly influenced by the size of vacuoles. Studies in *C. albicans* have led to the belief that it is actually the volume of the cytoplasm that is an important trigger for cell cycle progression. In its filamentous form, cell division is asymmetrical and the growth arrested subapical compartment is left with a small cytoplasmic volume and large vacuoles. Therefore, it is the ratio of cytoplasm volume to vacuole volume that is important for cell cycle progression (91). Other suggestions have been that large vacuoles play a role in nutrient limited conditions, as large vacuoles decrease the need for nutrients (92).

Sufficient pyrimidines are required for normal cell proliferation and depletion of pyrimidines leads to growth defects. An *A. fumigatus* strain with a mutation in the *pyrG* gene was unable to germinate; while the conidia were swelling, a germ tube never emerged (76). Addition of sufficient uridine and uracil restored growth. A *C. neoformans* strain with a *URA4* mutation displayed growth defects at high temperatures (74). In rapidly proliferating human lymphocytes, a greater increase in pyrimidine synthesis than purine synthesis was found, implying the greater role in cell proliferation for pyrimidines (75).

As shown in this section, pyrimidines are required for several processes, including DNA replication, RNA synthesis, protein and lipid synthesis, polysaccharide synthesis etc. Inhibition of pyrimidine biosynthesis in *A. fumigatus* by targeting DHODH with F901318 will affect all these processes and will most likely have a significant effect on growth, morphology and viability.

1.2.6.4 Pyrimidine synthesis and programmed cell death

In mammalian cells, it has been shown that inhibition of the pyrimidine biosynthesis pathway via DHODH, leads to the activation of tumor suppressor protein p53 (93, 94). This protein is a regulator in damaged cells, inducing apoptosis in cells too damaged to avoid their proliferation. Possibly, inhibition of DHODH by F901318 in *A. fumigatus* also causes apoptosis. An important read out for the possible induction of apoptosis is the mitochondrial membrane potential: a decrease has been associated with apoptotic cells. Furthermore, the onset of apoptosis involves several markers such as the cleavage of DNA, internalization of phosphatidylserine, activation of metacaspases and production of reactive oxygen species (95).

Apoptosis is a form of programmed cell death, of which other forms include necrosis and autophagy. The latter is known for the formation of so called autophagosomes: vesicles that take up toxic waste from the cytoplasm and then fuse with the vacuoles, where their contents are degraded (96). As a result of this, large vacuoles are often observed in autophagic cells.

An important regulator in these programmed cell death pathways is calcium. It serves as a second messenger and spikes of intracellular calcium levels often coincides with induced cell death (97, 98).

1.3 Aims of the project

1.3.1 FungiBrain

This project is part of a EU Marie Curie Initial Training Network (ITN) called FungiBrain. FungiBrain is a €3.9 million multi-centre training network grant funded by the EU to establish a detailed understanding of the conserved fungal signalling networks that regulate polarised and directed fungal cell growth in a wide range of fungal models and pathogens. This training network is a collaboration in fungal biology between eight European Universities and research institutes, and three leading

industrial partners. The project integrates genetic, biochemical, biophysical, cell biology and systems biology approaches to define common patterns of signal integration that regulate fungal cell growth and tropisms.

One of the overall aims of the FungiBrain project is to find novel antifungal drug targets. The FungiBrain project will also focus on establishing a detailed understanding of conserved fungal signalling networks that regulate polarised and directed fungal cell growth in a wide range of fungal models and pathogens. Furthermore, novel high throughput, live cell fungal tropism screens of mutant and chemical libraries will be developed.

1.3.2 Importance of the research area

The need for new antifungals is great. Resistance to the existing antifungal drugs, toxicity and spectrum of the existing drugs, the high mortality rates of invasive fungal infections, all indicate the need for new antifungals. Potential antifungal targets might be found in the fungal signalling networks, which is why these networks should be studied to establish a detailed understanding of them. A full understanding of these signalling networks will help finding novel targets.

In this project, specifically the inhibition of the pyrimidine synthesis pathway, via targeting DHODH was investigated in *A. fumigatus* using the new antifungal F901318. The effect on growth, cell morphology and intracellular structures was studied by confocal microscopy. Gaining knowledge of the effects of this drug on *A. fumigatus* will help to understand the consequences of inhibiting pyrimidine biosynthesis. Potentially new candidates for antifungal drug targets can be identified, in the *de novo* pyrimidine biosynthesis pathway itself or possibly in one of the pathways/structures affected by pyrimidine biosynthesis. Furthermore, ways to enhance the effects of this drug by for example combining it with another (antifungal) drug will help to improve antifungal therapy.

1.3.3 Main aims

The main aims that will be addressed in this PhD project are:

- Determine the effect of F901318 on growth and viability of *A. fumigatus*
- Determine the effects of DHODH inhibition, *i.e.*, pyrimidine biosynthesis inhibition, on *A. fumigatus* intracellular morphology
- Study uptake and localization of F901318

- Investigate how F901318 induces cell death (*i.e.* apoptosis, autophagy etc.)

1.3.4 Aim per chapter

Chapter 3:

Determine the effect of F901318 on growth and viability of conidia

Determine the effect of F901318 on growth and viability of germlings

Determine the effect of F901318 on growth and viability of hyphae

Chapter 4:

Tag DHODH with a GFP to determine its localization in *A. fumigatus*

Determine the effect of F901318 on cell wall structure and septation

Determine the effect of F901318 on vacuoles

Determine the effect of F901318 on nuclei

Chapter 5

Obtain a fluorescent F901318 analogue

Studying localization and uptake of F901318

Chapter 6

Investigate presence of apoptotic markers in F901318-treated hyphae

Investigate presence of autophagic markers

Investigate mitochondrial membrane potential

Measure intracellular calcium levels after F901318 addition

1.4 References

1. Blackwell M. 2011. The fungi: 1, 2, 3 ... 5.1 million species? American journal of botany 98:426–38.
2. Meyer V. 2008. Genetic engineering of filamentous fungi — Progress, obstacles and future trends. Biotechnology Advances 26:177–185.
3. Tuite NL, Lacey K. 2013. Overview of Invasive Fungal Infections, p. 1–23. *In* Methods in molecular biology (Clifton, N.J.).
4. Brown GD, Denning DW, Gow NAR, Levitz SM, Netea MG, White TC. 2012. Hidden killers: human fungal infections. Sci Transl Med 4:165rv13.
5. Havlickova B, Czaika VA, Friedrich M. 2008. Epidemiological trends in skin mycoses worldwide. Mycoses 51:2–15.
6. Denning DW. 1998. Invasive Aspergillosis. Clinical Infectious Diseases 26:781–803.

7. Pfaller MA, Diekema DJ. 2007. Epidemiology of invasive Candidiasis: a persistent public health problem. Clinical microbiology reviews 20:133–63.
8. Castelli MV, Butassi E, Monteiro MC, Svetaz LA, Vicente F, Zacchino SA. 2014. Novel antifungal agents: a patent review (2011 – present). Expert Opinion on Therapeutic Patents 24:323–338.
9. Canuto MM, Rodero FG. 2002. Antifungal drug resistance to azoles and polyenes. The Lancet Infectious diseases 2:550–63.
10. Latgé JP. 1999. *Aspergillus fumigatus* and aspergillosis. Clinical microbiology reviews 12:310–50.
11. Enoch DA, Ludlam HA, Brown NM. 2006. Invasive fungal infections: a review of epidemiology and management options. Journal of Medical Microbiology 55:809–818.
12. Skiada A, Pavleas I, Drogari-Apiranthitou M. 2017. Rare fungal infectious agents: a lurking enemy. F1000Research 6:1917.
13. Kronstad JW, Attarian R, Cadieux B, Choi J, D'Souza CA, Griffiths EJ, Geddes JMH, Hu G, Jung WH, Kretschmer M, Saikia S, Wang J. 2011. Expanding fungal pathogenesis: *Cryptococcus* species breaks out of the opportunistic box. Nature reviews Microbiology 9:193–203.
14. Park BJ, Wannemuehler KA, Marston BJ, Govender N, Pappas PG, Chiller TM. 2009. Estimation of the current global burden of cryptococcal meningitis among persons living with HIV/AIDS. AIDS 23:525–530.
15. Spampinato C, Leonardi D. 2013. Candida infections, causes, targets, and resistance mechanisms: traditional and alternative antifungal agents. BioMed research international 2013:204237.
16. Farid S, Mohamed S, Devbhandari M, Kneale M, Richardson M, Soon SY, Jones MT, Krysiak P, Shah R, Denning DW, Rammohan K. 2013. Results of surgery for chronic pulmonary Aspergillosis, optimal antifungal therapy and proposed high risk factors for recurrence--a National Centre's experience. Journal of cardiothoracic surgery 8:180.
17. van de Veerdonk FL, Gresnigt MS, Romani L, Netea MG, Latgé J-P. 2017. *Aspergillus fumigatus* morphology and dynamic host interactions. Nature Reviews Microbiology 15:661–674.
18. O'Gorman CM, Fuller HT, Dyer PS. 2009. Discovery of a sexual cycle in the opportunistic fungal pathogen *Aspergillus fumigatus*. Nature 457:471–474.
19. Smith NL, Denning DW. 2011. Underlying conditions in chronic pulmonary aspergillosis including simple aspergilloma. European Respiratory Journal 37:865–872.
20. Bowyer P, Denning DW. 2014. Environmental fungicides and triazole resistance in Aspergillus. Pest Management Science 70:173–178.
21. Denning DW, Pleuvry A, Cole DC. 2011. Global burden of chronic pulmonary aspergillosis as a sequel to pulmonary tuberculosis. Bulletin of the World Health Organization 89:864–72.
22. Denning DW, Hope WW. 2010. Therapy for fungal diseases: opportunities and priorities. Trends in microbiology 18:195–204.
23. Sanglard D. 2016. Emerging Threats in Antifungal-Resistant Fungal Pathogens. Frontiers in medicine 3:11.
24. Wiederhold NP. 2016. Echinocandin Resistance in *Candida* Species: a Review of Recent Developments. Current Infectious Disease Reports 18:42.
25. Scorzoni L, de Paula e Silva ACA, Marcos CM, Assato PA, de Melo WCMA, de Oliveira HC, Costa-Orlandi CB, Mendes-Giannini MJS, Fusco-Almeida

AM. 2017. Antifungal Therapy: New Advances in the Understanding and Treatment of Mycosis. Frontiers in Microbiology 8:36.
26. Chowdhary A, Sharma C, Meis JF. 2017. Azole-Resistant Aspergillosis: Epidemiology, Molecular Mechanisms, and Treatment. The Journal of Infectious Diseases 216:S436–S444.
27. Snelders E, Camps SMT, Karawajczyk A, Schaftenaar G, Kema GHJ, van der Lee HA, Klaassen CH, Melchers WJG, Verweij PE. 2012. Triazole fungicides can induce cross-resistance to medical triazoles in *Aspergillus fumigatus*. PloS one 7:e31801.
28. Dalhoff A. 2017. Does the use of antifungal agents in agriculture and in food foster polyene-resistance development? A reason for concern. Journal of Global Antimicrobial Resistance Epub ahead.
29. Odds FC. 2003. Antifungal agents: their diversity and increasing sophistication. Mycologist 17:51–55.
30. Pemán J, Cantón E, Espinel-Ingroff A. 2009. Antifungal drug resistance mechanisms. Expert Review of Anti-infective Therapy 7:453–460.
31. Kanafani ZA, Perfect JR. 2008. Resistance to antifungal agents: mechanisms and clinical impact. Clinical Infectious Diseases 46:120–8.
32. Vanden Bossche H. 1997. Mechanisms of antifungal resistance. Revista iberoamericana de micologia 14:44–9.
33. Balkis MM, Leidich SD, Mukherjee PK, Ghannoum MA. 2002. Mechanisms of fungal resistance: an overview. Drugs 62:1025–40.
34. Onyewu C, Blankenship JR, Del Poeta M, Heitman J. 2003. Ergosterol biosynthesis inhibitors become fungicidal when combined with calcineurin inhibitors against *Candida albicans*, *Candida glabrata*, and *Candida krusei*. Antimicrobial agents and chemotherapy 47:956–64.
35. Liu W, May GS, Lionakis MS, Lewis RE, Kontoyiannis DP. 2004. Extra copies of the *Aspergillus fumigatus* squalene epoxidase gene confer resistance to terbinafine: genetic approach to studying gene dose-dependent resistance to antifungals in *A. fumigatus*. Antimicrobial agents and chemotherapy 48:2490–6.
36. Graminha MAS, Rocha EMF, Prade RA, Martinez-Rossi NM. 2004. Terbinafine resistance mediated by salicylate 1-monooxygenase in *Aspergillus nidulans*. Antimicrobial agents and chemotherapy 48:3530–5.
37. Rocha EMF, Almeida CB, Martinez-Rossi NM. 2002. Identification of genes involved in terbinafine resistance in *Aspergillus nidulans*. Letters in applied microbiology 35:228–32.
38. Arvanitis M, Anagnostou T, Fuchs BB, Caliendo AM, Mylonakis E. 2014. Molecular and nonmolecular diagnostic methods for invasive fungal infections. Clinical microbiology reviews 27:490–526.
39. Pfaller MA, Sheehan DJ, Rex JH. 2004. Determination of fungicidal activities against yeasts and molds: lessons learned from bactericidal testing and the need for standardization. Clinical microbiology reviews 17:268–80.
40. Manavathu EK, Ramesh MS, Baskaran I, Ganesan LT, Chandrasekar PH. 2004. A comparative study of the post-antifungal effect (PAFE) of amphotericin B, triazoles and echinocandins on *Aspergillus fumigatus* and *Candida albicans*. Journal of Antimicrobial Chemotherapy 53:386–389.
41. Manavathu EK, Cutright JL, Chandrasekar PH. 1998. Organism-dependent fungicidal activities of azoles. Antimicrobial agents and chemotherapy 42:3018–21.

42. Espinel-Ingroff A. 2001. Germinated and nongerminated conidial suspensions for testing of susceptibilities of *Aspergillus* spp. to amphotericin B, itraconazole, posaconazole, ravuconazole, and voriconazole. Antimicrobial agents and chemotherapy 45:605–7.
43. Carmona EM, Limper AH. 2017. Overview of Treatment Approaches for Fungal Infections. Clinics in Chest Medicine 38:393–402.
44. Osherov N, Kontoyiannis DP. 2016. The anti-Aspergillus drug pipeline: Is the glass half full or empty? Medical Mycology 55:118–124.
45. Campitelli M, Zeineddine N, Samaha G, Maslak S. 2017. Combination Antifungal Therapy: A Review of Current Data. Journal of Clinical Medicine Research 9:451–456.
46. Halpern AB, Lyman GH, Walsh TJ, Kontoyiannis DP, Walter RB. 2015. Primary antifungal prophylaxis during curative-intent therapy for acute myeloid leukemia. Blood 126:2790–2797.
47. Cornely OA, Maertens J, Winston DJ, Perfect J, Ullmann AJ, Walsh TJ, Helfgott D, Holowiecki J, Stockelberg D, Goh Y-T, Petrini M, Hardalo C, Suresh R, Angulo-Gonzalez D. 2007. Posaconazole vs. Fluconazole or Itraconazole Prophylaxis in Patients with Neutropenia. New England Journal of Medicine 356:348–359.
48. Wilson D, Dimondi V, Johnson S, Jones T, Drew R. 2016. Role of isavuconazole in the treatment of invasive fungal infections. Therapeutics and Clinical Risk Management 12:1197–1206.
49. Shirley M, Scott LJ. 2016. Isavuconazole: A Review in Invasive Aspergillosis and Mucormycosis. Drugs 76:1647–1657.
50. Torrado JJ, Espada R, Ballesteros MP, Torrado-Santiago S. 2008. Amphotericin B formulations and drug targeting. Journal of Pharmaceutical Sciences 97:2405–2425.
51. Roemer T, Krysan DJ. 2014. Antifungal Drug Development: Challenges, Unmet Clinical Needs, and New Approaches. Cold Spring Harbor Perspectives in Medicine 4:a019703.
52. Victoria Castelli M, Gabriel Derita M, Noelí López S. 2017. Novel antifungal agents: a patent review (2013 - present). Expert Opinion on Therapeutic Patents 27:415–426.
53. Fuentefria AM, Pippi B, Lana DFD, Donato KK, de Andrade SF. 2017. Antifungals discovery: an insight into new strategies to combat antifungal resistance. Letters in Applied Microbiology Epub ahead.
54. Perfect JR. 2017. The antifungal pipeline: a reality check. Nature Reviews Drug Discovery 16:603–616.
55. McCarthy MW, Kontoyiannis DP, Cornely OA, Perfect JR, Walsh TJ. 2017. Novel Agents and Drug Targets to Meet the Challenges of Resistant Fungi. The Journal of Infectious Diseases 216:S474–S483.
56. Shibata T, Takahashi T, Yamada E, Kimura A, Nishikawa H, Hayakawa H, Nomura N, Mitsuyama J. 2012. T-2307 causes collapse of mitochondrial membrane potential in yeast. Antimicrobial agents and chemotherapy 56:5892–7.
57. Watanabe N-A, Miyazaki M, Horii T, Sagane K, Tsukahara K, Hata K. 2012. E1210, a new broad-spectrum antifungal, suppresses Candida albicans hyphal growth through inhibition of glycosylphosphatidylinositol biosynthesis. Antimicrobial agents and chemotherapy 56:960–71.
58. Ben Yaakov D, Rivkin A, Mircus G, Albert N, Dietl A-M, Kovalerchick D,

Carmeli S, Haas H, Kontoyiannis DP, Osherov N. 2016. Identification and characterization of haemofungin, a novel antifungal compound that inhibits the final step of haem biosynthesis. Journal of Antimicrobial Chemotherapy 71:946–952.
59. Mor V, Rella A, Farnoud AM, Singh A, Munshi M, Bryan A, Naseem S, Konopka JB, Ojima I, Bullesbach E, Ashbaugh A, Linke MJ, Cushion M, Collins M, Ananthula HK, Sallans L, Desai PB, Wiederhold NP, Fothergill AW, Kirkpatrick WR, Patterson T, Wong LH, Sinha S, Giaever G, Nislow C, Flaherty P, Pan X, Cesar GV, de Melo Tavares P, Frases S, Miranda K, Rodrigues ML, Luberto C, Nimrichter L, Del Poeta M. 2015. Identification of a New Class of Antifungals Targeting the Synthesis of Fungal Sphingolipids. mBio 6:e00647-15.
60. Krishnan BR, James KD, Polowy K, Bryant BJ, Vaidya A, Smith S, Laudeman CP. 2017. CD101, a novel echinocandin with exceptional stability properties and enhanced aqueous solubility. The Journal of Antibiotics 70:130–135.
61. Wring SA, Randolph R, Park S, Abruzzo G, Chen Q, Flattery A, Garrett G, Peel M, Outcalt R, Powell K, Trucksis M, Angulo D, Borroto-Esoda K. 2017. SCY-078 A First in Class Orally Active Antifungal Glucan Synthesis Inhibitor: Pre-Clinical Pharmacokinetics and Pharmacodynamic Target in Murine Models of Disseminated Candidiasis. Antimicrobial Agents and Chemotherapy AAC.02068-16.
62. Schell WA, Jones AM, Garvey EP, Hoekstra WJ, Schotzinger RJ, Alexander BD. 2017. Fungal CYP51 Inhibitors VT-1161 and VT-1129 Exhibit Strong *In Vitro* Activity against *Candida glabrata* and *C. krusei* Isolates Clinically Resistant to Azole and Echinocandin Antifungal Compounds. Antimicrobial agents and chemotherapy 61:e01817-16.
63. Shubitz LF, Trinh HT, Perrill RH, Thompson CM, Hanan NJ, Galgiani JN, Nix DE. 2014. Modeling nikkomycin Z dosing and pharmacology in murine pulmonary coccidioidomycosis preparatory to phase 2 clinical trials. The Journal of infectious diseases 209:1949–54.
64. Lamoth F, Juvvadi PR, Fortwendel JR, Steinbach WJ. 2012. Heat shock protein 90 is required for conidiation and cell wall integrity in *Aspergillus fumigatus*. Eukaryotic cell 11:1324–32.
65. Datta K, Hamad M. 2015. Immunotherapy of Fungal Infections. Immunological Investigations 44:738–776.
66. Posch W, Steger M, Wilflingseder D, Lass-Flörl C. 2017. Promising immunotherapy against fungal diseases. Expert Opinion on Biological Therapy 17:861–870.
67. Oliver JD, Sibley GEM, Beckmann N, Dobb KS, Slater MJ, McEntee L, du Pré S, Livermore J, Bromley MJ, Wiederhold NP, Hope WW, Kennedy AJ, Law D, Birch M. 2016. F901318 represents a novel class of antifungal drug that inhibits dihydroorotate dehydrogenase. PNAS 113:12809–12814.
68. Hope WW, McEntee L, Livermore J, Whalley S, Johnson A, Farrington N, Kolamunnage-Dona R, Schwartz J, Kennedy A, Law D, Birch M, Rex JH. 2017. Pharmacodynamics of the Orotomides against *Aspergillus fumigatus*: New Opportunities for Treatment of Multidrug-Resistant Fungal Disease. mBio 8:e01157-17.
69. Wiederhold NP, Law D, Birch M. 2017. Dihydroorotate dehydrogenase inhibitor F901318 has potent *in vitro* activity against *Scedosporium* species and *Lomentospora prolificans*. Journal of Antimicrobial Chemotherapy 72:1977–

1980.
70. Jones ME. 1980. Pyrimidine Nucleotide Biosynthesis in Animals: Genes, Enzymes, and Regulation of UMP Biosynthesis. Annual Review of Biochemistry 49:253–279.
71. Liu S, Neidhardt EA, Grossman TH, Ocain T, Clardy J. 2000. Structures of human dihydroorotate dehydrogenase in complex with antiproliferative agents. Structure 8:25–33.
72. Noble SM, Johnson AD. 2005. Strains and Strategies for Large-Scale Gene Deletion Studies of the Diploid Human Fungal Pathogen *Candida albicans*. Eukaryotic Cell 4:298–309.
73. Retallack DM, Heinecke EL, Gibbons R, Deepe GS, Woods JP. 1999. The URA5 gene is necessary for *Histoplasma capsulatum* growth during infection of mouse and human cells. Infection and immunity 67:624–9.
74. de Gontijo FA, Pascon RC, Fernandes L, Machado J, Alspaugh JA, Vallim MA. 2014. The role of the *de novo* pyrimidine biosynthetic pathway in *Cryptococcus neoformans* high temperature growth and virulence. Fungal Genetics and Biology 70:12–23.
75. Fairbanks LD, Bofill M, Ruckemann K, Simmonds HA. 1995. Importance of ribonucleotide availability to proliferating T-lymphocytes from healthy humans. Disproportionate expansion of pyrimidine pools and contrasting effects of de novo synthesis inhibitors. The Journal of biological chemistry 270:29682–9.
76. D'Enfert C, Diaquin M, Delit A, Wuscher N, Debeaupuis JP, Huerre M, Latge JP. 1996. Attenuated virulence of uridine-uracil auxotrophs of *Aspergillus fumigatus*. Infection and immunity 64:4401–5.
77. Munier-Lehmann H, Vidalain P-O, Tangy F, Janin YL. 2013. On Dihydroorotate Dehydrogenases and Their Inhibitors and Uses. Journal of Medicinal Chemistry 56:3148–3167.
78. Vyas VK, Ghate M. 2011. Recent developments in the medicinal chemistry and therapeutic potential of dihydroorotate dehydrogenase (DHODH) inhibitors. Mini reviews in medicinal chemistry 11:1039–55.
79. Garavito MF, Narváez-Ortiz HY, Zimmermann BH. 2015. Pyrimidine Metabolism: Dynamic and Versatile Pathways in Pathogens and Cellular Development. Journal of Genetics and Genomics 42:195–205.
80. Free SJ. 2013. Chapter Two – Fungal Cell Wall Organization and Biosynthesis, p. 33–82. *In* Advances in Genetics.
81. Milewski S, Gabriel I, Olchowy J. 2006. Enzymes of UDP-GlcNAc biosynthesis in yeast. Yeast 23:1–14.
82. Fang W, Du T, Raimi OG, Hurtado-Guerrero R, Urbaniak MD, Ibrahim AFM, Ferguson MAJ, Jin C, van Aalten DMF. 2013. Genetic and structural validation of *Aspergillus fumigatus* UDP-N-acetylglucosamine pyrophosphorylase as an antifungal target. Molecular Microbiology 89:479–493.
83. Do JH, Lim BO, Choi WS, Choi D-K. 2005. Exploring the Phospholipid Biosynthetic Pathways of *Aspergillus fumigatus* by Computational Genome Analysis. Engineering in Life Sciences 5:574–579.
84. Chang Y-F, Carman GM. 2008. CTP synthetase and its role in phospholipid synthesis in the yeast *Saccharomyces cerevisiae*. Progress in Lipid Research 47:333–339.
85. Fontaine T. 2017. Sphingolipids from the human fungal pathogen *Aspergillus fumigatus*. Biochimie 141:9–15.

86. Sant DG, Tupe SG, Ramana CV, Deshpande MV. 2016. Fungal cell membrane-promising drug target for antifungal therapy. Journal of Applied Microbiology 121:1498–1510.
87. Momany M, Taylor I. 2000. Landmarks in the early duplication cycles of *Aspergillus fumigatus* and *Aspergillus nidulans*: polarity, germ tube emergence and septation. Microbiology 146:3279–3284.
88. Dichtl K, Samantaray S, Aimanianda V, Zhu Z, Prévost M-C, Latgé J-P, Ebel F, Wagener J. 2015. *Aspergillus fumigatus* devoid of cell wall β-1,3-glucan is viable, massively sheds galactomannan and is killed by septum formation inhibitors. Molecular Microbiology 95:458–471.
89. Veses V, Richards A, Gow NAR. 2009. Vacuole inheritance regulates cell size and branching frequency of *Candida albicans* hyphae. Molecular microbiology 71:505–19.
90. Barelle CJ, Bohula EA, Kron SJ, Wessels D, Soll DR, Schäfer A, Brown AJP, Gow NAR. 2003. Asynchronous cell cycle and asymmetric vacuolar inheritance in true hyphae of *Candida albicans*. Eukaryotic cell 2:398–410.
91. Barelle CJ, Richard ML, Gaillardin C, Gow NAR, Brown AJP. 2006. *Candida albicans* VAC8 is required for vacuolar inheritance and normal hyphal branching. Eukaryotic cell 5:359–67.
92. Veses V, Richards A, Gow NA. 2008. Vacuoles and fungal biology. Current Opinion in Microbiology 11:503–510.
93. Khutornenko AA, Roudko V V, Chernyak B V, Vartapetian AB, Chumakov PM, Evstafieva AG. 2010. Pyrimidine biosynthesis links mitochondrial respiration to the p53 pathway. Proceedings of the National Academy of Sciences of the United States of America 107:12828–33.
94. Khutornenko AA, Dalina AA, Chernyak B V, Chumakov PM, Evstafieva AG. 2014. The Role of Dihydroorotate Dehydrogenase in Apoptosis Induction in Response to Inhibition of the Mitochondrial Respiratory Chain Complex III. Acta naturae 6:69–75.
95. Sharon A, Finkelstein A, Shlezinger N, Hatam I. 2009. Fungal apoptosis: function, genes and gene function. FEMS Microbiology Reviews 33:833–854.
96. Pollack J, Harris S, Marten M. 2009. Autophagy in filamentous fungi. Fungal Genetics and Biology 46:1–8.
97. Muñoz A, Marcos JF, Read ND. 2012. Concentration-dependent mechanisms of cell penetration and killing by the de novo designed antifungal hexapeptide PAF26. Molecular Microbiology 85:89–106.
98. Gonçalves AP, Cordeiro JM, Monteiro J, Muñoz A, Correia-de-Sá P, Read ND, Videira A. 2014. Activation of a TRP-like channel and intracellular Ca2+ dynamics during phospholipase-C-mediated cell death. Journal of cell science 127:3817–29.

CHAPTER 2

Materials and methods

2.1 Strains, culture and growth conditions

2.1.1 *Aspergillus* strains

All the *Aspergillus* strains that were used in this PhD project are listed in table 2.1. AF293 is a clinical isolate of *A. fumigatus* and was used to study the effect of F901318 on *A. fumigatus* morphology and growth. The genetically engineered strains that were used in this study were created in a *AKUB*^{KU80} background. KU80 is a protein that is required for non-homologous end joining and is encoded by *akuB* in *A. fumigatus*. Knocking out *akuB* has resulted in a strain with an increased frequency of homologous recombination, making it ideal for genetic manipulations. The *AKUB*^{KU80} knock-out was created in the *A. fumigatus* CEA17 strain (1).

DHODH is the target of F901318 and to study its localization, it was tagged with green fluorescent protein (GFP). As DHODH was assumed to have an N-terminal mitochondrial targeting sequence, it was tagged C-terminally with GFP. Two DHODH-GFP strains were generated; under control of the native promoter or the constitutive *gpdA* promoter. The P*gpdA*-DHODH-GFP strain gave the clearest GFP signal and was used to study localization. The DHODH-GFP strains were created in DHODH knock-out strain 11.1.1 that was previously created by Dr. Jason Oliver.

The cytoplasmic GFP strain was used to study the size ratio between the cytoplasm and the vacuoles, the H1-GFP strain to study nuclear morphology and the AEQ^{CEA10} strain to study intracellular calcium levels of *A. fumigatus* when exposed to F901318. All three strains were kindly given by Dr. Alberto Muñoz from the Manchester Fungal Infection Group (MFIG) at the University of Manchester.

Aspergillus flavus was utilized to study uptake and distribution of the fluorescent analogue F901848.

Table 2.1 Overview of all used and created *Aspergillus* strains. Apart from the *A. flavus* wildtype, all strains mentioned are *A. fumigatus*.

Strain	Function	Genotype	Parent strain	Source
AF293	Clinical isolate			NCPF 7367
***AKUB*^{KU80}**	Non-homologous recombination mutant	Δ*ku80*	CEA17	(1)
11.1.1	DHODH deletion	Δa*kuB::hph::pyrE*$^{-}$	*AKUB*^{KU80}	Dr Jason Oliver
DHODH-GFP	DHODH-GFP, native promoter	Δa*kuB::*[*pyrE-gfp*]	11.1.1	This work
PgpdA-DHODH-GFP	DHODH-GFP, constitutive promoter	Δa*kuB::*[P*gpdA-pyrE-gfp*]	11.1.1	This work
GFP-pyrG	Cytoplasmic GFP	Δa*kuB::ßtub::gfp::pyrG*$^{+}$	*AKUB*^{KU80}	MFIG
H1-GFP	Nuclear GFP	Δa*kuB::*[P*gpdA-H1-sgfp*]	*AKUB*^{KU80}	MFIG, (2)
AEQ^{CEA10}	Aequorin expressing	*his2A*^{t}*::*[P*gpdA-aeqS*-ptrA]	CEA10	(3)
A. flavus	Wildtype			

2.1.2 Conidia preparation and storage

A. fumigatus conidia from a -80 °C glycerol stock were inoculated in T25 culture flasks (Thermo Scientific Nunc) containing sabouraud dextrose agar (SAB agar, Oxoid) with the addition of supplements such as uracil and uridine when required. The conidia were incubated at 35 °C for 48 – 96 h. Conidia were harvested in phosphate buffered saline with 0.1% v/v Tween 80 (PBST). They were then filtered through sterile glass wool to remove any residue from the conidia. Conidia were quantified using an improved Neubauer hemocytometer. For long term storage, conidia were harvested and filtered as described and then mixed with sterile glycerol to a final concentration of 15% and stored at -80°C in cryovials.

2.1.3 Media and culture conditions

2.1.3.1 *Aspergillus*

Aspergillus strains were grown on either SAB agar, in SAB broth (Bacto) or on Vogel's minimal media (VMM) with, if appropriate, the addition of 10 mM uracil (added before autoclaving) and 10 mM uridine (added after autoclaving, filter sterilized). Contents for 50× Vogel's salts and Vogel's trace elements solution can be found in tables 2.2 and 2.3 (4). The final concentration of the Vogel's salts in VMM is 1x. Glucose was added to VMM to a final concentration of 1% w/v. Media used for transformations additionally contained 1.2M sorbitol. For solid VMM 1.5% agar (Bacto) was added. For hygromycin B selection, drug was added after autoclaving at 250 μg/ml.

Table 2.2 Contents of 1 L 50× Vogel's salts

Salts	Quantity
Sodium Citrate	125 g
KH_2PO_2, anhydrous	250 g
NH_4NO_3, anhydrous	100 g
MgSO4, $7H_2O$	10 g
$CaCl_2$, $2H_2O$	5 g
Vogel's trace elements solution	5 ml
Biotin Solution (0.1 mg/ml)	1.5 ml

Table 2.3 Contents of 100 ml Vogel's trace elements solution

Elements	Quantity
Citric acid, $1H_2O$	5 g
$ZnSO_4$, $7H_2O$	5 g
$Fe(NH_4)_2(SO_4)_4$, $6H_2O$	1 g
$CuSO_4$, $5H_2O$	0.25 g
$MnSO_4$, $4H_2O$	0.05 g
H_3BO_3, anhydrous	0.05 g
Na_2MOO_4, $2H_2O$	0.05 g

2.1.3.2 *Escherichia coli*

E. coli strains were maintained at 37 °C on LB media supplemented with 100 µg/ml ampicillin. For blue/white colony screening, the LB media was supplemented with 0.13 mM isopropyl-beta-D-thiogalactopyranoside (IPTG) and 76.5 nM 5-bromo-4-chloro-3-indolyl-beta-D-galacto-pyranoside (X-GAL).

2.1.4 Transformation

A protocol for Polyethylene Glycol (PEG)-mediated protoplast transformation was used. 50 ml liquid SAB media (with uridine and uracil added if appropriate (SABUU)) was inoculated with 10^6 conidia/ml, this was distributed over 5 90 mm petri dishes and wrapped with parafilm. The cultures were incubated overnight at 37 °C. Next day, biomass was collected over a J cloth and washed with sterile water. A 20 ml 5% glucanex (Novozymes) in KCl buffer (0.6M KCl, 50mM $CaCl_2$) solution was prepared and filter sterilized. Approximately 1 g of biomass was added to the glucanex-KCl mix. This was incubated at 30 °C, shaking at 100 rpm.

Protoplast formation was checked under a microscope after one hour. When enough protoplasts had formed, the protoplasts were filtered through lens tissue and collected in a 50 ml falcon tube. KCl buffer was added to 45 ml. This was then centrifuged at 1800 rpm at 4 °C for 9 min. Supernatant was discarded and the protoplasts were resuspended in 1 ml cold KCl and then topped up with KCl to 25 ml. Cold STC buffer (10 mM Tris HCl pH 7.5, 50 mM $CaCl_2$, 1.2 M Sorbitol) was then slowly added to 50 ml. This was centrifuged at 1900 rpm at 4 °C for 10 min. The pellet was re-suspended in 100-500 µl STC.

Protoplasts were counted with an improved Neubauer counting chamber. $\geq 10^6$ protoplasts were mixed with STC buffer and the appropriate DNA (1 – 3 µg) in 100 µl total volume. 200 µl sterile 60% PEG 6000 (in STC buffer) was added. This was incubated for 5 minutes at room temperature, then vortexed and plated directly onto VMM supplemented with 1.2 M Sorbitol. The transformation plates were incubated at 37 °C for 3 – 7 days.

2.1.5 Radial growth assay *Aspergillus flavus*

The radial growth assay of *A. flavus* in presence and absence of F901318 and F901848 was carried out on VMM and VMM with the addition of 10 mM uracil and 10 mM uridine. 10^4 spores were inoculated in the middle of each plate and the plates were incubated for 3 days at 35 °C, after which colony diameter was measured. Photos were taken with an Olympus SP-350.

2.2 Nucleic acid extraction and amplification

2.2.1 Genomic DNA isolation

Aspergillus strains were grown overnight in 10 ml SAB or SABUU broth at 35°C, shaking at 150 rpm. Next day, biomass was centrifuged for 20 minutes at 4°C at 3000 RCF in a falcon 6/3000. Supernatant was removed and mycelia was left to dry on Whatman (GE Healthcare) filterpaper for 0.5 to 1 hour. Genomic DNA was then extracted using the Fast DNA Spin Kit from MP Biomedicals. Afterwards, DNA integrity was checked by loading it onto an agarose gel (described in section 2.2.6).

2.2.2 RNA isolation

Spores were inoculated at a concentration of 10^6 spores/ml in 10 ml SAB broth and incubated at 37°C. Next the mycelium was harvested and 100 mg was used for RNA isolation. RNA was extracted mostly according to the FastRNA Pro Red Kit protocol from MP Biomedicals. The reagents provided by the kit were not used., RNA*pro* Solution was replaced with Tri Reagent (Fluka) and instead of Lysing Matrix C tubes 2 ml cryo vials filled with small glass beads were used. To remove any DNA contamination in the RNA, the turbo DNA-*free* kit by Ambion was used.

Afterwards RNA integrity was analyzed by loading 5 µl RNA onto an agarose gel (described in section 2.2.6). RNA concentration was measured with a spectrophotometer, measuring the OD_{260}.

2.2.3 Polymerase chain reaction

Amplification of DNA fragments was carried out with Phusion Hot Start II High-Fidelity DNA polymerase (Thermo Scientific). The reaction mix consisted of 1× Phusion HF buffer, 200 mM dNTPS, 1 pM-400 nM of each primer, 10 – 1000 ng DNA, 0.4 U Phusion Hot Start II High Fidelity DNA polymerase.

To analyze plasmid and genomic DNA DreamTaq Green PCR Master Mix (Thermo Scientific) was used. The reaction mix contained the following components: 1x master mix, 400 nM for each primer and genomic or plasmid DNA.

All primers used were synthesized by Eurofins. PCR reactions were carried out in a T3 thermocycler (Biometra) or a Bio-Rad-I-cycler. Cycling parameters were set up according to the manual, annealing temperature and extension time was adjusted accordingly for each set of primers and the length of the amplicon.

PCR products were either purified with AxyPrep PCR Clean-Up kit (Axygen) or the PCR products were extracted from an agarose gel with QIAquick Gel Extraction Kit (Qiagen).

2.2.4 Fusion PCR

Fusion PCR was used to create the DHODH-GFP fusion constructs. The protocol used was based on the protocol previously described by Szewczyk *et al* 2007 (5). The procedure is explained in Figure 2.1.

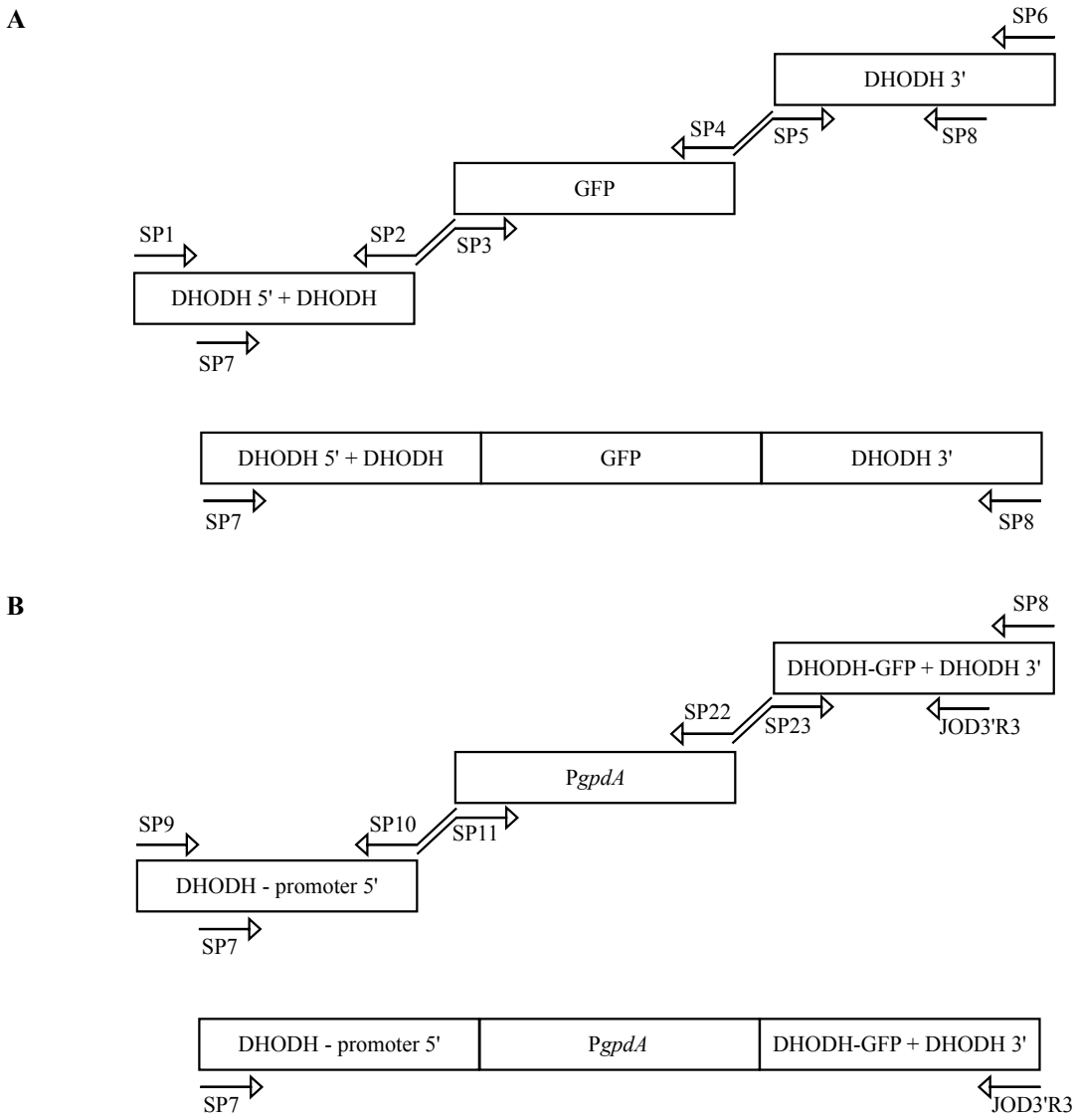

Figure 2.1 Protocol for fusion PCR to create the DHODH-GFP constructs. A) Construction of the DHODH-GFP construct. B) Construction of the PgpdA-DHODH-GFP construct. Note that the 5' flanking region of PgpdA was upstream of the DHODH promoter (DHODH – promoter 5').

Approximately 1.5 kbp long 5' and 3' DHODH flanking regions were amplified as described above with Phusion Hot Start II High Fidelity Polymerase. GFP was obtained from plasmid pFNO3, a reporter gene plasmid from the Fungal Genetics Stock Center (FGSC) kindly given by Dr. Mike Bromley from the University of Manchester. Constitutive promoter *gpdA* was amplified from pAN7.1. Linkers were used to facilitate homologous recombination between the fragments during fusion PCR. A Gly-Ala linker between DHODH and GFP was included to avoid interference of GFP with the DHODH protein structure. Nested primers were used for the actual fusion PCR, to increase the specificity and efficiency of the reaction.

The primers and the PCR cycling parameters for fusion PCR are listed in Table 2.4 and 2.5 respectively. The fusion PCR reaction mix contained the following component: 1× Phusion HF buffer, 200 µM dNTPs, 400 nM of each primer, 0.5 µl DNA templates, 2U Phusion Hot Start II DNA polymerase.

Table 2.4 Primers used for fusion PCR. Sequences in lower case represent the linker sequences.

Primer	Sequence (5' to 3')	DNA
SP1	GCCGACAAAACGAAATCACAG	pGTD2
SP2	ggcaccggctccagcgcctgcaccagctcc TTGACGGTTTTTCTTTTCCTCTCG	pGTD2
SP3	ggagctggtgcaggcgctggagccggtgccatg AGTAAAGGAGAAGAACTTTTCAC	pFNO3
SP4	atccacttaacgttactgaaatccta TTTGTATAGTTCATCCATGCC	pFNO3
SP5	gatttcagtaacgttaagtggat ACTGTTTCGTTTGGATACAGCG	pGTD2
SP6	CCAAGTGCGTATTGTCCATTCATC	pGTD2
SP7	CTGCTCCCCGATCTACAGG	(PgpdA-)DHODH-GFP
SP8	CTGGAGCTGACTCTTGACTCC	DHODH-GFP
SP9	ATCCTACTGACGTTGCTGTG	KU80 gDNA
SP10	gggagcatatcgttcagagc CTATTCGTCACTCATCTTGTCTTCG	KU80 gDNA
SP11	gctctgaacgatatgctccc GAATTCCCTTGTATCTCTACACAC	pAN7.1
SP22	ccggctcggtaacagaacta GGTTCTTGGATGGGAAGATG	pAN7.1
SP23	tagttctgttaccgagccgg ATGGTTGCCAATTCCACCAG	DGFP
JOD3'R3	ACTCAAGCCGAACGATCAAT	PgpdA-DHODH-GFP

Table 2.5 Cycling parameters for the fusion PCR

1×	98 °C for 30 s			
10×	98 °C for 10 s	70 °C for 1 s; to TM at 0.1 °C	TM for 30 s; to 72 °C at 0.1 °C/s	72 °C for 30 s/kb
5×	98 °C for 10 s	70 °C for 1 s; to TM at 0.1 °C	TM for 30 s; to 72 °C at 0.1 °C/s	72 °C for 30 s/kb, increase 5 s every cycle
10×	98 °C for 10 s	70 °C for 1 s; to TM at 0.1 °C	TM for 30 s; to 72 °C at 0.1 °C/s	72 °C for 30 s/kb, increase 20 s every cycle
1×	72 °C for 10 min	4 °C ∞		

2.2.5 Agarose gel electrophoresis

Agarose gel electrophoresis was carried out in a Horizon 58 Horizontal Gel Electrophoresis apparatus powered by a Biometra Power Pack P25. Electrophoresis was performed in 1× TAE (2 M TrisAcetate, 100 mM Na_2EDTA, pH 8.3), freshly made from a 50× stock solution (Flowgen Bioscience Ltd.). 1% (w/v) agarose gels (Agarose I, Amresco) in 1× TAE with the addition of ethidium bromide. Hyperladder I (Bioline) was used as a marker. Gels were imaged on a BioRad geldoc 2000.

2.3 Molecular cloning

2.3.1 pGEM-T easy vector cloning

Fusion PCR fragments were ligated into a pGEM-T easy vector (Promega). Because Phusion Hot Start II High-Fidelity DNA polymerase generates blunt ends, a poly-A tail was added to blunt ends. The A-tailing reaction was carried out by adding an equal amount DreamTaq Green DNA polymerase to the fusion PCR product and incubating the mixture for 20 min. at 72°C. The ligation mix consisted of 1x Rapid Ligation Buffer, 25-50 ng pGEM-T easy vector, 1:1 to 3:1 molar ratio of A-tailed fusion PCR product to the vector and 3 Weiss units of T4 DNA ligase. The reaction mix was incubated overnight at 4 °C.

2.3.2 *E. coli* transformation

Ligations and plasmids were either transformed into NEB 10-beta competent *E. coli* cells (New England BioLabs) or into MegaX DH10B T1 electrocompetent *E. coli* cells (Invitrogen).

From the chemically competent cells, 25 µl of thawed cells and 1 µl of plasmid DNA was added to the cell mixture. The mixture was placed on ice for 30 min, then the cells were heat shocked at 42 °C for 30 s and then placed on ice again for 5 minutes. The cells were then recovered in SOC outgrowth medium by placing them at 37 °C for 1 h, shaking at 250 rpm. Cells were then spread out on LB plates with 100 µg/ml ampicillin and incubated 16 h at 37 °C.

From the electrocompetent cells, 20 µl of thawed cells were added to 1 µl of plasmid DNA. This mixture was transferred to a 0.1-cm cuvette and electroporated under the following conditions: 1.75 kB, 200 Ω and 25 µF. Then 1 ml of recovery medium was added to the cells in the cuvette and this was then transferred to a 15-ml culture tube. The tube was incubated at 37 °C for 1 h, shaking at 225 rpm. Cells were then spread on LB plates containing 100 µg/ml ampicillin, X-GAL and IPTG for selection and incubated 16 h at 37 °C.

2.3.3 *E. coli* DNA isolation

Individual *E. coli* colonies were picked from the *E. coli* transformation plates and transferred into a tube liquid LB medium supplemented with ampicillin (100 µg/ml). Tubes were incubated 16 h at 37 °C in a shaker (225 rpm). Plasmid DNA was then purified from the bacterial cultures using the AxyPrep Plasmid Miniprep kit (Axygen). An overview of the used plasmids is listed in Table 2.6.

2.3.4 Restriction enzymes

Plasmid DNA was analyzed by digestion with restriction nucleases. Either the conventional enzymes by Fermentas or the FastDigest enzymes by ThermoScientific were used. The reaction mix was composed of 1 × buffer, 1 U enzyme and the appropriate amount of DNA. Incubation time was 1 h, except for the FastDigest enzymes, which were incubated for 15 min. Mix was incubated at 37 °C.

If the restriction analysis was positive, the plasmids were sent for sequencing to Source Bioscience Sequencing. Plasmids with pGEM-T easy vector as backbone were sequenced with T7 and SP6 RNA polymerase promoters.

The pGEM-T easy vectors containing transformation cassettes were digested with *XmnI* to linearize the plasmid for optimal homologous recombination during transformation into *A. fumigatus*.

2.3.5 Plasmids

An overview of all the plasmids used throughout this thesis are listed in table 2.6. Plasmid pGTD2 was previously created by Dr. Jason Oliver and is a pGEM-T easy vector in which DHODH and its flanking regions were cloned. Plasmid pFNO3 was kindly given by Dr. Mike Bromley from the MFIG at the University of Manchester. It contains a GFP gene, which was used for the construction for DHODH-GFP strains. Plasmid pAN7.1 was utilized to clone PgdpA from, which was fused to DHODH-GFP. Plasmids pDGFP and pPDGFP are pGEM-T easy vectors in which the DHODH-GFP and the PgpdA-DHODH-GFP fusion cassettes were cloned.

Table 2.6 Plasmids used in this thesis project.

Plasmid name	Content	Source
pGTD2	DHODH with flanking regions	Dr. Jason Oliver
pFNO3	Vector containing GFP	Dr. Mike Bromley, (6)
pAN7.1	Vector containing PgdpA	(7)
pDGFP	DHODH-GFP fusion cassette	This thesis
pPDGFP	PgpdA-DHODH-GFP fusion cassette	This thesis
pET-44-AFD	pET-44 vector *A.flavus* DHODH	This thesis

2.4 DHODH assay

2.4.1 Protein isolation

A. fumigatus DHODH was prepared as described in Oliver *et al* (8). *A. niger* DHODH was prepared in a similar fashion. The protein was cloned into a pET-44 vector (pET-44 Ek/LIC vector kit, Novagen), which adds a soluble Nus-tag and two His-tags to the protein and then transformed into *E. coli* NovaBlue GigaSingles (Novagen). The plasmid was sequenced to confirm the cloning had worked and no mutations had been introduced by PCR. The pET-44 vector, containing the *A. niger* DHODH, was transformed into *E. coli* Bl21 DE3 for protein expression, and grown in LB medium plus 100 µM FMN, 1% glucose and 100 µg/ml ampicillin at 37 °C until the OD600

reached approximately 0.5 when expression was induced by addition of 0.5 mM IPTG and incubation at 20 °C overnight. Protein was extracted using Bugbuster protein extraction reagent (Novagen), and the soluble fraction obtained after centrifugation at 16000 g, 20 min, 4 °C was then transferred to Ni-NTA His-bind resin (Novagen) for an hour with mixing on ice. The His-bind resin was transferred to a column, washed with 50 mM Na phosphate pH 8, 500 mM Na Cl, 20 mM imidazole 0.1% (w/v) Tween 20 and eluted with the same buffer except with the addition of 250 mM imidazole. A PD-10 column (GE healthcare) was used to exchange the buffer to DHODH assay buffer (50 mM Tris pH 8, 150 mM KCl, 10% (w/v) glycerol, 0.1% (w/v) Triton X100. Protein was stored at -80 °C.

2.4.2 DHODH enzyme assay

The redox indicator dye 2,6-dichloroindophenol (DCIP) was used as an artificial electron acceptor to follow the DHODH-catalysed oxidation of dihydroorotate to orotate. The reaction contained 1 mM DHO, 0.05 mM coenzyme Q2 and 0.1 mM DCIP in assay buffer. After addition of recombinant DHODH, DCIP reduction was followed by measuring the decrease in absorbance at 600 nm in clear 96-well microplates (Nunc) on a spectrophotometric plate reader (Tecan Safire). To measure the IC_{50} of F901848 against DHODH a range of drug concentrations were added to the assay wells and the decrease in activity plotted using XL-fit (IDBS), to calculate the concentration of drug giving 50% inhibition of DHODH.

2.5 Antifungal drugs

2.5.1 F901318 and other antifungals

F901318 was manufactured as previously described (8). Final concentration used in the microscopy experiments was 0.1 µg/ml, unless otherwise stated. Other antifungals were used at the following final concentrations: 1 µg/ml voriconazole, 4 µg/ml Amphotericin B and 0.5 µg/ml caspofungin. All antifungals were dissolved in dimethylsulfoxide (DMSO, Sigma).

2.5.2 Fluorescent F901318 analogues

To study uptake, distribution and localization of F901318, five fluorescent analogues of F901318 were synthesized. F902465, F902459, F901848 and F901821 were

labelled with 7-nitrobenzofurazan (NBD). F902430 was labelled with 6-Dimethylamino-napthalene. Compounds were dissolved in DMSO at a stock concentration of 5 mg/ml. Fluorescent scans were carried out on a Tecan Saffire plate reader to determine the excitation/emission peaks. The fluorescence spectra of the potentially fluorescent analogues were read at a concentration of 1.95 µg/ml.

2.6 Microscopy

2.6.1 Culture preparation

Conidia were incubated in Vogel's Minimal Media in a hydrophobic, uncoated µ-Slide 8 well (Ibidi). To obtain germ tubes or hyphae, conidia were pre-incubated for 8 h or 16 h respectively. Unless otherwise noted, inoculum for conidia and germ tubes was 10^5 conidia/ml and for hyphae 10^3 conidia/ml. The cultures were incubated at 37 °C.

2.6.2 Conidial diameter

Freshly harvested AF293 conidia were exposed to 0.1 µg/ml F901318 or 0.02% DMSO as a control. After 24, 48, 72, 96 and 120 h exposure, brightfield and Differential Interference Contrast (DIC) images of the treated and untreated conidia were acquired on a Nikon Eclipse TE2000-E widefield microscope, using a 60×/1.2 NA water objective. A Hamamatsu Orca-ER C4742-80 camera (Hamamatsu Photonics UK Ltd.) with Metamorph software (Molecular Devices) was used for acquisition.

2.6.3 46 h time lapse of F901318 treated germ tubes

AF293 germ tubes were treated with 0.1 µg/ml F901318. A brightfield time-lapse was acquired immediately after the addition of F901318, where z-stacks of 6 images 1 µm apart were taken every 10 min for 46 h on a Nikon Eclipse Ti widefield microscope with a 40×/0.6 NA dry objective using a 12-bit QI Cam cooled mono camera (QImaging, Canada) with Image Pro-Plus 7.0 (Media Cybernetics). The time lapse was acquired at 37 °C.

2.6.4 Confocal microscopy

A Leica TCS SP8X confocal laser microscope was used for live-cell imaging and for studying viability and morphology. Imaging took place at 37 °C in a temperature

controlled box (CUBE & BOX by Life Imaging Services). External light source was provided by a Leica EL6000, excitation light source was provided by a UV laser, SuperK White Light Laser or an argon laser. Either a 40×/0.85 NA dry objective, a 63×/1.2 NA water objective or a 63×/1.4 NA oil immersion objective was used. Leica Application Suite Advanced Fluorescence (LAS AF) was the image acquisition software. The FIJI image distribution of ImageJ was utilized for segmentation, measurements, quantification and processing (9).

2.6.4.1 16 h time lapses of growing germ tubes and hyphae

Germ tubes and hyphae were treated with 0.1 µg/ml F901318 or 0.02 % DMSO. Time lapses were started immediately after addition of F901318 or DMSO. Z-stacks of 6 images 1 µm apart were acquired every 10 min for 16 h.

2.6.4.2 H1-GFP

To observe nuclear morphology and mitosis, H1-GFP hyphae, either untreated or with F901318 (immediate or after 24 h treatment) were imaged for 2 h, taking a z-stack every min. Nuclei were counted in H1-GFP hyphal tips, over distance of 100 µm, that were either untreated or treated for 24 h with F901318.

2.6.4.3 Viability staining

Conidia, germ tubes and hyphae were treated with 0.1 µg/ml F901318 at 37 °C and viability was assessed after 24, 48, 72, 96 and 120 h of exposure using viability dye Bis-(1,3-Dibutylbarbituric Acid)Trimethine Oxonol (DiBAC, Molecular Probes). DiBAC was dissolved in DMSO and used at a final concentration of 2 µg/ml. Samples were incubated for 5 min at 37 °C prior to imaging. Excitation was set to 488 nm, emission was detected over a range of 500-590 nm. For conidia and germ tubes, the percentage of DiBAC staining was quantified. For hyphae, the area of DiBAC stained hyphae was quantified in FIJI by measuring the area of fluorescence/image.

Other viability dyes that were tested are Evans blue (Sigma), FUN-1 (Molecular Probes) and propidium iodide (PI, Sigma). PI and FUN-1 were dissolved in DMSO, Evans blue in water. Evans blue was used at a final concentration of 0.1%, FUN-1 at 5 µM and PI at 5 µg/ml. The excitation for FUN-1 was set to 488 nm and the emission to 500 – 550 nm and 580 – 630 nm. The excitation/emission for PI was set to 535/550-630 nm.

2.6.4.4 Apoptosis

To study F901318-treated hyphae undergo apoptosis, the presence of two apoptotic markers, production of reactive oxygen species (ROS) and activation of metacaspases, were studied. Dihydrorhodamine-123 (DHR-123, Sigma) was utilized to detect ROS and activation of metacaspases was observed with CaspACE™ (Promega). DHR-123) is normally non-fluorescent, but it becomes fluorescent when oxidized to rhodamine-123 by ROS. Rhodamine-123 is a green fluorescent mitochondrial dye. CaspACE FITC-VAD-FMK is a fluorescent analogue of caspase inhibitor Z-VAD-FMK (carbobenzoxy-valyl-alanyl-aspartyl-[O-methyl]-fluoromethylketone) conjugated to fluoroisothiocyanate (FITC). The inhibitor becomes fluorescent when it binds to activated caspases.

Hyphae were treated with F901318 for 24 h, after which DHR-123 and CaspACE^{TM} were applied. DHR-123 was dissolved in DMSO and used at a final concentration of 5 µg/ml. The marker was incubated for 2 h at 37 °C prior to imaging. CaspACE^{TM} was supplied as a 5 mM solution in DMSO and used at a final concentration of 10 µM. Dye was incubated for 20 min at 37 °C prior to imaging. Excitation/Emission for both dyes was set to 488/500-570 nm.

2.6.4.5 Fluorescent analogue imaging

F901848 was the fluorescent analogue utilized to study uptake and distribution in *A. flavus*. A final concentration of 0.8 µg/ml F901848 was added to hyphae after which a 1 h time lapse was acquired, taking images every 2 min, to study uptake of the fluorescent analogue. Excitation/emission was set to 488/500-560 nm.

To study uptake of F901848 when ATP synthesis is inhibited, *A. flavus* was pre-treated with sodium azide (NaN_3). Sodium azide was dissolved in water at a stock concentration of 0.3 M and used at a final concentration of 3 mM. After a 15-min incubation at 37 °C, 0.8 µg/ml F901848 was added and the fluorescence intensity was measured 15 min after addition.

To study uptake of F901848 after F901318 pre-treatment, 0.1 µg/ml F901318 was added to *A. flavus* hyphae for 2 or 24 h, after which 0.8 µg/ml F901848 was added. The fluorescence intensity was measured 15 min after addition.

2.6.4.6 Microscopy dyes

Various dyes were utilized to study the intracellular morphology after treating AF293 hyphae for 24 h with F901318. An overview of the dyes used is given in Table 2.6, which describes what the dye stains, the final concentration and excitation/emission spectrum. All dyes were dissolved in DMSO, except for the following; Aniline Blue was dissolved in 50 mM phosphate buffer (pH 8) as described by Beauvais *et al* 2001 (10), Calcofluor white was dissolved in water and Wheat germ agglutinin tetramethylrhodamine (WGA-orange) was dissolved in Phosphate Buffered Saline (PBS). Dyes were acquired from Sigma or Thermo Fisher Scientific (Molecular Probes). All dyes were incubated in the cultures for 30-60 min at 37 °C prior to imaging.

Table 2.7 All the dyes used in this thesis, including their solvents, the final concentration used and the excitation/emission.

Dye	Target	[Final]	Excitation/Emission
Aniline Blue	1,3-ß-glucan	25 µg/ml	405/420-470 nm
Calcofluor white	Chitin	0.1 µg/ml	405/420-470 nm
CMAC	Vacuoles	1 µM	405/420-470 nm
Concanavalin A	Mannose	10 µg/ml	488/500-550 nm
Filipin	Ergosterol	1 µg/ml	405/420-470 nm
FM4-64	Membranes	5 µM	515/550-700 nm
Nile red	Lipid droplets	10 µg/ml	514/530-600 nm
MitoTracker Red FM	Mitochondria	500 ng/ml	581/595-650 nm
Rhodamine-123	Mitochondria	10 µM	507/520-570 nm
WGA-orange	Chitin	5 µg/ml	555/570-630 nm

2.6.5 Transmission electron microscopy

Conidia (10^7 conidia/ml) and hyphae (pre-grown for 16 h) were treated with 0.1 µg/ml F901318 for 24 h in VMM at 37 °C. Controls were untreated freshly harvested conidia and 40 h untreated hyphae. Cultures were centrifuged and pellets fixed by high pressure freezing in a Leica EM PACT2 (Leica Microsystems, UK). Ultrathin sample sections were stained with lead citrate and uranyl acetate. Samples were examined with a JEM-1400 plus electron microscope and images were captured using AMT Image Capture Engine software.

2.7 Calcium measurements

The protocol used for the aequorin measurements is described in Muñoz *et al* 2015 (3). Conidia of the AEQ^{CEA10} strain (10^6 conidia/ml) in presence of 2.5 µM coelenterazine were incubated in 96-well plates, wrapped in foil, for 21 h at 25 °C. A multimode plate reader (Berthold Technologies TriStar LB 941 was used for the measurement of the luminescence after injection of the antifungal drug. 3 M $CaCl_2$ was used for the discharge control.

2.8 Statistics

Statistical analysis was performed in GraphPad Prism 7. For the conidial diameter, a two-way analysis of variance and Bonferroni's multiple comparison tests with 99% confidence intervals were performed. For the post-exposure effect biomass assay, a Student's T-test was performed with 99% confidence intervals. All experiments were performed in triplicate. Bars represent the Standard Deviation (SD).

2.9 References

1. da Silva Ferreira ME, Kress MRVZ, Savoldi M, Goldman MHS, Härtl A, Heinekamp T, Brakhage AA, Goldman GH. 2006. The akuB(KU80) mutant deficient for nonhomologous end joining is a powerful tool for analyzing pathogenicity in *Aspergillus fumigatus*. Eukaryotic cell 5:207–11.
2. Muñoz A, Harries E, Contreras-Valenzuela A, Carmona L, Read ND, Marcos JF. 2013. Two functional motifs define the interaction, internalization and toxicity of the cell-penetrating antifungal peptide PAF26 on fungal cells. PloS one 8:e54813.
3. Muñoz A, Bertuzzi M, Bettgenhaeuser J, Iakobachvili N, Bignell EM, Read ND, Goldman GH, De U, Paulo S. 2015. Different Stress-Induced Calcium Signatures Are Reported by Aequorin-Mediated Calcium Measurements in Living Cells of *Aspergillus fumigatus*. PLoS ONE 10:e0138008.
4. Vogel HJ. 1956. A Convenient Growth Medium for Neurospora crassa. Microbial Genetics Bulletin 13:42–47.
5. Szewczyk E, Nayak T, Oakley CE, Edgerton H, Xiong Y, Taheri-Talesh N, Osmani SA, Oakley BR. 2006. Fusion PCR and gene targeting in *Aspergillus nidulans*. Nature Protocols 1:3111–3120.
6. Yang L, Ukil L, Osmani A, Nahm F, Davies J, De Souza CPC, Dou X, Perez-Balaguer A, Osmani SA. 2004. Rapid production of gene replacement constructs and generation of a green fluorescent protein-tagged centromeric marker in *Aspergillus nidulans*. Eukaryotic cell 3:1359–62.
7. Punt PJ, Oliver RP, Dingemanse MA, Pouwels PH, van den Hondel CA. 1987. Transformation of *Aspergillus* based on the hygromycin B resistance marker from *Escherichia coli*. Gene 56:117–24.
8. Oliver JD, Sibley GEM, Beckmann N, Dobb KS, Slater MJ, McEntee L, du Pré

S, Livermore J, Bromley MJ, Wiederhold NP, Hope WW, Kennedy AJ, Law D, Birch M. 2016. F901318 represents a novel class of antifungal drug that inhibits dihydroorotate dehydrogenase. PNAS 113:12809–12814.
9. Schindelin J, Arganda-Carreras I, Frise E, Kaynig V, Longair M, Pietzsch T, Preibisch S, Rueden C, Saalfeld S, Schmid B, Tinevez J-Y, White DJ, Hartenstein V, Eliceiri K, Tomancak P, Cardona A. 2012. Fiji: an open-source platform for biological-image analysis. Nature Methods 9:676–682.
10. Beauvais A, Bruneau JM, Mol PC, Buitrago MJ, Legrand R, Latgé JP. 2001. Glucan synthase complex of *Aspergillus fumigatus*. Journal of bacteriology 183:2273–9.

CHAPTER 3

The effect of the novel antifungal drug F901318 on the growth and viability of *Aspergillus fumigatus*

Saskia du Pré,[a,b] Nicola Beckmann,[a] Mariana Cruz Almeida,[c] Graham E. M. Sibley,[a] Derek Law,[a] Alexandra C. Brand,[c] Mike Birch,[a] Nick D. Read,[b] Jason D. Oliver,[a]

F2G Ltd., Manchester, United Kingdom[a];
Manchester Fungal Infection Group, University of Manchester, United Kingdom[b]
Aberdeen Fungal Group, University of Aberdeen, United Kingdom[c]

Submitted to AAC

3.1 Abstract

F901318 is a novel antifungal drug that is highly active against *Aspergillus* species. Belonging to a new class of antifungals called the orotomides, F901318 targets dihydroorotate dehydrogenase (DHODH) in the *de novo* pyrimidine biosynthesis pathway. In this study, the antifungal effects of F901318 against *Aspergillus fumigatus* were investigated. Live-cell imaging revealed that at a low concentration of 0.1 µg/ml, F901318 completely inhibited germination, but conidia continued to expand by isotropic growth for >120 h. When this low F901318 concentration was applied to germ tubes or vegetative hyphae their elongation was completely inhibited within 10 h. Staining with the fluorescent viability dye bis-(1,3-dibutylbarbituric acid) trimethine oxonol (DiBAC) showed that prolonged exposure to F901318 (>24 h) led to vegetative hyphal swelling and a decrease in hyphal viability through cell lysis. The time-dependent killing of F901318 was further confirmed by measuring fungal biomass and growth rate in liquid culture. Compared to the untreated control, the ability of hyphal growth to recover in drug-free medium after 24 h exposure to F901318 was strongly impaired. A longer treatment of 48 h further improved the antifungal effect of F901318. Together, the results of this study indicate that F901318 initially has a fungistatic effect on *A. fumigatus* by inhibiting germination and growth, but prolonged exposure is fungicidal through hyphal swelling followed by cell lysis.

3.2 Introduction

F901318 is a new class of antifungal drug that acts through a novel mechanism and is currently in Phase I clinical development. It is highly active against all pathogenic *Aspergillus* species, with a low minimal inhibitory concentration (MIC) of < 0.1 µg/mL (1–3). F901318 is the first drug candidate from the new orotomide class of antifungals. Its cellular target is dihydroorotate dehydrogenase (DHODH), the fourth enzyme in the *de novo* pyrimidine biosynthesis pathway (4). Pyrimidine biosynthesis is vital for many cellular processes, including DNA/RNA synthesis (nucleobases cytosine, thymine and uracil), the cell cycle (DNA), protein synthesis (RNA), cell wall synthesis (via uridine triphosphate (UTP), which forms uridine diphosphate (UDP)-glucose) and phospholipid synthesis (via cytosine triphosphate (CTP)) (5).

The aim of this study was to investigate the antifungal effects of F901318 against the infective conidial form and the invasive hyphal form of *A. fumigatus*. Antifungal compounds are traditionally distinguished as being either fungistatic or fungicidal, the latter being preferred as fungistatic antifungals could allow the pathogen to regrow after cessation of treatment. However, it is not always straightforward to determine whether a compound is fungistatic or fungicidal, particularly for fungi that produce hyphae. The standardized method for *in vitro* antifungal susceptibility testing is the determination of the MIC, the lowest concentration of the antifungal which completely inhibits growth. For filamentous fungi, standardized methods for MICs were first developed for azoles by the European Committee on Antibiotic Susceptibility Testing (EUCAST 9.1) and the Clinical Laboratory Standards Institute (CLSI M38-A). However, these tests do not distinguish between fungistatic and fungicidal compounds, which is why other tests need to be employed to determine this (6). Over the years many methods have been developed to determine the degree of the fungicidal effect of antifungal compounds (reviewed in Pfaller *et al* 2004) (6). A common test is the determination of the minimal fungicidal concentration (MFC) where the clear wells of the MIC test are subcultured and colonies are counted. The lowest concentration with > 99.9% growth reduction is the MFC. More recently, fluorescent viability staining has been used to determine the fungicidal effect of antifungal compounds (7–9).

A further difficulty is that not every antifungal drug can be specifically classed as either fungistatic or fungicidal, as some are fungistatic against one species but fungicidal against another (10). Additionally, this can depend on the developmental stage of the fungus. For filamentous fungi, the MIC and MFC tests are typically carried out using conidia, even though it has been shown antifungals can have a different effect against ungerminated conidia, germinated conidia (germlings) or hyphae ((11), this study). Another factor in determining whether an antifungal compound is fungicidal, is the exposure time. For example, voriconazole was found to be fungistatic when exposed to *A. fumigatus* for 2 h (12). However, fungicidal effects were seen when the exposure time was increased to 24 h (13). Of the antifungal drug classes in clinical use, amphotericin B is usually considered to be a fungicidal drug, whereas azoles and echinocandins are either fungicidal or fungistatic depending on the species. Voriconazole, for example, is fungistatic against *Candida* species but shows fungicidal activity against the *Aspergillus* species (13). The three marketed echinocandins have

been widely considered fungicidal against *Candida* species, but fungistatic against *Aspergillus* species. However, recently it has been shown *in vitro* using high resolution, time-lapse, live-cell imaging that the effects of the echinocandin caspofungin on *A. fumigatus* is more complicated than previously appreciated. This latest study has shown that caspofungin causes hyphal hyperbranching coupled with repeated hyphal tip lysis followed by regenerative intrahyphal growth. This results in very compact colonies which continue to expand slowly. At high caspofungin concentrations after 40 h exposure to the drug, *A. fumigatus* intriguingly undergoes paradoxical growth (reversal of growth inhibition) by some unknown mechanism (14).

In this study, the fungicidal effect of F901318 towards three developmental stages of *A. fumigatus* - conidia, germlings and hyphae - was studied using time-lapse, live-cell imaging and viability staining. Additionally, the biomass and growth rate of F901318-treated hyphae shifted to drug-free medium were assessed to further analyze viability. Together, the results of this investigation have demonstrated that F901318 has a time-dependent killing effect on *A. fumigatus* of which the extent is dependent of the developmental stage to which the drug is exposed.

3.3 Materials and methods

3.3.1 Strain and cultures

Aspergillus fumigatus clinical isolate AF293 was used in this study. Conidia were either incubated in standard Vogel's Minimal Medium (VMM) (15) or Sabouraud (SAB) medium. Inoculum concentration varied from 10^3-10^7 conidia/ml (see relevant section). For microscopy, cultures were grown in VMM at 37 °C in uncoated μ-Slide 8 well chambers (Ibidi).

3.3.2 Antifungal drugs

F901318 was synthesized as previously described (2). Caspofungin, voriconazole and amphotericin B were acquired from Sigma-Aldrich. Stock solutions were prepared in dimethyl sulfoxide (DMSO, Sigma-Aldrich) and diluted to the required concentration in growth media.

3.3.3 Conidial diameter

Freshly harvested conidia were exposed to 0.1 µg/ml F901318 or 0.02% DMSO as a control. After 24, 48, 72, 96 and 120 h exposure, brightfield and differential interference contrast (DIC) images of the treated and untreated conidia were acquired on a Nikon Eclipse TE2000-E widefield microscope, using a 60× water immersion objective. A Hamamatsu Orca-ER C4742-80 camera (Hamamatsu Photonics UK Ltd.) with Metamorph software (Molecular Devices) was used for image acquisition.

3.3.4 Transmission electron microscopy

Conidia (10^7 conidia/ml) and hyphae (10^6 conidia/ml pre-grown for 16 h) were treated with 0.1 µg/ml F901318 for 24 h in VMM at 37 °C. Controls were untreated freshly harvested conidia and 40 h untreated hyphae. Cultures were centrifuged and pellets cryofixed by high pressure freezing in a Leica EM PACT2 (Leica Microsystems, UK) as described previously (16, 17). The pellets were subsequently embedded in Spurr's (epoxy) resin and ultrathin sample sections were stained with lead citrate and uranyl acetate. Samples were examined with a JEM-1400 plus electron microscope and images were captured using AMT Image Capture Engine software.

3.3.5 16 h time lapse, live-cell imaging of growing germ tubes and vegetative hyphae

Germ tubes were obtained by pre-incubating conidia for 8 h and vegetative hyphae were obtained by pre-incubating conidia for 16 h. The inoculum size was 10^5 conidia/ml, except for time-lapses of hyphae, in which case the inoculum size was 10^3 conidia/ml. Germ tubes and hyphae were treated with 0.1 µg/ml F901318 or 0.02 % DMSO (controls).

The 16 h brightfield time-lapse image series were acquired on a Leica SP8X confocal microscope with a 40×/0.85 NA dry objective, using an argon laser for illumination and transmitted light detector. Time lapse imaging was started immediately after the addition of F901318 or DMSO. Z-stacks of 6 images 1 µm apart were acquired every 10 min for 16 h using Leica Application Suite software (LAS-AF).

3.3.6 46 h time lapse imaging of F901318-treated germ tubes

Conidia were pre-incubated for 8 h at 37 °C to obtain germ tubes (germinated conidia) which were treated with 0.1 µg/ml F901318. Brightfield time-lapse, live-cell imaging was performed on a Nikon Eclipse Ti widefield microscope with a 40×/0.6 NA dry objective using a 12-bit QI Cam cooled mono camera (QImaging, Canada) with Image Pro-Plus 7.0 software (Media Cybernetics). The first image in the series was acquired immediately after the addition of F901318 with z-stacks of 6 images 1 µm apart captured every 10 min for 46 h.

3.3.7 Viability staining

Conidia, germlings and hyphae incubated in VMM were treated with 0.1 µg/ml F901318 at 37 °C and their viability assessed after 24, 48, 72, 96 and 120 h exposure with DiBAC (Molecular Probes) dissolved in DMSO and used at a final concentration of 2 µg/ml. Samples were incubated for 5 min at 37 °C prior to imaging.

Images of conidia, germlings and hyphae stained with DiBAC were acquired on a Leica SP8X confocal microscope with a 40×/0.85 NA dry objective using an argon or a white light laser for illumination. Excitation was set to 488 nm, emission was detected over the range of 500-590 nm. For conidia and germlings, the percentage of DiBAC staining was quantified. For hyphae, the area of DiBAC stained hyphae in images was quantified using the FIJI distribution of ImageJ (18) where images were segmented and the area of fluorescence/image was selected and measured.

3.3.8 Post-exposure recovery biomass assay

To obtain hyphae for this assay, 10^6 conidia/ml were grown in VMM for 18 h at 37 °C in flasks shaking at 200 rpm. Hyphae were treated with 0.1 µg/ml F901318, 1.0 µg/ml F901318 or 1 % DMSO for 24 h, after which they were harvested and washed. 0.3 g of wet weight was then transferred into fresh, drug-free VMM and incubated for 48 h, after which the hyphae were dried and their weight determined.

3.3.9 Post-exposure recovery growth rate assay

Hyphae were obtained for this assay by pre-growing 10^4 conidia/ml in SAB for 16 h at 35 °C in 96-well plates. Hyphae were treated with Phosphate Buffered Saline (PBS) or PBS containing 0.1 µg/ml F901318, 0.5 µg/ml caspofungin, 1 µg/ml voriconazole, 4 µg/ml amphotericin B or 1 % DMSO (control). Drug concentrations represented 2×

MIC. Plates were incubated for 24 h or 48 h at 35 °C. Hyphae were washed 3× with PBS Tween and placed in fresh SAB containing 10 µM uridine and 10 µM uracil. Plates were sealed with Breathe-Easy® sealing membrane (Sigma). The OD_{405nm} was determined every 10 min for 24 h.

3.3.10 Statistics

Statistical analyses were performed using GraphPad Prism 7. For the analysis of conidial diameter, a two-way analysis of variance and Bonferroni's multiple comparison tests with 99% confidence intervals were performed. For the post-exposure effect biomass assay, a Student's T-test was performed with 99% confidence intervals. All experiments were performed in triplicate. Bars represent the standard deviation (SD).

3.4 Results

3.4.1 F901318 inhibits germination, but not isotropic growth, of *A. fumigatus* conidia

To analyze the effects of 0.1 µg/ml F901318 on germination, *A. fumigatus* conidia were treated with the drug for up to five days and observed under the microscope every 24 h (Figure 3.1A). Within 24 h, untreated conidia had grown isotropically from an initial diameter of 3 µm to a final diameter of 8.7 µm with 100% germination. The F901318-treated conidia did not germinate, but continued to grow in diameter at a linear rate of ~1.5 µm/day. At day 5, germination was still not observed and the conidial diameter had increased to 10.5 µm. This was significantly larger than the 8.7 µm diameter of the germinated control conidia ($p<0.05$, Figure 3.1B). After exposure to F901318 for 8 days, there had been further isotropic growth of the conidia, without germination (data not shown).

Transmission electron microscopy (TEM) was utilized to determine whether exposure to F901318 had caused changes in their ultrastructure. Sections of freshly-harvested ungerminated conidia and conidia treated for 24 h were studied (Figure 3.1C). Treated conidia were larger than fresh ungerminated conidia, consistent with previous microscopy observations and measurements (Figure 3.1A and 3.1B), and contained highly enlarged vacuoles.

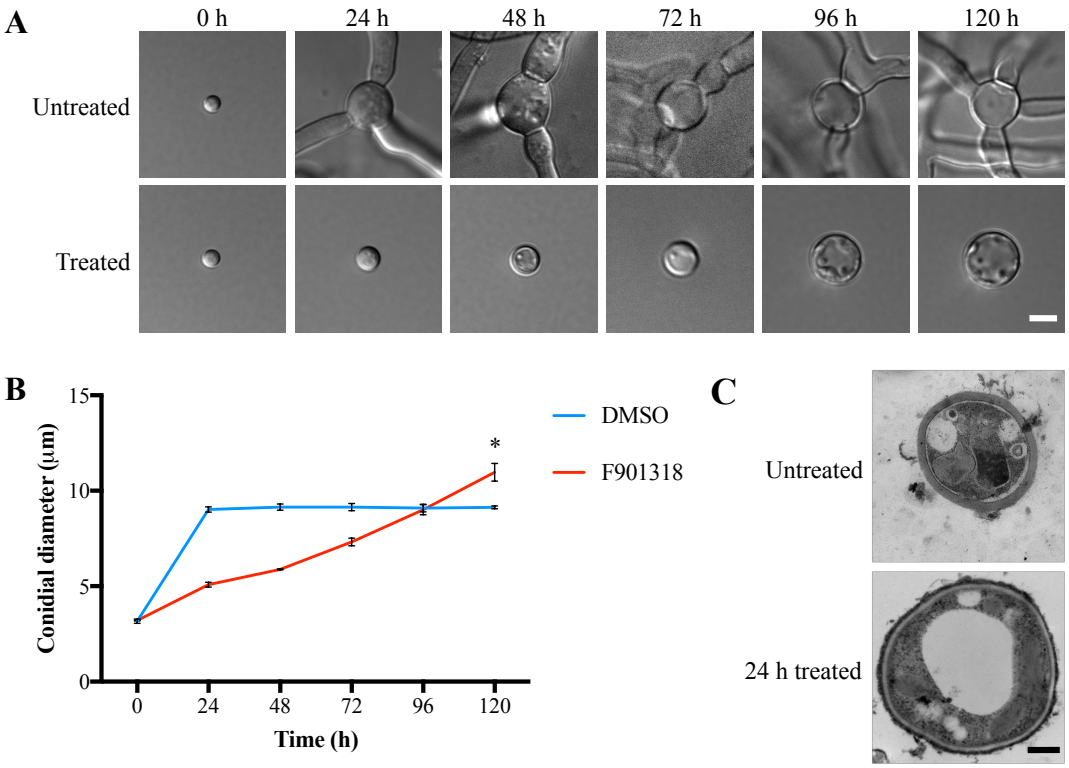

Figure 3.1 Conidia undergo isotropic growth but do not germinate when exposed to 0.1 µg/ml F901318. Conidia were imaged and their diameters measured 24, 48, 72, 96 and 120 h after addition of 0.1 µg/ml F901318. **A)** DIC images of untreated and treated conidia over time. Bar = 5 µm **B)** Conidial diameters of treated versus untreated conidia over time. Error bars represent SD. **C)** TEM images of an untreated conidium and 24 h treated conidium. Bar = 500 nm.

3.4.2 F901318 inhibits polarized hyphal growth

Time-lapse, live-cell imaging was used to study the effects of 0.1 µg/ml F901318 applied for 16 h to germ tubes and more mature vegetative hyphae of *A. fumigatus* (Figure 3.2A and supplementary movies S1-S4). The hyphal elongation rate in both germ tubes and hyphae slowed down after addition of F901318. A slight growth recovery was then observed, although the elongation rate of treated germ tubes was 6-fold slower than untreated germ tubes. For treated more mature vegetative hyphae, this was reduced by 12-fold compared to untreated hyphae. Hyphal elongation ceased completely 10 h addition of F901318 in both growth forms (Figure 3.2B).

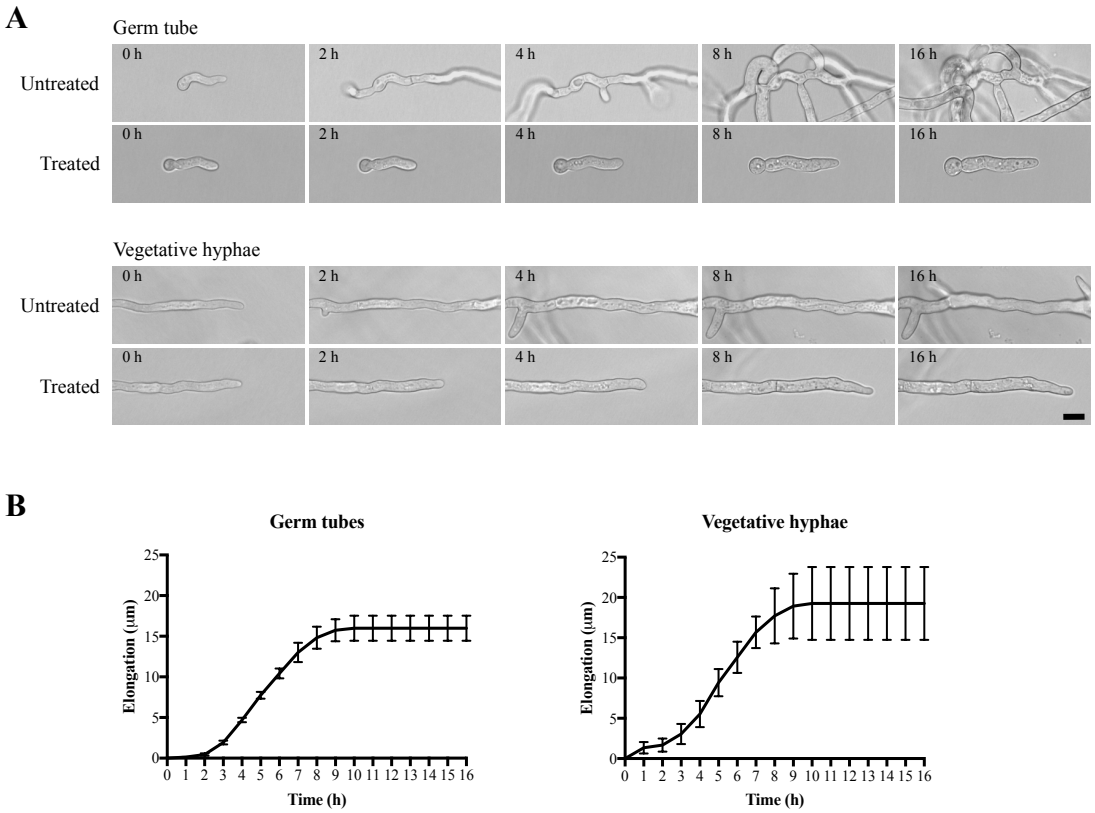

Figure 3.2 F901318 inhibits hyphal elongation in growing germlings and hyphae. 16 h time lapse sequences were captured of germ tubes and vegetative hyphae treated with 0.1 µg/ml F901318. **A)** Representative time points are shown from 16 h time lapse sequences of germ tubes and vegetative hyphae following treatment with F901318. Bar = 10 µm **B)** Hyphal elongation of germ tubes and vegetative hyphae after addition of F901318. Error bars represent SD.

3.4.3 F901318 causes isotropic growth and lysis of *A. fumigatus* hyphae

To investigate the effects of prolonged F901318 exposure, germlings exposed to 0.1 µg/ml F901318 were observed over a period of 46 h under the microscope. The images in Figure 3.3 represent different stages of a representative time lapse sequence (time lapse shown in video S1). In the first 8 h after adding the drug, germ tube width increased from approximately 4.5 µm to a more variable 5-7 µm. After 16 h the first septum had formed and a second formed after 32 h, dividing the germling into three compartments (Figure 3.3, black arrows). In the time lapse sequence shown, one hyphal compartment continued to swell and lysed to release its cellular contents 34 h after the addition of the drug (white arrows). However, lysis of hyphal compartments occurred at various times after the initiation of treatment, with the earliest occurring at 24 h. The occurrence of lysis may indicate significant and localized internal pressures and/or a site of weakening in the cell wall within this hyphal compartment. In Figure 3.3, the apical germling compartment had undergone considerable isotropic growth by

the 46 h time point (outlined arrow). These observations suggest that prolonged F901318 exposure leads to dysregulation of normal polarized growth and cell-wall deposition or cross-linking, accompanied by an inability to maintain cell wall integrity.

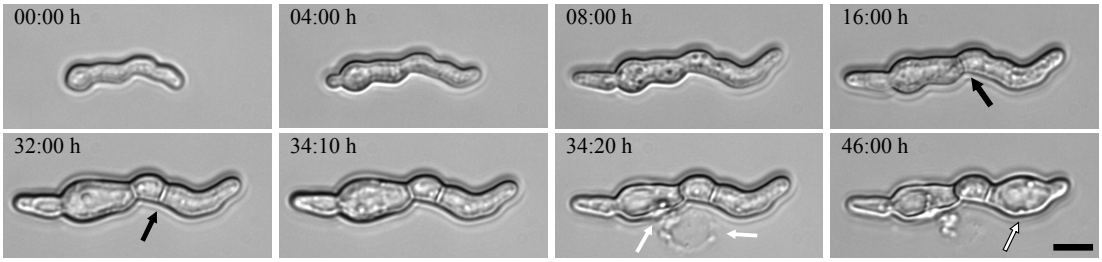

Figure 3.3 F901318 causes hyphal swelling and cell lysis. Representative images at time points of one of the 46 h time lapse sequences of germlings exposed to 0.1 µg/ml F901318. Arrows highlight the formation of two septa (black arrows), a lysed compartment and the consequent release of cellular contents (white arrows) and an apical swollen compartment (white arrow surrounded by black line). Bar = 10 µm.

TEM imaging of hyphae treated with F901318 for 24 h showed hyphal swelling (Figure 3.4A) and highly enlarged vacuoles (Figure 3.4B). Ruptured hyphal compartments lacking significant contents and possessing broken cell walls were evident following cell lysis in drug-treated samples (Figure 3.4C).

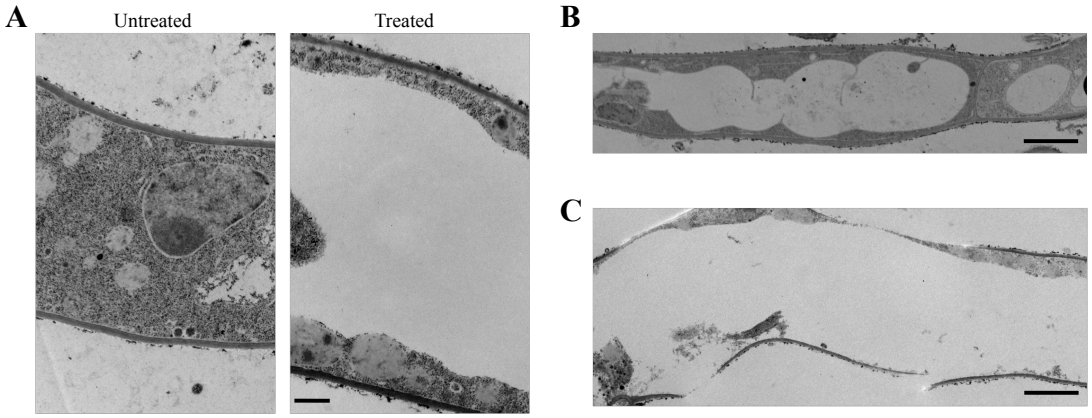

Figure 3.4 A) TEM image of an untreated hypha and a hypha treated for 24 h with 0.1 µg/ml F901318. Images show the increased diameter of the treated hypha. Bar = 0.5 µm. **B)** TEM image showing enlarged vacuoles in a hypha treated for 24 h with 0.1 µg/ml F901318. Bar = 2 µm. **C)** TEM image showing ruptured cell walls in a hypha treated for 24 h with 0.1 µg/ml F901318. Bar = 2 µm.

3.4.4 F901318 kills *A. fumigatus* in a time-dependent manner

As cell lysis was observed with prolonged treatment with 0.1 μg/ml F901318, the viability of *A. fumigatus* after exposure to F901318 was determined by staining with the fluorescent viability dye, DiBAC, which is an oxonol dye. Only dead cells were permeable to DiBAC, in which it binds to intracellular phospholipids to become fluorescent (19). No staining was observed in untreated cells.

Conidia, germlings and hyphae were treated with F901318 for up to 120 h, and their viability was measured every 24 h. Each of these three developmental stages lost their viability, but to varying extents, following treatment with F901318 (Figure 3.5). Germlings and vegetative hyphae were found to be more sensitive to drug treatment than conidia. Reduced viability in germlings and vegetative hyphae was observed after 24 h and in conidia after 48 h. After 120 h, 95% of the germlings were dead, whilst only 9.4% of conidia had lost viability at this stage. Microscopic examination showed that exposure to F901318 caused seemingly random cell lysis of individual apical and subapical compartments within a hypha. Direct quantitation of lysed compartments was difficult to determine, so for this purpose the total area of individual hyphae that exhibited DiBAC fluorescence in an image, was determined. Using this method, it was found that the area of dead hyphal compartments increased 25-fold from 77 μm^2 to 1922 μm^2 between the 24 h and 120 h time points. Together, these results suggest that the disruption of hyphal growth and homeostatic machinery by F901318 cannot be mitigated by *A. fumigatus*; it leads not only to a failure in growth but also to cell death.

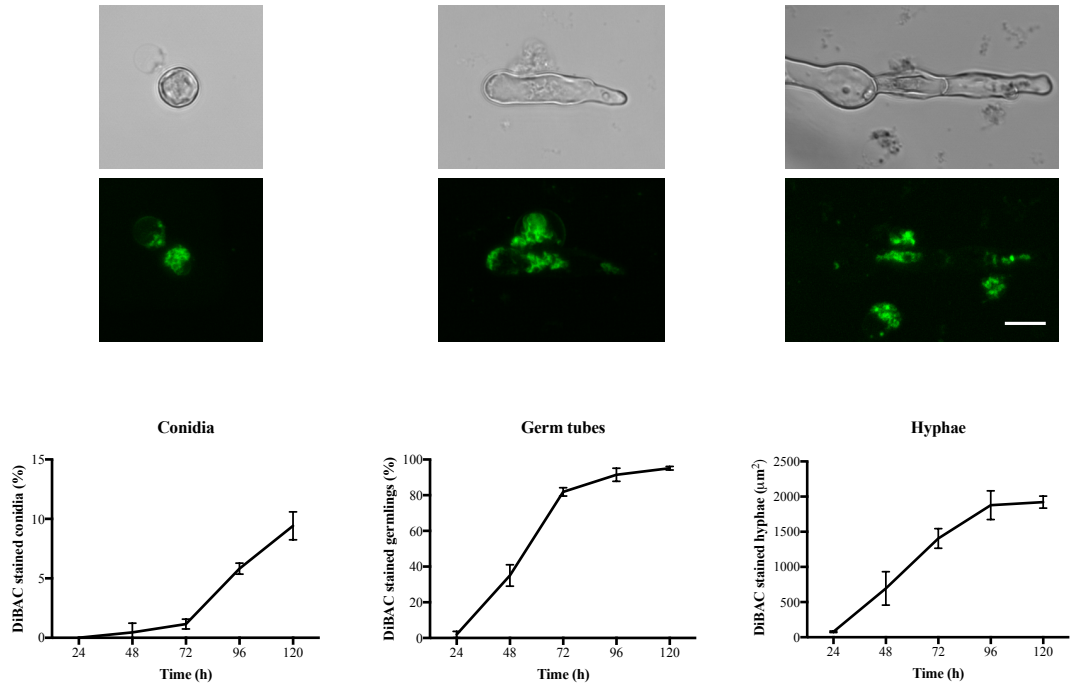

Figure 3.5 F901318 causes time-dependent cell lysis. The viability of conidia, germlings and hyphae treated with F901318 was quantified using DiBAC staining. Images show a representative conidium, germ tube and hypha stained with DiBAC. Histograms show the quantification of DiBAC staining (viability) of conidia, germlings and hyphae treated with F901318 over time. For conidia and germlings the percentage of DiBAC stained conidia and germlings was quantified. For hyphae, the area of DiBAC fluorescence in the images was quantified. Error bars represent SD. Bar = 10 µm.

3.4.5 *A. fumigatus* hyphae recover poorly following F901318 exposure

We next investigated whether the remaining drug-treated hyphal compartments that had not lysed, retained the ability to regrow once exposure to F901318 had ceased. After 24 h of treatment with 0.1 µg/ml or 1 µg/ml F901318, 0.3 g (wet weight) of hyphae were washed and transferred into drug-free growth medium for 48 h and their dry weights ascertained (Figure 3.6A). Regrowth of hyphae exposed to 0.1 µg/ml F901318 was reduced by 82-fold and almost completely inhibited when treated with 1.0 µg/ml F901318. The results suggest that *A. fumigatus* cannot substantially recover from the morphological changes induced by F901318.

3.4.6 Prolonged exposure to F901318 improves its antifungal effect

As staining with DiBAC had shown that longer F901318 treatment leads to a greater decrease in viability, growth recovery of hyphae treated for 24 h and 48 h with 0.1 µg/ml F901318 were compared. These results were compared with the ability of *A. fumigatus* to recover from exposure to other commonly-used antifungal drugs. For this

purpose, hyphae were treated with 0.1 µg/ml F901318, 0.5 µg/ml caspfungin, 1 µg/ml voriconazole or 4 µg/ml amphotericin B as comparators. After treatment for 24 h or 48 h, hyphae were washed to remove drug residues and transferred to SAB medium containing 10 µM uridine and 10 µM uracil (to mimic pyrimidine concentrations in human blood). The OD_{405} was then measured every 10 min for 24 h on a plate reader. As shown previously (20), regrowth following treatment with amphotericin B was almost undetectable, independent of the duration of treatment (Figure 3.6B). After 24 h of treatment, the F901318, caspofungin and voriconazole-treated hyphae, produced 74%, 69% and 89% respectively of the biomass produced by the control (Figure 3.6B, left graph). After 48 h of treatment this was reduced to 24%, 63% and 65% respectively (Figure 3.6B, right graph). These results show that prolonged treatment with these three antifungals leads to an increase of their antifungal effect. Compared to the 24 h treatment, the 48 h treatment led to a 1.06-fold increase in the antifungal effect of caspofungin and a 1.37-fold increase in the antifungal effect of voriconazole. An even stronger effect was observed for the 48 h F901318 treatment, with a 3.09-fold increase of its antifungal effect compared to the 24 h treatment. This result demonstrates that prolonged exposure increased the detrimental effect of F901318 on *A. fumigatus* hyphae, to a greater extent than prolonged exposure of caspofungin and voriconazole did.

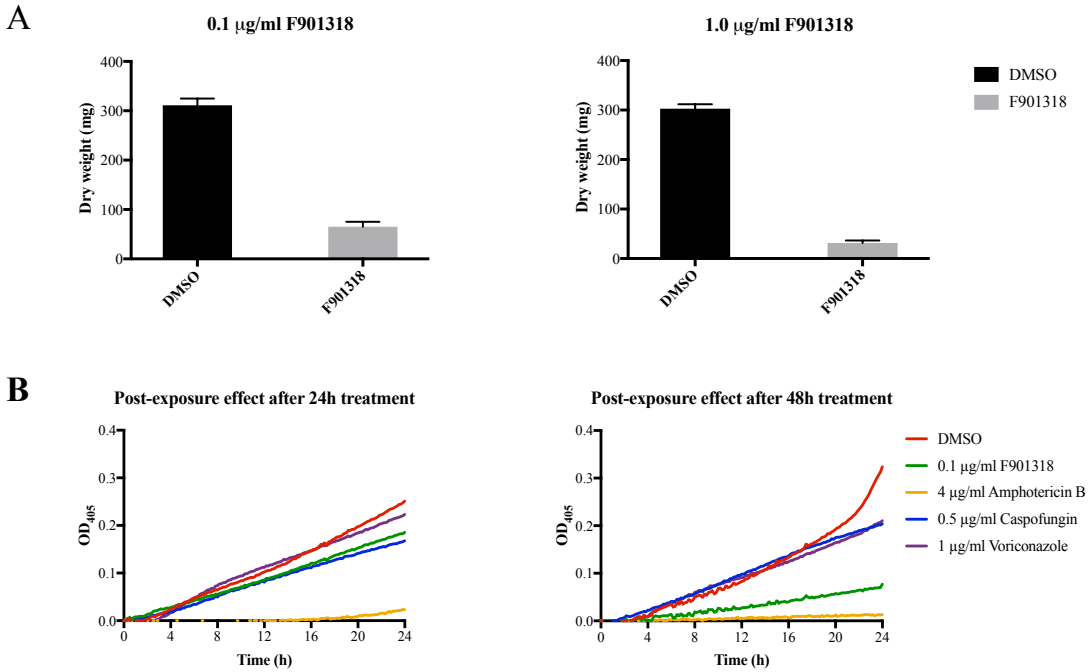

Figure 3.6 Recovery of F901318-treated hyphae in drug-free medium. **A)** Post-exposure recovery biomass assay of hyphae exposed to 0.1 μg/ml or 1.0 μg/ml F901318. Histograms show the reduction in dry weights of mycelia after being shifted to drug-free medium for 48 h. A higher concentration improved the antifungal effect of F901318. Error bars represent SD. **B)** Post-exposure recovery growth rate assay of hyphae treated with F901318, voriconazole, caspofungin and amphotericin B for 24 or 48h before being shifted to drug-free medium. Graphs show the growth recovery, which was measured by reading the OD at 405 nm on a plate reader every 10 min over 24h. Prolonged exposure to F901318 improved its antifungal effect.

3.5 Discussion

In this study, the inhibitory effects of the novel antifungal drug, F901318, on the growth and morphogenesis of different developmental stages (conidia, germ tubes and vegetative hyphae) was studied in the human pathogenic fungus, *Aspergillus fumigatus*. Additionally, the ability of hyphae to recover after treatment was investigated.

Conidia exposed to F901318 were not able to germinate, but they continued to grow isotropically (Figure 3.1). This result is similar to that reported in a previous study by d'Enfert *et al* (21) in which a pyrimidine biosynthesis mutant of *A. fumigatus* (*pyrG*$^{-}$) was observed to swell isotropically, without germinating. This is an important observation because the hyphal morphology is the penetrative form in invasive fungal infections, including invasive aspergillosis (22). Since F901318 also inhibits this pathway, it indicates that pyrimidine synthesis is vital for germination. However, it

also indicates that new synthesis of pyrimidines is not required for conidial isotropic growth, highlighting a possible fundamental difference between this process and hyphal tip growth, which may be associated with the mode of cell wall synthesis.
During germination, several metabolic processes are upregulated to allow conidia to transition from a dormant to an active state which is followed by the emergence of a germ tube and initiation of polarized hyphal growth (23–26). Proliferating cells require active *de novo* pyrimidine biosynthesis to meet the increased demand for pyrimidines for DNA/RNA synthesis, cell cycle regulation, protein synthesis, cell wall synthesis and phospholipid synthesis (27–30). When actively growing germ tubes and vegetative hyphae were exposed to F901318 for more than 10 h, tip growth was inhibited (Figure 3.2). Therefore, in ungerminated conidia, germ tubes and vegetative hyphae of *A. fumigatus*, it seems that polarized hyphal growth cannot be maintained when insufficient pyrimidines are present. *In vivo* infection studies with *A. fumigatus*, demonstrated that F901318 significantly improves survival, which indicated that hyphae cannot scavenge sufficient pyrimidines from the host (2).

Treatment of germ tubes or vegetative hyphae for less than 10 h resulted in a fungistatic effect of hyphal growth arrest. Prolonged exposure to F901318 caused excessive isotropic expansion of conidia in the absence of germination (Figure 3.1), and isotropic growth of individual hyphal compartments (Figure 3.2A), that subsequently underwent cell lysis (Figure 3.3). DiBAC staining demonstrated that extended exposure to F901318 led to a decreased viability of conidia, germlings and vegetative hyphae, indicating a time-dependent killing effect of F901318 (Figure 3.5). The extent of the killing effect was dependent on the developmental stage of *A. fumigatus*. Only 9.4% of conidia were killed after five days, showing that F901318 had mostly a fungistatic effect on these spores. This is in line with our unpublished data of MFC tests, also carried out with conidia, in which F901318 was concluded to have fungistatic effects. As conidia do not germinate in the presence of F901318 (Figure 3.1), there is no active hyphal growth, reducing the need for pyrimidines, allowing the conidia to survive for longer in presence of the drug than actively growing germlings and hyphae. Nevertheless, the isotropic growth of conidia still continued, which is interesting as inhibition of DHODH would be expected to lead to a reduced availability of UDP-sugars, which are essential during hyphal cell wall synthesis. This suggests that there are sufficient stores of pyrimidines to allow this growth, while

insufficient to support germination, or that the UDP-glucose requirements of the conidial cell wall are altered. The inhibition of conidial germination could imply a role for F901318 as a prophylactic drug by preventing conidia from germinating in the lungs of at risk patient populations. The number of DiBAC-stained germlings and hyphae increased more dramatically with time, demonstrating that F901318 has a stronger effect on these developmental stages. It seems likely that germlings and vegetative hyphae have a store of pyrimidines, allowing them to survive until this store is exhausted, after which the effects of pyrimidine starvation from F901318 exposure impact cell viability. This could explain the time-dependent killing effect of F901318 on germ tubes and vegetative hyphae.

The DiBAC staining results showed that only a small decrease in viability was observed 24 h after F901318 exposure. A biomass assay was performed to study whether 24 h treated hyphae could recover from F901318 treatment when placed in drug-free medium. The results show that growth recovery is strongly impaired after treatment with 0.1 µg/ml F901318 and even more so after treatment with 1.0 µg/ml (Figure 3.6A). So, even though the viability was only slightly decreased after treatment for 24 h, the hyphae were not able to fully recover from F901318, suggesting that the antifungal effect of F901318 is mostly irreversible. A post-exposure recovery growth rate assay showed that prolonged F901318 treatment increased the antifungal effect of F901318 (Figure 3.6B). Regrowth of the 48 h F901318-treated hyphae was 3.09-fold reduced when compared to the regrowth of 24 h treated hyphae. In line with the DiBAC staining results, this result again demonstrates that F901318 exposure decreases the viability of *A. fumigatus* in a time-dependent manner.

F901318 causes *A. fumigatus* hyphal compartments to swell, eventually leading to cell lysis. Hyphal swelling was also observed in a study in which *A. nidulans* hyphae were exposed to the DNA synthesis inhibitor hydroxyurea (25), suggesting that swelling could be a direct result of inhibiting DNA synthesis and/or downstream global effects on cell metabolism and regulation. Hyphal swelling and lysis has also been reported in caspofungin-treated *A. fumigatus* hyphae. However, the inhibitory effects of caspofungin cause increased septation, hyphal width and hyperbranching coupled with repeated hyphal tip lysis followed by regenerative intrahyphal growth (14). Interestingly, the continuous presence of caspofungin promotes excessive isotropic

growth of ungerminated conidia and a delay in germination (Moreno-Velasquez and Read, unpubl.). Caspofungin belongs to the echinocandins and drugs in this class inhibit 1,3-ß-glucan synthase, which is required for the formation of β-glucans in the fungal cell wall. One of the products of the pyrimidine synthesis pathway is uridine-5'-triphosphate (UTP), which is required for the formation of UDP-sugars, which are the substrates for the formation of the fungal cell wall polysaccharides chitin and 1,3-ß-glucans (5, 31). Inhibition of pyrimidine synthesis could therefore have downstream effects on the structure of the cell wall, ultimately resulting in cell lysis. Ruptured cell walls were frequently observed under the confocal microscope (Figure 3.5) and in TEM images of F901318 treated conidia (Figure 3.1C) and treated vegetative hyphae (Figure 3.4D). TEM also revealed apparently enlarged vacuoles in treated conidia (Figure 3.1C) and treated vegetative hyphae (Figure 3.4C). Vacuolar size has been linked to the cell cycle in *Candida albicans* (32), so it is possible that the larger vacuoles are a result of cell cycle disruption caused by inhibiting pyrimidine synthesis. It is likely that the formation of these large vacuoles play a role in the swelling that was observed in conidia, germlings and hyphae exposed to F901318 in combination with the isotropic growth that occurs. The vacuolar swelling may be due to an increased osmotic pressure that facilitates the lysis of the cell wall that has become weakened by F901318 treatment due to being starved of UDP-sugar precursors. Further work is required to investigate the effect of F901318 on the relationship between the formation of these large vacuoles, the osmotic homeostasis in the treated cells and the lysis of their cell walls.

The results of this study have demonstrated that although F901318 has a mostly fungistatic effect on conidia, it has more dramatic effects on germ tubes and hyphae. Prolonged exposure to the drug causes hyphal swelling and isotropic growth which leads to cell lysis, releasing cellular contents. It was therefore concluded that F901318 has a time-dependent killing effect against *A. fumigatus*. This study demonstrates that superficial observations of the effects of antifungal compounds do not always provide a straightforward distinction between whether the drug has fungistatic or fungicidal effects. Using classical methods of observation, F901318 would usually be regarded as a fungistatic agent. However, we have shown in this study by using time-lapse imaging that prolonged exposure to F901318 allows conidia to continue undergoing isotropic growth, but inhibits conidial germination whilst resulting in lysis of hyphal

cells. These results indicate that F901318 should be considered as a fungicidal agent against *Aspergillus* species.

3.6 Acknowledgements

We thank our colleagues at F2G Ltd. for their support in this work, as well as the Manchester Fungal Infection Group at the University of Manchester. We would also like to thank Gillian Milne and the Microscopy and Histology core facility at the University of Aberdeen, for their assistance with TEM. We also want to thank John Rex for critical reading of the manuscript. SdP is supported by the European grant Marie Curie ITN FungiBrain PITN-GA-2013-607963.

3.7 Author Contributions

SdP was the primary author, performed the live-cell imaging microscopy, TEM, viability staining and the analysis of the data. NB performed the post-exposure effect assays. MCA assisted with TEM. GEMS designed F901318. ACB, DL, MB, NDR and JDO provided guidance and assistance during this project and in the preparation of this manuscript.

3.8 References

1. Buil JB, Rijs AJMM, Meis JF, Birch M, Law D, Melchers WJG, Verweij PE. 2017. *In vitro* activity of the novel antifungal compound F901318 against difficult-to-treat *Aspergillus* isolates. Journal of Antimicrobial Chemotherapy.
2. Oliver JD, Sibley GEM, Beckmann N, Dobb KS, Slater MJ, McEntee L, du Pré S, Livermore J, Bromley MJ, Wiederhold NP, Hope WW, Kennedy AJ, Law D, Birch M. 2016. F901318 represents a novel class of antifungal drug that inhibits dihydroorotate dehydrogenase. PNAS 113:12809–12814.
3. Hope WW, McEntee L, Livermore J, Whalley S, Johnson A, Farrington N, Kolamunnage-Dona R, Schwartz J, Kennedy A, Law D, Birch M, Rex JH. 2017. Pharmacodynamics of the Orotomides against *Aspergillus fumigatus*: New Opportunities for Treatment of Multidrug-Resistant Fungal Disease. mBio 8:e01157-17.
4. Jones ME. 1980. Pyrimidine Nucleotide Biosynthesis in Animals: Genes, Enzymes, and Regulation of UMP Biosynthesis. Annual Review of Biochemistry 49:253–279.
5. Garavito MF, Narváez-Ortiz HY, Zimmermann BH. 2015. Pyrimidine Metabolism: Dynamic and Versatile Pathways in Pathogens and Cellular Development. Journal of Genetics and Genomics 42:195–205.
6. Pfaller MA, Sheehan DJ, Rex JH. 2004. Determination of fungicidal activities against yeasts and molds: lessons learned from bactericidal testing and the need for standardization. Clinical microbiology reviews 17:268–80.

7. Lass-Flörl C, Nagl M, Speth C, Ulmer H, Dierich MP, Würzner R. 2001. Studies of in vitro activities of voriconazole and itraconazole against *Aspergillus* hyphae using viability staining. Antimicrobial agents and chemotherapy 45:124–8.
8. Bowman JC, Hicks PS, Kurtz MB, Rosen H, Schmatz DM, Liberator PA, Douglas CM. 2002. The antifungal echinocandin caspofungin acetate kills growing cells of *Aspergillus fumigatus* in vitro. Antimicrobial agents and chemotherapy 46:3001–12.
9. Shirazi F, Kontoyiannis DP. 2013. Mitochondrial respiratory pathways inhibition in *Rhizopus oryzae* potentiates activity of posaconazole and itraconazole via apoptosis. PloS one 8:e63393.
10. Lewis II JS, Graybill JR. 2008. Fungicidal versus fungistatic: what's in a word? Expert Opin Pharmaco 9:927–935.
11. Espinel-Ingroff A. 2001. Germinated and nongerminated conidial suspensions for testing of susceptibilities of *Aspergillus* spp. to amphotericin B, itraconazole, posaconazole, ravuconazole, and voriconazole. Antimicrobial agents and chemotherapy 45:605–7.
12. Manavathu EK, Ramesh MS, Baskaran I, Ganesan LT, Chandrasekar PH. 2004. A comparative study of the post-antifungal effect (PAFE) of amphotericin B, triazoles and echinocandins on *Aspergillus fumigatus* and *Candida albicans*. Journal of Antimicrobial Chemotherapy 53:386–389.
13. Manavathu EK, Cutright JL, Chandrasekar PH. 1998. Organism-dependent fungicidal activities of azoles. Antimicrobial agents and chemotherapy 42:3018–21.
14. Moreno-Velásquez SD, Seidel C, Juvvadi PR, Steinbach WJ, Read ND. 2017. Caspofungin-Mediated Growth Inhibition and Paradoxical Growth in *Aspergillus fumigatus* involve Fungicidal Hyphal Tip Lysis Coupled with Regenerative Intrahyphal Growth and Dynamic Changes in β-1,3-Glucan Synthase Localization. Antimicrobial Agents and Chemotherapy AAC.00710-17.
15. Vogel HJ. 1956. A Convenient Growth Medium for *Neurospora crassa*. Microbial Genetics Bulletin 13:42–47.
16. Netea MG, Gow NAR, Munro CA, Bates S, Collins C, Ferwerda G, Hobson RP, Bertram G, Hughes HB, Jansen T, Jacobs L, Buurman ET, Gijzen K, Williams DL, Torensma R, McKinnon A, MacCallum DM, Odds FC, Van der Meer JWM, Brown AJP, Kullberg BJ. 2006. Immune sensing of *Candida albicans* requires cooperative recognition of mannans and glucans by lectin and Toll-like receptors. The Journal of clinical investigation 116:1642–50.
17. Ene I V., Adya AK, Wehmeier S, Brand AC, MacCallum DM, Gow NAR, Brown AJP. 2012. Host carbon sources modulate cell wall architecture, drug resistance and virulence in a fungal pathogen. Cellular Microbiology 14:1319–1335.
18. Schindelin J, Arganda-Carreras I, Frise E, Kaynig V, Longair M, Pietzsch T, Preibisch S, Rueden C, Saalfeld S, Schmid B, Tinevez J-Y, White DJ, Hartenstein V, Eliceiri K, Tomancak P, Cardona A. 2012. Fiji: an open-source platform for biological-image analysis. Nature Methods 9:676–682.
19. Bashford CL, Chance B, Smith JC, Yoshida T. 1979. The behavior of oxonol dyes in phospholipid dispersions. Biophysical journal 25:63–85.
20. Vitale RG, Mouton JW, Afeltra J, Meis JFGM, Verweij PE. 2002. Method for measuring postantifungal effect in *Aspergillus* species. Antimicrobial agents

and chemotherapy 46:1960–5.
21. D'Enfert C, Diaquin M, Delit A, Wuscher N, Debeaupuis JP, Huerre M, Latge JP. 1996. Attenuated virulence of uridine-uracil auxotrophs of *Aspergillus fumigatus*. Infection and immunity 64:4401–5.
22. Brand A. 2012. Hyphal growth in human fungal pathogens and its role in virulence. International journal of microbiology 2012:517529.
23. Lamarre C, Sokol S, Debeaupuis J-P, Henry C, Lacroix C, Glaser P, Coppée J-Y, François J-M, Latgé J-P. 2008. Transcriptomic analysis of the exit from dormancy of *Aspergillus fumigatus* conidia. BMC genomics 9:417.
24. van Leeuwen MR, Krijgsheld P, Bleichrodt R, Menke H, Stam H, Stark J, Wösten HAB, Dijksterhuis J. 2013. Germination of conidia of *Aspergillus niger* is accompanied by major changes in RNA profiles. Studies in mycology 74:59–70.
25. Osherov N, May G. 2000. Conidial germination in *Aspergillus nidulans* requires RAS signaling and protein synthesis. Genetics 155:647–56.
26. Bainbridge BW. 1971. Macromolecular Composition and Nuclear Division During Spore Germination in *Aspergillus nidulans*. Journal of General Microbiology 66:319–325.
27. Sigoillot FD, Berkowski JA, Sigoillot SM, Kotsis DH, Guy HI. 2003. Cell cycle-dependent regulation of pyrimidine biosynthesis. The Journal of biological chemistry 278:3403–9.
28. Quéméneur L, Gerland L-M, Flacher M, Ffrench M, Revillard J-P, Genestier L. 2003. Differential control of cell cycle, proliferation, and survival of primary T lymphocytes by purine and pyrimidine nucleotides. Journal of immunology 170:4986–95.
29. Fairbanks LD, Bofill M, Ruckemann K, Simmonds HA. 1995. Importance of ribonucleotide availability to proliferating T-lymphocytes from healthy humans. Disproportionate expansion of pyrimidine pools and contrasting effects of de novo synthesis inhibitors. The Journal of biological chemistry 270:29682–9.
30. Schröder M, Giermann N, Zrenner R. 2005. Functional analysis of the pyrimidine *de novo* synthesis pathway in solanaceous species. Plant physiology 138:1926–38.
31. Gow NAR, Latge J-P, Munro CA. 2017. The Fungal Cell Wall: Structure, Biosynthesis, and Function. Microbiology Spectrum 5.
32. Veses V, Richards A, Gow NA. 2008. Vacuoles and fungal biology. Current Opinion in Microbiology 11:503–510.

CHAPTER 4

The dynamic influence of F901318 on the morphology of *Aspergillus fumigatus*

Saskia du Pré[a,b], Graham E. M. Sibley[a], Mike Birch[a], Nick D. Read[b] and Jason D. Oliver[a]

F2G Ltd., Manchester, United Kingdom[a];
Manchester Fungal Infection Group, University of Manchester, United Kingdom[b]

4.1 Abstract

The first in class orotomide antifungal F901318 targets the *de novo* pyrimidine biosynthesis pathway by inhibiting dihydroorotate dehydrogenase (DHODH). The pyrimidines uracil, thymine and cytosine are building blocks of DNA and RNA, thus inhibition of their synthesis is likely to have multiple effects, including affecting cell cycle regulation and protein synthesis. Additionally, uridine-5'-triphosphate (UTP) is required for the formation of uridine-diphosphate glucose (UDP-glucose), which is an important precursor for several cell wall components. In this study, the effect of F901318 treatment on *A. fumigatus* hyphae was studied by microscopically investigating intracellular structures. Treatment with F901318 led to increased chitin content in the cell wall, increased septation, enlargement of vacuoles and inhibition of mitosis. Furthermore, a co-localization study of DHODH and MitoTracker Red FM confirmed for the first time that *A. fumigatus* DHODH is localized in the mitochondria. The results of this study show that F901318 treatment affects the morphology of several intracellular structures in *Aspergillus fumigatus*.

4.2 Introduction

Invasive fungal infections are threatening the lives of millions of people each year (1). Although progress has been made, infections of these kind remain difficult to diagnose and treat and mortality remains unacceptably high (2). Only four classes of antifungal drugs are currently available on the market (3). F901318 is a novel antifungal drug belonging to a new class of antifungal drugs, called the orotomides. F901318 inhibits the *de novo* pyrimidine biosynthesis by targeting dihydroorotate dehydrogenase (DHODH) (4).

DHODH catalyzes the fourth step in the pyrimidine biosynthesis pathway: a redox reaction in which dihydroorotate is oxidized to orotate, while the enzyme's flavin mononucleotide (FMN) prosthetic group is reduced to $FMNH_2$ (Figure 4.1) (5–8). $FMNH_2$ is re-oxidized to FMN by a cofactor of which the nature is different depending on the class of DHODH. There are two classes of DHODH recognized, class 1 and class 2, based on subcellular location and the cofactor used to re-oxidize $FMNH_2$. Class 1 DHODHs are cytosolic and are subdivided into class 1A and class 1B. Class 1A DHODHs are homodimeric proteins and use fumarate as cofactor. Class 1B DHODHs are heterotetrameric proteins, dimers of two heterodimers, and use NAD^+

as cofactor. Class 1 DHODHs are found for example in gram positive bacteria and some yeast, with some organisms possessing both class 1A and class 1B DHODHs. Class 2 DHODHs are membrane bound monomeric proteins and use ubiquinone (coenzyme Q (CoQ)) as a cofactor. In eukaryotes, the class 2 DHODH is inserted in the inner mitochondrial membrane, facing the intermembrane space, whereas in some prokaryotes that have a class 2 DHODH, including *Escherichia coli*, the enzyme is bound to the cytosolic membrane.

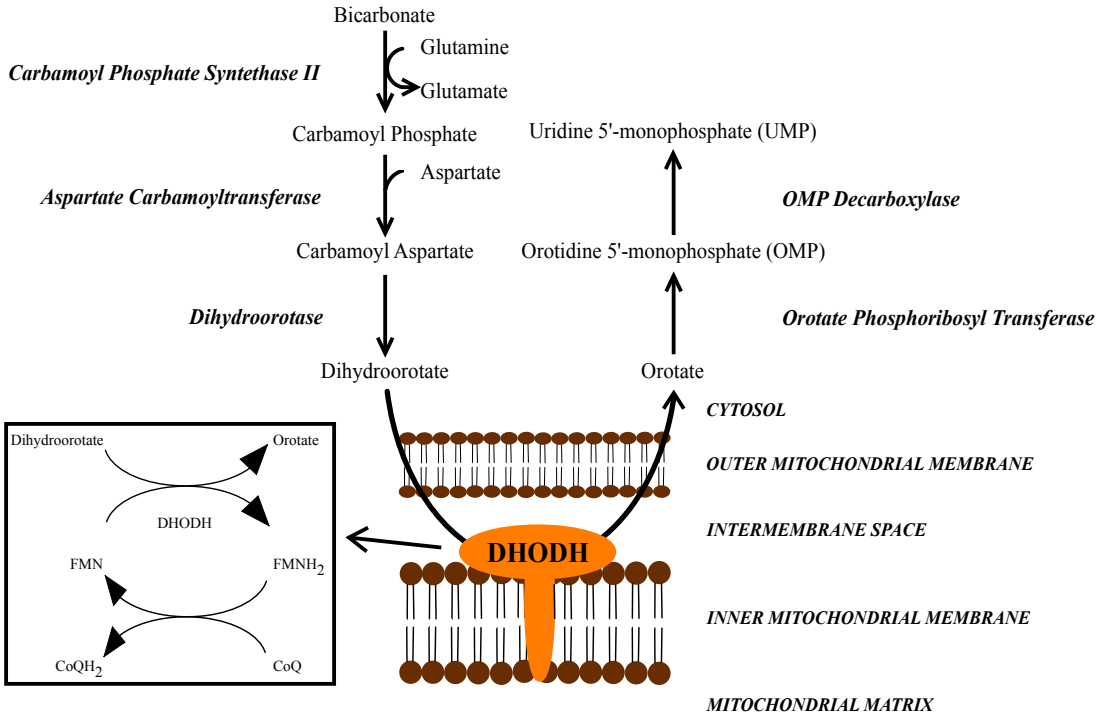

Figure 4.1 The *de novo* pyrimidine biosynthesis pathway. DHODH catalyzes a redox reaction where dihydroorotate is oxidized to orotate, while FMN is reduced to $FMNH_2$, which is then re-oxidized by CoQ (ubiquinone). DHODH = dihydroorotate dehydrogenase.

Although the class of DHODH in *A. fumigatus* has not yet been confirmed, it is likely to be a class 2 DHODH, due to the likely presence of a mitochondrial targeting sequence (MTS) and a transmembrane domain in its sequence. It has been suggested that F901318 inhibits DHODH by blocking the ubiquinone binding site (4). Previous research has shown that although F901318 is initially a static drug, based on accepted MFC assays, prolonged exposure leads to rupture of hyphae and the subsequent killing of *A. fumigatus*. Various morphological changes were observed upon exposing conidia, germ tubes and hyphae to F901318, most notably swelling which leads to cell lysis (chapter 3). As a result of this, ruptured cell walls were frequently observed

during transmission electron microscopy (TEM) and confocal microscopy of treated *A. fumigatus* hyphae.

Inhibiting DHODH and pyrimidine biosynthesis, leads to the inhibition of uridine-5'-monophosphate (UMP) and uridine-5'-triphosphate (UTP), which are important for several processes (Figure 4.2) (6, 7, 9). They are required for the formation of DNA/RNA building blocks uracil (UMP) and cytosine and thymine (UTP). UTP is also required for the formation of UDP-glucose and UDP-N-acetyl-glucosamine, respectively the substrates of 1,3-β-glucan synthase and chitin synthase. The products of these reactions, 1,3-β-glucan and chitin, form the main components in the structure of the fungal cell wall (10). Furthermore, UTP is the precursor for CTP (cytidine triphosphate), which is required for phospholipid synthesis.

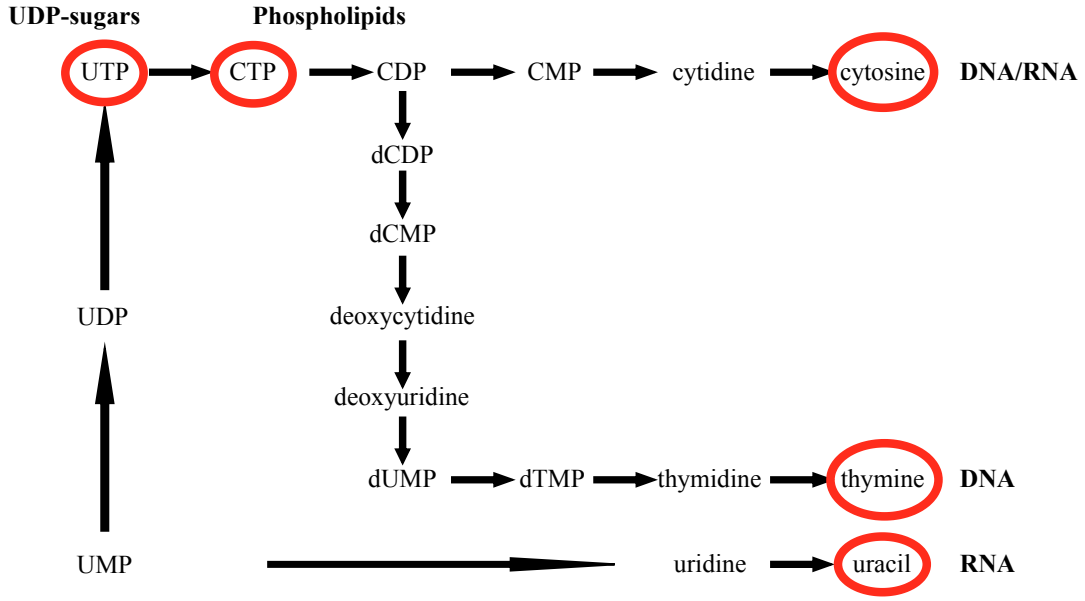

Figure 4.2 Pyrimidines are required for several cellular processes. They are required for cell cycle regulation (DNA), protein synthesis (RNA), cell wall synthesis (UDP-sugars and phospholipids synthesis (CTP). UMP = uridine monophosphate, UDP = uridine diphosphate, UTP = uridine triphosphate, CTP = cytidine triphosphate, CDP = cytidine diphosphate, CMP = cytidine monophosphate, dCDP = deoxycytidine diphosphate, dCMP = deoxycytidine monophosphate, dUMP = deoxyuridine monophosphate, dTMP = deoxythymidine monophosphate.

Uracil, cytosine and thymine are required to maintain the cell cycle (also known as the duplication cycle in filamentous fungi because cells are not actually separating). In the G1 phase, new cellular content is synthesized that is required to accommodate a new round of mitosis. A requirement of this is a significant increase in the availability of pyrimidines (11). Subsequently, the cell size starts to increase and when a threshold

size is reached and sufficient new cell material is present, the cell commits to a new round of mitosis, which was reported to take place synchronously, approximately every 45 min in *A. fumigatus* (12). After mitosis, new septa are usually formed depending on the size of the hyphal compartments.

Vacuoles are important contributors to cell size and vacuole dynamics are believed to play a role in cell cycle regulation (13). In the pathogenic dimorphic yeast *Candida albicans*, mutants in vacuole development were also found to be affected in the hyphal cell cycle (14). For *C. albicans*, it is believed that the volume of the cytoplasm is important for cell cycle progression through G1 (15). Asymmetrical cell division leaves the apical compartment with a larger cytoplasmic volume than the subapical compartments, which contain a larger vacuolar volume. Where the apical compartment continues to grow and divide, the subapical compartments are delayed. Therefore, it seems that the cytoplasm/vacuole ratio is important for cell cycle progression (16).

The aim of this study was to gain a better understanding of the effect of F901318 by investigating the intracellular morphological changes that take place in *A. fumigatus* upon exposure. The localization of DHODH was investigated as well as the cell wall contents of 1,3-β-glucan and chitin, septation, vacuolar volume and the effect on the cell cycle by utilizing a strain in which the nuclei are tagged with GFP (H1-GFP strain). An improved understanding of the intracellular rearrangements caused by F901318 could potentially lead to interesting suggestions for future work.

4.3 Materials and methods

4.3.1 Strains and cultures

Clinical isolate AF293 was used to study the cell wall, septation and the vacuoles. An *A. fumigatus* strain in which histone 1 was labelled with GFP (H1-GFP) was used to study nuclei and mitosis (17). For the purposes of this study, a GFP labelled DHODH strain was constructed under control of a constitutive *gpdA* promoter (PgpdA-DHODH-GFP). To obtain hyphae, 10^3 conidia/ml were pre-incubated for 16 h at 37 °C in Ibidi uncoated 8 well chambers (Thistle Scientific) for microscopy.

4.3.2 Construction of the PgpdA-DHODH-GFP strain

From its sequence, it appears that *A. fumigatus* DHODH has an N-terminal mitochondrial targeting sequence. To avoid interference with the targeting sequence,

DHODH was C-terminally tagged with GFP. The DHODH (*pyrE*) gene was deleted from an *A. fumigatus* KU80 strain and replaced by a hygromycin resistance cassette for selection (strain 11.1.1). A PgpdA-DHODH-GFP construct was created by fusion PCR, based on the method published by Szewczyck *et al* 2006 (18). This construct was then transformed into the DHODH knock-out strain, replacing the hygromycin resistance cassette, to obtain a GFP labelled DHODH strain, in which the native DHODH promoter was replaced by a constitutive *gpdA* promoter to enhance the GFP signal.

4.3.3 Antifungal drugs

F901318 was manufactured as previously described (4). F901318 was dissolved in dimethylsulfoxide (DMSO) at a stock concentration of 0.5 mg/ml and was used at a final concentration of 0.1 μg/ml.

4.3.4 Microscopy dyes

MitoTracker Red FM (Molecular probes) was dissolved in DMSO and used at a final concentration of 500 ng/ml. Aniline blue (Sigma) was dissolved in 50 mM phosphate buffer (pH 8) and used at a final concentration of 25 μg/ml (19). Calcofluor white (CFW, Sigma) was dissolved in water and used at a final concentration of 0.1 μg/ml. Cell tracker blue CMAC (7-amino-4-chloromethylcoumarin, Molecular Probes) was dissolved in DMSO and used at a final concentration of 1 μM. All dyes were added to the *A. fumigatus* cultures for at least 30 min at 37 °C prior to imaging.

4.3.5 Microscopy

All images were taken on Leica confocal SP8X microscope, using LAS AF for acquisition. Images were acquired using either a 40×/0.85 NA dry objective or a 63×/1.2 NA water objective. An argon laser was used for the excitation of the PgpdA-DHODH-GFP strain, the cytoplasmic GFP strain and the H1-GFP strain (excitation at 488 nm, emission at 500-550 nm) and a white light laser was used to excite MitoTracker Red FM (excitation at 581 nm, emission at 595-650 nm). A UV laser was used for the excitation of aniline blue, CFW and CMAC (excitation 405 nm, emission 420-470 nm). The FIJI distribution package of ImageJ was utilized for processing and measurements (20).

4.3.6 Statistics

Statistical analysis was performed in GraphPad Prism 7. Student's t-tests were performed with 99% confidence intervals. All experiments were performed in triplicate. * indicates a significant difference to control, $p<0.01$. Bars represent the standard deviation (SD).

4.4 Results

4.4.1 *A. fumigatus* has a class 2 DHODH located in the mitochondria

It had not been previously confirmed what class of DHODH *A. fumigatus* possesses. As most eukaryotes have a class 2 DHODH bound to the mitochondria, bioinformatics tools Predotar (21), TargetP (22) and MitoFates (23) were utilized to predict whether an N-terminal mitochondrial targeting sequence (MTS) is present in the protein sequence of DHODH (Afu2g11010). All three of these applications predicted that *A. fumigatus* DHODH possesses an MTS, suggesting it is a class 2 DHODH. To confirm that DHODH is localized in the mitochondria, a co-localization study was carried out in which MitoTracker Red FM was used to stain mitochondria in an *A. fumigatus* strain in which DHODH was labelled with GFP under expression of a constitutive *gpdA* promoter. The MitoTracker Red FM and the DHODH-GFP signal showed co-localization patterns consistent with the GFP tagged DHODH being present in the mitochondria (Figure 4.3). This confirms that *A. fumigatus* has a class 2 DHODH, bound to the mitochondria.

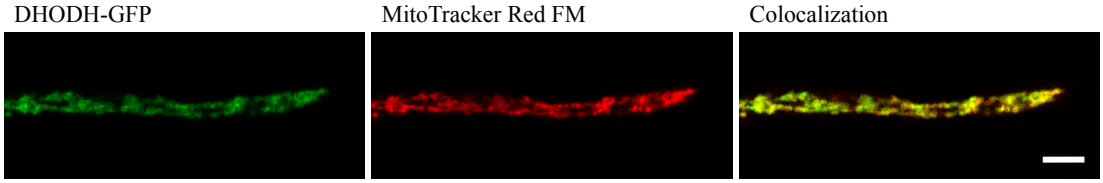

Figure 4.3 Co-localization of a PgpdA-DHODH-GFP strain with MitoTracker Red FM indicates that *A. fumigatus* has a class 2 DHODH that is localized in the mitochondria. Scale bar = 5 µm.

4.4.2 F901318 treatment leads to cell wall remodeling

As pyrimidines are involved in the formation of cell wall components 1,3-ß-glucan and chitin, the cell wall content of these two components was investigated. Aniline blue was used to stain 1,3-ß-glucan and chitin was stained with CFW. Hyphae were obtained by pre-incubating conidia for 16 h, after which they were treated with 0.1

µg/ml F901318. After 24 h, treated and untreated hyphae were stained with aniline blue or CFW and the relative fluorescence intensity of the dyes was measured. The fluorescence intensity represents the amount of 1,3-ß-glucan and chitin in the cell wall. After 24 h of F901318 exposure no significant decrease in overall 1,3-ß-glucan content was observed in the cell wall (Figure 4.4A). However, a significant decrease was observed specifically at the hyphal tips of the treated hyphae, with a 2.24-fold decrease in aniline blue fluorescence (Figure 4.4B). Chitin content was significantly increased, with a 3.75-fold increase in CFW fluorescence after 24 h treatment with F901318 (Figure 4.4C). This result demonstrates that F901318 treatment leads to cell wall remodeling by affecting the 1,3-ß-glucan and chitin content.

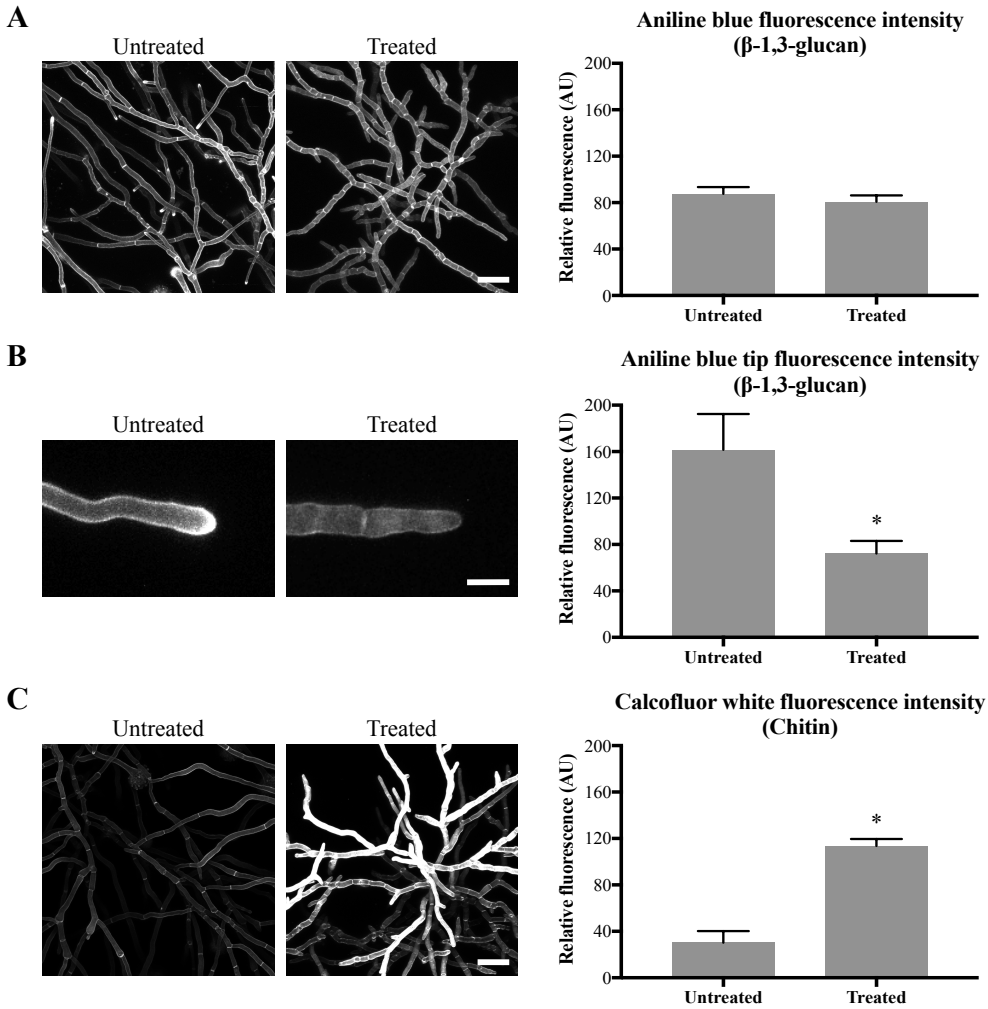

Figure 4.4 F901318 causes cell wall remodeling. Contents of cell wall components 1,3-ß-glucan and chitin were investigated by aniline blue and CFW staining respectively. Error bars represent the SD. A) No difference in overall fluorescence intensity for aniline blue. Scale bar = 40 µm. B) Specific reduction in aniline blue fluorescence intensity at the hyphal tip of treated hyphae. Scale bar = 10 µm. C) Chitin content was increased in the treated hyphae. Scale bar = 40 µm.

4.4.3 F901318 exposure increases hyphal septation

As previously reported (chapter 3), it appeared that additional septa were formed in F901318 treated germ tubes and hyphae. To investigate this further, the interseptal distance was measured in hyphae that were stained with aniline blue and CFW.

In the untreated hyphae, septa were 45 µm apart, whereas in 24 h treated hyphae this distance was 19 µm, which translates to 2.2 septa/100 µm in untreated hyphae and 5.3 septa/100 µm in F901318-treated hyphae, an increase of > 2-fold in the number of septa after drug treatment (Figure 4.5). This result indicates that although F901318 inhibits growth, formation of septa is not inhibited.

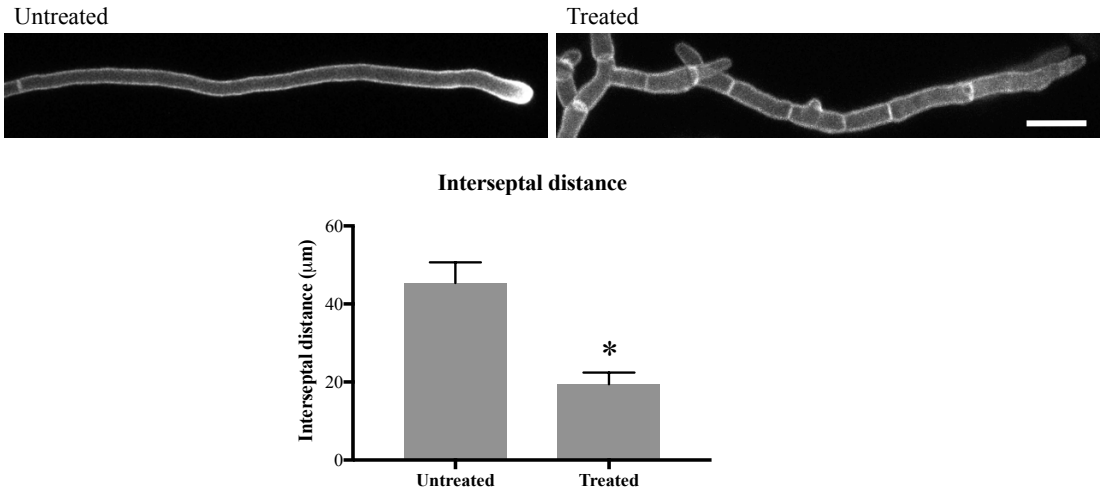

Figure 4.5 Interseptal distance in F901318-treated hyphae vs untreated hyphae. The distance between septa in treated hyphae was decreased, suggesting that although growth is inhibited by F901318, septa formation is not. Scale bar = 20 µm. Error bars represent SD.

4.4.4 Vacuolar volume increases upon F901318 exposure

Exposure to F901318 causes hyphae to significantly increase in size by swelling (chapter 3). Enlarged vacuoles were observed in F901318 treated conidia and hyphae. To further investigate this, vacuoles were stained with CellTracker Blue CMAC in a cytoplasmic GFP strain. The sizes of the cytoplasm and the vacuoles in subapical compartments were measured and a vacuole/cytoplasm ratio was determined.

In the hyphae exposed to F901318 for 24 h, vacuoles took up significantly more volume than the cytoplasm (Figure 4.6). In the untreated hyphae, vacuoles took up 39% of the cytoplasm, in the 24 h treated hyphae, this was nearly 68%. This is a 1.73-fold increase in vacuolar volume in the treated hyphae.

The vacuoles in the treated hyphae appeared to be fused together and form large lobes, whereas in untreated hyphae, various shapes (tubular and round) and sizes of vacuoles were observed. Furthermore, in untreated hyphae there were no vacuoles present in the hyphal tips, whereas in treated hyphae vacuoles took up a significant amount of space in the hyphal tips.

This data demonstrates that F901318 treatment leads to the formation of large vacuoles that take up a significant proportion of the hyphal compartments, decreasing the volume of the cytoplasm.

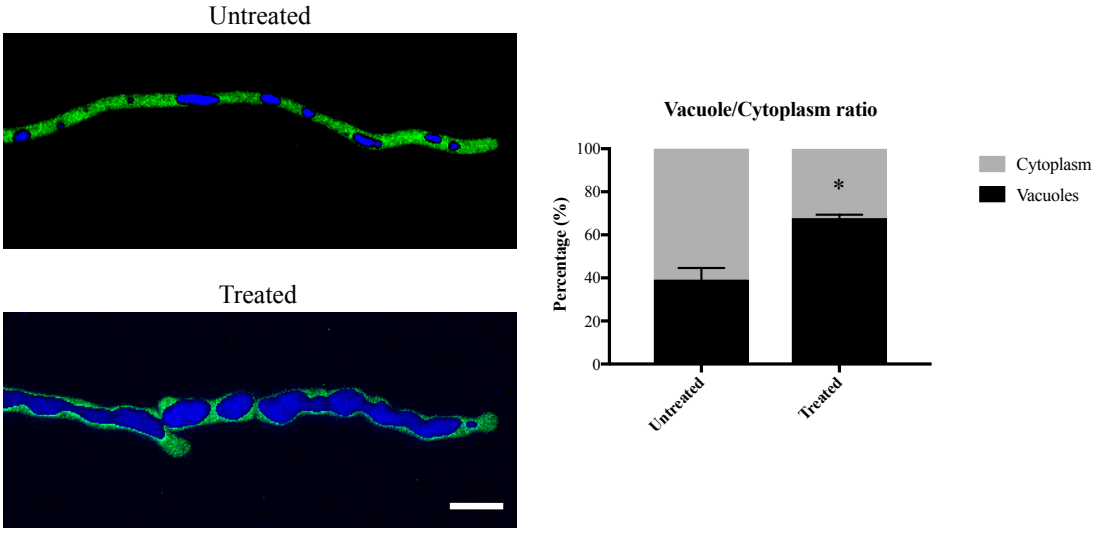

Figure 4.6 Vacuolar volume in untreated and 24 h treated F901318-treated hyphae. Vacuoles in a cytoplasmic-GFP strain were stained with CMAC and the vacuole/cytoplasm ratio was measured. Vacuolar volume was significantly enlarged after exposure to F901318, consequently reducing the volume of the cytoplasm. Scale bar = 10 µm. Error bars represent SD.

4.4.5 Prolonged F901318 exposure leads to inhibition of mitosis

Pyrimidine biosynthesis is important for DNA/RNA synthesis and cell cycle regulation. Therefore, the effect of F901318 on nuclei was studied using an *A. fumigatus* strain in which the nuclei were tagged with GFP (H1-GFP strain). Nuclei were observed over a course of 2 h to observe the effect on nuclear morphology and mitosis after adding F901318.

In the untreated control, nuclei were regularly shaped during interphase and would decrease in size during nuclear division, after which normal size was regained (Figure 4.6A left column, supplementary movie S6). Nuclei moved at a steady rate, which was slightly increased just after mitosis. When F901318 was added, a clear effect was seen on nuclear motility from 15-20 min after addition. The nuclei started to display rapid

movements, but ‘normal’ motility was restored 1-3 h after the drug was added (Figure 4.7A middle column, supplementary movie S7). In hyphae that had been treated for 24 h, nuclei were almost static and mitosis appeared to be inhibited (Figure 4.7A right column, supplementary movie S8).

To investigate whether mitosis was indeed inhibited, the number of nuclei over a distance of 100 µm from the hyphal tip was quantified. As hyphal elongation is inhibited by F901318, the result could be roughly translated to the number of rounds of mitosis that had taken place after the addition of F901318.
Over a distance of 100 µm from the hyphal tip, 8.4 nuclei were counted in the untreated hyphae and 27.3 nuclei in the 24 h treated hyphae (Figure 4.7B). This translates to an average of 1.5 (*i.e.* 1 or 2) rounds of mitosis that had taken place in the 24 h after the addition of F901318. It was previously reported that mitosis normally takes place every 45 min (12), however, under our conditions mitosis took place approximately every 60-75 min in the untreated hyphae. This means that normally over a period of 24 h at least 19 rounds of mitosis should take place.
These results show that over 24 h the number of rounds of mitosis is decreased from 19× to 1-2× in the F901318-treated hyphae. This result indicates that F901318 inhibits mitosis, which possibly suggests that F901318 treatment leads to cell cycle arrest.

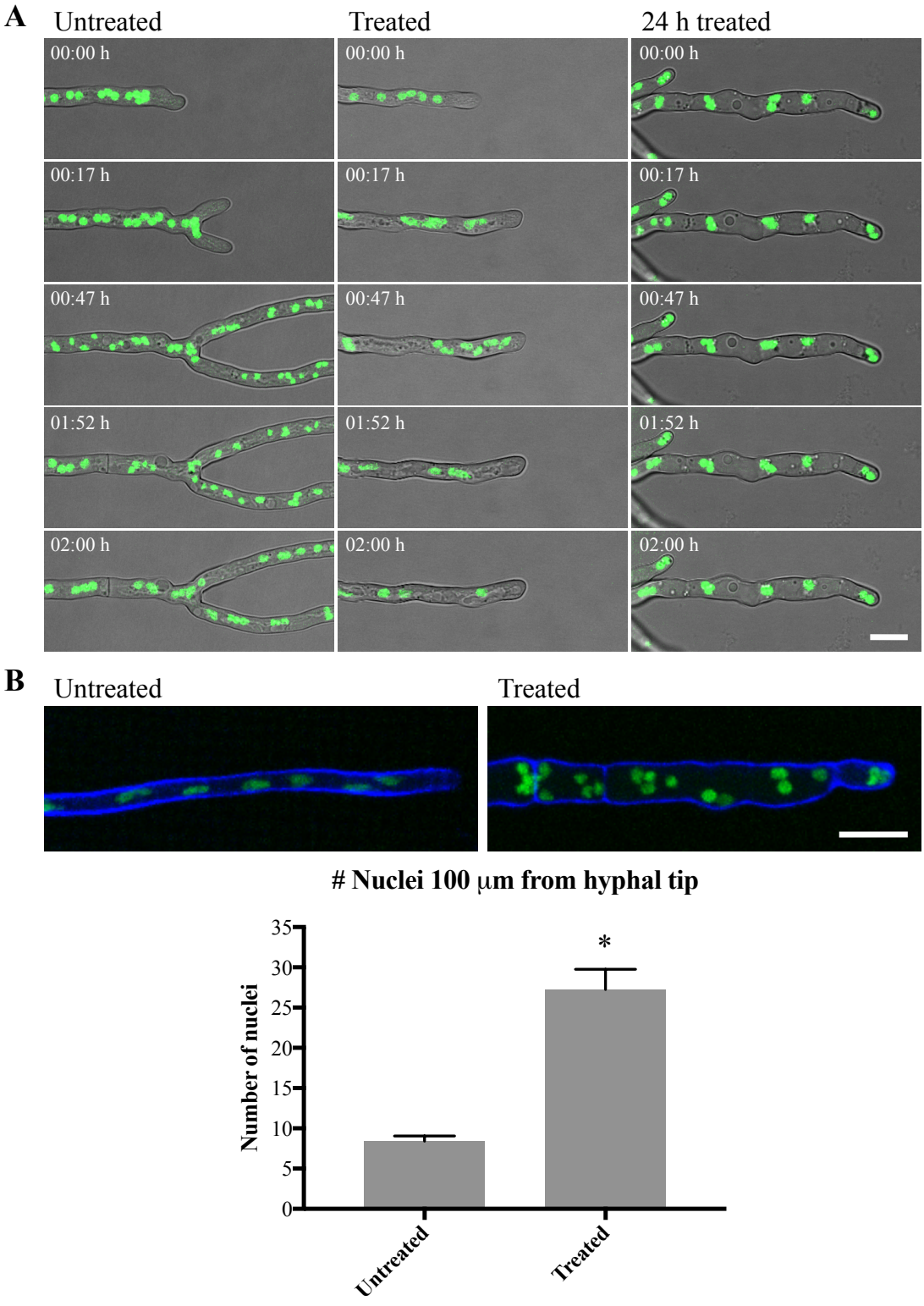

Figure 4.7 Effect of F901318 on nuclear morphology. A) In untreated hyphae, nuclei move at a steady rate, which increased 15-20 min after addition of F901318. In 24 h treated hyphae, nuclear motility was almost static. Scale bar = 10 μm B) Number of nuclei in 100 μm from the hyphal tip. Number of nuclei in the treated hyphae was increased, but as growth was inhibited, this number could be translated to the number of rounds of mitosis. Normally 19 rounds of mitosis should take place over 24 h. In the 24 h after addition of F901318 this was decreased to 1-2×. Scale bar = 10 μm. Error bars represent SD.

4.5 Discussion

In this study, the effect of the novel antifungal drug F901318 on the intracellular structure of the human pathogen *A. fumigatus* was investigated. Although the target of F901318 has been described (4), the downstream consequences for the cell, following exposure, are unknown. Therefore, the effect of F901318 treatment on several structures was investigated by either fluorescently staining or tagging with GFP to be able to microscopically investigate their morphology.

The exact nature of the DHODH class was also unknown. It was presumed that the *A. fumigatus* DHODH was a class 2 type located in the mitochondria and this was supported by bioinformatics tools that predicted a high probability of an MTS being present in the sequence. Co-localization of a PgpdA-DHODH-GFP strain and the mitochondrial dye MitoTracker Red FM confirmed that *A. fumigatus* DHODH is indeed localized in the mitochondria (Figure 4.3), confirming the initial theory of a Class II DHODH. Inhibition of DHODH by F901318 may therefore also have an effect on mitochondrial functioning. The mitochondrial membrane potential is an important measure of proper mitochondrial functioning and it would be interesting to investigate whether it is affected by F901318 exposure.

Pyrimidines are known to be incorporated into the cell wall via the intermediary UDP-glucose (10). In order to investigate the effects of UDP-glucose depletion on the cell wall structure following exposure to F901318, 1,3-ß-glucan and chitin were stained with aniline blue and CFW respectively and the fluorescence intensity was measured (Figure 4.4). No significant difference was found in overall aniline blue fluorescence, but specifically at the hyphal tip, the site of active growth, a significant decrease was found. In active growing hyphae addition of new cell wall material is constantly needed. F901318 inhibits pyrimidine biosynthesis, which presumably leads to a reduction in the availability of UTP. UTP is required for the synthesis of UDP-glucose, the substrate of 1,3-ß-glucan synthase. A decrease in 1,3-ß-glucan synthesis could explain the absence of aniline blue accumulation in the tips of the treated hyphae and possibly inhibition of hyphal growth.

In contrast to 1,3-ß-glucan, chitin content was significantly increased upon exposure to F901318. Potentially this chitin upregulation is a rescue mechanism of the fungus to avoid cell lysis. It does appear to be contradictory as UTP is required for the formation of chitin. Possibly, chitin upregulation is a relatively quick stress response after the addition of F901318 when sufficient pyrimidines are still available or perhaps it is regulated by an alternative cell wall salvage mechanism.
Interestingly, increased chitin content was also previously reported in *A. fumigatus* treated with caspofungin, an echinocandin which targets 1,3-ß-glucan synthase. Other similarities with caspofungin treated hyphae include hyphal swelling and (tip specific) cell lysis. Additionally, increased septation, observed in caspofungin-treated hyphae, was also observed in F901318-treated hyphae (Figure 4.5). Again, this could be a potential stress response, but also, more compartments allow for a better chance of some compartments avoiding cell lysis.

The similarities in morphology between F901318 and caspofungin treated hyphae lead to the interesting question if possibly F901318 and caspofungin can act synergistically and together exert a stronger antifungal effect against *A. fumigatus*. The echinocandins are regarded as fungistatic against *Aspergillus* species, as the hyphae are able to recover to some extent via intrahyphal growth (24, 25). As F901318 inhibits hyphal elongation, intrahyphal growth may be inhibited when both antifungals are combined. Additionally, as both antifungals cause cell lysis, together caspofungin and F901318 may have a faster fungicidal effect. Furthermore, it may also be interesting to combine F901318 with chitin synthase inhibitors such as Nikkomycin Z.

F901318-treated hyphae were found to contain enlarged vacuoles (Figure 4.6). In filamentous fungi, vacuolar appearance is highly dynamic and depends on the state of the fungus. Older hyphal compartments usually contain enlarged vacuoles, while younger compartments contain long tubular vacuoles that play a role in cell signaling and cell biogenesis, hyphal tips usually do not contain any vacuoles. It is believed that in nutrient limited conditions, large vacuoles are formed to decrease the volume of the cytoplasm, which decreases the need for nutrients and protein synthesis (26). Furthermore, compartments containing large vacuoles were previously found to be cell cycle arrested. The cytoplasmic volume is believed to be an important trigger in the G1 start event. As large vacuoles decrease the volume of the cytoplasm, highly

vacuolated compartments are therefore believed to be arrested in G1. When F901318 was added to an H1-GFP strain, nuclear motility became increased for 1-3 h after addition of the drug, before returning to previous levels (Figure 4.7A). In the 24 h after the addition of F901318, only 1 or 2 rounds of mitosis take place and it appears that no further mitosis occurs after 24 h treatment (Figure 4.7B). F901318 blocks the formation of pyrimidines found in DNA and RNA – cytosine, thymine and uridine. It is reasonable to assume that a decrease in the cellular levels of pyrimidines may lead to an inability to replicate the full set of DNA, which blocks the onset of mitosis and possibly causes a cell cycle arrest.

The results of this study have given an insight into the intracellular rearrangements in *A. fumigatus* exposed to F901318. It is clear that pyrimidines are crucial for many cellular processes and not just DNA/RNA. Hence, drugs that interfere with the pyrimidine biosynthesis pathway could potentially be very promising.

4.6 Acknowledgements

From the Manchester Fungal Infection Group, we would like to thank Dr. Mike Bromley for providing us with the pFNO3 plasmid and Dr. Alberto Munoz for providing us with the *A. fumigatus* H1-GFP strain. Furthermore, we would like to thank our colleagues at F2G for their help and support in this project.

4.7 References

1. Brown GD, Denning DW, Gow NAR, Levitz SM, Netea MG, White TC. 2012. Hidden killers: human fungal infections. Sci Transl Med 4:165rv13.
2. Denning DW, Bromley MJ. 2015. How to bolster the antifungal pipeline. Science 347:1414–1416.
3. Campoy S, Adrio JL. 2016. Antifungals. Biochemical Pharmacology.
4. Oliver JD, Sibley GEM, Beckmann N, Dobb KS, Slater MJ, McEntee L, du Pré S, Livermore J, Bromley MJ, Wiederhold NP, Hope WW, Kennedy AJ, Law D, Birch M. 2016. F901318 represents a novel class of antifungal drug that inhibits dihydroorotate dehydrogenase. PNAS 113:12809–12814.
5. Jones ME. 1980. Pyrimidine Nucleotide Biosynthesis in Animals: Genes, Enzymes, and Regulation of UMP Biosynthesis. Annual Review of Biochemistry 49:253–279.
6. Liu S, Neidhardt EA, Grossman TH, Ocain T, Clardy J. 2000. Structures of human dihydroorotate dehydrogenase in complex with antiproliferative agents. Structure 8:25–33.
7. Vyas VK, Ghate M. 2011. Recent developments in the medicinal chemistry and therapeutic potential of dihydroorotate dehydrogenase (DHODH) inhibitors.

Mini reviews in medicinal chemistry 11:1039–55.
8. Munier-Lehmann H, Vidalain P-O, Tangy F, Janin YL. 2013. On Dihydroorotate Dehydrogenases and Their Inhibitors and Uses. Journal of Medicinal Chemistry 56:3148–3167.
9. Garavito MF, Narváez-Ortiz HY, Zimmermann BH. 2015. Pyrimidine Metabolism: Dynamic and Versatile Pathways in Pathogens and Cellular Development. Journal of Genetics and Genomics 42:195–205.
10. Gow NAR, Latge J-P, Munro CA. 2017. The Fungal Cell Wall: Structure, Biosynthesis, and Function. Microbiology Spectrum 5.
11. Fairbanks LD, Bofill M, Ruckemann K, Simmonds HA. 1995. Importance of ribonucleotide availability to proliferating T-lymphocytes from healthy humans. Disproportionate expansion of pyrimidine pools and contrasting effects of de novo synthesis inhibitors. The Journal of biological chemistry 270:29682–9.
12. Momany M, Taylor I. 2000. Landmarks in the early duplication cycles of *Aspergillus fumigatus* and *Aspergillus nidulans*: polarity, germ tube emergence and septation. Microbiology 146:3279–3284.
13. Richards A, Veses V, Gow NAR. 2010. Vacuole dynamics in fungi. Fungal Biology Reviews 24:93–105.
14. Veses V, Richards A, Gow NAR. 2009. Vacuole inheritance regulates cell size and branching frequency of *Candida albicans* hyphae. Molecular microbiology 71:505–19.
15. Gow NAR, Gooday GW. 1982. Vacuolation, Branch Production and Linear Growth of Germ Tubes of *Candida albicans*. Journal of General Microbiology 128:2195–2198.
16. Barelle CJ, Richard ML, Gaillardin C, Gow NAR, Brown AJP. 2006. *Candida albicans* VAC8 is required for vacuolar inheritance and normal hyphal branching. Eukaryotic cell 5:359–67.
17. Muñoz A, Harries E, Contreras-Valenzuela A, Carmona L, Read ND, Marcos JF. 2013. Two functional motifs define the interaction, internalization and toxicity of the cell-penetrating antifungal peptide PAF26 on fungal cells. PloS one 8:e54813.
18. Szewczyk E, Nayak T, Oakley CE, Edgerton H, Xiong Y, Taheri-Talesh N, Osmani SA, Oakley BR. 2006. Fusion PCR and gene targeting in *Aspergillus nidulans*. Nature Protocols 1:3111–3120.
19. Beauvais A, Bruneau JM, Mol PC, Buitrago MJ, Legrand R, Latgé JP. 2001. Glucan synthase complex of *Aspergillus fumigatus*. Journal of bacteriology 183:2273–9.
20. Schindelin J, Arganda-Carreras I, Frise E, Kaynig V, Longair M, Pietzsch T, Preibisch S, Rueden C, Saalfeld S, Schmid B, Tinevez J-Y, White DJ, Hartenstein V, Eliceiri K, Tomancak P, Cardona A. 2012. Fiji: an open-source platform for biological-image analysis. Nature Methods 9:676–682.
21. Small I, Peeters N, Legeai F, Lurin C. 2004. Predotar: A tool for rapidly screening proteomes forN-terminal targeting sequences. PROTEOMICS 4:1581–1590.
22. Emanuelsson O, Nielsen H, Brunak S, von Heijne G. 2000. Predicting Subcellular Localization of Proteins Based on their N-terminal Amino Acid Sequence. Journal of Molecular Biology 300:1005–1016.
23. Fukasawa Y, Tsuji J, Fu S-C, Tomii K, Horton P, Imai K. 2015. MitoFates: improved prediction of mitochondrial targeting sequences and their cleavage

sites. Molecular & cellular proteomics : MCP 14:1113–26.
24. Walker LA, Lee KK, Munro CA, Gow NAR. 2015. Caspofungin Treatment of *Aspergillus fumigatus* Results in ChsG-Dependent Upregulation of Chitin Synthesis and the Formation of Chitin-Rich Microcolonies. Antimicrobial agents and chemotherapy 59:5932–41.
25. Moreno-Velásquez SD, Seidel C, Juvvadi PR, Steinbach WJ, Read ND. 2017. Caspofungin-Mediated Growth Inhibition and Paradoxical Growth in *Aspergillus fumigatus* involve Fungicidal Hyphal Tip Lysis Coupled with Regenerative Intrahyphal Growth and Dynamic Changes in β-1,3-Glucan Synthase Localization. Antimicrobial Agents and Chemotherapy AAC.00710-17.
26. Veses V, Richards A, Gow NA. 2008. Vacuoles and fungal biology. Current Opinion in Microbiology 11:503–510.

CHAPTER 5

Analysis of uptake and intracellular distribution of the orotomide antifungal agent F901318 using a fluorescent analogue

Saskia du Pré[a,b], Graham E. M. Sibley[a], Nicola Beckmann[a], Nick D. Read[b], Mike Birch[a] and Jason D. Oliver[a]

F2G Ltd., Manchester, United Kingdom[a];
Manchester Fungal Infection Group, University of Manchester, United Kingdom[b]

5.1 Abstract

To investigate how novel antifungal drug F901318 is taken up and distributed in *Aspergillus* species, fluorescent analogues were synthesized. F901848 is a F901318 analogue labelled with 7-nitrobenzofurazan that gave a bright fluorescence signal. Although it was not active against *A. fumigatus*, it did demonstrate antifungal activity against *A. flavus, A. terreus* and *A. niger*. An *in vitro* enzyme assay showed that *A. niger* DHODH activity was reduced by F901848, confirming that the fluorescent analogue also targets DHODH. It was also confirmed for *A. flavus* that the pyrimidine biosynthesis pathway is targeted by F901848: in a growth assay, excess uridine and uracil reversed the inhibitory growth effect of F901848. Live-cell, time lapse microscopy of F901848 with *A. flavus* showed that the analogue was taken up by hyphae minutes after addition, with the fluorescence intensity increasing over time, indicating the accumulation of the analogue. F901848 was distributed in the cytoplasm, but accumulated at specific structures, that were identified as the mitochondria, the site of DHODH. Sodium azide treatment did not lead to a delay in uptake of F901848, indicating that the analogue is taken up via an energy-independent transport mechanism such as diffusion. Finally, uptake of F901848 was decreased when hyphae were pre-treated with F901318, but not when hyphae were pre-treated with caspofungin, indicating that F901318 and F901848 compete for the same target site and also possibly that F901318 treatment leads to decreased membrane permeability. The design and synthesis of a fluorescent analogue of F901318 is a useful tool for the investigation of the actions of the new orotomide class of antifungals and particularly useful in studying drug uptake and distribution.

5.2 Introduction

Invasive aspergillosis is a life-threatening disease which is difficult to diagnose and treat (1). Only a limited number of antifungal agents are available to treat this disease and the development of antifungals acting on novel targets is difficult (2, 3). F901318 is a novel drug, from the brand new antifungal class, the orotomides, that is in clinical development for invasive aspergillosis. It targets dihydroorotate dehydrogenase (DHODH) in the pyrimidine biosynthesis pathway (4). Recently, studies have employed the use of fluorescently labelled antifungals to assist in understanding how antifungals are taken up and where they localize. Antifungal peptide PAF26 was

fluorescently labelled and used to study its uptake and localization (5). It was found that the peptide is taken up via active transport and either localizes to the vacuoles until cell death is induced, when it is transported in the cytoplasm (low concentration) or it localizes in the cytoplasm and then in the other organelles when cell death is induced (high concentration). Another example is a fluorophore-conjugated posaconazole, which was used to study its localization in both epithelial cells and *A. fumigatus* (6). The fluorescent posaconazole was found to localize in epithelial cells and was transferred into *A. fumigatus* upon membrane contact. It concentrated within cell membranes, especially the endoplasmic reticulum (ER), where it co-localized with its target CYP51a. Finally, a fluorescently labelled version of caspofungin was suggested to have potential as a diagnostic tool for invasive fungal infections, as it fluorescently stained *Candida* and *Aspergillus*, but not bacteria, showing its specificity (7).

The mechanisms of drug import are not known for every antifungal. In *Candida albicans* it has been found that flucytosine is transported by facilitated diffusion, using membrane transport proteins called permeases (8). It has been suggested that azoles are also imported via facilitated diffusion in a number of pathogenic fungi (9, 10).
In this study, various fluorescent analogues of F901318 were synthesized and the susceptibility of *Aspergillus* species to these analogues was tested. The most promising fluorescent analogue was utilized to study its uptake and intracellular localization in the *Aspergillus* species. The results demonstrate the advantage of a fluorescent drug analogue as a tool to study antifungal drugs *in vitro*.

5.3 Materials and methods

5.3.1 Culture conditions

Strains of *A. fumigatus* (AF293) *A. flavus*, *A. terreus* and *A. niger* were tested for their susceptibility to F901318 and the fluorescent analogues. For the growth assays of *A. fumigatus* and *A. flavus* with F901318 and F901848, 10^3 conidia were spotted onto the centre of the agar and incubated for 48 h at 37 °C on petri dishes containing Vogel's Minimal Medium (VMM). Medium was supplemented with 10 mM uridine and 10 mM uracil when indicated (VMMUU). *A. flavus* was utilized for microscopy with

F901848. Hyphae were obtained by pre-incubating 10^3 conidia/ml in VMM for 16 h at 37 °C in uncoated Ibidi 8-well chambers.

5.3.2 Antifungal compounds

F901318 was synthesized as previously described. F902465, F902459, F901848 and F901821 were labelled with 7-nitrobenzofurazan (NBD). F902430 was labelled with 6-Dimethylamino-naphtalene. Compounds were dissolved in dimethylsulfoxide (DMSO) to a stock concentration of 5 mg/ml. For microscopy, F901848 was dissolved in DMSO at a stock concentration of 2 mg/ml and used at a final concentration of 0.8 µg/ml. For the pre-treatments, F901318 was used at a final concentration of 0.1 µg/ml. Caspofungin was dissolved in water at a stock concentration of 25 µg/ml and used at a final concentration of 0.5 µg/ml.

5.3.3 Fluorescence spectra

The fluorescence spectra of the F901318 analogues were determined in black 96-well plates (Nunc) on a fluorimetric plate reader (Tecan Safire) at a concentration of 1.95 µg/ml. Both the excitation and emission wavelength ranges were set at 230 nm to 850 nm with 10 nm steps to give an extensive scan of the fluorescence spectrum of each compound.

5.3.4 Minimal inhibitory concentration (MIC)

The MICs of the fluorescent analogues against *Aspergillus* species was determined according to a standard method by the Clinical & Laboratory Standards Institute (CLSI). Conidia were inoculated in RPMI-1640 medium and exposed to the compounds at concentrations ranging from 0.05 to 50 µg/ml. The MIC was determined as the lowest drug concentration that prevented growth after 48 h incubation at 35 °C.

5.3.5 Protein isolation

A. fumigatus DHODH was prepared as described in Oliver *et al* (4). *A. niger* DHODH was prepared in a similar fashion. The DHODH cDNA was cloned into a pET-44 vector (pET-44 Ek/LIC vector kit, Novagen), which adds a soluble Nus-tag and two His-tags to the protein and then transformed into *E. coli* NovaBlue GigaSingles (Novagen). The plasmid was sequenced to confirm the cloning had worked and no

mutations had been introduced by PCR. The pET-44 vector, containing the *A. niger* DHODH, was transformed into *E. coli* Bl21 DE3 for protein expression, and grown in LB media plus 100 µM FMN, 1% glucose and 100 µg/ml ampicillin at 37 °C until the OD600 reached approximately 0.5 when expression was induced by addition of 0.5 mM IPTG and incubation at 20 °C overnight. Protein was extracted using Bugbuster protein extraction reagent (Novagen), and the soluble fraction obtained after centrifugation at 16000 g, 20 min, 4 °C was then transferred to Ni-NTA His-bind resin (Novagen) for an hour with mixing on ice. The His-bind resin was transferred to a column, washed with 50 mM Na phosphate pH 8, 500 mM Na Cl, 20 mM imidazole 0.1% (w/v) Tween 20 and eluted with the same buffer except with the addition of 250 mM imidazole. A PD-10 column (GE healthcare) was used to exchange the buffer to DHODH assay buffer (50 mM Tris pH 8, 150 mM KCl, 10% (w/v) glycerol, 0.1% (w/v) Triton X100. Protein was stored at -80 °C.

5.3.6 DHODH enzyme assays

The redox indicator dye 2,6-dichloroindophenol (DCIP) was used as an artificial electron acceptor to follow the DHODH-catalyzed oxidation of dihydroorotate to orotate. The reaction contained 1 mM DHO, 0.05 mM coenzyme Q2 and 0.1 mM DCIP in assay buffer. After addition of recombinant DHODH, DCIP reduction was followed by measuring the decrease in absorbance at 600 nm in clear 96-well microplates (Nunc) on a spectrophotometric plate reader (Tecan Safire). To measure the IC_{50} of F901848 against DHODH a range of drug concentrations were added to the assay wells and the decrease in activity plotted using XL-fit (IDBS), to calculate the concentration of drug giving 50% inhibition of DHODH.

5.3.7 Pre-treatments and staining

To study the effect on F901848 uptake in energy-depleted conditions, hyphae were pre-treated with sodium azide (NaN_3), an ATP synthesis inhibitor. The inhibitor was dissolved in water to a stock concentration of 0.3 M and used at a final concentration of 3 mM. The hyphae were incubated for 15 min with sodium azide, after which either F901848 or FM4-64 was added. FM4-64 (N-(3-triethylammoniumpropyl)-4-(6-(4-(diethylamino) phenyl) hexatrienyl) pyridinium dibromide, Molecular Probes) is a styryl dye with excitation/emission maxima of 515/640 nm and was used at a final

concentration of 5 μM. MitoTracker Red FM was dissolved in DMSO and used at a final concentration of 500 nM. The excitation/emission was set to 581/595-650 nm.

5.3.8 Microscopy

The fluorescent analogue was imaged on a Leica SP8X confocal microscope with a 63×/1.2 NA water immersion objective, using an argon laser for illumination. Images were acquired with Leica Application Suite Advanced Fluorescence (LAS AF) software at 37 °C. For F901848 the excitation was set to 488 nm and the emission was detected over a range of 500-550 nm. The FIJI distribution of ImageJ was used for image processing and measurements (11).

5.3.9 Statistics

Statistical analysis was performed in GraphPad Prism 7. One-way ANOVA was performed with multiple comparisons. Tests were performed with 95% confidence intervals. All experiments were performed in triplicate. * indicates a significant difference to control, $p<0.05$. Bars represent the standard deviation (SD).

5.4 Results

5.4.1 Fluorescent analogues F901848 and F901821 exhibit fluorescence

As F901318 has no intrinsic fluorescence, it was decided to try and design new compounds that were fluorescent for utilization as a tool to study uptake and distribution of the orotomide antifungals. Five analogues for F901318 were synthesized; F902465, F902459, F902430, F901848 and F901821.

To study whether the compounds exhibited any fluorescence, their relative fluorescence was measured on a plate reader. Figure 5.1 displays the structures and fluorescence spectra of F901318 (top left) and the five fluorescent analogues. As mentioned before, F901318 did not exhibit any fluorescence. F902430, labelled with 6-dimethylamino-naphtalene, exhibited slight fluorescence and had an excitation/emission peak of 360/490 nm, as was consistent with the fluorophore's spectral properties. The other four compounds were labelled with NBD, but only F901848 and F901821 exhibited fluorescence, with an excitation/emission peak of 490/550 nm, consistent with NBD's spectral properties. The structures of F902465 and F902459 contain a ring between the fluorophore and the orotomide, whereas F901848

and F901821 do not. Possibly, the ring in the structures of F902465 and F902459 decreases the flexibility of the compound and interferes with the fluorophores' spectral properties. In the structures of F901848 and F901821 this ring is replaced by a linear linker, which possibly increases the flexibility of the compounds and thereby facilitates their spectral properties.

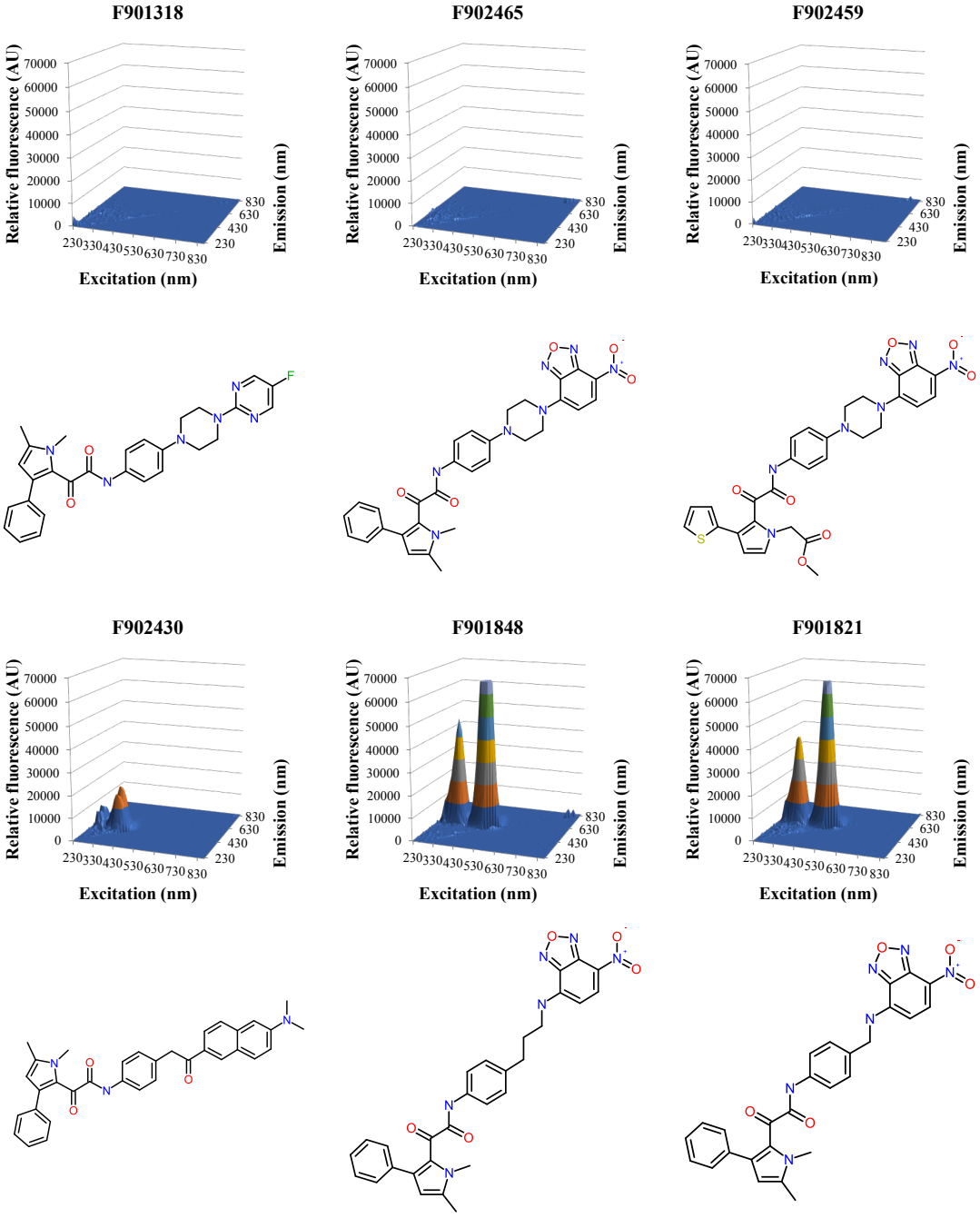

Figure 5.1 Fluorescence spectra and structures of F901318 and five analogues.

5.4.2 F901848 is active against *A. niger* and *A. flavus*

To assess the susceptibility of various *Aspergillus* species to the F901318 analogues, the minimal inhibitory concentrations (MICs) were determined (Table 5.1).

Table 5.1 Minimal Inhibitory Concentrations (µg/ml)

Compound	*A. niger*	*A. fumigatus*	*A. terreus*	*A. flavus*
F901318	0.015 – 0.06	0.008 – 0.06	0.004 – 0.03	0.015 – 0.06
F902465	>50	>50	>50	>50
F902459	>50	>50	>50	>50
F902430	>50	>50	>50	>50
F901848	0.8	>50	6.3	0.8
F901821	>50	>50	>50	>50

None of the compounds showed significant antifungal activity against *A. fumigatus*. F901848 was the only compound that showed some activity against *A. terreus*, but especially against *A. niger* and *A. flavus* with a sub 1.0 µg/ml MIC. It is likely that the addition of a fluorophore changes the SAR (structure-activity relationship) in such a way that the analogues cannot fit in their binding sites as efficiently as the original compound, explaining the absence of potent antifungal activity of most of the analogues. Of the five analogues, only F901848 and F901821 exhibited fluorescence. F901848 contains a longer linker between the fluorophore and the orotomide and this possibly creates a more flexible compound, which improves its SAR.

The inhibitory activity of F901848 against DHODH was further tested by setting up *in vitro* enzyme assays using recombinant DHODH protein from *A. fumigatus* and *A. niger*. The half maximal inhibitory concentration (IC_{50}) was determined for F901318 and F901848 (Table 5.2).

Table 5.2 IC_{50} of F901318 and F901848 against DHODH from *A. fumigatus* and *A. niger* (nM)

	F901318	**F901848**
A. fumigatus	44	1042
A. niger	30	37

The results show that the IC_{50} of F901848 against *A. niger* DHODH was similar to F901318, showing that this analogue inhibits DHODH activity. Interestingly, the IC_{50} of F901318 and F901848 against *A. niger* DHODH was similar, but the MIC of F901848 was higher than the extremely potent F901318, although it still had very good potency compared to other antifungals. This possibly indicates that although the fluorescent analogue efficiently binds its DHODH binding site, it is either being taken up less well by *A. niger* or is transported less efficiently across the mitochondrial membranes (DHODH is located on the inner mitochondrial membrane). Taken together the results show that F901848 exhibited fluorescence and had good activity against *A. niger* and *A. flavus*.

5.4.3 F901848 targets the pyrimidine biosynthesis pathway in *A. flavus*

To further confirm that F901848 is active against *A. flavus* and that it targets the pyrimidine biosynthesis pathway, a growth assay was performed (Figure 5.2). Both *A. flavus* and *A. fumigatus* were not able to grow in presence of F901318. As expected from the MIC results (Table 5.1), growth was observed for *A. fumigatus* in presence of F901848, although growth was slightly deteriorated at a higher concentration of 1.0 µg/ml F901848. *A. flavus* grew slightly in presence of 0.1 µg/ml F901848, but at 1.0 µg/ml growth was hardly visible. When 10 mM uridine and 10 mM uracil (UU) was added to the media, growth was restored for *A. flavus* and *A. fumigatus* in presence of F901318 and F901848. Exogenous addition of high concentrations of the pyrimidines uridine and uracil reverses the effect of pyrimidine biosynthesis inhibition. Therefore, this result indicates that, like F901318, F901848 inhibits the pyrimidine biosynthesis pathway in *A. flavus*.

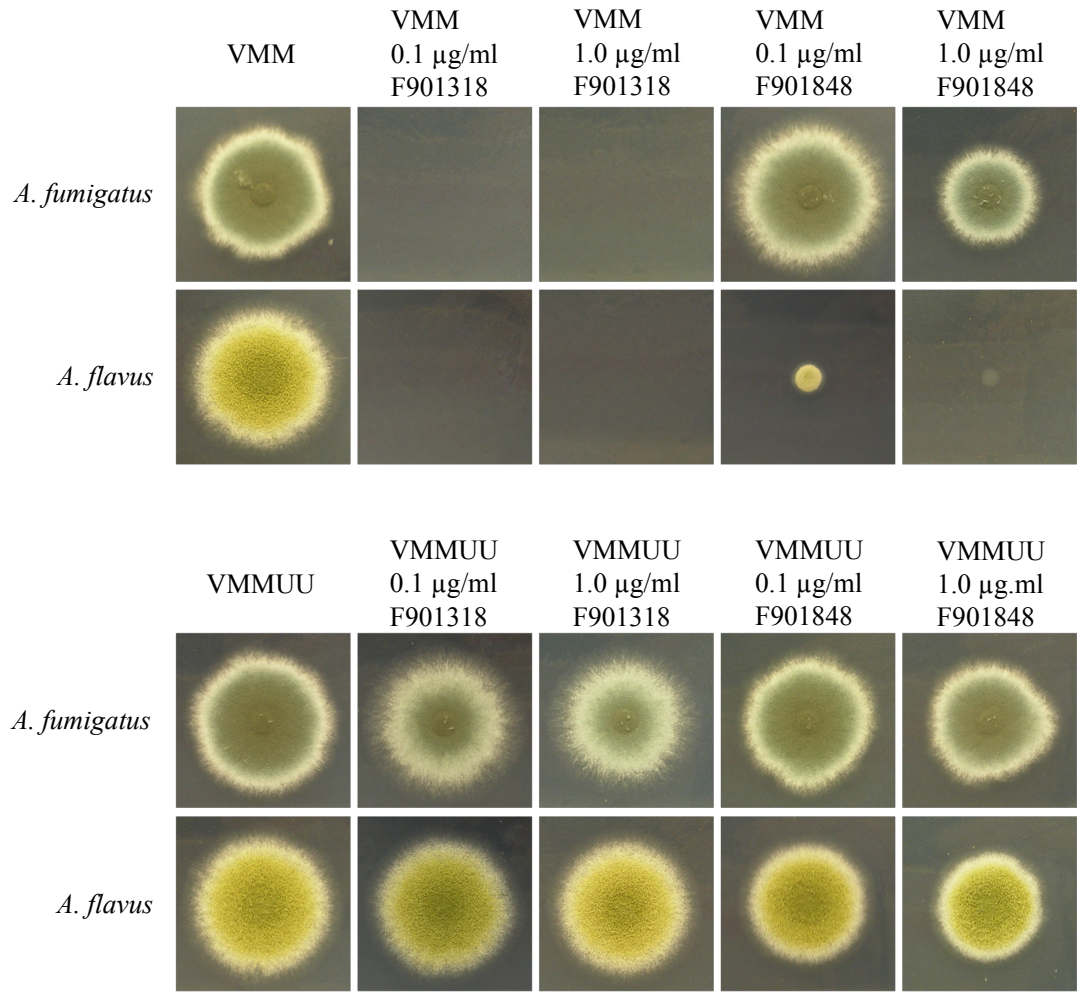

Figure 5.2 Growth assay of *A. fumigatus* and *A. flavus* in presence of F901318 or F901848. Growth of *A. flavus* was abolished in presence of F901848, but could be restored by the addition of uridine and uracil (VMMUU), indicating that F901848 inhibits the pyrimidine biosynthesis pathway in *A. flavus*. VMM = Vogel's minimal medium, VMMUU = VMM containing uridine and uracil.

5.4.4 F901848 is taken up at a linear rate

To investigate the uptake of F901848 by *A. flavus*, the fluorescent analogue was added to hyphae, after which a 1 h time lapse, taking images every 2 min, was initiated to monitor the uptake at 37 °C. Low levels of fluorescence were observed first, but the intensity increased over time (Figure 5.3A, supplementary movie S9). The F901848 fluorescence intensity accumulated over time at a linear rate for approximately 40 min after addition, after which increase ceased (Figure 5.3B). This result indicates that F901848 uptake progresses linearly at 37 °C, with maximum uptake achieved after approximately 40 min.

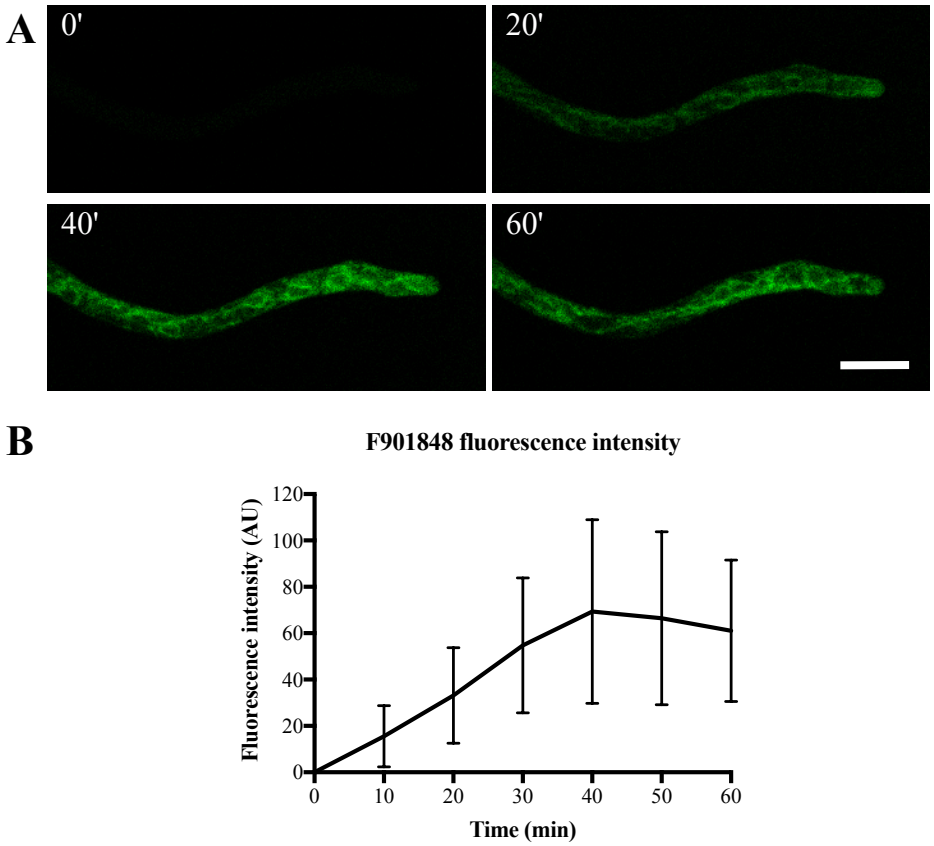

Figure 5.3 F901848 uptake in *A. flavus*. Fluorescence intensity was monitored over time, which revealed that uptake took place at a linear rate, achieving maximum uptake after approximately 40 min. Bar = 10 µm. Error bars represent SD.

5.4.5 F901848 accumulates in the mitochondria

As can be seen in Figure 5.3, F901848 was distributed throughout the cytoplasm, but over time accumulations at specific structures were evident. As DHODH is localized in the mitochondria, it was investigated whether the sites of these F901848 accumulations were the mitochondria. A co-localization study was carried out with MitoTracker Red FM and F901848, 30 min after its addition, which showed that the accumulations indeed co-localized with the mitochondrial dye. This result indicates that although the fluorescent analogue spreads throughout the cytoplasm, it accumulates at the site of target DHODH (Figure 5.4).

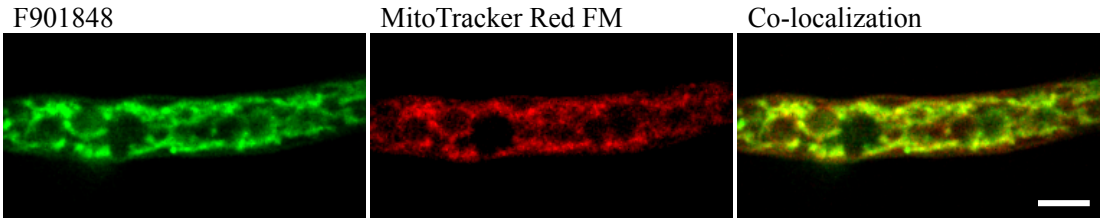

Figure 5.4 Co-localization of F901848 and MitoTracker Red FM. Although the fluorescent analogue spreads throughout the cytoplasm, it accumulates in the mitochondria. Bar = 5 µm.

5.4.6 F901848 is taken up by an ATP-independent process

To investigate the transport mechanism via which F901848 is taken up by *A. flavus*, hyphae were treated with sodium azide for 15 min prior to the addition of F901848. As a control, the membrane dye FM4-64 was utilized, which is taken up via endocytosis, a form of active transport. F901848 uptake was not inhibited in hyphae pre-treated with sodium azide, whereas uptake of FM4-64 was (Figure 5.5A). The fluorescence intensity of F901848 was measured 15 min after addition and this showed that it was increased in the sodium azide pre-treated hyphae (Figure 5.5B). These results indicate that F901848 is not being taken up via an energy driven transport mechanism and that sodium azide pre-treatment enhances F901848 uptake.

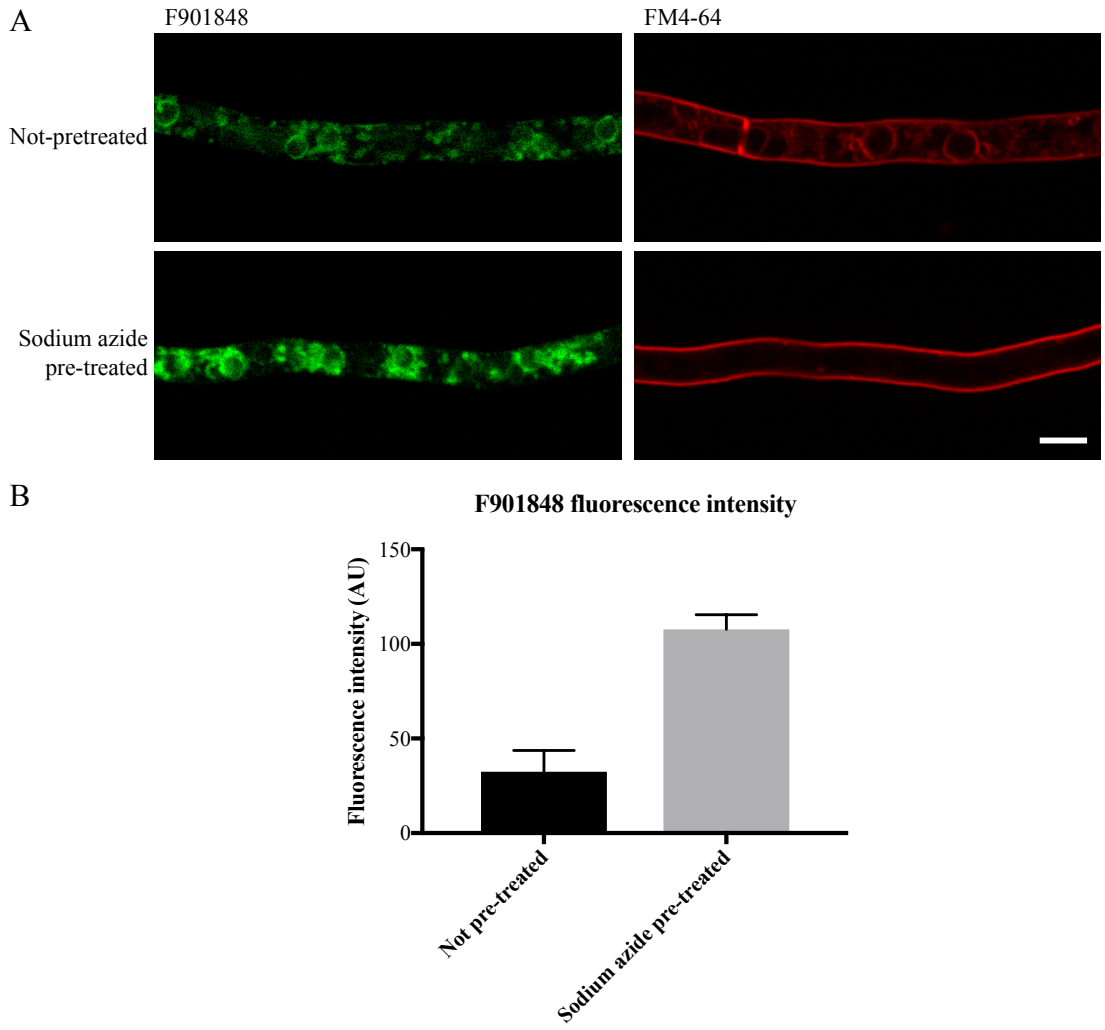

Figure 5.5 Uptake of F901848 when ATP-synthesis is inhibited by sodium azide. Pre-treatment with sodium azide did not lead to decreased F901848 uptake, whereas uptake of FM4-64 was inhibited. This result suggests that F901848 is not being taken up by an energy-driven transport mechanism. Bar = 5 µm. Error bars represent SD.

5.4.7 F901318 pre-treatment decreases F901848 uptake

To investigate whether F901318 treatment affects uptake of F901848, *A. flavus* hyphae were pre-treated for 2 or 24 h with 0.1 µg/ml F901318. F901848 was then added and the fluorescence intensity was measured after 15 min. Caspofungin was used as a control as it has a similar effect on morphology as F901318, such as hyphal swelling, increased chitin content and increased septation, even though it has a different target (1,3-ß-glucan synthase). Hyphae pre-treated with F901318 showed a decreased F901848 fluorescence intensity, compared to uptake of hyphae that were not pre-treated (Figure 5.6). F901848 fluorescence intensity was significantly decreased in hyphae that were pre-treated with F901318 for 24 h. F901848 fluorescence intensity was not decreased in caspofungin pre-treated hyphae, in fact it was slightly increased

(Figure 5.6). Increasing the pre-treatment to 24 h even further increased F901848 fluorescence intensity. These results suggest that F901318 occupying the DHODH binding site prevents the accumulation of F901848 at the same binding site. Possibly, F901318 treatment also leads to decreased membrane permeability, thereby also preventing F901848 uptake.

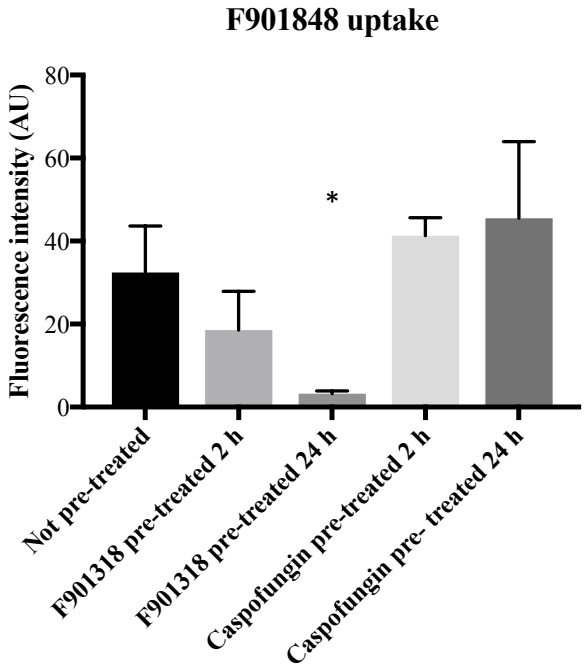

Figure 5.6 Fluorescence intensity of F901848 after pre-treatment with F901318 and caspofungin. F901318 pre-treatment leads to a reduced F901848 fluorescence intensity, whereas it is slightly increased in caspofungin pre-treated hyphae. This possibly indicates competition between F901318 and F901848 for the DHODH binding site and possibly that F901318 treatment leads to inhibition of transport. Error bars represent SD, n = 10.

5.5 Discussion

In this study, a fluorescent analogue of the novel antifungal drug F901318 was utilized as a tool to study uptake and cellular localization in the *Aspergillus* species. Five analogues were synthesized, of which the most promising, F901848, was labelled with NBD-CL, a small green fluorophore, which was previously shown to be a good label for PAF26 (12) (Figure 5.1). Although F901848 was not active against all of the *Aspergillus* species, it showed potent activity against *A. niger* and *A. flavus* (Table 5.1). An *in vitro* enzyme assay where the activity of F901848 against recombinant *A. niger* DHODH protein was tested showed that the analogue inhibits DHODH activity (Table 5.2). It was also confirmed for *A. flavus* that F901848 targets the pyrimidine

biosynthesis pathway by a growth assay in which uridine and uracil were shown to reverse the effect of F901848 (Figure 5.2). *A. flavus* was utilized to investigate the uptake and localization of F901848.

Interestingly, although the MIC of F901848 against *A. niger* was higher than the MIC of F901318, the IC_{50} was similar for both compounds. This possibly indicates that the fluorescent analogue has a similar level of activity against DHODH, but it is either being taken up less well by *A. niger*, or it is less efficiently transported across the mitochondrial membranes to the site of DHODH. Another possibility is that the analogue is being pumped out.

Table 5.1 shows that the MICs of the fluorescent analogues were significantly different compared to the MIC of F901318. It is reasonable to assume that the addition of a fluorophore will affect the uptake of such compounds and their SAR. Additionally, the fluorophores themselves might also display a degree of antifungal activity against the *Aspergillus* species. Therefore, to investigate this, MICs should be carried out with the fluorophores alone as well.

To investigate the uptake of F901848 into *A. flavus* hyphae, the fluorescence intensity was monitored over an hour after addition of the analogue. The fluorescence intensity increased at a linear rate, with maximum uptake detected after approximately 40 min, after which the fluorescence intensity would no longer increase (Figure 5.3). A slight decrease was measured, but this was not significant and is possibly because the fluorescence was not equally distributed in the hyphae, affecting the measurement and explaining the large error bars. Although the analogue appeared to spread throughout the cytoplasm, from approximately 15 min after addition accumulations at specific sites started to become evident. As the target DHODH is located in the mitochondria, a co-localization study of F901848 and the mitochondrial dye MitoTracker Red FM was carried out (Figure 5.4). The accumulations of F901848 indeed showed co-localization with MitoTracker Red FM, indicating that F901848 spreads throughout the cytoplasm and accumulates at the site of its target DHODH. To make sure the accumulation of fluorescence in the mitochondria is not due to the conjugated fluorophore, uptake of the fluorophore NBD-CL alone in *A. flavus* needs to be studied and a co-localization study with MitoTracker Red FM should be carried out.

To investigate the transport mechanism via which F901848 is taken up the *A. flavus* hyphae, ATP synthesis inhibitor sodium azide was utilized. Hyphae were treated with 3 mM sodium azide prior to addition of F901848 (13, 14). This treatment did not decrease F901848 fluorescence intensity, instead it was 3-fold increased (Figure 5.5). The styryl dye FM4-64 was used as a control as it is taken up via endocytosis, a form of active transport. Indeed, in sodium azide pre-treated hyphae, no fluorescence was visible inside the hyphae 15 min after addition of FM4-64, whereas in hyphae that had not been pre-treated, the membranes of the vacuoles were stained (Figure 5.5A). These results strongly suggest that F901848 is not being taken up via an energy driven process, it is more likely that is taken up via diffusion. More work is needed to analyze via what form of diffusion F901848 is being taken up. Possibly it is a form of ATP-independent facilitated diffusion, as was found before for azole import in *A. fumigatus* and has been suggested to be a conserved mechanism across fungal species (10).

Interestingly, as mentioned, sodium azide pre-treatment seemed to increase the uptake of F901848. Only one study was found where cell-to-cell diffusion was increased in staminal hairs of *Setcreasea purpurea* after azide treatment (15). The authors suggested that molecules that normally cannot pass the membrane, can pass under stress conditions due to enlarged pores. Possibly, azide treatment in fungi increases membrane permeability, allowing more compounds to enter the hyphae.

To study whether F901318 affects F901848 uptake, F901848 was added to hyphae that had been pre-treated with F901318 or caspofungin, which was used a control as it has a similar effect as F901318, such as hyphal swelling, increased septation and increased chitin content (chapter 4). When F901848 was added to hyphae that had been pre-treated with F901318, the fluorescence intensity was decreased, but not in hyphae that were pre-treated with caspofungin (Figure 5.6). This result possibly indicates the competition between F901848 and F901318 for binding the same target, DHODH, with F901318 occupying the DHODH site, F901848 cannot accumulate leading to a reduced fluorescence intensity. As caspofungin has a different target, 1,3-ß-glucan synthase, no decrease in F901848 fluorescence intensity was observed as it is not competing for the same binding site. This was also found before in studies with fluorescent caspofungin and posaconazole, where pre-treatment with the original compounds prevented the accumulation of the fluorescently tagged analogues (6, 7).

The decreased uptake of F901848 after F901318 pre-treatment may also suggest that that F901318 treatment leads to decreased membrane permeability. F901318 targets pyrimidine biosynthesis and pyrimidines play important roles in various processes such as DNA/RNA synthesis, cell wall synthesis, but also lipid synthesis. It may be that F901318 treatment leads rearrangements in the membrane structure, thereby decreasing its permeability, which leads to a decrease in uptake. As the F901848 fluorescence intensity wasn't decreased in caspofungin-treated hyphae, it is unlikely that the decreased uptake of F901848 in F901318 pre-treated hyphae is due to the increased chitin in the cell wall, as caspofungin also causes increased chitin synthesis. Interestingly, the fluorescence intensity of F901848 was slightly increased in caspofungin-treated hyphae compared to hyphae that were not pre-treated, although this difference was not statistically significant (Figure 5.6). This could be a result of caspofungin affecting the cell wall and possibly increasing membrane permeability, allowing for F901848 to be taken up more quickly. This is consistent with findings in a previous study, where rhodamine-123 was utilized to measure uptake and an increased fluorescence intensity was found in caspofungin-treated hyphae (16).

Taken together, the results with the fluorescent analogue of F901318, F901848 show that such a tool is very useful to study the distribution and uptake of antifungal drugs.

5.6 References

1. Brown GD, Denning DW, Gow NAR, Levitz SM, Netea MG, White TC. 2012. Hidden killers: human fungal infections. Sci Transl Med 4:165rv13.
2. Denning DW, Bromley MJ. 2015. How to bolster the antifungal pipeline. Science 347:1414–1416.
3. Campoy S, Adrio JL. 2016. Antifungals. Biochemical Pharmacology.
4. Oliver JD, Sibley GEM, Beckmann N, Dobb KS, Slater MJ, McEntee L, du Pré S, Livermore J, Bromley MJ, Wiederhold NP, Hope WW, Kennedy AJ, Law D, Birch M. 2016. F901318 represents a novel class of antifungal drug that inhibits dihydroorotate dehydrogenase. PNAS 113:12809–12814.
5. Muñoz A, Marcos JF, Read ND. 2012. Concentration-dependent mechanisms of cell penetration and killing by the de novo designed antifungal hexapeptide PAF26. Molecular Microbiology 85:89–106.
6. Campoli P, Perlin DS, Kristof AS, White TC, Filler SG, Sheppard DC. 2013. Pharmacokinetics of posaconazole within epithelial cells and fungi: insights into potential mechanisms of action during treatment and prophylaxis. The Journal of infectious diseases 208:1717–28.
7. Pratt A, Garcia-Effron G, Zhao Y, Park S, Mustaev A, Pillai S, Perlin DS. 2013. Evaluation of fungal-specific fluorescent labeled echinocandin probes as

diagnostic adjuncts. Medical Mycology 51:103–107.
8. Hope WW, Tabernero L, Denning DW, Anderson MJ. 2004. Molecular mechanisms of primary resistance to flucytosine in *Candida albicans*. Antimicrobial agents and chemotherapy 48:4377–86.
9. Mansfield BE, Oltean HN, Oliver BG, Hoot SJ, Leyde SE, Hedstrom L, White TC. 2010. Azole drugs are imported by facilitated diffusion in *Candida albicans* and other pathogenic fungi. PLoS pathogens 6:e1001126.
10. Esquivel BD, Smith AR, Zavrel M, White TC. 2015. Azole Drug Import into the Pathogenic Fungus *Aspergillus fumigatus*. Antimicrobial Agents and Chemotherapy 59:3390–3398.
11. Schindelin J, Arganda-Carreras I, Frise E, Kaynig V, Longair M, Pietzsch T, Preibisch S, Rueden C, Saalfeld S, Schmid B, Tinevez J-Y, White DJ, Hartenstein V, Eliceiri K, Tomancak P, Cardona A. 2012. Fiji: an open-source platform for biological-image analysis. Nature Methods 9:676–682.
12. Zhao C, Fernandez A, Avlonitis N, Vande Velde G, Bradley M, Read ND, Vendrell M. 2016. Searching for the Optimal Fluorophore to Label Antimicrobial Peptides. ACS Combinatorial Science 18:689–696.
13. Atkinson HA, Daniels A, Read ND. 2002. Live-cell imaging of endocytosis during conidial germination in the rice blast fungus, *Magnaporthe grisea*. Fungal Genetics and Biology 37:233–44.
14. Hoffmann J, Mendgen K. 1998. Endocytosis and Membrane Turnover in the Germ Tube of *Uromyces fabae*. Fungal Genetics and Biology 24:77–85.
15. Tucker EB. 1993. Azide treatment enhances cell-to-cell diffusion in staminal hairs of *Setcreasea purpurea*. Protoplasma 174:45–49.
16. Altwasser R, Baldin C, Weber J, Guthke R, Kniemeyer O, Brakhage AA, Linde J, Valiante V. 2015. Network Modeling Reveals Cross Talk of MAP Kinases during Adaptation to Caspofungin Stress in *Aspergillus fumigatus*. PLOS ONE 10:e0136932.

CHAPTER 6

F901318-induced killing of *A. fumigatus*: an investigation into the mechanism of cell death

Saskia du Pré[a,b], Nick D. Read[b], Mike Birch[a] and Jason D. Oliver[a]

F2G Ltd., Manchester, United Kingdom[a];
Manchester Fungal Infection Group, University of Manchester, United Kingdom[b]

6.1 Abstract

F901318 is a novel antifungal drug that inhibits *de novo* pyrimidine biosynthesis by targeting dihydroorotate dehydrogenase (DHODH). It causes time-dependent swelling and cell lysis in *A. fumigatus*. In this study, the mechanism behind this F901318-induced cell lysis was investigated. The possibility of it being regulated by programmed cell death was investigated by looking for presence of markers for apoptosis and autophagy in F901318-treated *A. fumigatus* hyphae. Apoptotic markers of activated metacaspases and ROS production appear to be present in the lysed hyphae, however, the morphological rearrangements and the presence of vesicle-like structures in F901318-treated hyphae also suggest a cell death mechanism via autophagy. Furthermore, the mitochondrial membrane potential, associated with programmed cell death, appears to be decreased in F901318-treated hyphae. DHODH localization in the mitochondria did not appear to be affected by F901318 treatment. Finally, calcium levels, associated with regulated cell death, appeared to steadily increase after addition of F901318, possibly indicating that F901318-induced cell death is indeed regulated. Together, the results in this study suggest that F901318-induced cell death in *A. fumigatus* is caused by a form of programmed cell death, but further work is required to fully understand the mechanism of cell death.

6.2 Introduction

Invasive fungal infections are an increasing threat to our health, with an estimated 1.5 million deaths each year (1). Species from the *Aspergillus* genus are amongst the most common of human fungal pathogens, but at the moment only four classes of antifungal drugs are available for treatment of invasive aspergillosis (2). They either target the cell wall (echinocandins), the cell membrane (azoles and polyenes) or DNA/RNA synthesis (flucytosine). Newly approved antifungal drugs usually belong to one of the existing classes and as a result of repeated prescription of drugs acting on the same target, resistance to the existing antifungal drug classes has started to emerge, which is why it is important that antifungal drugs are developed that act on different targets (3).

F901318 is a new orotomide antifungal drug that is currently in clinical development for invasive aspergillosis (4). It works via a novel mode of action, blocking the *de novo*

pyrimidine biosynthesis pathway by inhibiting dihydroorotate dehydrogenase (DHODH) (5). When *A. fumigatus* is exposed to F901318, it initially has a static effect by inhibiting hyphal growth, however, prolonged exposure eventually leads to cell lysis (Chapter 3). Although the target of the drug was known, the exact mechanism behind this cell lysis was not well understood. An investigation of various markers of cell death was undertaken to attempt to elucidate the process leading to F901318-induced cell lysis. Cell death can be caused by different mechanisms, such as apoptosis, autophagy and necrosis; with the former two processes traditionally thought of as programmed cell death (PCD). Although especially well described in higher eukaryotes, it is now accepted that some forms of PCD also occur in yeast and filamentous fungi and has been associated with development and stress response (6).

In mammalian cells, it has previously been reported that downregulation of the *de novo* pyrimidine biosynthesis pathway, and also specifically DHODH, leads to an increase of the p53 tumor suppressor, which plays an important role in cell growth regulation and induces apoptosis (7, 8). This suggests the possibility that, when DHODH is inhibited in *A. fumigatus* by F901318, apoptosis may be triggered. However, the morphological rearrangements that have previously been shown to occur in response to F901318 treatment, appear to point to autophagy. F901318-treated hyphae become swollen due to the formation of large vacuoles (chapters 3 and 4), a typical hallmark of autophagy, due to sequestering of vesicles (autophagosomes) that contain cytosolic material, which is subsequently degraded in the vacuoles (9). Autophagy has been associated with nutrient starvation (9), so perhaps it can be induced during any type of deficiency, such as pyrimidine starvation.

In most eukaryotes, including *A. fumigatus* (chapter 4), DHODH is localized in the mitochondria (10). The functions of the mitochondria and DHODH are connected by the use of ubiquinone. In the mitochondria ubiquinone is used in the electron transport chain (ETC), where it plays a role as an electron carrier to cytochrome C, while DHODH utilizes ubiquinone as a terminal electron acceptor to re-oxidize the flavin mononucleotide co-factor, allowing further rounds of dihydroorotate oxidation (11, 12). Thus, the inhibition of DHODH by F901318 has the potential to affect mitochondrial functioning. The mitochondrial membrane potential (MMP) is essential for mitochondrial function as it is required for the ETC and a decrease in potential has

been associated with apoptosis (13, 14). The MMP can be assessed by using fluorescent mitochondrial dyes, such as Rhodamine-123 and JC-1. Fluorescence intensity of the dye is directly related to the MMP.

Calcium plays an important role as an intracellular signal (second messenger) in eukaryotes, including filamentous fungi, and is involved in various pathways, including PCD-related processes (15). Cells commonly respond to cell death stimuli with increased intracellular levels of calcium (16). Calcium levels can be measured using a calcium sensitive photoprotein called aequorin (17). Aequorin is isolated from the jellyfish *Aequorea victorea* and is a two-unit photoprotein composed of apoaequorin and the prosthetic group coelenterazine, and has a high affinity for free calcium. On binding calcium, the coelenterazine is oxidized to coelenteramide, which releases energy in the form of blue light (469 nm). The amount of luminescence is dependent upon the concentration of free calcium, which is why it can be used to report the cytosolic calcium concentration. This way, it is possible to test whether an antifungal agent causes an increase in intracellular calcium levels.

The aim of this study was to investigate how F901318 induces cell death in *A. fumigatus*. The presence of two apoptotic markers was investigated; production of reactive oxygen species (ROS) and activation of metacaspases. To determine whether autophagy plays a role, the presence of autophagosomes in F901318-treated hyphae was investigated. Additionally, the mitochondrial membrane potential was investigated, using the fluorescent mitochondria dyes MitoTracker Red FM and Rhodamine-123. Finally, calcium levels in *A. fumigatus* were investigated upon F901318 exposure using aequorin.

6.3 Materials and Methods

6.3.1 Strains and cultures

A. fumigatus clinical isolate AF293 was utilized for the apoptosis, autophagy and mitochondrial membrane potential studies. A cytosolic-GFP strain was also utilized to study presence of autophagic vesicles. A strain in which DHODH was C-terminally tagged with GFP under expression of the constitutive *gpdA* promoter was used for studying localization of DHODH before and after F901318 treatment (PgpdA-

DHODH-GFP strain, described in Chapter 4). The AEQ^{CEA10} strain (18) was used to measure calcium levels after addition of F901318. *A. fumigatus* was grown in Vogel's Minimal Medium (VMM) (19). For microscopy, hyphae were obtained by incubation of *A. fumigatus* conidia (10^3 conidia/ml) for 16 h at 37 °C in uncoated µ-slide 8 well chambers (Ibidi).

6.3.2 Antifungal drugs

F901318 was synthesized as previously described (4). The drug was dissolved in dimethylsulfoxide (DMSO) at a stock concentration of 0.5 mg/ml and used at a final concentration of 0.1 µg/ml.

6.3.3 Apoptotic markers

Dihydrorhodamine-123 (DHR-123, Sigma) was utilized to detect ROS and activation of metacaspases was observed with CaspACE™ (Promega). Dihydrorhodamine 123 (DHR-123) is normally non-fluorescent, but becomes fluorescent when oxidized to rhodamine-123 by ROS. CaspACE™ FITC-VAD-FMK is a fluorescent analogue of caspase inhibitor Z-VAD-FMK (carbobenzoxy-valyl-alanyl-aspartyl-[O-methyl]-fluoromethylketone) conjugated to fluoroisothiocyanate (FITC). The inhibitor becomes fluorescent when it binds to activated caspases.

The markers were added to hyphae that had been exposed to F901318 for 24 h. CaspACE™ was supplied as 5 mM solution in dimethylsulfoxide (DMSO) and used at a final concentration of 10 µM. DHR-123 was dissolved in DMSO and used at a final concentration of 2 µg/ml. CaspACE™ and DHR-123 were incubated for 20 min and 2 h respectively prior to imaging.

6.3.4 Fluorescent dyes

CellTracker™ Blue CMAC (7-amino-4-chloromethylcoumarin, molecular probes), staining the vacuoles was used at a final concentration of 1 µM. Filipin (Sigma), a polyene staining phospholipids in the cell membrane, was used at a final concentration of 1 µg/ml. Nile red (Sigma), a lipophilic stain for detection of intracellular lipid droplets, was used at a final concentration of 10 µg/ml.

To stain the mitochondria, MitoTracker Red FM (Molecular probes) and rhodamine-123 (Sigma) were used. They were dissolved in DMSO and used at a final

concentration of 500 nM and 10 μM respectively. Dyes were incubated for 45 – 60 min at 37 °C prior to imaging.

6.3.5 Microscopy

A Leica confocal SP8X microscope was utilized for the imaging, using Leica Application Suite Advanced Fluorescence (LAS AF) software for acquisition. Imaging took place in a temperature-controlled box (CUBE & BOX, Life Imaging Services). Excitation light source was provided by a UV laser, SuperK White Light Laser or an argon laser. A 40×/0.85 NA dry objective was utilized for the apoptosis marker experiments. A 63×/1.2 NA water objective was used for the vesicle and mitochondria staining. The FIJI distribution of ImageJ was utilized for processing (20).

The excitation for CaspACE^{TM} and the GFP strains was set to 488 nm and emission was detected over a range of 500-570 nm. For Nile red, DHR-123 and rhodamine-123 it was set to 514/530-600 nm. The excitation/emission for MitoTracker Red FM was 581/595-650 nm and for CMAC and filipin 405/415-450 nm.

6.3.6 Calcium aequorin measurements

The protocol used for the aequorin measurements is described in Muñoz *et al* 2015 (18). Conidia of the AEQ^{CEA10} strain (1×10^6 conidia/ml) in presence of 2.5 μM coelenterazine were incubated in 96-well plates, wrapped in foil, for 21 h at 25 °C. A multimode plate reader (Berthold Technologies TriStar LB 941) was used for the measurement of the luminescence after injection of the antifungal drug. 3 M $CaCl_2$ was used for the discharge control.

6.4 Results

6.4.1 Apoptotic markers appear to be present after F901318 exposure

To study whether F901318 induces apoptosis, the presence of apoptotic markers, namely metacaspase activation and ROS production, was investigated. DHR-123 or CaspACE^{TM} were applied to hyphae that had been exposed to F901318 for 24 h. In the treated hyphae, fluorescence of both DHR-123 and CaspACE^{TM} was detected in only a few hyphal compartments (Figure 6.1). This result suggests that after 24 h of treatment, F901318 does not widely induce apoptosis.

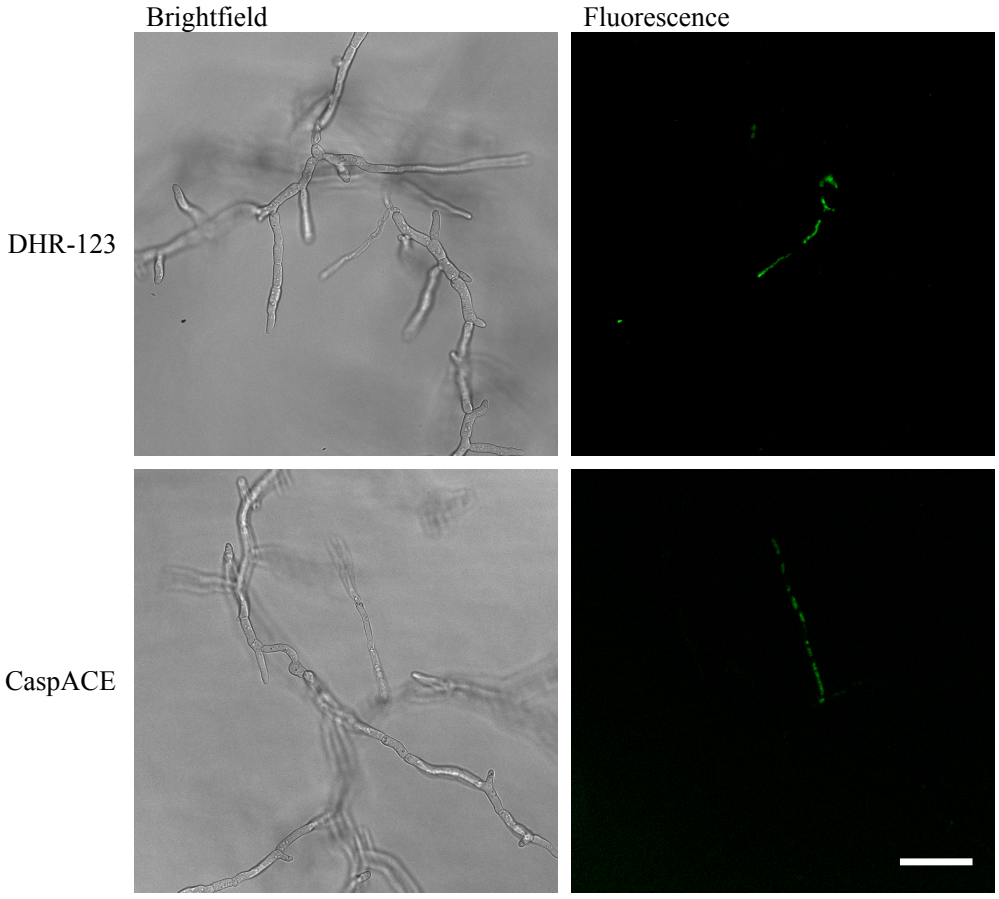

Figure 6.1 Presence of apoptotic markers for ROS production (DHR-123) and activation of metacaspases (CaspACE) in 24 h F901318-treated hyphae. Only few hyphal compartments were stained by the dyes, suggesting no significant induction of apoptosis after 24 h of F901318 treatment. DHR-123 = dihydrorhodamine-123. Bar = 50 µm.

6.4.2 F901318-treated hyphae contain vesicle-like structures

F901318-treated hyphae were studied for presence of autophagosomes. In hyphae that had been treated with F901318, distinctive vesicle-like structures could be observed, which were absent from untreated hyphae (indicated with arrows in Figure 6.2, top image). When vacuoles were stained with CMAC, the vesicle-like structures remained unstained and appeared to be distinct from the vacuoles (Figure 6.2, second row). Likewise, when a cytosolic-GFP (Cyto-GFP) strain was treated with F901318, no fluorescence was observed in the vesicles, suggesting the vesicles were discontinuous from the cytosol (Figure 6.2, third row). The vesicular structures were not stained by filipin, indicating that their membrane does not contain any sterol (Figure 6.2 fourth row). Neither did they co-localize with Nile red, excluding the possibility of the structures being lipid droplets (Figure 6.2, fifth row). The results show that the vesicle-like structures are distinct from both the cytoplasm and the vacuoles, and although

their exact nature remains to be confirmed, there exists the possibility that they are autophagosomes.

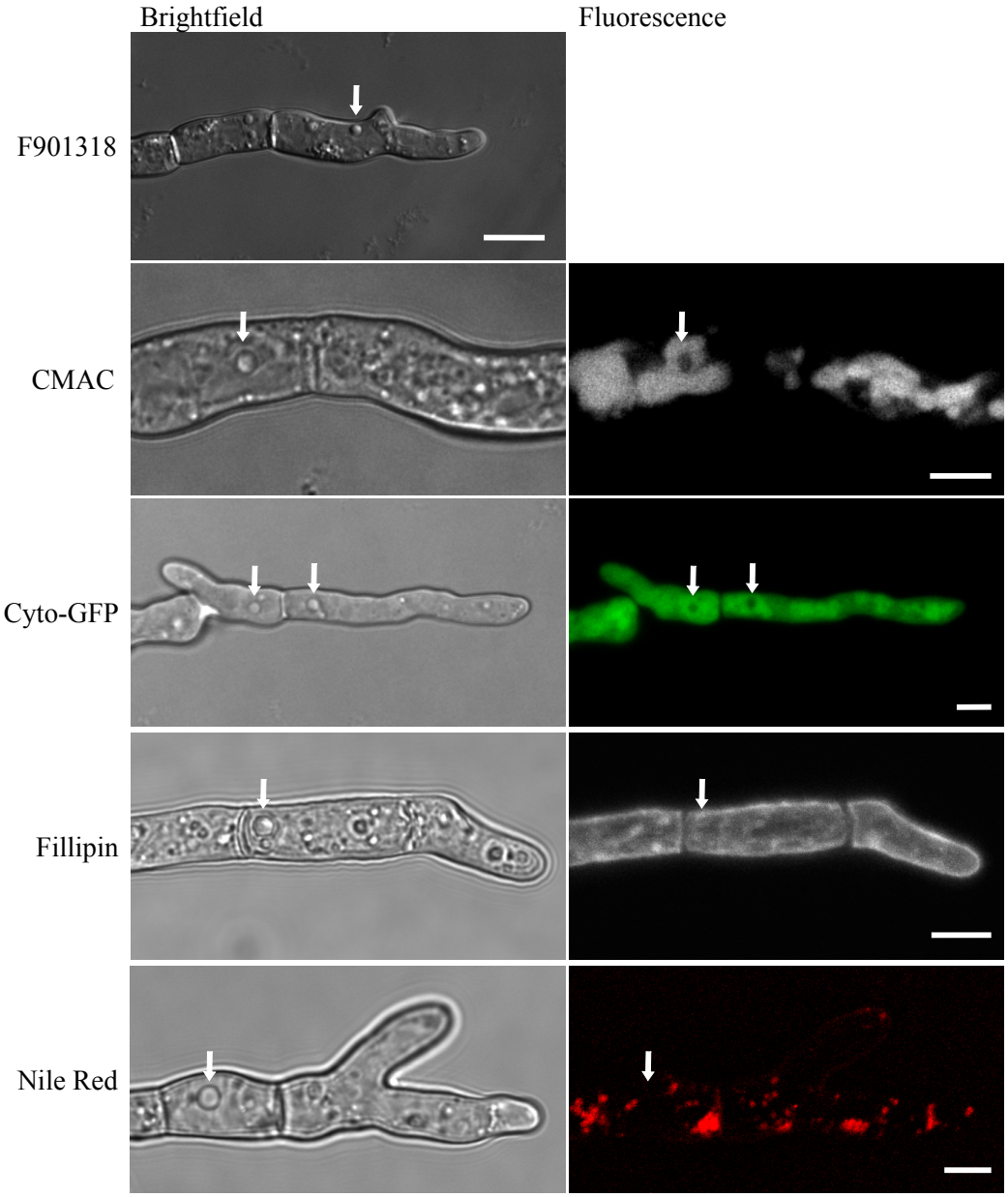

Figure 6.2 In F901318-treated hyphae vesicle-like structures were observed as indicated in the top DIC image (bar = 10 µm). The structures were excluded from the vacuoles (CMAC) and the cytosol (cyto-GFP), they were also not stained by filipin (sterol) or Nile red (lipid droplets) (bars = 5 µm).

6.4.3 F901318 appears to reduce the mitochondrial membrane potential

The MMP is important for mitochondrial functioning due its role in the ETC and a change in the potential has been associated with apoptosis. To assess the mitochondrial membrane potential after 24 h treatment with F901318, MitoTracker Red FM and

Rhodamine-123 were utilized. For both dyes fluorescence was observed in the untreated hyphae, but the fluorescence intensity was decreased in the F901318-treated hyphae (Figure 6.3). MitoTracker Red FM appeared to be accumulating at the cell wall, suggesting that it is not able to enter treated hyphae (Figure 6.3, top row). A faint rhodamine-123 was observed in the treated hyphae, suggesting the MMP was decreased (Figure 6.3, second row). However, as the fluorescence signal was very low with 10 µM rhodamine-123, it was repeated with a higher amount of 100 µM. This time, fluorescence was observed in the treated hyphae (Figure 6.3, third row). Although the results with MitoTracker Red FM and a low amount of rhodamine-123 appear to indicate a decrease in MMP, the result with a higher amount of the latter dye seems to contradict this.

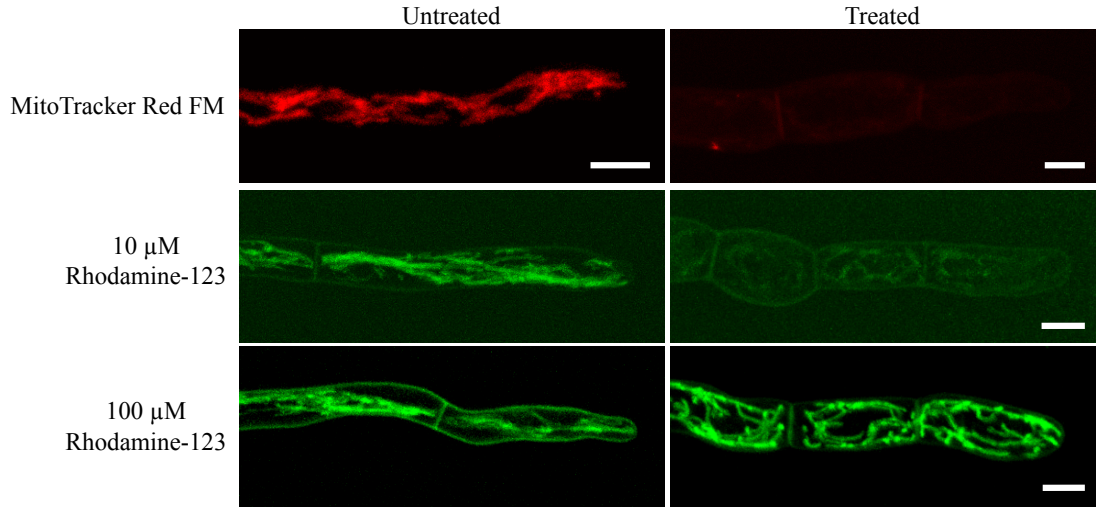

Figure 6.3 The MMP was investigated by utilizing the mitochondrial dyes MitoTracker Red FM and rhodamine-123. MitoTracker Red FM and 10 µM rhodamine-123 show reduced fluorescence in the treated hyphae, indicating the MMP is reduced. However, a bright signal is detected with 100 µM rhodamine-123, making the result unclear. Bar = 5 µm.

6.4.4 DHODH appears to remain in the mitochondria after F901318 treatment

To study the localization of DHODH after F901318 treatment, the PgpdA-DHODH-GFP strain was treated for 24 h, after which localization was studied. As co-localization with MitoTracker Red FM could not be carried out due to the dye not being taken up by treated hyphae (Figure 6.3, top row), the morphology of the DHODH-GFP signal was studied. The DHODH-GFP signal in both the untreated and the treated hyphae was localized in long filamentous structures (Figure 6.4). The structures and distribution of the signal appears to be similar to the rhodamine-123

staining in Figure 6.3 (third row). Although more accurate assays need to be carried out, this result appears to suggest that DHODH remains localized in the mitochondria after F901318 treatment.

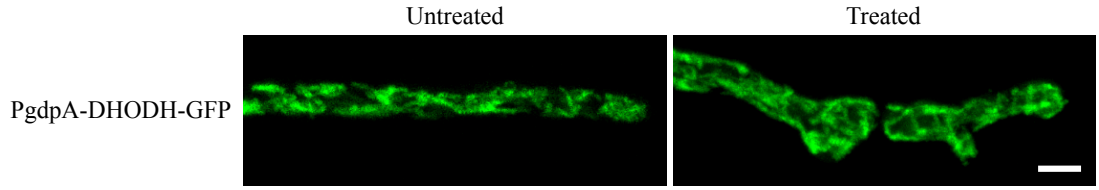

Figure 6.4 PgpdA-DHODH-GFP before and after F901318 treatment. After treatment, DHODH appears to remain localized in long filamentous structures, which possibly suggests that DHODH is still localized in the mitochondria after drug treatment. Bar = 5 μm.

6.4.5 F901318 does not cause immediate calcium spikes

To examine the effects of stress induced by F901318 on the intracellular calcium concentrations ($[Ca^{2+}]_c$), *A. fumigatus* strain AEQ^{CEA10} was utilized to measure aequorin luminescence. Calcium levels were measured over a period of 2 h (7200 s), starting when 1 or 5 μg/ml F901318 or no drug as a control was added (Figure 6.4). In the no drug control, luminescence remained steady, indicating no change in intracellular calcium levels. When F901318 was added, calcium levels appeared to steadily increase. In the no drug control, after two hour the intracellular calcium concentration ($[Ca^{2+}]c$) was 0.052 μM. When 1.0 or 5.0 μg/ml F901318 was added, this increased to 0.078 and 0.113 μM respectively, the latter concentration being a significant increase from the no drug control. This result appears to suggest that the intracellular levels of calcium increase over time when F901318 is added.

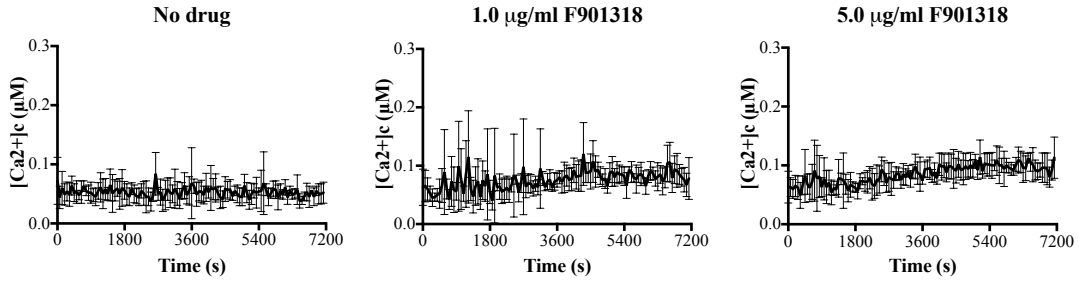

Figure 6.5 Intracellular calcium levels in *A. fumigatus* treated with 1 or 5 μg/ml F901318 or no drug as a control. Levels appear to increase over time after addition of the drug.

6.5 Discussion

In this study, the mechanism behind the cell death caused by F901318 treatment in *A. fumigatus* was investigated. Two forms of PCD, apoptosis and authophagy, were investigated by detecting whether any apoptotic or autophagic markers were present in the treated hyphae.

In mammalian cells inhibiting DHODH and disrupting *de novo* pyrimidine biosynthesis leads to induction of apoptosis (7, 8), in a p53-mediated mechanism. To investigate whether apoptosis was triggered in *A. fumigatus*, two apoptotic markers were studied: the activation of metacaspases (CaspACE^{TM}) and the production of ROS (DHR-123). In the treated hyphae, both CaspACE^{TM} and DHR-123 fluorescence was observed in a few hyphal compartments (Figure 6.1). This indicates that apoptosis is not widely induced after 24 h of F901318 treatment. However, as there are several apoptotic markers that are produced during apoptosis induction, it will be useful to investigate these, such as DNA cleavage (TUNEL assay) and externalization of phosphatidylserine (Annexin V) (6). Additionally, these results should be compared to a control that is known to induce apoptosis, such as TPEN (N,N,N',N'-Tetrakis(2-pyridylmethyl)ethylenediamine).

Autophagy is another form of programmed cell death and its main hallmark is the formation of vesicles called autophagosomes that contain cytoplasmic waste. They fuse with the vacuoles, where the waste is degraded, which leads to hyper vacuolization and large vacuolar. Previously it was described that in *A. fumigatus* large vacuoles were formed following treatment with F901318 (chapter 4), which may suggest the activation of authophagy. During autophagy, toxic cytoplasmic contents are sequestered in so called autophagic bodies (autophagosomes), which fuse with the vacuoles, where the contents are released and subsequently degraded (9). This leads to the formation of larger vacuoles, as seen in F901318-treated hyphae (Chapter 4). Presence of autophagic bodies is an important hallmark for autophagy, which is why treated hyphae were investigated for presence of such vesicles. Vesicle-like structures were indeed observed in hyphae that had been exposed to F901318. To further investigate these vesicles, treated hyphae were stained to highlight the vacuoles (CMAC), sterol (filipin) and lipid droplets (Nile red), and additionally, a cytosolic-

GFP strain was utilized (Figure 6.2). It was clear that the vesicles were excluded from both vacuoles and the cytosol. The structures were also not stained by filipin or Nile red. The latter dye excludes the possibility of the structures being lipid droplets. The vesicles were also not stained by filipin, suggesting that their membranes do not contain any sterol. It will be useful to stain with FM4-64, which stains up membranes. To truly determine whether the vesicles are autophagosomes, a strain should be utilized where autophagy-related protein 8 (ATG8) is tagged with GFP. ATG8 is associated with autophagosomes, so if the GFP tagged ATG8 would co-localize with the vesicles, this would strongly indicate the activation of autophagy by F901318 (9, 21).

The MMP is essential for proper mitochondrial functioning and as DHODH and the mitochondria are associated with each other by localization and their use of ubiquinone, the MMP was investigated using fluorescent dyes MitoTracker Red FM and rhodamine-123. Both dyes produce a fluorescent signal in the mitochondria that is dependent on the MMP. MitoTracker Red FM did not produce a signal in the F901318-treated hyphae, 10 μM rhodamine 123 did give a signal, but it appeared to be decreased when compared to the untreated hyphae (Figure 6.3). However, when an excess amount of 100 μM rhodamine-123 was applied, a bright fluorescence signal was detected. Therefore, it is not entirely clear whether the MMP was decreased by F901318. The reason why an excess amount of rhodamine-123 does give a signal, may be due to the fact that more dye can accumulate at the mitochondria. It may be useful to utilize another dye such as JC-1 to investigate the MMP and confirm whether or not F901318 treatment leads to a decrease in the MMP.

The fact that MitoTracker Red FM did not give signal in the F901318-treated hyphae, may indicate that the dye can simply no longer be taken up by hyphae exposed to the drug. Possibly, this could be due to inhibition of transport. In a study where a fluorescent F901318 analogue was utilized to investigate uptake of the drug, it was suggested that F901318 possibly inhibits active transport, as the analogue was not taken up in hyphae that were pre-treated with F901318 for 24 h (chapter 5). Rhodamine-123 was able to enter the hyphae, but as this is a smaller molecule than MitoTracker Red FM, it may be taken up via diffusion.

Localization of DHODH was also investigated after treatment with F901318. Although it could not be confirmed by co-localization with MitoTracker Red FM, it appeared as though DHODH was still localized in long filamentous structures, that could be the mitochondria (Figure 6.4). Sometimes target mislocalization is observed after treatment with an antifungal, as is the case with 1,3-ß-glucan synthase when *A. fumigatus* is treated with caspofungin (22). However, DHODH is anchored in the inner mitochondrial membrane due to its mitochondrial targeting sequence, so it may be expected to remain *in situ*.

Calcium also plays in a role in PCD, acting as a second messenger in associated pathways. Therefore, calcium levels in response to F901318 treatment were measured using aequorin. No change in calcium level was detected in the untreated control, but when F901318 was added, the calcium level started to slowly increase in time (Figure 6.5). It was previously reported that other antifungals induce calcium spikes, but this was not observed for F901318. However, these antifungals were cidal agents with a more immediate killing effect, whereas F901318 does not immediately kill *A. fumigatus*, rather it has a time-dependent killing effect, which possibly explains why no calcium peaks were observed for F901318. The viability of *A. fumigatus* exposed to F901318 decreases with prolonged exposure. With aequorin the calcium level of a population of germ tubes is measured. Therefore, it is possible that calcium peaks may never be observed for F901318 treatment, but rather the calcium level keeps rising steadily as an increasing number of germ tubes are killed. To confirm this, it would be interesting to repeat the aequorin measurements over a longer period of time. It would be even more interesting to utilize an *A. fumigatus* GCaMP strain, which contains a genetically encoded calcium indicator (GECI) (23). It could be used to monitor germ tubes exposed to F901318 over time, similar to the 46 h timelapse in chapter 3, to observe whether calcium spikes can be observed in individual germ tubes when they undergo cell lysis.

Some initial evidence in this study suggests that a type of PCD may be induced in F901318-treated hyphae. Although it appears as if markers for both apoptosis and autophagy are present, a role for autophagy seems to be more likely with presence of large vacuoles and possible autophagic bodies. Further investigation is required to confirm the effectiveness of the apoptosis markers used and additionally, other

apoptotic markers, such as DNA cleavage and phosphatidylserine internalization, can be investigated. To further study autophagy, it would be useful to generate a ATG8-GFP strain and use this strain to see whether ATG8 localizes in the vesicle-like structures found in treated hyphae.

6.6 References

1. Brown GD, Denning DW, Gow NAR, Levitz SM, Netea MG, White TC. 2012. Hidden killers: human fungal infections. Sci Transl Med 4:165rv13.
2. Campoy S, Adrio JL. 2016. Antifungals. Biochemical Pharmacology.
3. Kanafani ZA, Perfect JR. 2008. Resistance to antifungal agents: mechanisms and clinical impact. Clinical Infectious Diseases 46:120–8.
4. Oliver JD, Sibley GEM, Beckmann N, Dobb KS, Slater MJ, McEntee L, du Pré S, Livermore J, Bromley MJ, Wiederhold NP, Hope WW, Kennedy AJ, Law D, Birch M. 2016. F901318 represents a novel class of antifungal drug that inhibits dihydroorotate dehydrogenase. PNAS 113:12809–12814.
5. Jones ME. 1980. Pyrimidine Nucleotide Biosynthesis in Animals: Genes, Enzymes, and Regulation of UMP Biosynthesis. Annual Review of Biochemistry 49:253–279.
6. Sharon A, Finkelstein A, Shlezinger N, Hatam I. 2009. Fungal apoptosis: function, genes and gene function. FEMS Microbiology Reviews 33:833–854.
7. Khutornenko AA, Roudko V V, Chernyak B V, Vartapetian AB, Chumakov PM, Evstafieva AG. 2010. Pyrimidine biosynthesis links mitochondrial respiration to the p53 pathway. Proceedings of the National Academy of Sciences of the United States of America 107:12828–33.
8. Khutornenko AA, Dalina AA, Chernyak B V, Chumakov PM, Evstafieva AG. 2014. The Role of Dihydroorotate Dehydrogenase in Apoptosis Induction in Response to Inhibition of the Mitochondrial Respiratory Chain Complex III. Acta naturae 6:69–75.
9. Pollack J, Harris S, Marten M. 2009. Autophagy in filamentous fungi. Fungal Genetics and Biology 46:1–8.
10. Rawls J, Knecht W, Diekert K, Lill R, Löffler M. 2000. Requirements for the mitochondrial import and localization of dihydroorotate dehydrogenase. European journal of biochemistry 267:2079–87.
11. Liu S, Neidhardt EA, Grossman TH, Ocain T, Clardy J. 2000. Structures of human dihydroorotate dehydrogenase in complex with antiproliferative agents. Structure 8:25–33.
12. Vyas VK, Ghate M. 2011. Recent developments in the medicinal chemistry and therapeutic potential of dihydroorotate dehydrogenase (DHODH) inhibitors. Mini reviews in medicinal chemistry 11:1039–55.
13. Robson GD. 2006. Programmed cell death in the aspergilli and other filamentous fungi. Medical Mycology 44:S109–S114.
14. Bras M, Queenan B, Susin SA. 2005. Programmed cell death via mitochondria: different modes of dying. Biochemistry Biokhimiia 70:231–9.
15. Hajnóczky G, Davies E, Madesh M. 2003. Calcium signaling and apoptosis. Biochemical and biophysical research communications 304:445–54.
16. Gonçalves AP, Cordeiro JM, Monteiro J, Muñoz A, Correia-de-Sá P, Read ND, Videira A. 2014. Activation of a TRP-like channel and intracellular Ca2+

dynamics during phospholipase-C-mediated cell death. Journal of cell science 127:3817–29.
17. Bonora M, Giorgi C, Bononi A, Marchi S, Patergnani S, Rimessi A, Rizzuto R, Pinton P. 2013. Subcellular calcium measurements in mammalian cells using jellyfish photoprotein aequorin-based probes. Nature Protocols 8:2105–2118.
18. Muñoz A, Bertuzzi M, Bettgenhaeuser J, Iakobachvili N, Bignell EM, Read ND, Goldman GH, De U, Paulo S. 2015. Different Stress-Induced Calcium Signatures Are Reported by Aequorin-Mediated Calcium Measurements in Living Cells of *Aspergillus fumigatus*. PLoS ONE 10:e0138008.
19. Vogel HJ. 1956. A Convenient Growth Medium for *Neurospora crassa*. Microbial Genetics Bulletin 13:42–47.
20. Schindelin J, Arganda-Carreras I, Frise E, Kaynig V, Longair M, Pietzsch T, Preibisch S, Rueden C, Saalfeld S, Schmid B, Tinevez J-Y, White DJ, Hartenstein V, Eliceiri K, Tomancak P, Cardona A. 2012. Fiji: an open-source platform for biological-image analysis. Nature Methods 9:676–682.
21. Pinar M, Pantazopoulou A, Peñalva MA. 2013. Live-cell imaging of *Aspergillus nidulans* autophagy: RAB1 dependence, Golgi independence and ER involvement. Autophagy 9:1024–43.
22. Moreno-Velásquez SD, Seidel C, Juvvadi PR, Steinbach WJ, Read ND. 2017. Caspofungin-Mediated Growth Inhibition and Paradoxical Growth in *Aspergillus fumigatus* involve Fungicidal Hyphal Tip Lysis Coupled with Regenerative Intrahyphal Growth and Dynamic Changes in β-1,3-Glucan Synthase Localization. Antimicrobial Agents and Chemotherapy AAC.00710-17.
23. Akerboom J, Chen T-W, Wardill TJ, Tian L, Marvin JS, Mutlu S, Calderón NC, Esposti F, Borghuis BG, Sun XR, Gordus A, Orger MB, Portugues R, Engert F, Macklin JJ, Filosa A, Aggarwal A, Kerr RA, Takagi R, Kracun S, Shigetomi E, Khakh BS, Baier H, Lagnado L, Wang SS-H, Bargmann CI, Kimmel BE, Jayaraman V, Svoboda K, Kim DS, Schreiter ER, Looger LL. 2012. Optimization of a GCaMP calcium indicator for neural activity imaging. The Journal of neuroscience 32:13819–40.

CHAPTER 7

General discussion and future work

7.1 General discussion

Treatment options for invasive fungal infections are limited with only four classes of antifungal drugs available on the market (1). The latest class to be approved for clinical use were the echinocandins in 2001 (2). High mortality rates call for the urgent need of new antifungal drugs acting on novel targets. F901318 is a novel antifungal drug belonging to a new class of antifungals called the orotomides and is currently in clinical development for invasive aspergillosis. F901318 inhibits *de novo* pyrimidine biosynthesis by targeting DHODH, the fourth enzyme in this pathway (3). Pyrimidines are required for DNA and RNA synthesis, which in turn are important for cell cycle regulation and protein synthesis. Additionally, pyrimidines are involved in other processes, such as phospholipid synthesis and cell wall formation. In this PhD project, the effects of the novel antifungal drug F901318 on the human pathogenic fungus *Aspergillus fumigatus* were investigated.

7.1.1 Chapter 3: the effect of the novel antifungal drug F901318 on the growth and viability of *Aspergillus fumigatus.*

Chapter 3 focused on the effect of F901318 on growth and viability, discussing whether the drug has a static or a cidal effect against *A. fumigatus*. According to the determination of the MFC, F901318 is a fungistatic drug (not published). Live-cell, time lapse microscopy indeed showed that F901318 inhibits germination and tip growth, but no immediate decrease in viability was observed (Figure 3.1 and 3.2). However, when the exposure to F901318 was prolonged to >24 h, conidia, germ tubes and hyphae became swollen and this would lead to cell lysis (Figure 3.3). DiBAC staining revealed that the decrease in viability was especially evident for germ tubes and vegetative hyphae, conidia were more resistant, which is consistent with the MFC result (Figure 3.5). Additionally, it was found that the effect of F901318 in non-lysed hyphae, was largely irreversible as little regrowth was observed after washing out the drug (Figure 3.6). The results show that prolonged treatment with F901318 leads to cell lysis and therefore it was concluded that F901318 should be regarded as a time-dependent fungicidal drug against *A. fumigatus*. Furthermore, as F901318 inhibits germination, the drug could be considered for prophylaxis.

The results of this chapter show that an antifungal compound should not always be distinguished as either fungistatic or fungicidal. It rather depends on various factors, such as the concentration of the drug, exposure time and the developmental stage of the fungus. In this chapter, the focus was mainly on the latter two factors and less on the concentration of the drug. For all the experiments, a concentration of 0.1 µg/ml F901318 was used (selected as it is roughly twice the MIC), but in section 3.3.5 a biomass assay was performed in which hyphae were treated with either 0.1 or 1.0 µg/ml F901318. The results in this section show that the effect of 1.0 µg/ml was stronger than the effect of 0.1 µg/ml, which possibly indicates that the antifungal effect of F901318 is concentration dependent. Therefore, it may be interesting to investigate whether higher concentrations of the drug have a stronger cidal effect on *A. fumigatus*.

7.1.2 Chapter 4: the dynamic influence of F901318 on the morphology of *Aspergillus fumigatus*.

In chapter 4, the localization of DHODH and the effect of F901318 on intracellular structures were investigated. Co-localization of a PgpdA-DHODH-GFP strain with the mitochondrial dye MitoTracker Red FM indicated that *A. fumigatus* harbours a class 2 DHODH that is located in the mitochondria (Figure 4.3). Cellular structures predicted to be affected by inhibition of pyrimidine biosynthesis, such as the cell wall, the vacuoles and the nuclei, were studied using fluorescent confocal microscopy. In the cell wall, the 1,3-β-glucan content was specifically decreased at the F901318-treated hyphal tips, while the overall chitin content and septation was increased (Figure 4.4 and 4.5). Vacuolar volume was increased in F901318-treated hyphae, while the volume of the cytoplasm was decreased (Figure 4.6). Analyses with an H1-GFP strain revealed that 15-20 min after addition of F901318, nuclear motility increased for 1-3 h and that F901318 inhibits mitosis (Figure 4.7). These results show that inhibiting pyrimidine biosynthesis has a dynamic effect on the entire cell, affecting several key processes.

Taking together results from chapter 3 and 4, it appears that the effects of F901318 treatment have some similarities with the effects of caspofungin treatment. Both drugs induce swelling, cell lysis, increased chitin synthesis and increased septation. However, caspofungin is widely regarded as being static against *A. fumigatus*, as it does not completely inhibit growth. It causes tip specific cell lysis, from which the

fungus recovers by regenerative intrahyphal growth, leading to small hyperbranched colonies. F901318 does inhibit hyphal growth and additionally also causes cell lysis. The similarities and differences in the effects exerted by F901318 and caspofungin on *A. fumigatus* lead to the question whether these two antifungals can work together synergistically and create a more direct loss in viability, with both F901318 and caspofungin causing cell lysis and F901318 also inhibiting (intrahyphal) growth.

In this work, the two main components of the cell wall, 1,3-ß-glucan and chitin, were investigated. However, the cell wall also contains 1,6-ß-glucan, 1,3-α-glucan, galactomannan and galactosaminoglycan (GAG), additionally, conidia contain a melanin and rodlet layer (4). It would be interesting to study these other components by fluorescence microscopy and TEM, to fully understand the effect of F901318 on other cell wall components. A start was made by investigating mannose by staining with concanavalin A (Appendix). Furthermore, cell wall integrity is regulated by a number of pathways, which includes the core protein kinase C pathway, but also the Ca^{2+}/calcineurin pathway and the HOG pathway (4). Together, the pathways maintain cell wall integrity and regulate cell wall remodeling when the cell wall is compromised. A common cell wall stress response is the upregulation of chitin, which was also observed in F901318-treated hyphae (5). It would be interesting to investigate this further with chitin synthase mutants, especially since UTP is required for chitin synthesis. A potential role for transcription factor CrzA could also be investigated, as it was shown to be involved in the caspofungin-induced chitin synthase upregulation (6). Furthermore, the cell wall thickness can be measured, to assess whether the chitin increase leads to a thicker cell wall. This can be done perhaps from TEM images, alternatively, thickness can be measured using high resolution fluorescence microscopy with a specific (outer) cell wall and membrane dye. Additionally, the hyphal swelling and the consequent cell lysis observed in F901318-treated hyphae leads to the assumption that this increases the pressure on the cell wall. Therefore, it will be interesting to investigate this further, also whether the increased chitin content allows the fungus to withstand more pressure, delaying the onset of cell lysis. Various methods have been described to measure turgor pressure, either indirectly or directly, such as utilizing a pressure probe (7). Another method is the utilization of microchambers, by measuring the deformation of the plastic caused by hyphae (8, 9). In this respect, it would also be interesting to investigate whether combining F901318

with a chitin synthesis inhibitor, such as Nikkomycin Z, would increase the onset of cell lysis.

An increased number of septa were measured in the F901318-treated hyphae. This has also been observed in caspofungin-treated hyphae and it has been suggested that this is to increase survival of the fungus. Increased compartmentalization increases the length of a hypha that is left intact after one compartment lyses. To investigate this further, it would be interesting to analyze the effect of F901318 treatment on hyphae where the formation of septa is disrupted. This could be achieved for example by treatment with hydroxyurea or by utilizing a *Rho4* mutant, which was shown to contain a reduced number of septa (10–12).

F901318 treatment was shown to lead to increased vacuolar volume. It has been suggested that the vacuolar volume is indirectly important for cell cycle progression as it affects cytoplasmic volume. Therefore, it will be interesting to investigate the effect of F901318 treatment on vacuole development mutants. This will also be useful to further understand the role of the vacuoles in cell cycle regulation.

Analyses with the H1-GFP strain has revealed an interesting phenomenon, where nuclear motility was increased from approximately 15 min to 3 h after addition of F901318. An explanation for this phenomenon was not found, but interestingly there seems to be a correlation between this effect and the initial inhibition of growth found in chapter 3 (section 3.3.2). Tip growth is halted about 15-30 min after addition of the drug and approximately 2 h later, tip growth is initiated again, albeit at a far slower rate. This suggests that during this increased motility, hyphal tip growth cannot proceed. It will be interesting to further investigate this effect on the nuclei, perhaps by analyzing the morphology and dynamics of actin and the microtubules, as the cytoskeleton is important for both nuclear motility and mitosis. To further investigate the effect on the cell cycle, it could be analyzed by flow cytometry with, for example, propidium iodide (PI) DNA staining. The DNA content varies throughout the phases of the cell cycle and PI binds in proportion to the amount of DNA present in a cell. This way, the fluorescence intensity of PI, measured by flow cytometry, can tell in what phase of the cell cycle F901318-treated *A. fumigatus* is arrested. Alternatively, the Vybrant® DyeCycle™ dyes from Molecular probes could be utilized.

7.1.3 Chapter 5: analysis of uptake and intracellular distribution of the orotomide antifungal agent F901318 using a fluorescent analogue.

Chapter 5 concentrated on the utilization of a fluorescent analogue as a tool to study distribution and uptake of F901318. Several analogues were synthesized, of which F901848 was both fluorescent and showed promising antifungal activity against *A. flavus* and *A. niger* (Figure 5.1 and 5.2, Table 5.1 and 5.2). Uptake and distribution of the fluorescent analogue was studied in *A. flavus*. After addition, the fluorescence intensity increased over time, achieving maximum fluorescence after approximately 40 min (Figure 5.3). Although fluorescence was observed throughout the entire cytoplasm, accumulations at specific sites were clear and co-localization with MitoTracker Red FM confirmed that these were the mitochondria, where DHODH is localized (Figure 5.4). F901848 uptake was not inhibited by ATP synthesis inhibitor sodium azide, which strongly suggests that the analogue is not taken up via an energy driven process (Figure 5.5). Hyphae that were pre-treated with F901318, showed decreased uptake of F901848, whereas hyphae pre-treated with caspofungin did not (Figure 5.6). This possibly indicates the competition between F901318 and F901848 for their DHODH binding site and also that possibly F901318 treatment leads to a decreased membrane permeability. The results in this chapter show that a fluorescent analogue is a valuable tool in studying uptake and distribution of antifungal drugs.

Adding a fluorophore to a compound undoubtedly affects the activity of the compound and this was evident in the different F901318 analogues that were synthesized. None of the analogues retained the same level of activity of F901318, with only F901848 exhibiting fluorescence and antifungal activity against three *Aspergillus* species. However, this analogue has shown its value in studying uptake and distribution in *A. flavus*. Unfortunately, in this work the *in vitro* enzyme assay could not be performed for *A. flavus* due to issues with the purification of its DHODH. It will be useful to reattempt purifying *A. flavus* DHODH so an *in vitro* enzyme assay can be performed to confirm that F901848 is also active against *A. flavus* DHODH.

It will be interesting to further investigate whether F901318 decreases membrane permeability. Pyrimidines are involved in the lipid synthesis pathway and thereby contribute to the structure of the cell membrane. During this PhD, several dyes have been utilized to study the intracellular morphology of *A. fumigatus* after F901318 exposure (chapter 4). However, it was found that some dyes did not stain the F901318-

treated hyphae, suggesting they were not taken up. This was the case for FM4-64 and MitoTracker Red FM. The first is taken up via active transport, which is possibly inhibited by F901318 due to the link between DHODH and mitochondrial function, which possibly leads to decreased ATP synthesis (chapter 6). MitoTracker Red FM is taken up via diffusion and its fluorescence is dependent on the mitochondrial membrane potential (chapter 6). No signal was detected in F901318-treated hyphae, which could indicate loss of the mitochondrial membrane potential (MMP), however an accumulation at the cell wall suggests it is simply no longer being taken up (chapter 6). However, other dyes used in this work, such as CMAC and rhodamine 123, were taken up by F901318-treated hyphae. The main difference between the latter dyes and MitoTracker Red FM is their molecular weight, with MitoTracker Red FM having a higher molecular weight. This possibly indicates that F901318 treatment leads to a decrease of compounds that are allowed to diffuse through the cell membrane, with only small compounds being able to enter hyphae. It will be interesting to further investigate the effect of F901318 on the cell membrane.

7.1.4 Chapter 6: F901318-induced killing of *A. fumigatus*: an investigation into the mechanism of cell death.

In the final results chapter 6, it was investigated whether F901318 induces programmed cell death in *A. fumigatus*. Apoptotic markers activation of metacaspases and production of ROS appeared to be present in F901318-treated hyphae (Figure 6.1). However, vesicle-like structures present in the F901318-treated hyphae, distinct from the cytoplasm and the vacuoles, may be autophagosomes (Figure 6.2). Furthermore, the mitochondrial membrane potential (MMP) was investigated and the results appear to indicate that F901318 treatment leads to a decrease in MMP (Figure 6.3). Finally, localization of DHODH did not appear to be affected by F901318 treatment (Figure 6.4) and aequorin measurements showed that the intracellular calcium levels appear to slowly rise after F901318 addition (Figure 6.5). Although the results seem to suggest that F901318-treated hyphae do exhibit markers of programmed cell death, more work is required to gain a full understanding.

Although this chapter is merely the beginning of an investigation into whether F901318 causes programmed cell death and a more in-depth analysis is needed, it does give some insights into to possible induction of programmed cell death by F901318.

The results appear to indicate the presence of apoptotic markers of ROS production and activation of metacaspases, however, more markers need to be investigated to confirm, such as DNA fragmentation (TUNEL assay) and translocation of phosphatidylserine (Annexin V).

Interestingly, the formation of the vesicle-like structures seemed to indicate the formation of autophagosomes and thus induction of autophagy. To further investigate this, a GFP-ATG8 strain could be used to study co-localization between the vesicles and ATG8, a known component of autophagosomes.

A further investigation into the MMP is required, as the results in this chapter were not entirely clear. In 24 h F901318-treated hyphae, MitoTracker Red FM did not give a signal, however, as an accumulation was observed at the cell wall, it is possible that it was no longer able to enter the cell. This could be due to a limitation in transport caused by F901318, as mentioned before. When Rhodamine-123 was utilized, a signal was observed in the treated hyphae, although it appeared to be slightly lower in the treated hyphae, but the results were not entirely clear. More work is required to investigate the MMP in response to F901318 treatment and possibly use of another dye such as JC-1, a further indicator of mitochondrial health and MMP.

Finally, no clear calcium spikes were observed after addition of F901318, although this was previously observed for other antifungals. Instead calcium levels appear to slowly increase, but it is possibly that calcium spikes might be observed prior to cell lysis. An *A. fumigatus* strain carrying a genetically encoded calcium indicator, such as the GcAMP6 strain will be useful to further investigate this. Furthermore, as the Ca^{2+}/calcineurin pathway is also involved in maintaining cell wall integrity, synergy of F901318 and calcineurin inhibitors should be explored (4). Calcineurin is a phosphatase that senses intracellular calcium levels and transduces this signal to transcription factor CrzA. Previous research demonstrated synergy between caspofungin and calcineurin inhibitors (such as FK506) in attenuating growth of *Aspergillus* spp. (13).

7.1.5 Conclusion

Taken together, the results in this PhD project have led to a greater understanding of the effects of DHODH inhibition in *A. fumigatus* by the novel antifungal drug F901318. The drug causes a variety of effects on growth, viability and the intracellular

structure, which are summarized in figure 7.1. A description of a suggested sequence of events that occur after the addition of F901318 to *A. fumigatus* is given below.

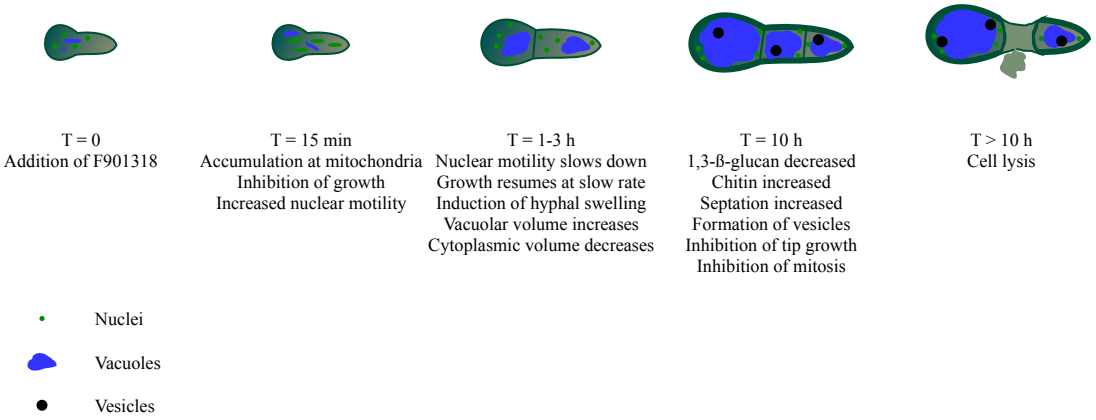

Figure 7.1 Sequence of events after addition of F901318.

F901318 is taken up at a linear rate and accumulates at the mitochondria from approximately 15 min after addition (chapter 5). This then leads to inhibition of hyphal elongation and causes increased nuclear motility (chapters 3 and 4). Nuclear motility is slowed down to pre-drug levels 1-3 h after addition of the drug, after which hyphal growth resumes at a slow rate (chapters 3 and 4). During the resumed growth, the hyphae start to swell significantly, presumably caused by an increase in vacuolar volume (chapter 4). This increase in vacuolar volume could be a consequence of pyrimidine starvation and leads to a decrease in the cytoplasmic volume which in turn possibly causes cell cycle arrest and inhibition of mitosis (chapter 4). Meanwhile, formation of 1,3-ß-glucan is decreased due to a reduced availability in UDP-glucose and perhaps as a consequence of this and the hyphal swelling, chitin production is increased for compensation and to create a stronger cell wall, to try and prevent cell lysis (chapter 4). Septation also increases, perhaps to increase survival, as it allows most of the hypha to survive as one compartment lyses (chapter 4). Furthermore, distinct vesicle-like structures are formed, and intracellular calcium levels increase, which could be indications that programmed cell death is induced (chapter 6). 10 h after addition hyphal growth is completely ceased and cell lysis occurs in a time-dependent fashion (chapter 3).

The results in this work show that inhibition of *de novo* pyrimidine biosynthesis via DHODH causes a dynamic effect throughout the fungal hyphae, that ultimately leads

to cell death. This shows that the pyrimidine biosynthetic pathway is a very promising antifungal drug target and F901318 could be the first antifungal approved for clinical use that acts on this pathway. F901318 is currently in clinical development for treatment of aspergillosis and scedosporiosis. Pre-clinical testing in animals has shown that longer treatment improves outcome, which is consistent with the results in chapter 3 (14). Prolonging the exposure of F901318 increases its effectiveness against *A. fumigatus* to a greater level than prolonging the exposure of voriconazole and caspofungin (chapter 3). This could potentially indicate that F901318, once approved for clinical use, may be favorable for treatment of Aspergillosis. Additionally, the results in chapter 3 also indicate the potential use of F901318 as a prophylactic drug, as conidia cannot germinate in presence of this drug.

Taken together, the results in this thesis support a role for F901318 in the treatment of aspergillosis. Clinical testing is currently in progress which will hopefully lead to F901318 being approved for clinical use. Additional *in vitro* research of F901318 should be continued to further understand the mechanism of F901318 induced cell death of *A. fumigatus*. The next section provides an overview of suggested future work that will further unravel the effect of F901318 treatment on *A. fumigatus*. The work focuses on researching whether the effect is concentration dependent, whether F901318 can synergize with caspofungin and other (non-antifungal) drugs, expand on the effect on the cell wall, on programmed cell death, uptake, transport, etc. Together the results of these experiments will provide an understanding of the mechanism of F901318 activity, while also improving our understanding of the cell biology of *A. fumigatus*. The result of this work could potentially lead to suggestions for treatment and possibly even to suggestions for novel antifungal drug targets.

7.2 Future work

The general discussion has highlighted several suggestions for future work. In this section, the suggested future work and experiments is summarized.

- Is the antifungal effect of F901318 concentration dependent?

  Repeat the DiBAC experiment in section 3.3.5 with higher concentrations of F901318.

- Does F901318 work synergistically with caspofungin, chitin synthase inhibitors (Nikkomycin Z) and/or calcineurin inhibitors (FK506)?

Use live-cell, time-lapse microscopy with the cytoplasmic-GFP strain to observe induction of cell death (15) *in presence of both drugs, either added at the same time or in sequence.*

- How is the cell wall remodeled in response to F901318 treatment?

Investigate content of other cell wall components using fluorescent dyes/lectins. Investigate the mechanism behind chitin increase by utilizing chitin synthase mutants and inhibitors. Measure cell wall thickness from either TEM images or high-resolution fluorescence microscopy. Measure pressure on the cell wall either by utilization of a pressure probe or microchambers (7–9).

- Is increased septation important for survival in presence of F901318?

Treat hyphae with a septation inhibitor such as hydroxyurea prior to adding F901318, alternatively use a rho4 mutant, in which septation is decreased (10–12).

- Does the vacuolar volume play a role in F901318 induced swelling?

Treat vacuole development mutants in presence of the drug and measure volume of the cytosol and the vacuoles as described in this thesis.

- Are F901318-treated hyphae arrested in the G1 phase of the cell cycle?

Flow cytometry analysis of the cell cycle using a dye such as PI or Vybrant (Molecular Probes).

- Is F901848 taken up via facilitated diffusion utilizing permeases?

As it has been suggested that utilization of permeases for drug import is important in fungal species, it will be interesting to investigate whether the fluorescent F901318 analogue F901848 is also imported with the help of permeases. This could be studied in permease knock-out strains.

- Does F901318 affect transport?

Results in chapters 5 and 6 seemed to suggest that F901318 affects uptake of certain compounds. Larger molecules such as MitoTracker Red FM and F901848 were being taken up very poorly in 24 h F901318-treated hyphae. As pyrimidines are also required for phospholipid synthesis, it is possible that the cell membrane is affected by F901318 treatment. To further study this, the cell membrane composition could be analyzed by utilizing probes for lipids and membranes (Molecular Probes).

- Is F901318 retained within the hyphae, even after washing out the drug from the media?

As a follow up from section 3.3.6, where it was found that hyphae cannot fully recover after F901318 exposure. Perhaps after washing out the drug from the media, F901318 is retained in the hyphae. To investigate this, hyphae could be treated with the fluorescent analogue F901848, then wash it out and measure the fluorescence intensity.

- Does F901318 induce apoptosis?

Investigate apoptotic markers such as DNA cleavage (TUNEL assay) and internalization of phosphatidylserine (Annexin V) (16).

- Are the vesicle-like structures observed in F901318-treated hyphae autophagosomes?

Study co-localization of the vesicles in a GFP-ATG8 strain (17).

- Does F901318 cause changes in the mitochondrial membrane potential?

Use Rhodamine-123 or another dye, such as JC-1 to quantify fluorescence intensity, which correlates with the MMP.

- Does F901318 cause an increase in the intracellular calcium concentration?

Repeat aequorin measurements over a longer period of time. Use GCaMP imaging to observe whether calcium spikes are observed prior to lysing.

- Do the effects exerted by F901318 *in vitro*, also occur during infection?

Imaging human cell lines that have been infected with A. fumigatus and treated with F901318 could be utilized.

7.3 References

1. Denning DW, Hope WW. 2010. Therapy for fungal diseases: opportunities and priorities. Trends in microbiology 18:195–204.
2. Denning DW. 2003. Echinocandin antifungal drugs. The Lancet 362:1142–1151.
3. Oliver JD, Sibley GEM, Beckmann N, Dobb KS, Slater MJ, McEntee L, du Pré S, Livermore J, Bromley MJ, Wiederhold NP, Hope WW, Kennedy AJ, Law D, Birch M. 2016. F901318 represents a novel class of antifungal drug that inhibits dihydroorotate dehydrogenase. PNAS 113:12809–12814.
4. Gow NAR, Latge J-P, Munro CA. 2017. The Fungal Cell Wall: Structure, Biosynthesis, and Function. Microbiology Spectrum 5.
5. Popolo L, Gualtieri T, Ragni E. 2001. The yeast cell-wall salvage pathway. Medical mycology 39 Suppl 1:111–21.
6. Ries LNA, Rocha MC, de Castro PA, Silva-Rocha R, Silva RN, Freitas FZ, de Assis LJ, Bertolini MC, Malavazi I, Goldman GH. 2017. The *Aspergillus fumigatus* CrzA Transcription Factor Activates Chitin Synthase Gene Expression during the Caspofungin Paradoxical Effect. mBio 8:e00705-17.
7. Bastmeyer M, Deising HB, Bechinger C. 2002. Force exertion in fungal infection. Annu Rev Biophys Biomol Struct 31:321–41.
8. Minc N, Boudaoud A, Chang F. 2009. Mechanical Forces of Fission Yeast Growth. Current Biology 19:1096–1101.
9. Davì V, Minc N. 2015. Mechanics and morphogenesis of fission yeast cells. Current opinion in microbiology 28:36–45.
10. Dichtl K, Samantaray S, Aimanianda V, Zhu Z, Prévost M-C, Latgé J-P, Ebel F, Wagener J. 2015. *Aspergillus fumigatus* devoid of cell wall β-1,3-glucan is viable, massively sheds galactomannan and is killed by septum formation inhibitors. Molecular Microbiology 95:458–471.
11. Dichtl K, Helmschrott C, Dirr F, Wagener J. 2012. Deciphering cell wall integrity signalling in *Aspergillus fumigatus*: identification and functional characterization of cell wall stress sensors and relevant Rho GTPases. Molecular microbiology 83:506–19.
12. Si H, Justa-Schuch D, Seiler S, Harris SD. 2010. Regulation of septum formation by the Bud3-Rho4 GTPase module in *Aspergillus nidulans*. Genetics 185:165–76.
13. Kontoyiannis DP, Lewis RE, Osherov N, Albert ND, May GS. 2003. Combination of caspofungin with inhibitors of the calcineurin pathway attenuates growth *in vitro* in *Aspergillus* species. The Journal of antimicrobial chemotherapy 51:313–6.
14. Hope WW, McEntee L, Livermore J, Whalley S, Johnson A, Farrington N, Kolamunnage-Dona R, Schwartz J, Kennedy A, Law D, Birch M, Rex JH. 2017. Pharmacodynamics of the Orotomides against *Aspergillus fumigatus*: New Opportunities for Treatment of Multidrug-Resistant Fungal Disease. mBio 8:e01157-17.

15. Moreno-Velásquez SD, Seidel C, Juvvadi PR, Steinbach WJ, Read ND. 2017. Caspofungin-Mediated Growth Inhibition and Paradoxical Growth in *Aspergillus fumigatus* involve Fungicidal Hyphal Tip Lysis Coupled with Regenerative Intrahyphal Growth and Dynamic Changes in β-1,3-Glucan Synthase Localization. Antimicrobial Agents and Chemotherapy AAC.00710-17.
16. Sharon A, Finkelstein A, Shlezinger N, Hatam I. 2009. Fungal apoptosis: function, genes and gene function. FEMS Microbiology Reviews 33:833–854.
17. Pinar M, Pantazopoulou A, Peñalva MA. 2013. Live-cell imaging of *Aspergillus nidulans* autophagy: RAB1 dependence, Golgi independence and ER involvement. Autophagy 9:1024–43.

APPENDIX

APPENDIX A

This PhD thesis was written in an alternative format, with each results chapter written in journal paper style. This appendix describes some additional experiments that were performed during this PhD project, but were not included in the results chapters/papers.

A1 Viability dyes

A1.1 Introduction

Chapter 3 describes how the viability of *A. Fumigatus* after exposure to F901318 was assessed by staining with the fluorescent viability dye DiBAC (Figure 3.5). This dye was chosen after testing a total of four viability dyes, which besides DiBAC were Evans blue, Propidium Iodide (PI) and FUN-1. Evans blue is a (non-fluorescent) viability dye that is not able to enter living cells. It is only able to enter cells with a permeable membrane, where it then stains the cytoplasm blue. FUN-1 is a two-color fluorescent viability dye specifically for yeast and fungi, which has the added advantage that it stains both live and dead cells, but in different patterns. Live cells are stained green with red vacuolar structures, dead cells are stained yellow-green. PI is a red fluorescent dye that is only able to enter permeable cells, where it stains nucleic acids.

A1.2 Results

Conidia were pre-grown for 16 h in VMM and the resulting hyphae were then treated with either 2 μg/ml Amphotericin B or left untreated as a control. After 24 h of treatment, hyphae were stained with Evans blue (Figure A1A). Untreated hyphae were not stained by Evans blue, while parts of treated hyphae were stained. However, the staining pattern did not appear to be uniform; some hyphae were stained more intense than other, although no apparent difference in viability was observed. Furthermore, swollen but viable hyphae were stained by Evans blue, whereas hyphae that had lysed were not stained, although these were clearly killed. Additionally, hyphae that were killed by treatment with the fungicidal agent Amphotericin B were also not clearly stained.

For FUN-1 staining, conidia were pre-grown for 8 h in VMM to obtain germ tubes which were then treated with 0.15 µg/ml F901318 and after 24 h of treatment, FUN-1 was applied (Figure A1B). Viable germ tubes were stained green with clear red vacuolar structures. However, the dye was not retained in lysed germ tubes; hardly any fluorescence was observed in lysed germ tubes.

PI was applied to hyphae that had been treated with F901318 for 72 h (Figure A1C). Viable compartments of the hyphae were not stained by PI, as expected. Compartment that had lysed were partially stained, but especially the released cellular contents were clearly stained by PI.

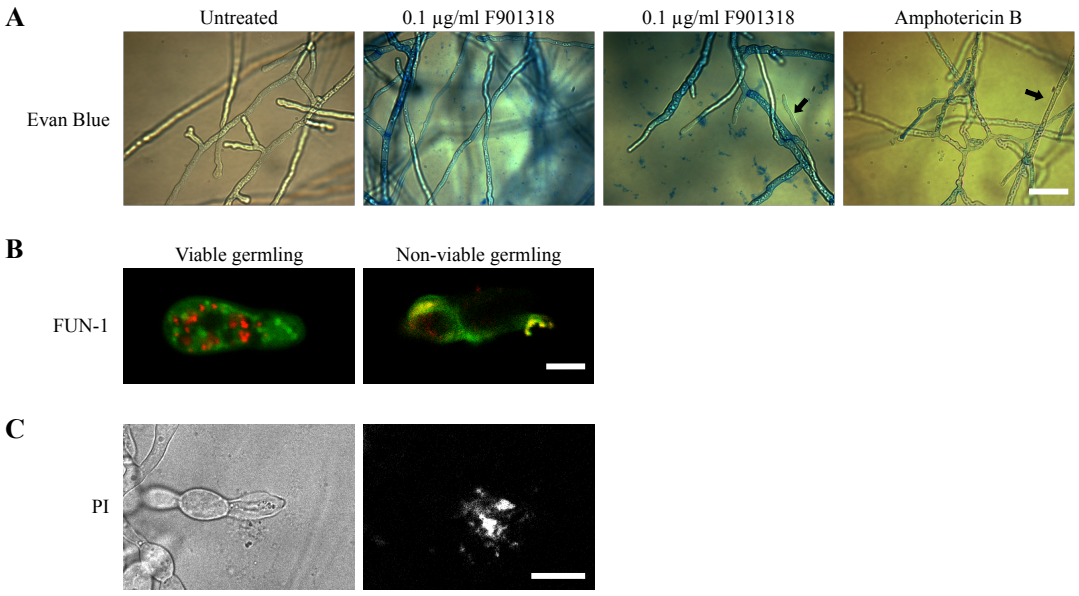

Figure A1 Microscopy images showing the staining of patterns of different viability dyes. A) Evans blue. Bar = 20 µm. B) FUN-1 Bar = 5 µm. C) Propidium Iodide (PI). Bar = 20 µm.

A1.3 Discussion

Different viability dyes were tested for quantification of viability after F901318 treatment. F901318 causes cell lysis which consequently leads to the release of cellular contents. Hyphae without any cellular content are more difficult to stain by viability dyes, this was especially evident with Evans blue and FUN-1 staining. The staining pattern for Evans blue was not consistent; viable compartment could also be stained, whereas not all dead compartments were stained. Although FUN-1 has the added advantage that it stains both live and dead cells in a different pattern, fluorescence was significantly reduced in lysed cells. Therefore, both Evans blue and FUN-1 were not considered to be suitable for quantification of viability after F901318 exposure. PI and

DiBAC gave a similar staining pattern, staining especially the released cellular contents. As DiBAC stained the actual lysed hyphae slightly better and was generally brighter than PI, this dye was chosen to quantify the viability of *A. fumigatus* after F901318 exposure (Figure 3.5).

A2 Cell wall

A2.1 Introduction

In Chapter 4, the cell wall structure was studied by quantifying the fluorescence intensity of CFW (chitin) and Aniline blue (1,3-ß-glucan). Aniline blue fluorescence was reduced specifically at the tip, while CFW fluorescence was significantly increased in general. The cell wall structure was also studied with lectins that bind to carbohydrate proteins. Wheat germ agglutinin (WGA) and Concanavalin A (ConA) bind to chitin (surface) and mannose respectively. The lectins used were conjugated to fluorescent proteins for visualization, WGA with tetramethylrhodamine and ConA with fluorescein.

A2.2 Results

WGA-orange fluorescence intensity was significantly increased in the F901318 treated hyphae. ConA fluorescence intensity also appeared to be increased, however, this result was not significant.

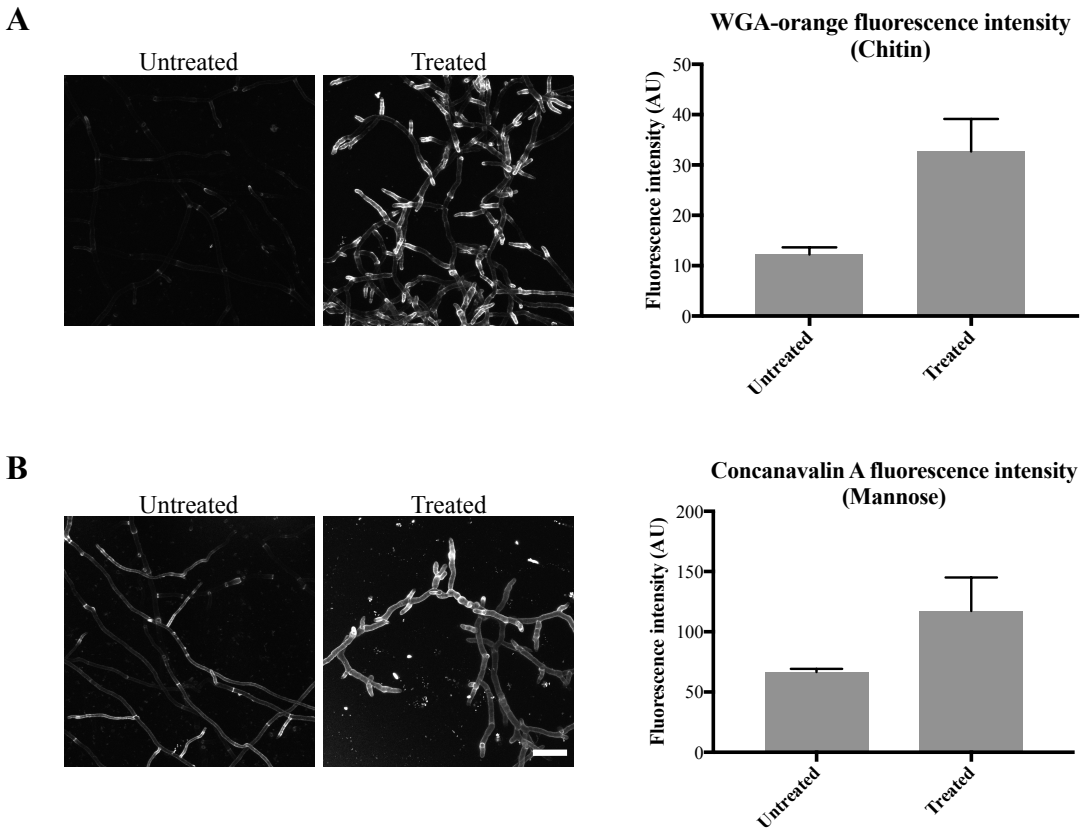

Figure A2 Fluorescence intensity of cell wall lectins WGA-orange and Concanavalin A. Bar = 40 μm.

A2.3 Discussion

As was observed with CFW staining, WGA-orange fluorescence intensity was increased in the hyphae treated for 24 h with F901318, confirming that chitin content in the cell wall is upregulated upon exposure to the drug. ConA binds to mannose and although it appears as if the fluorescence intensity in the treated hyphae is increased, the difference is not significant. The ConA staining was repeated only twice, so it might be interesting to repeat this staining to verify the fluorescence intensity. It may also be useful to determine cell wall thickness.

APPENDIX B

During this PhD project, I was a co-author on a paper titled "F901318 represents a novel class of antifungal drug that inhibits dihydroorotate dehydrogenase" by my supervisor Dr. Jason Oliver. The paper was published in *Proceedings of the National Academy of Sciences* (PNAS) in 2016. A copy of this paper is included in this appendix.

F901318 represents a novel class of antifungal drug that inhibits dihydroorotate dehydrogenase

Jason D. Oliver[a,1], Graham E. M. Sibley[a], Nicola Beckmann[a], Katharine S. Dobb[a], Martin J. Slater[b], Laura McEntee[c], Saskia du Pré[a], Joanne Livermore[c], Michael J. Bromley[a,2], Nathan P. Wiederhold[d], William W. Hope[c], Anthony J. Kennedy[a], Derek Law[a], and Mike Birch[a]

[a]F2G Ltd., Manchester M30 0LX, United Kingdom; [b]Cresset, Litlington SG8 0SS, United Kingdom; [c]Antimicrobial Pharmacodynamics and Therapeutics, Department of Molecular and Clinical Pharmacology, University of Liverpool, Liverpool L69 3GE, United Kingdom; and [d]Fungus Testing Laboratory, Departments of Pathology and Medicine/Infectious Diseases, University of Texas Health Science Center at San Antonio, San Antonio, TX 78229

Edited by Carl F. Nathan, Weill Medical College of Cornell University, New York, NY, and approved September 27, 2016 (received for review May 24, 2016)

There is an important medical need for new antifungal agents with novel mechanisms of action to treat the increasing number of patients with life-threatening systemic fungal disease and to overcome the growing problem of resistance to current therapies. F901318, the leading representative of a novel class of drug, the orotomides, is an antifungal drug in clinical development that demonstrates excellent potency against a broad range of dimorphic and filamentous fungi. In vitro susceptibility testing of F901318 against more than 100 strains from the four main pathogenic *Aspergillus* spp. revealed minimal inhibitory concentrations of ≤0.06 μg/mL—greater potency than the leading antifungal classes. An investigation into the mechanism of action of F901318 found that it acts via inhibition of the pyrimidine biosynthesis enzyme dihydroorotate dehydrogenase (DHODH) in a fungal-specific manner. Homology modeling of *Aspergillus fumigatus* DHODH has identified a predicted binding mode of the inhibitor and important interacting amino acid residues. In a murine pulmonary model of aspergillosis, F901318 displays in vivo efficacy against a strain of *A. fumigatus* sensitive to the azole class of antifungals and a strain displaying an azole-resistant phenotype. F901318 is currently in late Phase 1 clinical trials, offering hope that the antifungal armamentarium can be expanded to include a class of agent with a mechanism of action distinct from currently marketed antifungals.

antifungal drug | *Aspergillus fumigatus* | mechanism of action | dihydroorotate dehydrogenase

A recent estimate puts the annual death toll from serious fungal infections at 1.5 million (1). As one of the four greatest killers, *Aspergillus* species are opportunistic human pathogens, particularly affecting immunocompromised persons, such as transplant recipients and those with hematologic malignancies. Invasive aspergillosis has a high mortality (30–90%) and is estimated to affect more than 200,000 people annually. Other diseases caused by *Aspergillus* species, including allergic bronchopulmonary aspergillosis (2) and chronic pulmonary aspergillosis (3), have a significant global impact, affecting millions of patients.

There has been a dearth of new drug classes developed to treat systemic fungal infections arriving in the clinic, with the most recent being the echinocandins, introduced in 2001. Only three other classes of antifungal drugs are currently available for the treatment of invasive fungal disease: polyenes (amphotericin B), azoles (e.g., voriconazole, posaconazole, and the recently licensed isavuconazole), and flucytosine (4). These agents work via a limited range of cellular targets. Echinocandins, such as caspofungin, inhibit β-(1,3)-glucan synthase, exploiting the most striking difference between the fungal cell and its human counterpart—the cell wall. Two antifungal drug classes target the cell membrane: azoles inhibit ergosterol biosynthesis, and polyenes disrupt fungal membranes via ergosterol binding. Flucytosine is a pyrimidine analog, converted to 5-fluorouracil within fungal cells, that disrupts DNA and RNA synthesis; however, owing to rapid development of resistance, it is used primarily in combination therapy.

Issues exist with current therapies, including overt toxicity, drug–drug interactions, variable pharmacokinetics, and increasing levels of drug resistance (5, 6). In particular, the development of resistance to the azole class of antifungals is concerning, because they are currently the sole orally available antifungal agent for the treatment of aspergillosis (7). Azole-resistant clinical isolates of *Aspergillus fumigatus* have been observed and isolated from patients worldwide, including Europe, the United States, Asia, Africa, Australia, and the Middle East (8, 9). Apparently exacerbated by the environmental use of azole fungicides in agriculture (10), reported rates of azole resistance have approached 30% at certain sites in Europe, with rates outside Europe varying between 0.6% and 11.2% (9).

Results

Discovery of F901318. With the aim of identifying new antifungal chemistries, a library of 340,292 small molecules was screened in vitro against *A. fumigatus*, and multiple chemical series with antifungal activity were identified. The initial hits in one such series, originally termed the "F3 series," were developed by a medicinal chemistry program that was driven by classical structure–activity relationships based on in vitro activity. This series was characterized by excellent in vitro potency against *Aspergillus* spp., but was devoid of activity against *Candida* spp. This unusual

Significance

New antifungal drugs that act via novel mechanisms are urgently needed to combat the high mortality of invasive fungal disease and the emergence of resistance to existing therapies. We describe the discovery, structure, activity, and mechanism of action of F901318, a new antifungal agent. A member of a novel class of antifungals, the orotomides, F901318 acts via inhibition of dihydroorotate dehydrogenase, an enzyme of de novo pyrimidine biosynthesis. F901318 is currently in clinical development for the treatment of invasive aspergillosis.

Author contributions: J.D.O., G.E.M.S., M.J.S., M.J.B., N.P.W., W.W.H., A.J.K., D.L., and M.B. designed research; J.D.O., G.E.M.S., N.B., K.S.D., M.J.S., L.M., S.d.P., J.L., N.P.W., and D.L. performed research; M.J.B. contributed new reagents/analytic tools; J.D.O., G.E.M.S., N.B., M.J.S., J.L., N.P.W., W.W.H., A.J.K., D.L., and M.B. analyzed data; and J.D.O., G.E.M.S., M.J.S., N.P.W., W.W.H., A.J.K., D.L., and M.B. wrote the paper.

Conflict of interest statement: J.D.O., G.E.M.S., N.B., S.d.P., A.J.K., D.L., and M.B. are employees of F2G Ltd. K.S.D. and M.J.B. are ex-employees of F2G Ltd. J.D.O., G.E.M.S., K.S.D., A.J.K., D.L., and M.B. are shareholders of F2G Ltd. W.W.H. has received research funding from Pfizer, Gilead, Astellas, AiCuris, and F2G, and has acted as a consultant and/or given talks for Pfizer, Basilea, Astellas, F2G, Nordic Pharma, Mayne Pharma, and Pulmocide. G.E.M.S., D.L., J.D.O., and M.B. are listed as inventors on patent WO2009130481. J.D.O., M.J.B., G.E.M.S., and M.B. are listed as inventors on patent WO200913379.

This article is a PNAS Direct Submission.

[1]To whom correspondence should be addressed. Email: joliver@f2g.com.

[2]Present address: Manchester Fungal Infection Group, Institute of Inflammation and Repair, University of Manchester, Manchester M13 9NT, United Kingdom.

This article contains supporting information online at www.pnas.org/lookup/suppl/doi:10.1073/pnas.1608304113/-/DCSupplemental.

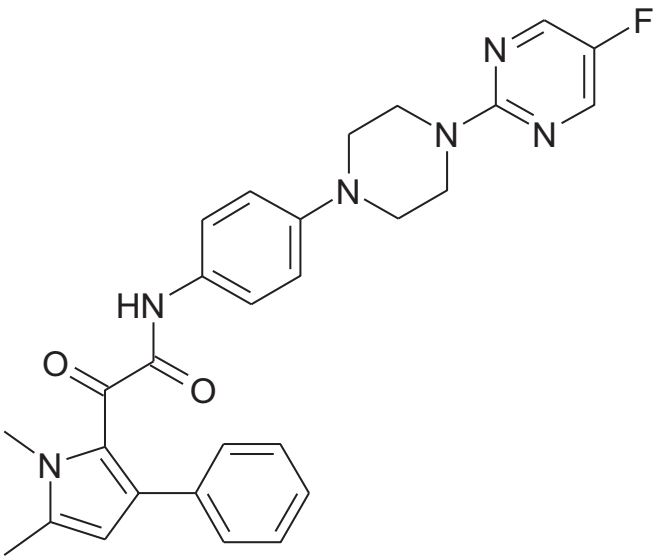

Fig. 1. Structure of F901318.

pattern perhaps explains why similar chemicals have not been found previously. Typically, antifungal screens have depended on first finding activity against *Candida*. Modifications to improve physicochemical properties, antifungal potency, pharmacokinetics, ADMET (absorption, distribution, metabolism, excretion, and toxicity) properties, in vivo efficacy in infection models, and toxicology have led to the development of F901318 (Fig. 1). Antifungal susceptibility testing of F901318 using standardized techniques demonstrated its potent activities against clinical isolates of aspergilli, with minimum inhibitory concentrations (MICs) of <0.1 μg/mL against multiple strains of *A. fumigatus*, *Aspergillus terreus*, *Aspergillus niger*, and *Aspergillus flavus*, including isolates resistant to other antifungal agents (Table 1).

Mechanism of Action Screen. Initially, owing to the method of discovery, the mechanism of action of this series was unknown. A combination of microbiological, genetic, and biochemical approaches were used to identify the target of this drug series. A genetic screen, similar to a multicopy suppressor screen, was performed to identify genes that, when present in multiple copies, provided resistance to F901318. This approach was previously validated for the antifungal drugs itraconazole and terbinafine, by demonstrating that the presence of additional copies of cytochrome P450 C-14 lanosterol α-demethylase and squalene epoxidase, respectively, led to resistance to those agents (11, 12). In the present study, *Aspergillus nidulans* spores that had been transformed with an *A. nidulans* genomic library carried by the autonomously replicating plasmid pAMA1 were exposed to F901318. Four independent resistant clones were obtained, pAMA1 DNA was isolated, and the genomic DNA insert was sequenced. All resistant clones contained inserts that mapped to the same region of chromosome I (Fig. S1*A*). Although sequence data from five genes was retrieved, only one gene—ANIA_05909—was intact in all four genomic fragments. This gene, named *pyrE* in *Aspergillus* spp., encodes the pyrimidine biosynthesis enzyme dihydroorotate dehydrogenase (DHODH; EC 1.3.5.2).

To confirm that extra copies of *pyrE* led to F901318 resistance, the recovered plasmid pAMA1_18.1 was treated with a bacterial transposon (Tn5) to disrupt either *pyrE* or a neighboring gene, ANIA_05910, and the resulting plasmids were transformed into *A. nidulans*. Strains carrying the intact pAMA1_18.1 or the ANIA_05910 disruptant exhibited resistance to F901318; however, on disruption of *pyrE*, the strain returned to wild-type (WT) levels of susceptibility to F901318 (Fig. S1*B*). This finding confirmed that extra copies of the gene encoding DHODH were responsible for the resistance to F901318, implicating DHODH as the target of the drug.

DHODH Is the Target of F901318. DHODH is an oxidoreductase that catalyzes the fourth step of the pyrimidine biosynthesis pathway (Fig. S2), the conversion of dihydroorotate to orotate. Confirmation that the drug disrupts pyrimidine biosynthesis was obtained after the addition of exogenous pyrimidines (uridine and uracil) to the media during susceptibility testing. A reversal of the antifungal effect of F901318 on *A. fumigatus* was observed, but only at millimolar concentrations of pyrimidines (5 mM and above; Fig. S3). Interestingly, human serum contains low levels of pyrimidines, estimated to be ∼15 μM (13), which are insufficient to reverse the effect of F901318 on *A. fumigatus* in vivo. Indeed, mutants of *A. fumigatus* (14), *Candida albicans* (15), *Histoplasma capsulatum* (16), and *Cryptococcus neoformans* (17), which are disrupted in pyrimidine biosynthesis, have exhibited attenuated virulence in animal models of infection, indicating that targeting pyrimidine synthesis is a valid antifungal strategy.

Biochemical evidence confirming that the target of F901318 was DHODH was obtained from in vitro enzyme assays that were set up with recombinant *A. fumigatus* DHODH using 2,6-dichloroindophenol as a redox indicator. F901318 inhibited *A. fumigatus* DHODH in a dose-dependent manner, with an IC_{50} of 44 ± 10 nM (n = 11; Fig. 2). DHODH is also present in mammals, although there is a low overall identity to *Aspergillus* DHODH (∼30%; Fig. S4). A known inhibitor of human DHODH, teriflunomide (18), which is used to treat multiple sclerosis in man, did not inhibit *A. fumigatus* DHODH in vitro. Species selectivity of F901318 was confirmed in an assay in which little inhibition of human DHODH was observed, whereas teriflunomide inhibited human DHODH, as expected. In fact, the IC_{50} value for F901318 against human DHODH was not reached at 100 μM, the highest concentration used in these experiments, indicating that F901318 was

Table 1. Antifungal potency of F901318 and other antifungal drugs against the major *Aspergillus* species

Drug	Parameter	*A. fumigatus* (n = 55)	*A. terreus* (n = 21)	*A. flavus* (n = 19)	*A. niger* (n = 19)
F901318	MIC mean, μg/mL	0.029	0.014	0.021	0.031
	MIC range, μg/mL	0.008–0.06	0.004–0.03	0.015–0.06	0.015–0.06
Amphotericin B	MIC mean, μg/mL	1.55	2.07	1.39	0.46
	MIC range, μg/mL	0.5–2	1–4	1–2	0.25–1
Caspofungin	MEC* mean, μg/mL	0.096	0.112	0.06	0.062
	MEC* range, μg/mL	0.06–0.12	0.06–0.12	0.06	0.06–0.12
Voriconazole	MIC mean, μg/mL	0.69	0.59	0.96	0.77
	MIC range, μg/mL	0.25–16	0.25–1	0.5–1	0.5–16

The MICs (in μg/mL) of F901318, amphotericin B, and voriconazole were determined for the *Aspergillus* spp. indicated (n, number of different strains tested). *For caspofungin, the MEC is shown, because growth is not completely inhibited with this drug. Data are displayed as the geometric mean of the MICs and the range of MIC from lowest to highest for the strains of a particular species.

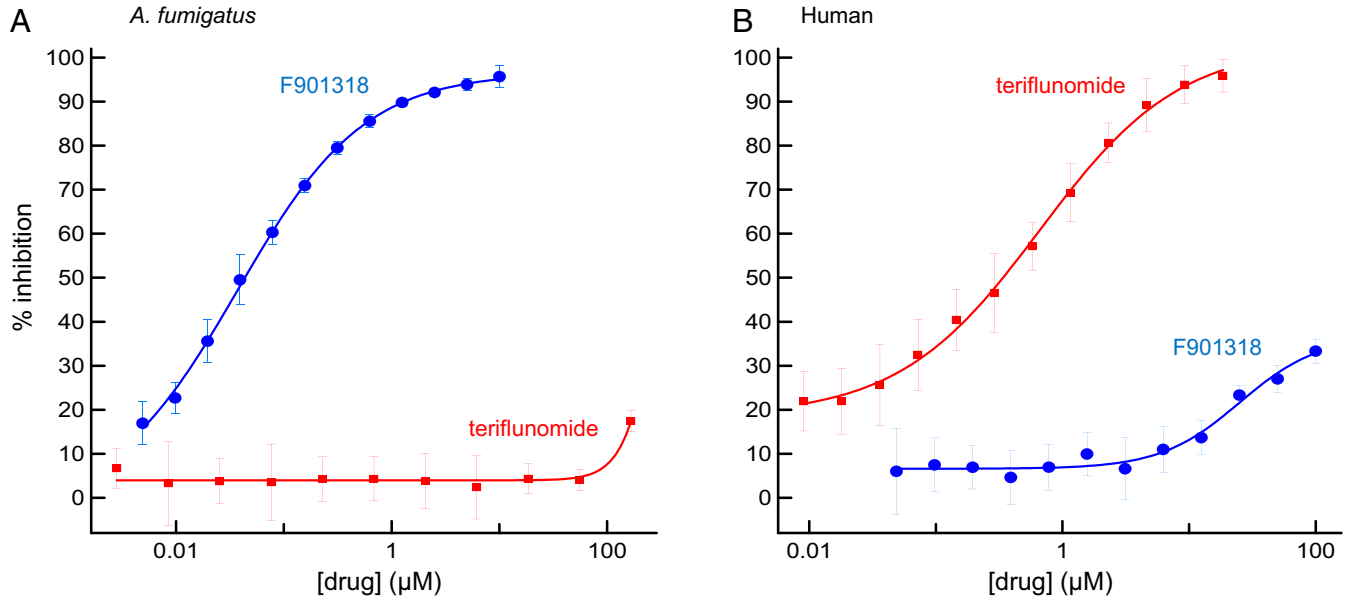

Fig. 2. F901318 inhibits *A. fumigatus* DHODH in vitro. Recombinant *A. fumigatus* DHODH (*A*) and human DHODH (*B*) were incubated in the presence and absence of varying concentrations of F901318 and teriflunomide. The activity of the enzymes was measured for each drug concentration, and the percent inhibition compared with no drug controls was calculated.

>2,200-fold more potent against the *A. fumigatus* enzyme. Thus, fungal DHODH was confirmed as the target of F901318, and despite the presence of a mammalian version of the enzyme, no target-based toxicity was predicted. On elucidation of the mechanism of action, the F3 series was renamed the orotomides, combining the mechanism (dihydroorotate) with the chemistry (α-ketoamide).

Further enzyme kinetic experiments revealed that F901318 is a reversible inhibitor of *A. fumigatus* DHODH (Fig. S5*A*) and is a competitive inhibitor with respect to the ubiquinone (coenzyme Q) cofactor, which functions as an electron acceptor in the reaction (Fig. S5*B*). This latter property is perhaps not unexpected, given that structural studies have shown that known inhibitors of human DHODH (teriflunomide and brequinar) (19) and the *Plasmodium falciparum* enzyme (DSM265) (20) bind in a region of the protein predicted to be a channel through which the ubiquinone enters the molecule from the inner mitochondrial membrane.

Structural Insights of F901318 Binding to *A. fumigatus* DHODH. In the absence of a crystal structure, we investigated the binding of F901318 to *A. fumigatus* DHODH by creating a homology model of *A. fumigatus* DHODH (Fig. S6) using the structural information provided by other class 2 DHODH enzymes, including the structure of human DHODH (19). F901318 and other members of the series were used to identify a likely binding mode. Key residues for binding were identified (Fig. 3*A*). Validation of the importance of two of these residues was obtained by mutagenesis of *C. albicans* DHODH. The WT *C. albicans* DHODH was not inhibited by F901318, but mutation of two residues, Phe_{162} and Val_{171}, to the residues predicted to occupy the same positions in the *A. fumigatus* enzyme, Val_{200} and Met_{209}, respectively, created a mutant *C. albicans* DHODH that was inhibited by F901318 (Fig. 3*B*). The IC_{50} of the mutant *C. albicans*_V_{162}_M_{171} was still ∼40-fold higher than the IC_{50} of F901318 against the *A. fumigatus* enzyme, indicating the existence of other important differences in DHODH between the two species; however, both of these residues are clearly important for inhibition. These data, along with the observed competition between F901318 and coenzyme Q in the in vitro assay, suggest that the orotomides bind in the "quinone channel," where ubiquinone enters the enzyme from the inner mitochondrial membrane, preventing reoxidation of the dihydroflavin mononucleotide ($FMNH_2$) cofactor essential for the reaction to proceed (Fig. S2).

Spectrum, Resistance, and in Vivo Efficacy of F901318. Although we observed no activity against *Candida* spp. and the zygomycetes in antifungal susceptibility testing, F901318 displayed excellent potency against a broad range of pathogenic filamentous and dimorphic fungi, including *Penicillium* spp., *Coccidiodes immitis*, *H. capsulatum*, *Blastomyces dermatitidis*, *Fusarium* spp., and the difficult-to-treat *Scedosporium* spp. This spectrum appears to be sequence-driven, given that the sensitive organisms were found to be grouped together in a phylogenetic analysis of DHODH (Fig. S7). This finding is consistent with observations that other DHODH inhibitors exhibit specificity of action owing to interspecies variations in the architecture of the hydrophobic channel in which the inhibitors are predicted to bind (19–21). Thus, the unique spectrum of F901318 is a reflection of the structure of the target, DHODH, and the binding mode of the orotomides.

We investigated the resistance to F901318 in *A. fumigatus* by repeated exposure to a concentration gradient of the drug on an agar plate and selection from the margins of growth. This was carried out for 50 passages, with no change in the MIC observed for the first 40 passages and only a modest increase thereafter (Fig. S8). In contrast, voriconazole exhibited an increase in the MIC between 10 and 15 passages. Based on these results, it appears that F901318 resistance is not easily induced in *A. fumigatus*.

Pharmacokinetic studies in mice have identified good distribution of F901318 to tissues including the kidney, liver, and lung, with detection in the brain, albeit at lower levels, suggesting that the drug reaches key sites of infection. The efficacy of F901318 was demonstrated in a neutropenic murine model of invasive pulmonary aspergillosis. After infection with a well-characterized *A. fumigatus* strain (NIH 4215), survival was significantly improved by F901318 treatment (Fig. 4*A*). Treatment with the triazole drug posaconazole also increased survival after infection with this strain.

Mutations in the gene encoding the target molecule of the azole class of antifungal drugs, *Cyp51A*, that cause resistance have been identified. Several azole-resistant strains of *A. fumigatus* carry a combination of a tandem repeat in the promoter and a point

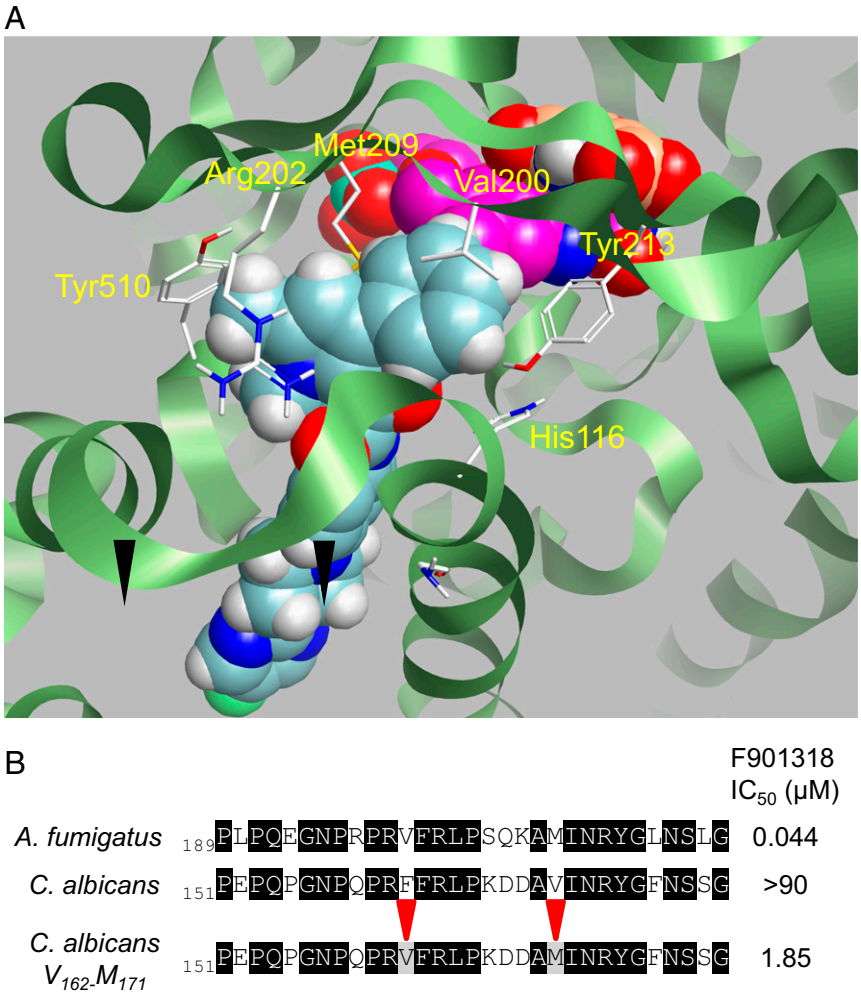

Fig. 3. (*A*) Binding of F901318 to *A. fumigatus* DHODH. A homology model of *A. fumigatus* DHODH was created, and the binding mode of F901318 (cyan) was estimated. The product orotate (orange) and the cofactor flavin mononucleotide (FMN; magenta) are also shown. Residues predicted to be close to the molecule are highlighted. (*B*) F901318 inhibits a mutant version, but not the WT version, of *C. albicans* DHODH. Recombinant *C. albicans* DHODH residues Phe_{162} and Val_{171} were mutated to Val and Met, respectively (their predicted equivalents in *A. fumigatus* DHODH). The IC_{50} of F901318 inhibition of the WT and mutant DHODH proteins is displayed in the right-hand column (*A. fumigatus* IC_{50}, $n = 11$, SD = 0.01 μM; WT *C. albicans* IC_{50}, $n = 7$, all seven replicates had an IC_{50} >90 μM; *C. albicans_V162_M171* IC_{50}, $n = 7$, SD = 0.91 μM).

mutation in the coding sequence. One such strain, *A. fumigatus* F16216, carrying the TR34/L98H mutation of *Cyp51A*, has proven to be resistant to multiple azole drugs, including itraconazole, voriconazole, and posaconazole (22). In vitro, *A. fumigatus* F16216 displayed no resistance to F901318, with an MIC of 0.03 μg/mL, which is comparable to the data presented in Table 1. In vivo, in the pulmonary aspergillosis model, *A. fumigatus* F16216 caused an infection that cannot be treated with posaconazole (Fig. 4*B*); however, F901318 therapy led to a significant increase in survival in this severe model, demonstrating that the different mechanism of action of the orotomides enables F901318 to overcome azole resistance caused by *Cyp51A* mutations.

Preclinical safety pharmacology and toxicology studies of F901318 have supported the progression and evaluation of this antifungal in Phase 1 oral and i.v. single and repeated dose trials.

Discussion

As highlighted by Denning and Bromley (23), the antifungal pipeline has failed to produce new antifungal drugs with mechanisms of action different from those of existing classes in the years since caspofungin was licensed in 2001. Many potential antifungal targets have been investigated, but translating these early stage projects into clinical candidates has proven elusive. This difficulty has mirrored the issues with target-based screening encountered in the antibacterial arena (24). In fact, a review of new mechanism, first-in-class medicines approved by the US Food and Drug Administration between 1999 and 2008 revealed that target-based screens were responsible for the discovery of only 3 of 10 drugs for infectious disease, with the majority discovered by phenotypic screening (i.e., "whole-cell screens" for antibiotics/antifungals) (25). The orotomides were discovered via a whole-cell screening approach, providing hits that were known to have antifungal activity from the start, but with no knowledge of mechanism of action. This classical approach was coupled with a genetic screen to identify the target of the drug, DHODH. A recent review of antifungal drug discovery suggested that similar approaches, taking advantage of genetic tools such as haploinsufficiency strain collections and new technologies such as next-generation sequencing, may accelerate the translation of antifungal chemistries toward the clinic (26).

Pyrimidines are essential to the cell, not just for the synthesis of DNA and RNA, but also for the formation of precursors for lipid and carbohydrate metabolism. For example, synthesis of the cell wall requires UDP-activated sugars at multiple stages, including

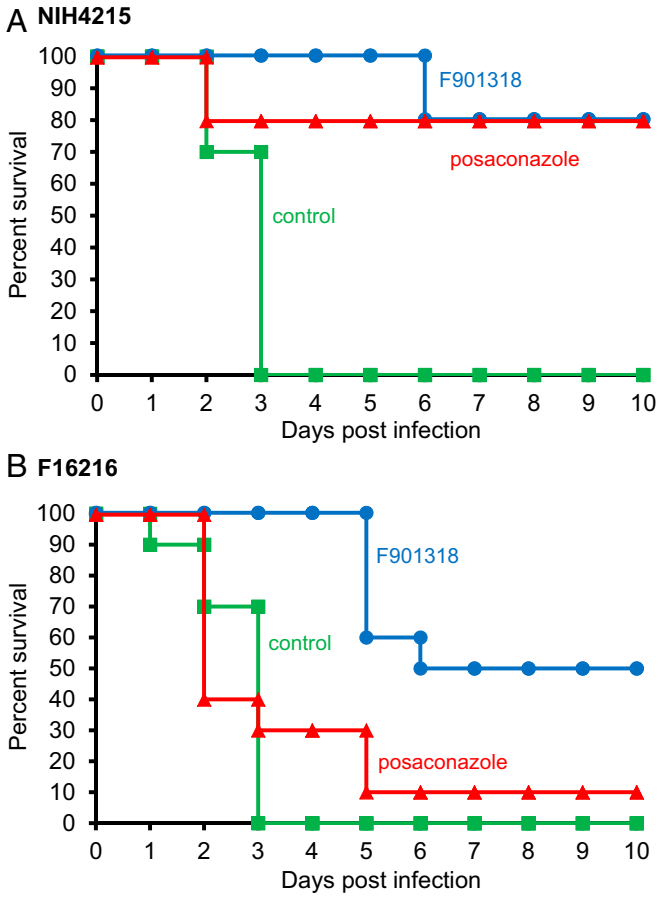

Fig. 4. In vivo efficacy of F901318 in a murine model of *A. fumigatus* infection. Groups of 10 immunosuppressed mice were infected intranasally with *A. fumigatus* NIH 4215 (*A*) or the azole-resistant *A. fumigatus* F16216 (*B*) conidia on day 0. Treatment with F901318 (15 mg/kg i.v., three times daily; blue circles), posaconazole (7.5 mg/kg orally, once daily; red triangles), or control (green squares) was initiated at 6 h postinfection. Kaplan–Meier curves of surviving mice in each group were plotted. After infection with NIH 4215, F901318 treatment significantly improved survival compared with controls ($P < 0.001$, Mantel–Haenszel test). After infection with F16216, F901318 treatment significantly improved survival compared with controls ($P < 0.001$) and compared with posaconazole treatment ($P < 0.005$).

UDP-glucose for β-(1,3)-glucan synthesis. Pyrimidines are synthesized in the de novo pyrimidine biosynthesis pathway (Fig. S2), in which DHODH is a key enzyme, but they also can be scavenged by fungi from the environment via the salvage pathway. The pyrimidine salvage pathway appears to be inefficient for *A. fumigatus*, however (Fig. S3). In animal models of infection, pyrimidine biosynthesis mutants from several pathogenic fungi are highly attenuated for virulence, including studies on *A. fumigatus* (14), *C. albicans* (15), *H. capsulatum* (16), and *C. neoformans* (17). In *Saccharomyces cerevisiae*, a *ura3* deletion strain lacking the orotidine-5′-phosphate (OMP) decarboxylase enzyme of pyrimidine biosynthesis was unable to survive in vivo, exhibiting a decrease in the competitive index versus a WT or reconstituted strain observed after just 4 h (27). In *C. albicans*, *URA3* has been commonly used as a selectable marker, but concerns have been raised that in some virulence studies, the ectopic expression of *URA3*, leading to reduced OMP decarboxylase activity, had a greater effect on virulence compared with the disruption of the target gene of interest (28). Thus, the evidence in the literature supports the targeting of pyrimidine biosynthesis as a valid antifungal strategy.

Identifying DHODH as the target of the orotomides has helped explain the spectrum of antifungal activity that we observed. F901318 has activity against numerous pathogenic filamentous and dimorphic fungi, including *Aspergillus* spp., *H. capsulatum*, *Blastomyces dermatitides*, and *C. immitis*, along with the difficult-to-treat *Scedosporium prolificans*. These F901318-susceptible organisms group together on the phylogenetic tree of DHODH (Fig. S7), whereas DHODH from *Candida* spp., *C. neoformans*, and the human and *Plasmodium* enzymes are more distantly related while still classified as class 2 DHODH enzymes. DHODH from the zygomycota, such as *Rhizopus* and *Mucor*, align more closely with class 1A DHODHs, cytosolic enzymes that occur in Gram-positive bacteria and the trypanosomatids that use alternative cofactors, such as fumarate.

DHODH has been suggested as a target for therapy in multiple diverse disease areas, including oncology, rheumatoid arthritis, multiple sclerosis, and infectious diseases caused by such agents as *Plasmodium*, bacteria, and viruses (21, 29). There are currently two marketed agents that have activity against human DHODH: leflunomide for rheumatoid arthritis and teriflunomide for multiple sclerosis. DSM265 is an antimalarial drug targeting plasmodial DHODH that is currently in Phase 2 clinical trials (20); however, to our knowledge, no other human antifungal therapies have progressed with DHODH as a target.

Although at first consideration, the breadth of therapeutic areas for which DHODH has been proposed as a drug target is surprising, in each case limiting the pool of pyrimidines prevents proliferation of a population of cells. In some cases, the host cells are targeted, such as lymphocytes in autoimmune diseases and proliferating cancerous cells in oncology. Alternatively, the DHODH of invading pathogens is targeted to selectively limit the pyrimidine pools of the infective agent. Between these two effects, antiviral action has been reported for human DHODH inhibitors, given that viruses require host pyrimidines for replication (29).

In conclusion, to combat the increasing problem of resistance to existing antifungal therapies, the discovery of new cellular targets for antifungals, along with viable chemistry against these new targets (23), is vitally important. F901318 is an antifungal drug, currently in both intravenous and oral Phase 1 clinical trials (ClinicalTrials.gov identifiers: NCT02142153, NCT02342574, NCT02394483, and NCT02737371), that acts via inhibition of the pyrimidine biosynthesis enzyme DHODH, validating an alternative target for antifungal drug discovery.

Materials and Methods

Primers. The sequences of the primers used in this work are listed in Table S1. Primers were supplied by Eurofins MWG.

Synthesis of F901318. The 2-(1,5-dimethyl-3-phenyl-1H-pyrro-2-yl)-*N*-(4-[4-(5-fluoro-pyrimidin-2-yl-piperazin-1yl]-phenyl)-2-oxo-acetamide (F901318) was prepared as described in *SI Materials and Methods*.

In Vitro Antifungal Susceptibility Testing. MICs of antifungal drugs were determined according to Clinical and Laboratory Standards Institute (CLSI) protocol M38-A2 in RPMI 1640 medium buffered to pH 7.0 with MOPS buffer at 35 °C. For caspofungin, the minimum effective concentration (MEC) was defined as the lowest drug concentration causing abnormal growth (i.e., short-branching hyphae).

Mechanism of Action Screen. An *A. nidulans* genomic library carried on the pRG3-AMA1-NotI vector was obtained from the Fungal Genetic Stock Center. Protoplasts from *pyrG*- strains of *A. nidulans* (A767) were transformed with the genomic library by PEG-mediated transformation. Transformants were exposed to lethal concentrations of F901318 on Vogel's minimal agar (30). Plasmid DNA was extracted from resistant colonies and sequenced.

DHODH Assays. These assays were carried out using recombinant DHODH prepared from *A. fumigatus* cDNA, *C. albicans* gDNA, or, for the human protein, IMAGE clone 6064723 (Geneservice Ltd.) cloned into the vector pET44 (Novagen) minus the N-terminal 88 (*A. fumigatus*), 56 (*C. albicans*), or 28 (human) amino acids. For *C. albicans*, CTG-encoded serines were mutated

to TCG. Further mutations altered Phe_{162} and Val_{171} to become Val and Met to create the mutant protein *C. albicans*_V_{162}_M_{171}. Primers are listed in Table S1, and further methodological details are provided in *SI Materials and Methods*. The assay was conducted as described elsewhere (31).

Homology Modeling of *A. fumigatus* DHODH. Human DHODH [Protein Data Bank (PDB) ID code 1D3G] served as the protein template for construction of the *A. fumigatus* DHODH model. Other DHODH structures from human (PDB ID codes 1PRH, 2PRL, 2PRM, 3G0X, 3KVM, 2WV8, and 2FQI), rat (PDB ID codes 1UUM and 1UUO), *Trypanosoma cruzi* (PDB ID code 2E68), *P. falciparum* (PDB ID codes 3I68, 1ITV, and 3O8A) *Leishmania major* (PDB ID code 3MJY), and *Escherichia coli* (PDB ID code 1F76) also informed the process. Coarse refinement of the structure with Discovery Studio 4.1 (Accelerys) was followed by fine refinement with XEDraw (Cresset). More details of the homology modeling process and ligand binding are provided in *SI Materials and Methods*.

Resistance Testing. *A. fumigatus* 210 conidia were inoculated onto Sabouraud agar (Oxoid) in a 9-cm Petri dish. An 8-mm-diameter circle of agar was removed from the center of the plate to create a well. 100 μL of 500 μg/mL drug was loaded into the well and allowed to diffuse into the agar, creating a concentration gradient. After 4 d of incubation at 35 °C, a zone of inhibition was observed, and conidia were collected from the margins of growth and then used to create the next plate. After every fifth passage, the MIC was determined as described above.

In Vivo Efficacy Testing. All experiments were conducted under U.K. Home Office project license 40/3630 and approved by the University of Liverpool's Animal Welfare Committee. Groups of 10 CD-1 mice were immunosuppressed with 200 mg/kg cyclophosphamide i.p. at 4 d before infection and with cyclophosphamide and 250 mg/kg cortisone acetate s.c. at 1 d before infection. *A. fumigatus* F16216 carries an L98H mutation of *cyp51A* and a 34-bp tandem repeat in the *cyp51A* promoter, leading to resistance to azole drugs (22). Conidia from this strain and from the WT *A. fumigatus* NIH 4215 were administered intranasally on day 0. Treatment with F901318 (15 mg/kg i.v. three times daily) or posaconazole (7.5 mg/kg/day orally) was initiated at 6 h postinfection.

ACKNOWLEDGMENTS. We thank John Rex, Richard White, and Markus Heep for their critical reading of the manuscript. S.d.P. is supported by the European Union Grant PITN-GA-2013-607963.

1. Brown GD, et al. (2012) Hidden killers: Human fungal infections. *Sci Transl Med* 4(165):165rv13.
2. Denning DW, Pleuvry A, Cole DC (2013) Global burden of allergic bronchopulmonary aspergillosis with asthma and its complication, chronic pulmonary aspergillosis, in adults. *Med Mycol* 51(4):361–370.
3. Denning DW, Pleuvry A, Cole DC (2011) Global burden of chronic pulmonary aspergillosis as a sequel to pulmonary tuberculosis. *Bull World Health Organ* 89(12): 864–872.
4. Pound MW, Townsend ML, Dimondi V, Wilson D, Drew RH (2011) Overview of treatment options for invasive fungal infections. *Med Mycol* 49(6):561–580.
5. Denning DW, Hope WW (2010) Therapy for fungal diseases: Opportunities and priorities. *Trends Microbiol* 18(5):195–204.
6. Nett JE, Andes DR (2016) Antifungal agents: Spectrum of activity, pharmacology, and clinical indications. *Infect Dis Clin North Am* 30(1):51–83.
7. Verweij PE, Chowdhary A, Melchers WJ, Meis JF (2016) Azole resistance in *Aspergillus fumigatus*: Can we retain the clinical use of mold-active antifungal azoles? *Clin Infect Dis* 62(3):362–368.
8. Rivero-Menendez O, Alastruey-Izquierdo A, Mellado E, Cuenca-Estrella M (2016) Triazole resistance in *Aspergillus* spp.: A worldwide problem? *J Fungi* 2(3):21.
9. Gonçalves SS, Souza AC, Chowdhary A, Meis JF, Colombo AL (2016) Epidemiology and molecular mechanisms of antifungal resistance in *Candida* and *Aspergillus*. *Mycoses* 59(4):198–219.
10. Chowdhary A, Kathuria S, Xu J, Meis JF (2013) Emergence of azole-resistant *Aspergillus fumigatus* strains due to agricultural azole use creates an increasing threat to human health. *PLoS Pathog* 9(10):e1003633.
11. Osherov N, Kontoyiannis DP, Romans A, May GS (2001) Resistance to itraconazole in *Aspergillus nidulans* and *Aspergillus fumigatus* is conferred by extra copies of the *A. nidulans* P-450 14α-demethylase gene, *pdmA*. *J Antimicrob Chemother* 48(1): 75–81.
12. Liu W, May GS, Lionakis MS, Lewis RE, Kontoyiannis DP (2004) Extra copies of the *Aspergillus fumigatus* squalene epoxidase gene confer resistance to terbinafine: Genetic approach to studying gene dose-dependent resistance to antifungals in *A. fumigatus*. *Antimicrob Agents Chemother* 48(7):2490–2496.
13. Parry TE, Blackmore JA (1974) Serum "uracil plus uridine" levels in normal subjects and their possible significance. *J Clin Pathol* 27(10):789–793.
14. D'Enfert C, et al. (1996) Attenuated virulence of uridine-uracil auxotrophs of *Aspergillus fumigatus*. *Infect Immun* 64(10):4401–4405.
15. Noble SM, Johnson AD (2005) Strains and strategies for large-scale gene deletion studies of the diploid human fungal pathogen *Candida albicans*. *Eukaryot Cell* 4(2): 298–309.
16. Retallack DM, Heinecke EL, Gibbons R, Deepe GS, Jr, Woods JP (1999) The *URA5* gene is necessary for *Histoplasma capsulatum* growth during infection of mouse and human cells. *Infect Immun* 67(2):624–629.
17. de Gontijo FA, et al. (2014) The role of the de novo pyrimidine biosynthetic pathway in *Cryptococcus neoformans* high-temperature growth and virulence. *Fungal Genet Biol* 70:12–23.
18. Bar-Or A, Pachner A, Menguy-Vacheron F, Kaplan J, Wiendl H (2014) Teriflunomide and its mechanism of action in multiple sclerosis. *Drugs* 74(6):659–674.
19. Liu S, Neidhardt EA, Grossman TH, Ocain T, Clardy J (2000) Structures of human dihydroorotate dehydrogenase in complex with antiproliferative agents. *Structure* 8(1): 25–33.
20. Phillips MA, et al. (2015) A long-duration dihydroorotate dehydrogenase inhibitor (DSM265) for prevention and treatment of malaria. *Sci Transl Med* 7(296):296ra111.
21. Vyas VK, Ghate M (2011) Recent developments in the medicinal chemistry and therapeutic potential of dihydroorotate dehydrogenase (DHODH) inhibitors. *Mini Rev Med Chem* 11(12):1039–1055.
22. Howard SJ, Pasqualotto AC, Denning DW (2010) Azole resistance in allergic bronchopulmonary aspergillosis and *Aspergillus* bronchitis. *Clin Microbiol Infect* 16(6): 683–688.
23. Denning DW, Bromley MJ (2015) Infectious disease: How to bolster the antifungal pipeline. *Science* 347(6229):1414–1416.
24. Payne DJ, Gwynn MN, Holmes DJ, Pompliano DL (2007) Drugs for bad bugs: Confronting the challenges of antibacterial discovery. *Nat Rev Drug Discov* 6(1):29–40.
25. Swinney DC, Anthony J (2011) How were new medicines discovered? *Nat Rev Drug Discov* 10(7):507–519.
26. Roemer T, Krysan DJ (2014) Antifungal drug development: Challenges, unmet clinical needs, and new approaches. *Cold Spring Harb Perspect Med* 4(5):a019703.
27. Goldstein AL, McCusker JH (2001) Development of *Saccharomyces cerevisiae* as a model pathogen: A system for the genetic identification of gene products required for survival in the mammalian host environment. *Genetics* 159(2):499–513.
28. Brand A, MacCallum DM, Brown AJ, Gow NA, Odds FC (2004) Ectopic expression of *URA3* can influence the virulence phenotypes and proteome of *Candida albicans* but can be overcome by targeted reintegration of *URA3* at the *RPS10* locus. *Eukaryot Cell* 3(4):900–909.
29. Munier-Lehmann H, Vidalain PO, Tangy F, Janin YL (2013) On dihydroorotate dehydrogenases and their inhibitors and uses. *J Med Chem* 56(8):3148–3167.
30. Vogel HJ (1956) A convenient growth medium for *Neurospora* (medium N). *Microbiol Genet Bull* 13:42–43.
31. Zameitat E, Gojković Z, Knecht W, Piskur J, Löffler M (2006) Biochemical characterization of recombinant dihydroorotate dehydrogenase from the opportunistic pathogenic yeast *Candida albicans*. *FEBS J* 273(14):3183–3191.
32. Sibley GEM, et al. (2009) Pyrrole antifungal agents. Patent Cooperation Treaty Appl WO2009130481.
33. Copeland RA, et al. (1995) Recombinant human dihydroorotate dehydrogenase: Expression, purification, and characterization of a catalytically functional truncated enzyme. *Arch Biochem Biophys* 323(1):79–86.
34. Dereeper A, et al. (2008) Phylogeny.fr: Robust phylogenetic analysis for the non-specialist. *Nucleic Acids Res* 36(Web Server issue):W465–469.
35. Rawls J, Knecht W, Diekert K, Lill R, Löffler M (2000) Requirements for the mitochondrial import and localization of dihydroorotate dehydrogenase. *Eur J Biochem* 267(7):2079–2087.

Supporting Information

Oliver et al. 10.1073/pnas.1608304113

SI Materials and Methods

Fungal Strains. For susceptibility testing, a range of clinical isolates were tested for each species plus standard strains: *A. fumigatus* AF210, *A. niger* AN1, *A. terreus* AT4, *A. flavus* AFl1, *C. albicans* CA6862, *E. coli* NCTC 10418, and *Staphylococcus aureus* Oxford strain NCTC 6571. *A. nidulans* A4 (WT) and *A. nidulans* A767 (*pyrG89 nicA*) were used for the mechanism of action screen. *A. fumigatus* NIH4215 and *A. fumigatus* F16216 were used for efficacy testing.

Synthesis of F901318. The synthesis of 1,2-dimethyl-4-phenyl-1H-pyrrole was done as described previously (32).

(1,5-Dimethyl-3-phenyl-1H-pyrrol-2-yl)-oxo-acetyl chloride. Oxalyl chloride (78.42 mL, 0.91 mol) was slowly added to a cooled solution of 1,2-dimethyl-4-phenyl-1H-pyrrole (105.5 g, 0.61 mol) in dry dichloromethane (3 × 200 mL) at 0 °C. The reaction mixture was then warmed to room temperature and stirred for 1 h. The solvent was evaporated to dryness in vacuo to afford 124 g (78% yield) of (1,5-dimethyl-3-phenyl-1H-pyrrol-2-yl)-oxo-acetyl chloride as a brown oily liquid, which was used directly in the next step (TLC system: EtOAc:pet ether, 3:7; Rf value, 0.65).

5-Fluoro-2-[4-(4-nitro-phenyl)-piperazin-1-yl]-pyrimidine. 2-Chloro-5-fluoropyrimidine (78.76 mL, 0.64 mol) was added to suspension of 1-(4-nitro-phenyl)-piperazine (110 g, 0.53 mol) and potassium carbonate (367.2 g, 2.65 mol) in acetonitrile (3 L). The reaction mixture was refluxed for 48 h. On completion of reflux, the mixture was cooled to 0 °C and then filtered, and the residue was taken in water (3 L) and stirred for 30 min. The suspension was filtered, the solid cake was washed with water (1 L) and pet ether (1 L) and then dried under vacuum to afford 148 g (92%) of 5-fluoro-2-[4-(4-nitro-phenyl)-piperazin-1-yl]-pyrimidine as a yellow-colored solid. (TLC system: EtOAc:pet ether, 3:7; Rf value, 0.70). ^{1}H NMR (300 MHz, CDCl3): δ 8.24 (s, 2 H), 8.17–8.13 (d, J = 9.6 Hz, 2 H), 6.87–6.84 (d, J = 9.6 Hz, 2 H), 3.97–3.94 (m, 4 H), 3.55–3.52 (m, 4 H). m.p. 205–206 °C. (*m*/*z*, ES, positive scan): 304.21 (100%; M+H).

4-[4-(5-Fluoro-pyrimidin-2-yl)-piperazin-1-yl]-phenyl amine. A solution of 5-fluoro-2-[4-(4-nitro-phenyl)-piperazin-1-yl]-pyrimidine (80 g, 0.26 mol) in methanol (1 L) was hydrogenated over Raney Nickel (30 g) under 70-psi pressure at room temperature for 6 h. The reaction mixture was filtered over celite, and the filtrate was concentrated in vacuo to yield a crude product, which was washed with hexane (500 mL) to afford 52 g (72%) of 4-[4-(5-fluoro-pyrimidin-2-yl)-piperazin-1-yl]-phenyl amine as a brown-colored solid (TLC system: methanol:chloroform, 1:9; Rf value, 0.50). ^{1}H NMR (300 MHz, CDCl3): δ 8.21 (s, 2 H), 6.86–6.84 (d, J = 8.7 Hz, 2 H), 6.68–6.65 (d, J = 9.0 Hz, 2 H), 3.92–3.89 (m, 4 H), 3.45 (broad s, 2 H, NH2), 3.09–3.06 (m, 4 H). m.p. 138–139 °C. (*m*/*z*, ES, positive scan): 288.14 (100%; M+H).

2-(1,5-Dimethyl-3-phenyl-1H-pyrro-2-yl)-N-{4-[4-(5-fluoro-pyrimidin-2-yl)-piperazin-1-yl]-phenyl}-2-oxo-acetamide F901318. A solution of 1,5-dimethyl-3-phenyl-1H-pyrrol-2-yl)-oxo-acetyl chloride (64.65 g, 0.24 mol) in dichloromethane (500 mL) was added to a stirred solution of 4-[4-(5-fluoro-pyrimidin-2-yl)-piperazin-1-yl]-phenyl amine (45 g, 0.16 mol) and triethylamine (46 mL, 0.32 mol) in dichloromethane (150 mL) at 0 °C. The reaction mixture was warmed to room temperature and then stirred for 30 min. The reaction mixture was quenched with water and extracted with dichloromethane (6 × 500 mL). The combined organic layers were washed successively with saturated sodium bicarbonate solution (1.5 L), water (1 L), and brine (1.5 L), and finally dried over anhydrous sodium sulfate. The organic layer was stirred with neutral alumina (500 g) at room temperature for 30 min and then filtered. The filtrate was concentrated in vacuo to yield the crude product, which was washed successively with diethyl ether (300 mL) and hexane (200 mL) to afford 60 g (73%) of 2-(1,5-dimethyl-3-phenyl-1H-pyrro-2-yl)-*N*-{4-[4-(5-fluoro-pyrimidin-2-yl-piperazin-1yl]-phenyl}-2-oxo-acetamide F901318 as a yellow-colored solid (TLC system: EtOAc:pet ether, 1:1; Rf value, 0.65). ^{1}H NMR (400 MHz, CDCl3): δ 8.21 (s, 2 H), 8.19 (broad s, 1 H), 7.32–7.22 (m, 5 H), 7.10 (d, J = 8.7 Hz, 2 H), 6.83 (d, J = 8.7 Hz, 2 H), 6.13 (s, 1 H), 3.92–3.88 (m, 4 H), 3.81 (s, 3 H), 3.19–3.15 (m, 4 H), 2.33 (s, 3 H). m.p. 194–197 °C. (*m*/*z*, APCI, positive scan): 499.41 (100%; M+H).

Mechanism of Action Screen. *A. nidulans* A767 protoplasts were prepared from fungal biomass by digestion with 5% (wt/vol) glucanex (Novozymes) in 0.6 M KCl and 50 mM $CaCl_2$ for 60–120 min at 30 °C with shaking at 100 rpm. The protoplasts were washed in 0.6 M KCl and 50 mM $CaCl_2$, isolated by centrifugation at 820 × *g* for 9 min at 4 °C, and then washed and resuspended in STC buffer (1.2 M sorbitol, 50 mM $CaCl_2$, and 10 mM Tris·HCl pH 7.5). Then 2–5 μg of an *A. nidulans* genomic library carried on the pRG3-AMA1-NotI vector (Fungal Genetic Stock Center) was transformed into protoplasts in the presence of 40% (wt/vol) PEG 6000 in STC buffer for 5 min, followed by vortexing and inoculation onto Vogel's minimal medium, 1.2 M sorbitol, and 5 μg/mL nicotinic acid. The plates were incubated at 37 °C for 5 d, after which the spores were collected in PBS-0.1% Tween 80 and filtered through glass wool. A total of 10^5 spores were inoculated onto Vogel's minimal medium (30) plus 0.25 μg/mL F901318, and the plates were incubated at 37 °C for 7 d. DNA was isolated from resistant colonies using the FastDNA Spin Kit (MP Biomedicals), and plasmid DNA was transformed into *E. coli* (MegaX DH10B T1R Electrocomp cells; Invitrogen).

DNA was mutagenized using the EZ-Tn5 bacterial transposon system (Epicentre Biotechnologies). A DNA fragment comprising *A. fumigatus pyrG* (GenBank accession no. Y11303.1), followed by the EM7 promoter upstream of the *She ble* ORF (codes for resistance to zeocin: 1,924–2,426 bp of pEM7/zeo; Invitrogen) with Tn5 mosaic ends at both ends, was included in the transposase reaction. After transformation into *E. coli*, insertion of the Tn5 transposon was detected by growth in the presence of 50 μg/mL zeocin, and PCR established the insertion site.

Cloning, Expression, and Purification of DHODH. To overcome initial problems with solubility of *A. fumigatus* DHODH expressed in *E. coli*, the N-terminal 88 amino acids consisting of the mitochondrial targeting sequence and transmembrane domain were omitted, and the truncated DHODH (amino acids 89–531) was cloned into pET44 (Novagen) that codes for an N-terminal NusA fusion protein to aid solubility. *A. fumigatus* cDNA was prepared from *A. fumigatus* RNA using AMV reverse transcriptase (Promega). PCR of N-truncated *A. fumigatus* DHODH coding cDNA was carried out using primers AF_DHODH_F1 and AF_DHODH_R1 (primer sequences given in Table S1) and KOD DNA polymerase (Novagen). This product was cloned into pET44 by ligation-independent cloning (Novagen). N-truncated (amino acids 29–395) human DHODH cDNA was cloned from IMAGE clone 6064723 (MGC70636; Geneservice) into pET44 after PCR with primers HS_DHODH_F1 and HS_DHODH_R1.

C. albicans DHODH contains two CTG-encoded serine residues at codons 11 and 78 that were mutated to TCG codons by incorporating the new codons in two overlapping fragments, which were subsequently joined by fusion PCR. The fragments were created by

PCR from gDNA with primer pairs CA_DHODH_mutF1 with CA_DHODH_mutR1 and CA_DHODH_mutF2 with CA_DHODH_mutR2. The fusion PCR used primers CA_DHODH_fusF1 with CA_DHODH_fusR1, and the product was cloned into pGEM-Teasy (Promega) and sequenced. N-truncated (amino acids 57–444) *C. albicans* DHODH cDNA was cloned into pET44 for protein expression. Previous studies on recombinant DHODH from a variety of organisms, including human (33) and *C. albicans* (31), have found that removal of the N terminus, including the mitochondrial targeting sequence and transmembrane regions, improves expression, simplifies purification, and has little effect on kinetics.

C. albicans DHODH was further mutated at two residues. Phe_{162} and Val_{171} were altered to become Val and Met, respectively, using the Phusion Site-Directed Mutagenesis Kit (Thermo Fisher Scientific). PCR was carried out with phosphorylated primers CA_DHODH_VM_F and CA_DHODH_FV_R and template pET44_CA_DHODH. The product was religated into a plasmid using T4 DNA ligase to create pET44_CA_DHODH_V_{162}_M_{171}.

Protein expression plasmids were transformed into *E. coli* BL21 (DE3) cells, and expression was stimulated with 0.5 mM isopropyl β-D-1-thiogalactopyranoside, followed by incubation in LB broth in the presence of 100 μg/mL ampicillin and 100 μM flavin mononucleotide at 18–20 °C for 16–18 h. Bacterial pellets were lysed with BugBuster (Novagen), and His-tagged DHODH protein was isolated by immobilized metal affinity chromatography using His-Bind resin (Novagen) according to the manufacturer's instructions.

DHODH Assays. These assays were carried out broadly as described elsewhere (31). Approximately 2 μg of recombinant *A. fumigatus* DHODH or 0.5 μg of recombinant human DHODH was incubated in the presence of 1 mM L-dihydroorotic acid, 0.05 mM coenzyme Q2, and 0.1 mM 2,6-dichlorindophenol in 50 mM Tris·HCl, 150 mM KCl, 10% (wt/vol) glycerol, and 0.1% (wt/vol) Triton X-100, pH 8 at 25 °C. DHODH activity was determined using the redox indicator 2,6-dichloroindophenol by measuring the decrease in absorbance at 600 nm. Initial reaction velocities were determined, and the percent inhibition in the presence of the drug was calculated compared with controls in the absence of drug. The inhibition curve data were fitted to a four-parameter sigmoidal plot (r^2 >0.998 for IC_{50} plots) using XLFit (IDBS), and the IC_{50} value was calculated as the concentration of drug causing 50% inhibition.

Homology Modeling of *A. fumigatus* DHODH. A range of DHODH structures, including those from human, rat, *P. falciparum*, and *E. coli*, were compared with the fungal sequences for *Candida* and *Aspergillus* strains. Sequences were aligned manually with reference to the protein superimpositions (PyMOL). RCSB PDB ID codes for the structures used were as follows: 1D3G, 1PRH, 2PRL, 2PRM, 3G0X, 3KVM, 2WV8, 2FQI (human); 1UUM, 1UUO (rat); 2E68 (*Trypanosoma cruzi*); 3I68, 1ITV, 3O8A (*P. falciparum*); 3MJY (*Leishmania major*); and 1F76 (*E. coli*) (www.rcsb.org).

Human DHODH (PDB ID code 1D3G) (19) served as the protein template for construction of the *A. fumigatus* DHODH model. Residue replacement, bump checking, and coarse refinement were done in Discovery studio 4.1 (Accelrys). Fine residue refinement and new secondary structure or loop insertions were built in XEDraw (Cresset's internal research software, results of which can be visualized in Torch; www.cresset-group.com/products/torch/). When no information was known for a given loop, the loop was constructed manually based on the local environment and the nature of the primary sequence (i.e., using the predicted beta sheet or helical secondary structural preference) to yield appropriate packing that minimized the exposure of lipophilic residues and maximized the exposure of polar and charged residues to solvent. The final protein was coarse minimized (0.1 rmsd) using the XED force field.

In parallel to the initial protein analysis, the fungal inhibitor data were compared with known DHODH activities for which X-ray data were available. Full multiple ligand alignments were generated, and 3DQSAR was performed for the fungal inhibitors (Forge; Cresset; www.cresset-group.com/products/forge/).

All of the available information for the ligand centric and protein complex data were combined to provide a best estimate of correct placement of the F901318 inhibitor structure in the homology model. The resultant complex was then reminimized in place initially using shell minimization in XEDraw and then using full minimization to 0.01 rmsd (Fig. S6*A*).

The homology model was assessed using a Ramachandran plot (Fig. S6*C*). This plot exhibited good geometries for the core, with the only discrepancies being distant from the ligand and confined to more speculative regions of the model, i.e., where no homology existed.

By bringing both the protein sequence and structural data together with ligand SAR and field data, we were able to conclude with reasonable confidence the most likely nature of the interactions of this DHODH inhibitor chemotype. As with known inhibitors, a bidirectional H-bonding arrangement was observed for these fungal ligands, in keeping with the likely interactions within the putative ubiquinone-binding site. These interactions, from observation across multiple examples, involve equivalents of His_{116}, Arg_{202}, Tyr_{213}, and Tyr_{505} (*A. fumigatus* residue numbering) as the corresponding H-bonding partners (Fig. 3*A*). From the sequence, structure analysis, and ligand field analysis, further lipophilic contacts—Val_{200}, Met_{209}, and Tyr_{510}—were defined. This ligand-binding model is supported by the mutagenesis of the *C. albicans* recombinant protein (Fig. 3*B*). Phe_{162} and Val_{171} of *C. albicans* align with Val_{200} and Met_{209} of *A. fumigatus* DHODH, respectively. Mutating these residues to their *A. fumigatus* equivalents introduced inhibition of DHODH activity by F901318 in the mutant, where no inhibition had occurred with the WT enzyme.

Creation of DHODH Phylogenetic Trees. DHODH sequences were obtained from searching sequence databases held by the National Center for Biotechnology Information, EnsemblFungi, and the Joint Genome Initiative (JGI). The accession codes for the proteins are as follows, with alternative fungal names in parentheses: *Absidia idahoensis* (*Lichtheimia ramosa*), CDS13591.1; *Acremonium_alcalophilum*, jgi|Acral2|2024193; *Alternaria alternata*, jgi|Altal1|982905; *Alternaria brassicicola*, jgi|Altbr1|1659; *A. flavus*, XP_002379410.1; *A. fumigatus*, XP_755434.1; *Aspergillus lentulus*, GAQ06647.1; *A. niger*, XP_001399431.2; *A. terreus*, protein sequence derived from gene ATEG_01477 (EnsemblFungi); *Bipolaris sorokiniana*, XP_007699125.1; *B. dermatitidis* (*Ajellomyces dermatitidis*), EEQ85598.1; *C. albicans*, XP_723522.1; *Candida glabrata*, XP_449903.1; *Candida krusei* (*Pichia kudriavzevii*), KGK37337.1; *Candida parapsilosis*, CCE41941.1; *Candida tropicalis*, XP_002549089.1; *Chaetomium globosum*, XP_001223311.1; *C. immitis*, XP_001240778.2; *C. neoformans*, XP_569657.1; *E. coli*, WP_001330055.1; *Exophiala dermatitidis*, XP_009159400.1; *Fusarium oxysporum*, EGU79150.1; *Fusarium solani* (*Nectria hematococca*), XP_003046434.1; *H. capsulatum* (*Ajellomyces capsulatus*), EGC45332.1; *Homo sapiens*, NP_001352.2; *Magnaporthe_oryzae*, XP_003719157.1; *Malassezia globosa*, XP_001729892.1; *Microsporum canis* (*Arthroderma otae*), XP_002849178.1; *Microsporum gypseum*, XP_003175518.1; *Mucor circinelloides*, EPB81175.1; *Neurospora crassa*, XP_961804.1; *Paecilomyces variotii* (*Byssochlamys spectabilis*), GAD93826.1; *Paracoccidioides brasiliensis*, XP_010757420.1; *Penicillium chrysogenum*, jgi|Pench1|33932; *Penecillium marneffei* (*Talaromyces marneffei*), KFX48065.1; *Phycomyces blakesleeanus*, jgi|Phybl2|177367; *P. falciparum*, XP_966023.1; *Pneumocystis jirovecii*, CCJ31177.1; *Rhizopus delemar*, EIE79352.1; *Scedosporium apiospermum*, JOWA01000121.1; *Sporothrix schenckii*, ERT03286.1;

Trichoderma reesei, XP_006962857.1; *Trichophyton mentagrophytes* (*Arthroderma benhamiae*), XP_003012466.1; *Trichophyton rubrum*, XP_003234264.1; and *Ustilago maydis*, XP_011389794.1.

Sequences in FASTA format were submitted for phylogenetic analysis at www.phylogeny.fr using the "Advanced" analysis (34). Sequences were aligned using MUSCLE ("Full mode") and curated with GBlocks (default settings). Phylogeny was established by the maximum likelihood method in PhyML using the approximate likelihood ratio test set to SH-like with the WAG substitution method. The tree was visualized in TreeDyn.

Class 2 DHODH sequences are present in all mammals, many fungi, and some bacteria, including *E. coli* (29). They are membrane-bound (integral mitochondrial membrane proteins in mammals and some fungi; membrane-associated in some bacteria) monomers that have a catalytic serine and use ubiquinone as a terminal electron acceptor. Class 1A and 1B DHODHs are soluble and multimeric, have a catalytic cysteine, and use fumarate or NAD as a terminal electron acceptor. Class 2 DHODHs (Fig. S7*A*) were analyzed separately from the zygomycete DHODHs (Fig. S7*B*), which appear to be from class 1A.

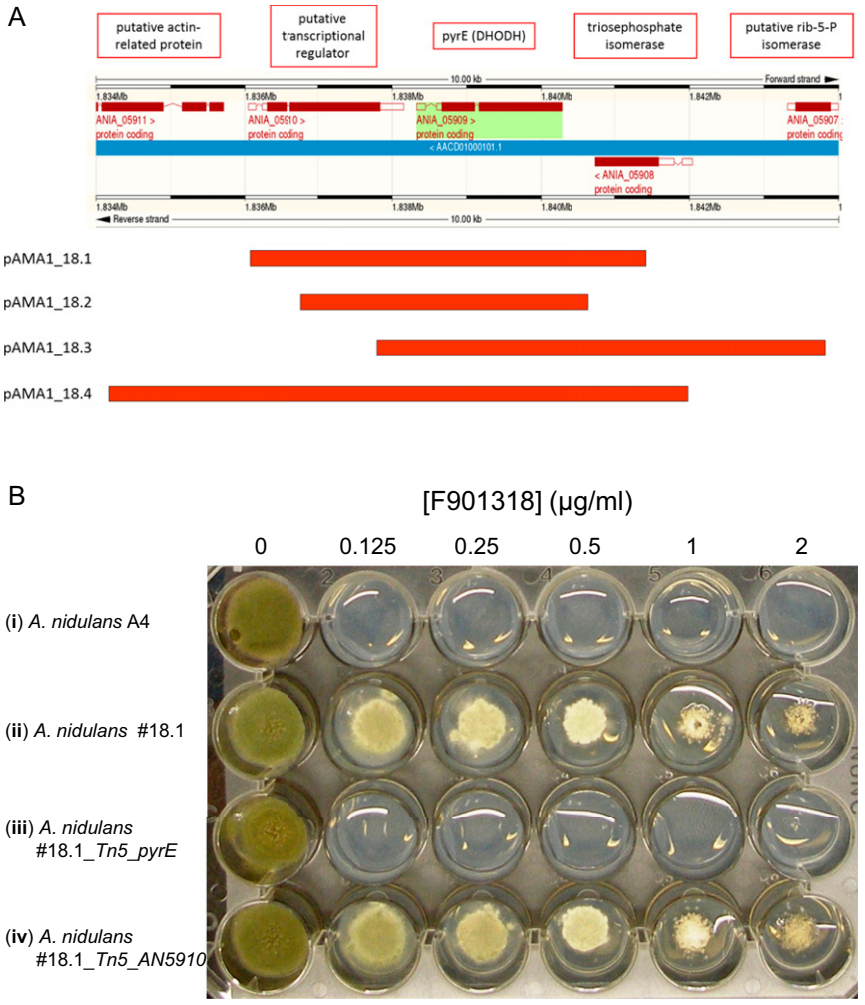

Fig. S1. (*A*) Map of AMA inserts recovered from the mechanism of action screen. An *A. nidulans* genomic screen was performed for genes that when present in a high copy number provided resistance to F901318 (*Materials and Methods*). pAMA1 clones 18.1–18.4 were recovered from four independent colonies that were resistant to F901318. DNA was extracted from the resistant *A. nidulans* and transformed into *E. coli*. Plasmid DNA was isolated and sequenced, and the genomic inserts (red bars) found were mapped to the *A. nidulans* genome using EnsemblFungi. (*B*) *A. nidulans* carrying extra copies of *pyrE* is resistant to F901318. The pAMA1_18.1 plasmid was transformed into *A. nidulans* A767 before (#18.1; *ii*) and after mutagenesis with the EZ-Tn5 bacterial transposon system. The transposon disrupted the pyrE gene (#18.1_Tn5_*pyrE*; *iii*) or the neighboring ANIA_05910 gene (#18.1_Tn5_*AN5910*; *iv*). Conidia from the resulting transformants and from the WT *A. nidulans* A4 (*i*) were inoculated onto media in the presence and absence of varying concentrations of F901318 and incubated at 37 °C for 4 d.

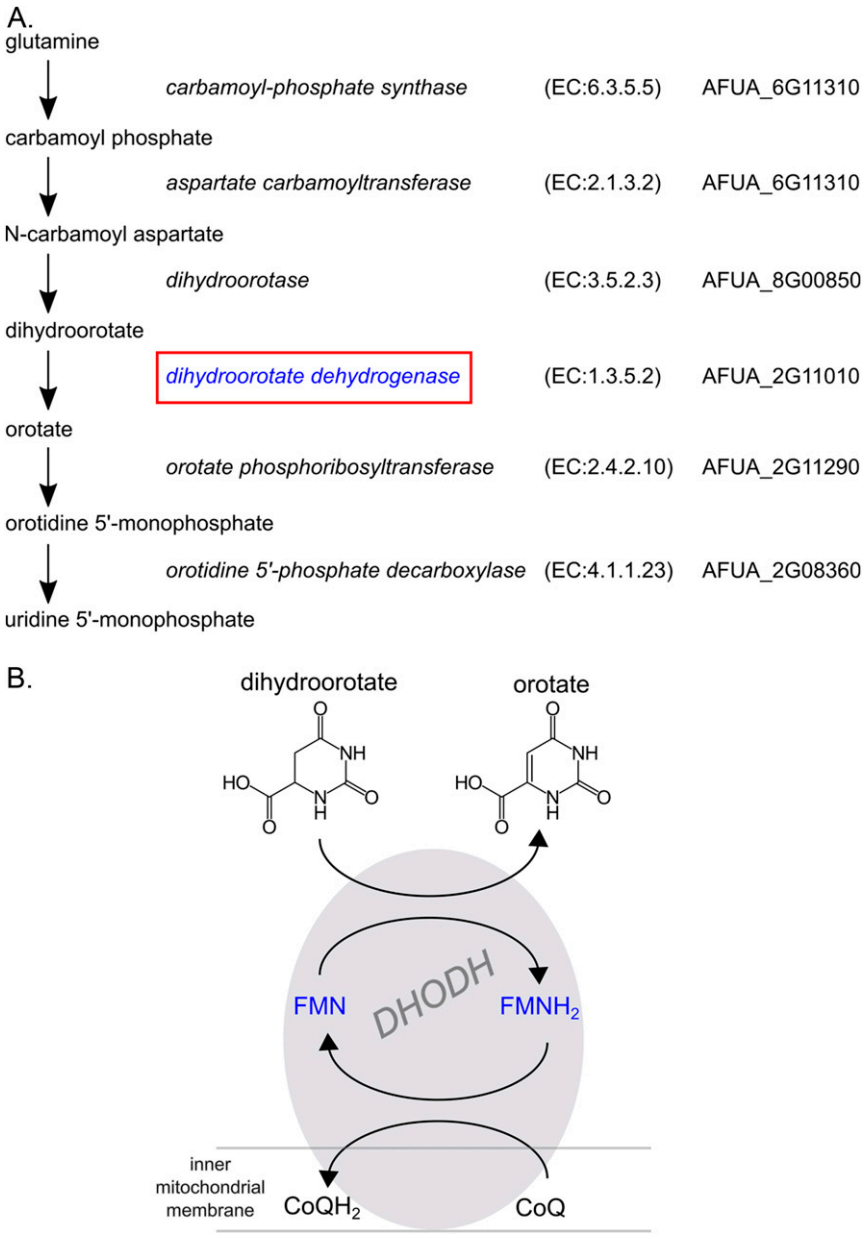

Fig. S2. DHODH is an enzyme of pyrimidine biosynthesis. (*A*) Pathway of de novo pyrimidine biosynthesis in *A. fumigatus*. Enzyme names, classification (according to the Nomenclature Committee of the International Union of Biochemistry and Molecular Biology; www.chem.qmul.ac.uk/iubmb/enzyme/), and predicted *A. fumigatus* genes (from KEGG; www.genome.jp/kegg/ and EnsemblFungi; www.fungi.ensembl.org/index.html/) are listed next to each step of the pathway. (*B*) Reaction catalyzed by DHODH. In mammals and many fungi, DHODH is located at the mitochondria, where a transmembrane domain anchors the enzyme to the outside of the inner mitochondrial membrane. In the intermembrane space, DHODH catalyzes the oxidation of dihydroorotate to orotate. FMN and ubiquinone from the mitochondrial membrane (coenzyme Q) act as electron acceptors in the reaction.

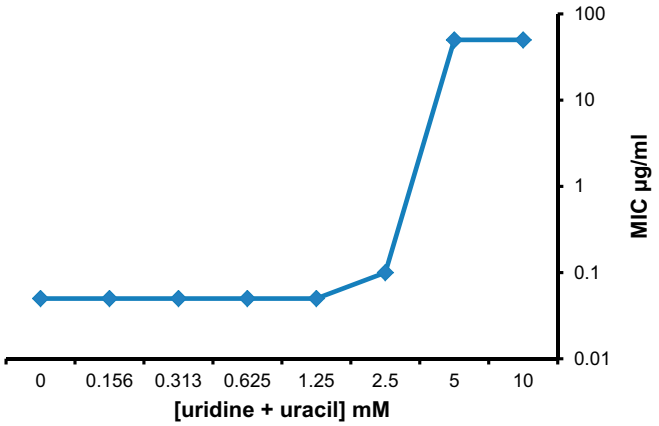

Fig. S3. Reversal of the antifungal effect of F901318 at high pyrimidine concentrations. Antifungal susceptibility testing of F901318 against *A. fumigatus* AF293 was carried out according to CLSI protocol M38-A2 in the presence of different concentrations of uridine and uracil. The MIC of F901318 was obtained for each pyrimidine concentration.

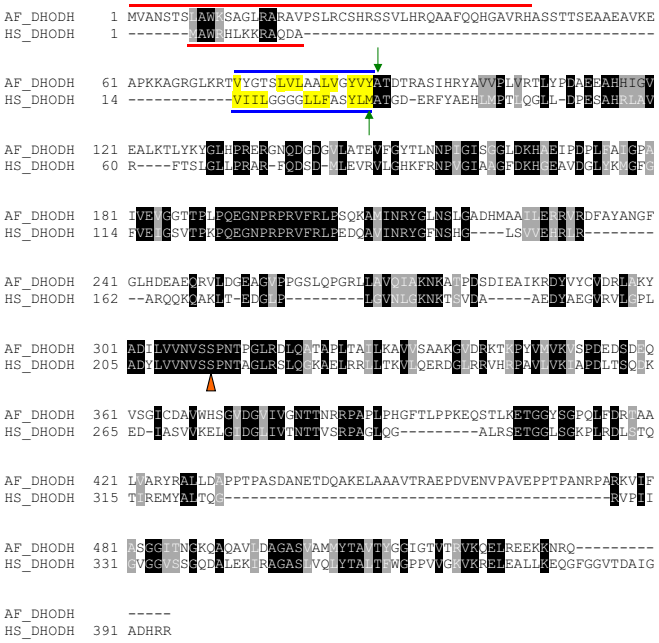

Fig. S4. Alignment of *A. fumigatus* (AF_DHODH) and human (HS_DHODH) DHODH amino acid sequences. The DHODH protein sequences for *A. fumigatus* and human were aligned using CLUSTALW, followed by minor realignment of the mitochondrial targeting sequences and transmembrane domains, defined previously for the human sequence (35). The conserved residues are highlighted in black, and similar residues are highlighted in gray (using BOXSHADE), except in the transmembrane domain, where hydrophobic residues are highlighted in yellow. Mitochondrial targeting sequences are denoted by a red line; transmembrane sequences, by a blue line. Green arrows denote the first residue of the expressed recombinant proteins. The conserved catalytic serine is labeled with an orange triangle.

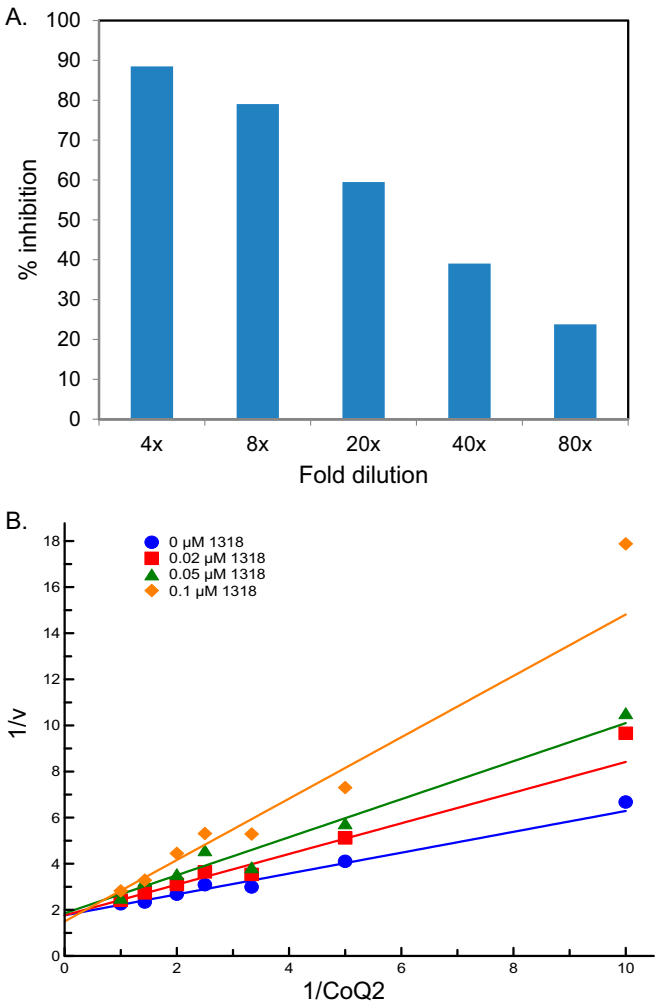

Fig. S5. Kinetics of F901318 inhibition of *A. fumigatus* DHODH. (*A*) F901318 is a reversible inhibitor of *A. fumigatus* DHODH. *A. fumigatus* DHODH was incubated in the presence or absence of 4 µM F901318 for 30 min at room temperature. Aliquots were then diluted in assay buffer [50 mM Tris·HCl, 150 mM KCl, 10% (wt/vol) glycerol and 0.1% (wt/vol) Triton X-100, pH 8] and then further diluted by addition of the mixture that starts the reaction (1 mM L-dihydroorotic acid, 0.05 mM coenzyme Q2, and 0.1 mM 2,6-dichlorindophenol in assay buffer). The final dilution was 4- to 80-fold, giving a final drug concentration of 1–0.05 µM. DHODH activity was calculated for each condition in duplicate and expressed as percent inhibition compared with no drug controls. Dilution of the inhibitor-enzyme mixture releases drug from the enzyme, increasing the activity (and hence decreasing the inhibition) with greater dilution. Thus, F901318 is a reversible inhibitor of *A. fumigatus* DHODH. (*B*) F901318 is a competitive inhibitor of *A. fumigatus* DHODH. Lineweaver Burk analysis of F901318 inhibition of *A. fumigatus* DHODH. The reciprocal of the coenzyme Q2 concentration (in mM) is plotted vs. the reciprocal of the reaction velocity (v, nmol min^{-1}). For a competitive inhibitor, the lines should cross the *y*-axis at the same place.

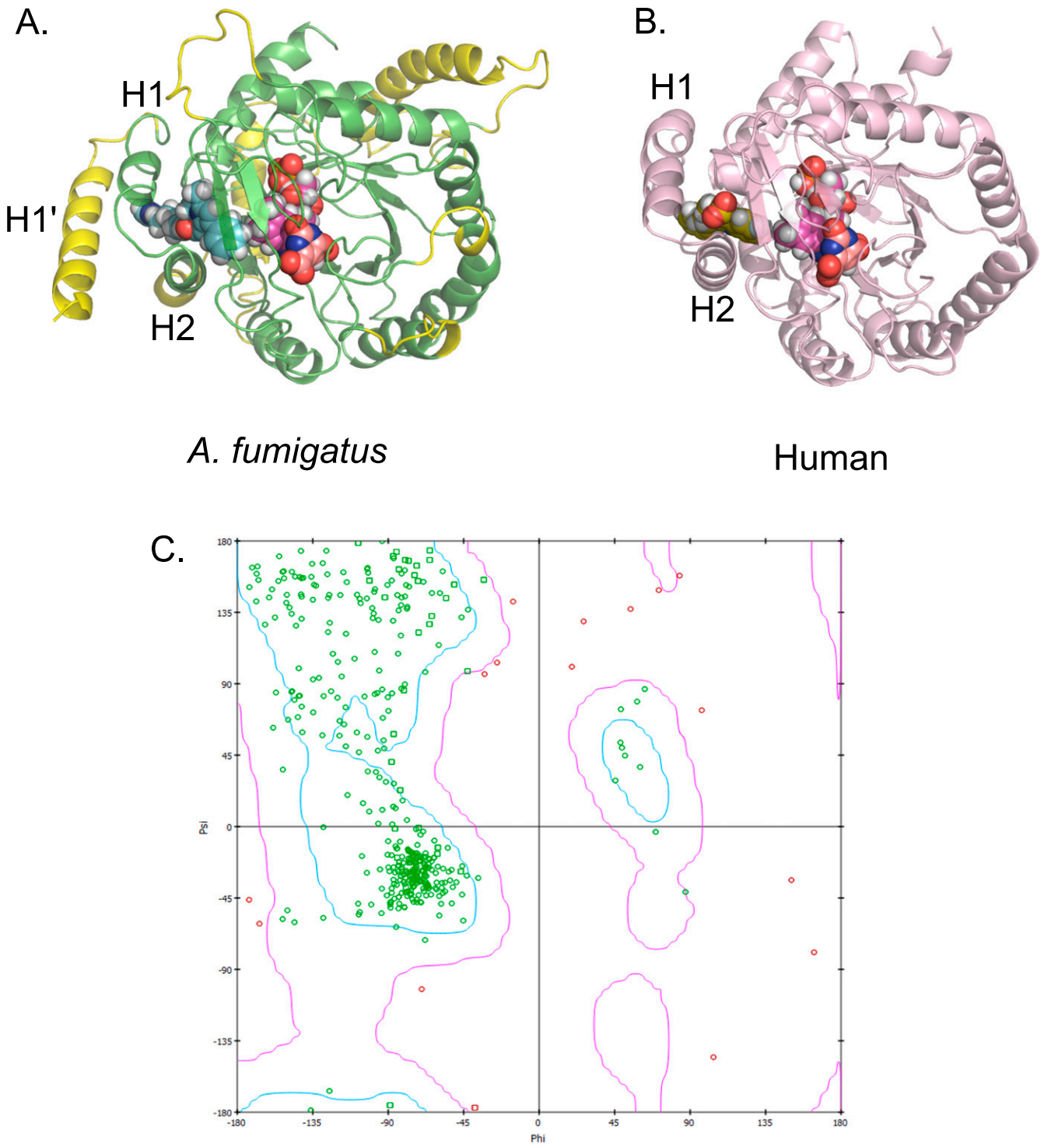

Fig. S6. Inhibitor binding to DHODH. (A) Homology model of *A. fumigatus* DHODH with the estimated binding mode of F901318. The *A. fumigatus* DHODH was modeled using information from known class 2 DHODH structures, with the human structure (PDB ID code 1D3G) forming the protein template. Manually modeled loop/helix insertions are shown in yellow and include an extra N-terminal alpha-helix (H1′) compared with the human protein. Helices H1 and H2 are common to these structures and are predicted to be the entry point for ubiquinone from the mitochondrial membrane (19). F901318 is shown as cyan spheres, FMN is in magenta, and orotate is in orange. (*B*) Brequinar bound to human DHODH (PDB ID code 1D3G). Adapted from Liu et al. (19). Brequinar is in green; FMN, in magenta; orotate, in orange. (*C*) Ramachandran plot of an *A. fumigatus* DHODH homology model. The model was assessed by calculating the ϕ and ψ torsional angles of the amino acid residues in the model. The bulk of the model appears to be energetically allowable (green residues). All residues with ϕ–ψ angle irregularities are exclusively in regions with lower homology to known structures and thus are more speculative. These discrepancies (pink residues) occur in residues distant from the predicted inhibitor-binding region and should not affect the derived ligand-binding hypothesis.

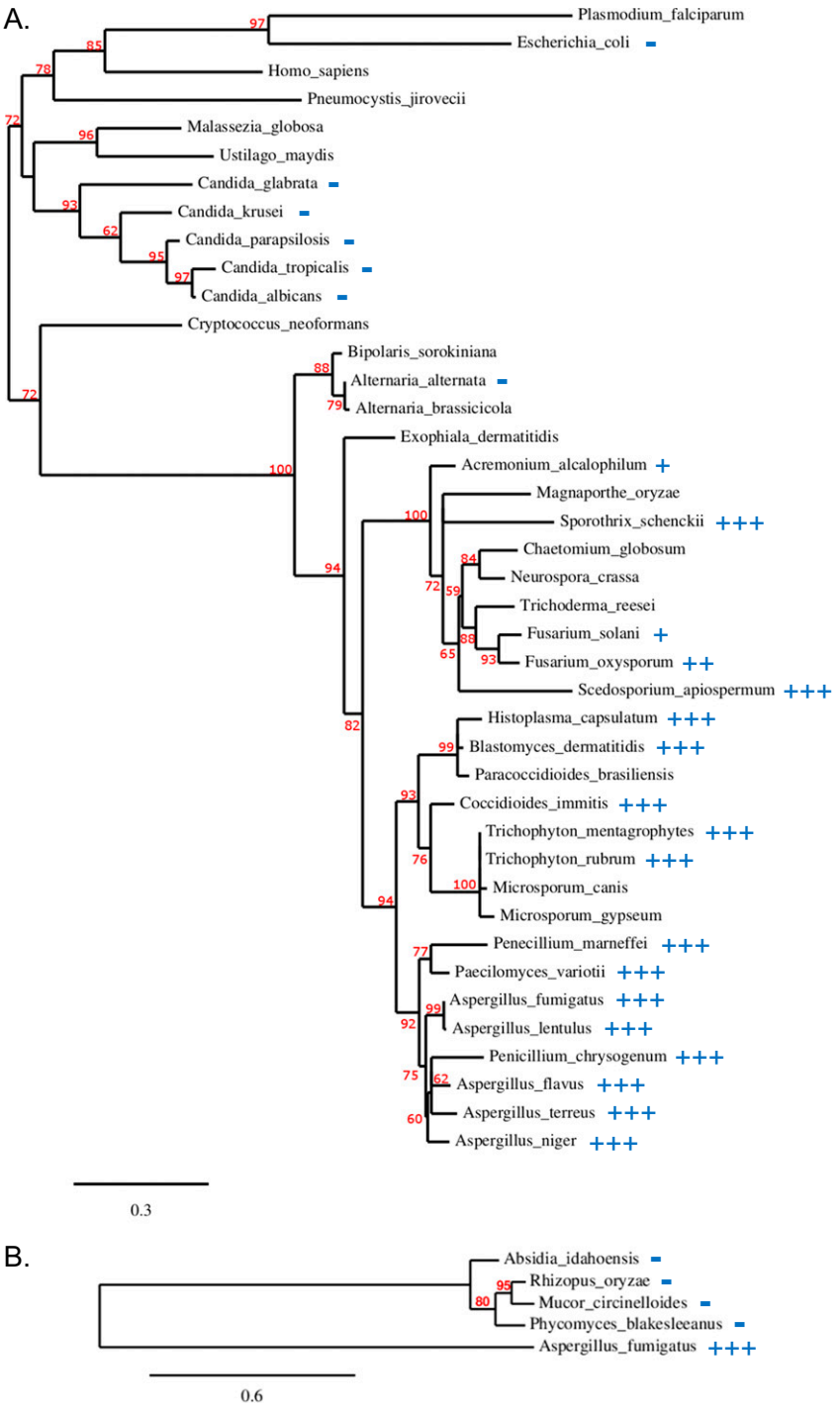

Fig. S7. Phylogeny of DHODH and F901318 susceptibility. (*A*) Class 2 DHODH sequences from fungi and selected other organisms. (*B*) Zygomycete DHODH phylogeny. Branch support values expressed as a percentage are indicated in red. The scale bar corresponds to the branch length for an expected number of 0.3 and 0.6 substitution per site in *A* and *B*, respectively. Antifungal susceptibility testing of F901318 against the species indicated was carried out according to CLSI protocol M38-A2. For the fungi with a score, at least five different strains were tested, except for the following organisms: *A. lentulus*, $n = 4$; *F. solani*, $n = 3$; *F. oxysporum*, $n = 2$; *S. apiospermum*, $n = 2$; and *P. variotti*, $n = 3$. For *S. prolificans*, three different strains were tested, all giving an MIC of ≤0.06 μg/mL, but no DHODH sequence could be obtained for phylogenetic analysis. MIC scoring: +++, MIC ≤0.06 μg/mL; ++, MIC = 0.125–0.5 μg/mL; +, MIC = 1–2 μg/mL; −, MIC >32 μg/mL.

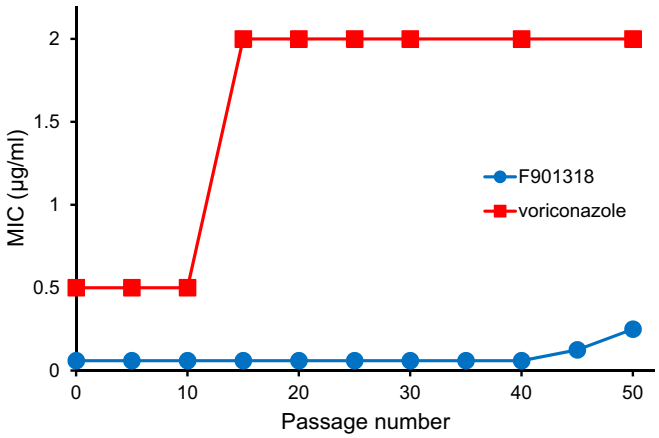

Fig. S8. Effect on MIC of repeated exposure of *A. fumigatus* to F901318 or voriconazole. *A. fumigatus* 210 conidia were inoculated on Sabouraud agar. Then 100 μL of 500 μg/mL F901318 (blue circles) or voriconazole (red squares) was dispensed into a well in the center of the plate and allowed to diffuse. After incubation at 35 °C for 4 d, conidia were collected from the margins of growth and used to inoculate the next plate. After every five passages, the MIC of the conidia was determined.

Table S1. Sequences of the primers used in this study

Primer	Sequence 5′–3′
AF_DHODH_F1	GACGACGACAAGATGGCGACGGATACCAGGGCAAG
AF_DHODH_R1	GAGGAGAAGCCCGGTCTATTGACGGTTTTTCTTTTCC
HS_DHODH_F1	GACGACGACAAGATGGCCACGGGAGATGAGCG
HS_DHODH_R1	GAGGAGAAGCCCGGTTCACCTCCGATGATCTGCTC
CA_DHODH_fusF1	ATGTTTCGTCCAAGTATCAAATTC
CA_DHODH_fusR1	TCACTTATCATCAGAGCCAA
CA_DHODH_mutF1	ATGTTTCGTCCAAGTATCAAATTCAAACAGTCGACTTTGTCC
CA_DHODH_mutR1	CCAACTTATGTCCCGACTCTGCATCTGTGAAAGT
CA_DHODH_mutF2	CACAGATGCAGAGTCGGGACATAAGT
CA_DHODH_mutR2	TCACTTATCATCAGAGCCAATTATTTGCTC
CA_DHODH_F1	GACGACGACAAGATGTCAAGATCAGCAATCCATGA
CA_DHODH_R1	GAGGAGAAGCCCGGTTCACTTATCATCAGAGCCAA
CA_DHODH_VM_F	CCAAAAGATGATGCTATGATTAACAGAT
CA_DHODH_FV_R	CAATCTGAAAACTCTTGGCTGA